Protection contre les courts-circuits des réseaux à courant continu de forte puissance

Justine Descloux

UNIVERSITÉ DE GRENOBLE

THÈSE

Pour obtenir le grade de

DOCTEUR DE L'UNIVERSITÉ DE GRENOBLE

Spécialité : **Génie Électrique**

Arrêté ministériel : 7 août 2006

Présentée par

Justine DESCLOUX

Thèse dirigée par **Bertrand RAISON**
et codirigée par **Jean-Baptiste CURIS**

préparée au sein du **Laboratoire de Génie Électrique de Grenoble (G2Elab)** dans l'**École Doctorale Électronique, Électrotechnique, Automatique et Traitement du Signal**

Protection contre les courts-circuits des réseaux à courant continu de forte puissance

THÈSE SOUTENUE PUBLIQUEMENT LE **20 septembre 2013,**

DEVANT LE JURY COMPOSÉ DE :

M. Jean-Claude MAUN Professeur, École Polytechnique de Bruxelles	Rapporteur
M. Mario PAOLONE Professeur, École Polytechnique Fédérale de Lausanne	Rapporteur
Mme. Anne-Marie DENIS Ingénieur, RTE	Examinateur
M. Stephen FINNEY Professeur, University of Strathclyde	Examinateur
M. Wolfgang GRIESHABER Docteur, Alstom Grid	Examinateur
M. Xavier GUILLAUD Professeur, École Centrale de Lille	Examinateur
M. Jean-Baptiste CURIS Ingénieur, RTE	Encadrant
M. Bertrand RAISON Professeur, Université de Grenoble	Directeur

Remerciements

Mes premiers remerciements vont à toi Bertrand, qui a dirigé cette thèse en apportant toute l'originalité dont tu disposes dans le monde bien carré du contrôle commande des réseaux électriques. En plus de ton investissement incontestable dans ces travaux et de ton encadrement au jour le jour, ce malgré tes responsabilités administratives, je te remercie aussi pour l'immense réconfort que tu m'as apporté lors des phases où la pertinence des résultats de simulations n'était pas évidente à appréhender seule. Merci de t'être adapté à mes déplacements de fin de rédaction jusqu'à effectuer les dernières corrections de ce manuscrit par mail et directement dans les .tex. J'ai été ravie de travailler avec toi pendant ces trois années, mais aussi de discuter météo montagne, skitour, cuisine (à caractère digeste ou non) ou autre sujet hors cadre avec toi en partageant un café, et de découvrir tes lectures on ne peut plus inattendues lors des déplacements en train. Mille mercis !

Merci Jean-Baptiste d'avoir suivi assidûment ces travaux et apporté l'expérience des réseaux réels. Merci de t'être déplacé à Grenoble pour chaque réunion, et d'avoir maintenu un regard critique même après ton changement de poste. Merci aussi pour tes messages de soutien chaleureux dans les dernières lignes droites, qui m'ont aidés à garder le cap.

Je remercie Xavier Guillaud d'avoir accepté de présider le jury de cette thèse, ainsi que les rapporteurs, Jean-Claude Maun et Mario Paolone, pour la rapidité avec laquelle ils ont lu mon manuscrit et l'intérêt qu'ils ont porté à mon travail.

Merci également aux autres membres du jury qui ont accepté de juger ce travail: Anne-Marie Denis, Stephen Finney et Wolfgang Grieshaber, pour leurs apports, leurs commentaires sur le manuscrit et les questions qu'ils ont posées lors de la sou-

tenance.

J'associe à ces remerciements l'ensemble du personnel du G2Elab: direction, personnels administratifs, techniques, enseignants et chercheurs avec qui j'ai eu l'occasion de discuter ou simplement pour leurs bonjours souriants qui participent à l'aura de bonne humeur générale du labo. Merci particulièrement aux membres de l'équipe Syrel pour leurs éclaircissements sur des questions techniques ou pratiques, à Camille pour les travaux communs sur les limiteurs de courant supraconducteurs, ainsi qu'à Delphine, Daniel et Lauric pour avoir partagé les encadrements de TP.

Je remercie également toutes les personnes de RTE qui ont suivi ces travaux dans le cadre du projet Twenties, et surtout Anne-Marie Denis, Olivier Despouys, Samuel Nguefeu et Jean-Pierre Taisne pour les échanges que nous avons eu et leur expertise sur le domaine du transport d'électricité en courant continu.

Je remercie Pierre Rault pour les échanges sur notre sujet commun, et pour le support EMTP-rv ! Sans toi je me serais arrachée les cheveux bien de nombreuses fois à cause des changements de version du logiciel. Je te souhaite tout le courage qu'il faut pour les dernières lignes de ton manuscrit et ta soutenance.

Merci à toutes les personnes du L2EP de m'avoir accueillie dans leur laboratoire de Lille pour réaliser les tests sur le démonstrateur Twenties, et en particulier à Fred, Hicham et Sid qui ont travaillé très dur sur cette maquette.

Je remercie Jean Mahseredjian et Sébastien Dennetière pour leur aide et les réponses qu'ils ont apportées à mes questions de modélisation des câbles.

Aussi, j'aimerais remercier mes amis et ma famille, toutes les personnes auxquelles je pense évidemment quand je me remémore ces trois ans.

Un immense merci à Jean-Louis, avec qui j'ai partagé le même bureau, les week ends et les soirées, les déprimes et les rigolades. Merci pour tout ton réconfort et ton écoute quand il fallait. Merci d'avoir fabriqué le petit vélo blanc qui m'accompagnait sur tous mes trajets de dernière année (oui, sauf quand il pleut ou qu'il neige ou

qu'il fait froid), merci de regarder aux mêmes endroits quand on est assis à côté, merci d'être mon ami même si j'habite à Paris !

Merci à Rémi de m'avoir transformée en skieuse de poudreuse, de m'avoir appris à mettre des crampons et à utiliser un piolet, de m'avoir forcée à courir autour de chaque massif sous des trombes d'eau et de monter 2000m de dev avec 30 kg sur le dos, et de savoir expliquer n'importe quel principe d'électrotechnique (voire astrophysique) sauf comment fonctionnent les protections. Merci à Titouan pour les ateliers peinture collectifs et fartage de ski, merci à Archie de s'intéresser à la mode et de ne pas se laisser aller sous la dictature des GrenobleX en GoreTex, merci à Raph d'être exactement le contraire pour créer le débat, merci à Teu pour les soirées à l'ouest ou autres échanges sans fin dans les maisons lilloises. Merci Imane de m'avoir prêté ton lit quand mon appartement était rempli de cafards, merci Tim et Anto pour les sorties grosse popo et au hazard. Merci Isa, Néné, Aurélien, les deux Xaviers et tous les autres jojos parisiens de m'avoir fait croire pendant trois ans que vous étiez d'accord avec moi sur le fait que, une thèse, c'est un vrai travail, et de m'avoir malgré tout prévenue que je serai fatiguée les premiers mois à Paris. Merci à Luce d'avoir cusiné une semaine pour faire le meilleur pot de thèse, et merci aussi à Anna, Célia et Zazou pour toute leur aide.

Merci Gaspard pour ta manière unique de construire des phrases exclusivement composées d'acronymes ou de mots anglais, peu importe le sujet, mais surtout merci d'oublier de temps en temps la rationalité et de me faire partager toutes tes qualités dont je ne ferai pas la liste ici.

À ma soeur Caro, merci de lutter contre la déformation professionnelle et de ne pas te focaliser uniquement sur le gaz en me posant des questions sur le transport d'électricité, et merci de m'avoir donné un peu de ton expérience sur les entreprises de la branche IEG. Merci à mon frère/beau-frère Bertrand de pousser l'esthétisme jusque dans les power point (qui sont, je le sais, passés de mode). Merci à vous deux d'être aussi mes amis, et de m'avoir logée nourrie et blanchie chez vous, dans des petits appartements ou des grandes maisons, avant chacune de mes réunions à Paris et toutes les autres fois. À ma soeur Élo, merci de m'avoir permis de rédiger les dernières lignes de ce manuscrit sur une île paradisiaque et d'avoir fait tomber

le stress de la dernière ligne droite en me prêtant ton paddle sur l'îlot Tenia !

Merci à toi maman pour toutes tes petites attentions poétiques qui réchauffent, pour tous ces albums-photos-historiques que tu crées à chaque évènement afin de se souvenir des bons moments. Merci à toi papa pour tes conseils et ton avis toujours bien tranché, merci d'adapter ton organisation sans faille quand je suis là alors que tu détestes l'incertitude, de t'attendrir malgré ton (mon) caractère sanguin, par amour et confiance masquée, que tu ne dévoiles qu'aux moments opportuns. Merci à vous deux pour cette proximité qui n'a pas besoin de mots pour s'installer.

Merci enfin à tous ceux qui sont venus le 20 septembre 2013 à Grenoble écouter cette soutenance et célébrer la fin de ces trois ans avec moi.

Contents

List of Figures

List of Tables

General introduction

General introduction

The development and investigation of new transmission solution is emphasized by the required global energy transition due to consumption increase and sustainable development concerns, currently subjected to numerous debates.

In this context, the European Union launched a climate and energy package, adopted by the European Parliament on December 2008. The package focuses on greenhouse gases emissions cuts, renewable and energy efficiency, and supports the so called *three 20 target*, which is actually composed of four objectives:

- To reduce emissions of greenhouse gases by 20% by 2020.
- To increase energy efficiency to save 20% of European Union energy consumption by 2020.
- To reach 20% of renewable energy in the total energy consumption in the EU by 2020.
- To reach 10% of biofuels in the total consumption of vehicles by 2020.

In the frame of the energy transition, the expected reduction of electrical consumption, the increase of decentralized renewable resources and the storage capacity development hope let imagine lower needs in electricity transmission. Beside, the transmission grid is often associated to centralized production due to nuclear power plants. In [Maillard, 2013], the Chairman of the RTE Management Board reviews this idea. Among his arguments, the remoteness of the renewable plants from the consumption centers, the impossibility to locally absorb large power production and the limits in storage facilities are highlighted. The German example is reminded since the country is currently experiencing a physical and economical waste due to the lack of sufficient transmission grid, which sometimes lead to restrain the renewable production. His conclusion is that no matter the choices that are kept for the

future, the transmission grid adjustment is a real challenge and must be carried out, otherwise, no possible energy transition is foreseeable.

As a part of those challenges, RTE participates to the reinforcement of a pan-European grid, and to the creation of a Supergrid over long term. Numerous European project emerged in that sense, and many Supergrid concept were born. As the DESERTEC[1] concept considers long transmission lines to link Europe to photovoltaics farms producing bulk power in Africa, other grids meshing the North Sea (see Fig.1) were investigated.

Figure 1: Meshed grid example, http://www.greenunivers.com

Supergrids appears as a complementary and required solution to the market mechanisms that already exist to support the integration of renewable resources. By reinforcing interconnections between all European countries, and by reinforcing the mutualization of the electricity produced by the most efficient infrastructures, the Supergrids might reduce the total cost of energy for each participating countries, and improve the European energy independence.

In this context, the European Commission launched in 2010 the project called

[1] www.desertec.org

TWENTIES[2], which aims to sustain the integration of large scale renewable energy resources into the transmission grid. The 26 partners are mainly Transmission System Operatiors (TSO), manufacturers and universities, for a total budget of 56.8M€ (Fig.2).

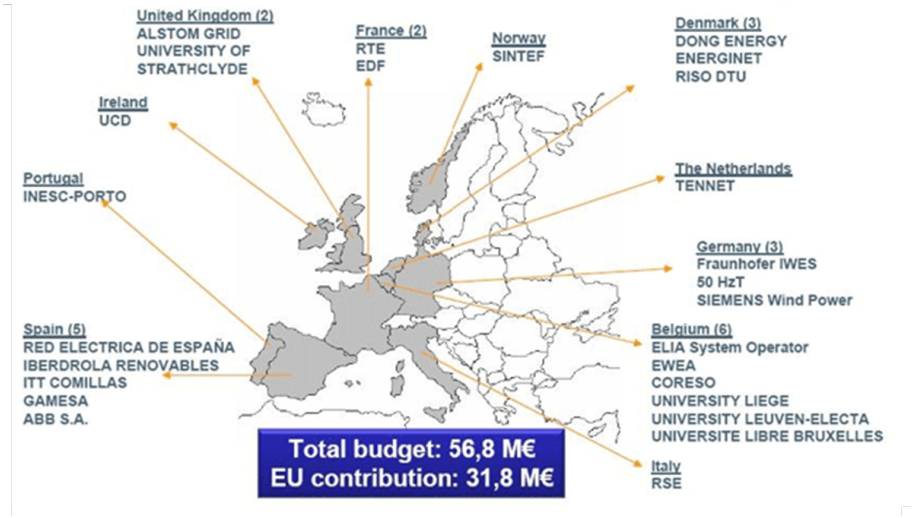

Figure 2: TWENTIES project features, source: http://www.twenties-project.eu

As a partner of the TWENTIES project, RTE is the leader of 2 Working Packages (WP.5 and WP.11), and its role is to assess the technical and economical feasibility of submarine Direct Current (DC) grids. Indeed, this transmission solution is considered to link remote offshore wind farms to the onshore Alternative Current (AC) grid. While WP.5 is more related to R&D aspects, WP.11 aims to build a demonstrator (named DEMO 3) to prove the results of the theoretical studies investigating High Voltage Direct Current (HVDC) grids.

Alternative current is worldwide used for electric power transmission, as a result of the battle between alternative and direct current, with their respective advocates Nicola Tesla and Thomas A. Edison. The battle was won by AC transmission at the end of the eighteen eighties. Electromagnetic transformers were the key to the success of AC transmission, since the DC voltage transformation was too difficult, expensive, and inefficient, the solution was given up and only found in few cities. However, recent developments of power electronics implied a renewed potential for the use of DC transmission. Thanks to the technologies improvements, many direct

[2]**T**ransmission system operation with large penetration of **W**ind and other renewable **E**lectricity sources in **N**etworks by means of innovative **T**ools and **I**ntegrated **E**nergy **S**olutions, http://www.twenties-project.eu, 7th framework program, ref 249812

current interconnection were built in several countries, where AC transmission was less effective. This is the case for long transmission line aiming to transmit bulk power, which is why the Direct Current solution was considered in the TWENTIES project. RTE investigated two main problematics, namely:

- the control of converter stations composing the considered DC grid,
- the protection of the DC grid.

Research work were thus supervised by RTE and lead to two Ph.D projects. The first one on control were conducted by Pierre Rault at the Laboratory of Electrical Engineering and Power Electronics of Lille (L2EP), and the second one on protections was conducted in Grenoble Electrical Engineering laboratory (G2Elab), and is presented in this manuscript.

This thesis, untitled "Protection plan for a Multi-Terminal and High Voltage Direct Current grid" aims thus to investigate possible protection systems for DC grid applications against short-circuit faults due to insulation breakdown or external constraints, in order to propose a complete protection plan, including a main protection and one or several backup principles in case one component fails.

In Chapter 1, the relevance of DC application is explained and the technologies composing such infrastructures are discussed. Chapter 2 goes into details in the topic by developing the fault phenomenon and reviewing the possible protection strategies that were found in the literature. Then, Chapter 3 presents the models that were used to investigate the DC grid behavior under fault conditions. The parameters influence on the signals resulting of a fault are subjected to a parametric study addressed in Chapter 4. In Chapter 5, the constraints related to DC grid protection are expressed and a complete protection plan proposal is given. Finally, the related protection system is validated and its limits are discussed in Chapter 6. The validation was performed using simulations and a low-scale physical demonstrator (TWENTIES DEMO 3), implemented in the L2EP. This thesis will end with a conclusion providing the major points addressed by this work and a proposition of further works to ensure the development of Multi-Terminal Direct Current (MTDC) grid protection plans.

CHAPTER 1

Relevance of HVDC applications and thesis objectives

Chapter 1

Relevance of HVDC applications and thesis objectives

This chapter presents the relevance of HVDC links and the reason of their large development. Projects related to the interconnection between France and its neighbor countries are mentioned. Finally, the AC - DC conversion technologies are detailed.

1 Development of HVDC links

Alternative Current is widely used for the transmission of electrical power. Nevertheless, High Voltage Direct Current grids turn out to be more attractive and less costly for certain applications. It allows, for example, to interconnect two non-synchronous systems or with different frequencies, but above all, HVDC links characteristics became a very popular solution when they aim to transmit bulk power over long distances. Indeed, from a certain amount of power to transmit, there is a critical length beyond which AC transmission is not viable anymore. This is due to the fact that the intrinsic losses and undervoltages need to be compensated for. Even though it is possible to use voltage standing up station for overhead lines, the capacitive effect inherent to AC transmission based on underground or undersea cables is too large, leading the DC solution to be less expansive and more efficient [Valenza and Cipollini, 1995]. The cost of AC - DC converters is compensated by the gain of active power that can be transmitted. Fig.1.1 justifies the DC choice, by illustrating the transmitting power capacity for several link cases, as a function

of the link length and for several voltage levels.

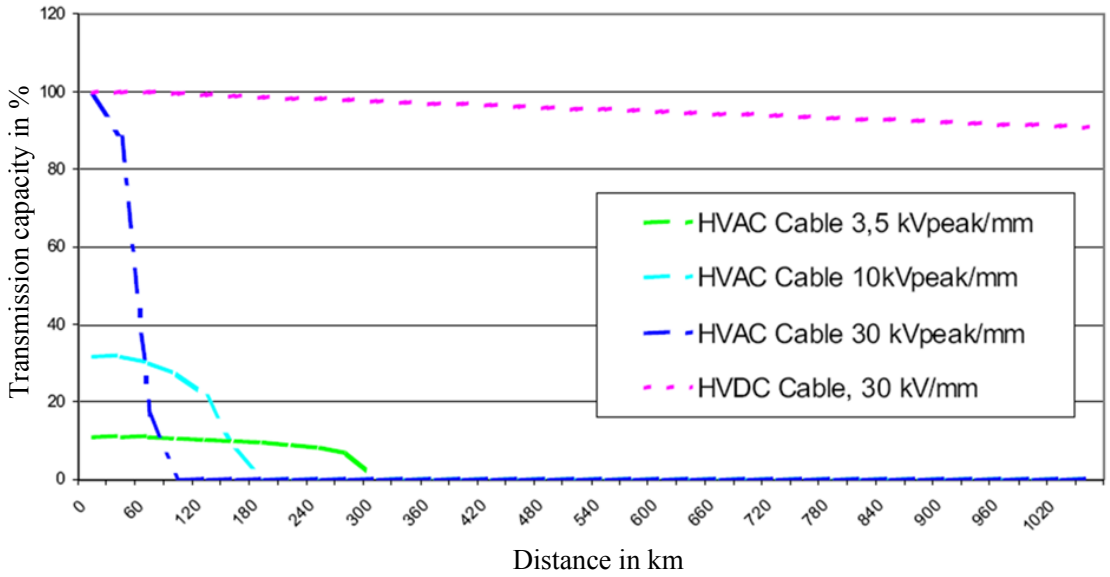

Figure 1.1: Transmission capacity of HVAC and HVDC links, [Asplund, 2004]

Consequently, HVDC links are under a wide development phase, especially for application related to offshore grids, either for countries interconnection or for offshore wind farms connection. Nonetheless, those links require very complex power electronics systems to ensure the AC - DC conversion at each connection point with AC grid or source, which are extremely costly. HVDC links based on Voltage Source Converters (VSC) are the most interesting, particularly because those converters permit the control of the active and reactive power independently, and also to reverse the power flow very quickly [Guo and Zhao, 2009]. By this way, the VSC can be controlled in the four quadrants and so to feed or to absorb active and reactive power. This converter type offers the possibility to connect several converter stations in order to create a true DC grid, that can have several structures (meshed, looped, ...). Those so called Multi-Terminal High Voltage DC grids (MT-HVDC or MTDC) are not developed yet, and the technical barriers are still under investigation in several institutions.

While the research on the control of the VSC is still ongoing in several institutions (KU Leuven - Belgium, École Centrale de Lille - France, ...), this thesis focuses on the protection of MTDC grid in case of a fault event, resulting of insulation breakdown or external constraints. Even though the detection of a fault in

the DC zone can be performed by several existing methods, the identification of the faulty element is still unknown.

2 General operation of HVDC links

HVDC links consist in converting the energy produced in the form of alternative current in direct current or voltage thanks to AC - DC converter stations, to transmit the power to another station which will convert it back in alternative form. This would replace a three phase AC link, considering the bulk power to transmit. Apart from facilitating the operation thanks to the absence of reactive power and the flexibility of the control of the power electronics devices, HVDC links can eventually reduce the cost in the way that two conductors (even only one in some cases) are required instead of three in the alternative solution. Fig.1.2 explains the operating principle.

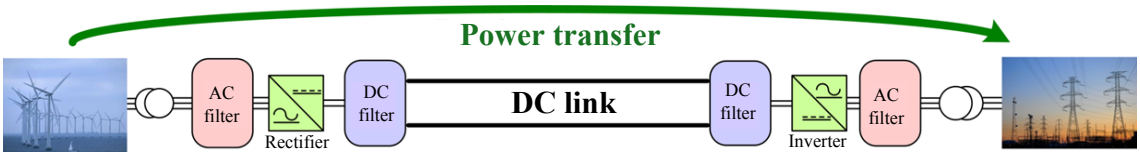

Figure 1.2: HVDC link scheme

Aspects related to converters will be developed in the next section. Filters enables to smooth the current and to maintain the DC voltage to a constant value, and to compensate for the harmonics in the AC side currents.

The transformers need to be sized in order to support high variations of current that can occur in the DC zone, and has to correspond to a large short-circuit impedance so that they limit the impact on the AC grid. The DC link can be made up with overhead lines, underground or undersea cables, and several topologies can be found.

Most common structures are presented in [Sabonnadière and Hadjsaïd, 2007] and are summarized below.

2.1 Possible HVDC link structures

a) $+U$ Link with ground or sea return

The advantage of this technology is that it uses only one monopolar link, which is less costly. The current return path is the ground or the sea.

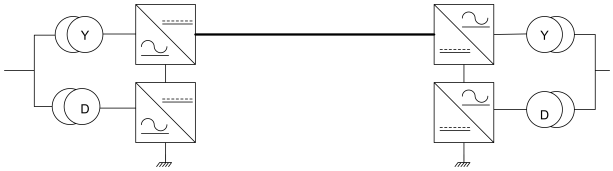

Figure 1.3: $+U$ monopolar link scheme with ground return

b) $\pm U$ link with grounded middle point

When the return current cannot be done by ground or sea, which is usually the case, especially for submarine links due to the magnetic field that can create perturbations prohibited by navigating instrumentation of boats, the return is made in a cable of opposite polarity.

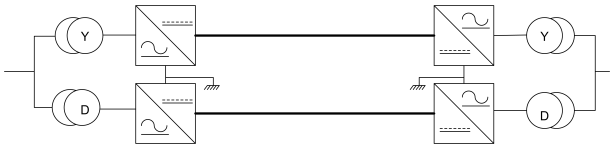

Figure 1.4: $\pm U$ bipolar link scheme with grounded middle point

c) $\pm U$ bipolar link with monopolar operation possibility

For this kind of structure, electrodes are remote to the station in order to constitute a preferred return current path by ground, in case a monopolar operation is required. This would be the case for example when there is a problem in one cable.

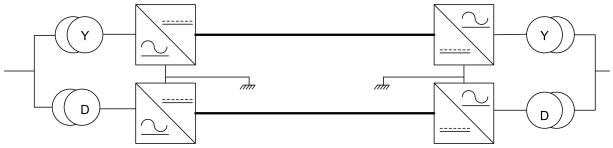

Figure 1.5: $\pm U$ bipolar link scheme with monopolar operation possibility

d) $\pm U$ bipolar link with neutral conductor for monopolar operation

This topology is employed in order to have a high reliability. Indeed, the neutral conductor presence enables to operate the system as a monopolar link, with an identical current but a voltage of only one polarity, so corresponding to a power transfer of the half of the nominal value.

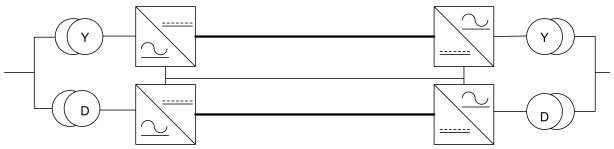

Figure 1.6: $\pm U$ bipolar HVDC link with neutral conductor

e) $+U_1, -U_2$ link

For application with very high voltage ratings, and hence with large voltage drops, this kind of structure is often employed. U_2, with negative polarity, is the highest voltage. Indeed, the dielectric constraints are easier to withstand when the voltage polarity is negative.

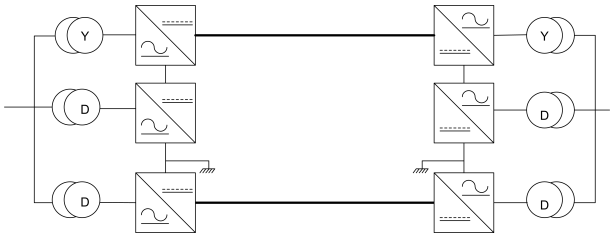

Figure 1.7: $+U_1, -U_2$ HVDC link

f) Back-to-back links

Those links are widely used to connect non-synchronous grids, or grids operating at different frequencies. The cables are extremely short (in the range of one meter), since the aim is only to connect two grids with different characteristics and not to transmit power over long distances.

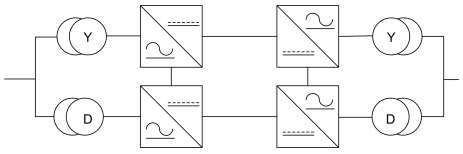

Figure 1.8: Back-to-back HVDC link scheme

2.2 HVDC links currently under operation in Europe and planed installations

Worldwide, many HVDC links were developed. The offshore links currently under operation are shown in red on Fig.1.9. They are mainly point-to-point interconnections between countries (only one link between two terminals). For the France case, the most famous one is the Cross-Channel link (now IFA2000, standing for *Interconnection France Angleterre 2000MW*).

France and United Kingdom were first linked in 1961, thanks to a link called IFA160 (standing for 160MW). However, the system was too weak because the cables, that were wired at the sea floor, were often caught by trawler boats [RTE, 2006].

This is why the two counties decided, in 1974, to build a new link in which the cables are wired in submarine trenches. The objective was an availability up than 95%. The rated power was improved to 2000MW, and the main features of the link are displayed in Tab.1.1. The link is based on Line Commutated Converters (LCC). This converter technology, also called natural commutation converter, uses thyristors.

Characteristic	Value
Voltage	±270kV
Active power	2000MW
Distance	78km
Conductor	4 DC cables pairs
Wiring	Trenches, 1.5 meter under sea floor
Converter	LCC

Table 1.1: IFA2000 main features, [TechnoScience, 2012]

Other HVDC links were developed and others are currently planed, as shown on Fig.1.9 for the North Sea area.

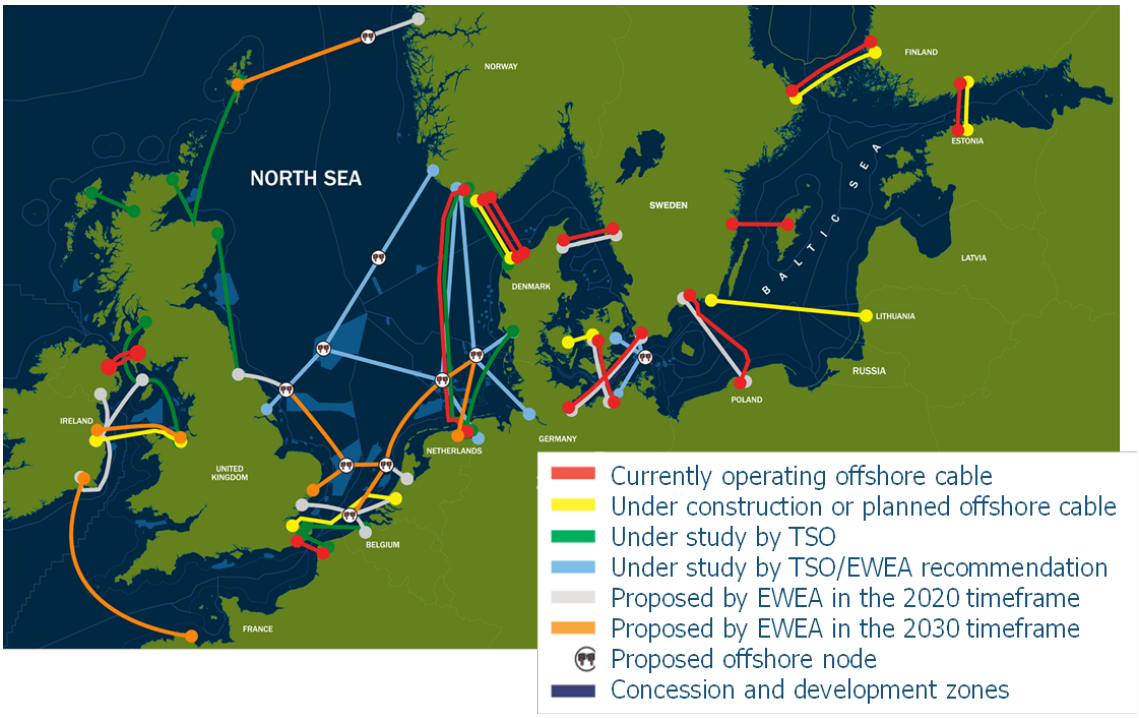

Figure 1.9: Development of offshore wind farms in North Sea, source: http://www.greenunivers.com

Among the planned projects, some of them are linking multiple terminals (more than two), and are no longer point-to-point links but Multi-Terminal grids. Those grids cannot be based on LCC technology. Indeed, for LCC technologies, the power flow reverse is done by inverting the voltage polarity. It is thus impossible to build MTDC grids because they would operate at a constant voltage polarity, which leads to the development of a new converter type, namely Voltage Source Converter. This solution is detailed in the next section.

3 New conversion technologies

Voltage Source Converters uses transistors instead of thyristors. The Insulated Gate Bipolar Transistors (IGBT) which compose the VSC can be controlled to be blocked or conducting. A large number of IGBT are connected in series in each arm. They are controlled to change their state simultaneously, with an accuracy close to the microsecond [Nee and Angquist, 2010a]. The output voltage is built thanks to

the Pulse Width Modulation (PWM) technique.

The main advantage of VSC is that as mentioned earlier, they enables a simultaneous control of the active and reactive power exchanged between the converter and the grid connected to it.

Besides, the power flow direction change does not require the voltage polarity reversal, which is the case for LCC converters. VSC are hence appropriate for Multi-Terminal DC grids since the voltage polarity can now be maintained constant. The main differences between LCC and VSC are given in Tab.1.2.

LCC	**VSC**
Thyristors	Transistors
Unidirectional current	Constant voltage polarity
Consume reactive power	Produce or consume reactive power
Low frequency harmonics generation (requires large filters)	High frequency harmonics generation (easily filtered)

Table 1.2: LCC and VSC comparison, [Vissouvanadin Soubaretty, 2011]

Most conventional technologies are composed of two or three levels, as illustrated on Fig.1.10 and Fig.1.11.

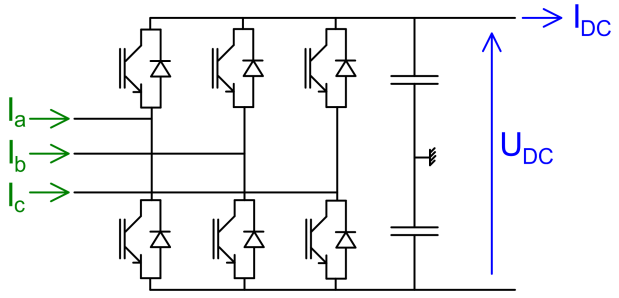

Figure 1.10: 2-level converter

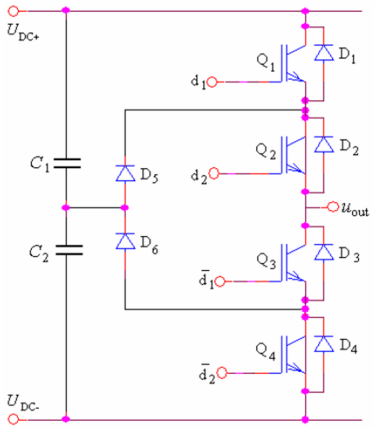

Figure 1.11: 3-level converter, [Ikonen et al., 2005]

However, new structures are springing up, called Multi-Modular Converters (MMC) or multi-level converters. The circuit is thus composed of sub-modules that are constituted by a DC capacitor and a half-bridge, as shown on Fig.1.12. Each arm contains series connections of these sub-modules, as illustrated on Fig.1.13. The half-bridge enables to insert or to bypass the DC capacitor in the sub-module chain connected in series. The control system maintains the mean number of sub-modules connected in series in the two arms at a constant value, in order to balance the DC voltage. The desired terminal voltage is built thanks to the variation in the difference between the number of sub-modules inserted in the superior and inferior arms.

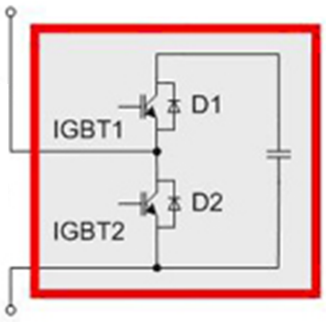

Figure 1.12: Half-bridge sub-module scheme, [http://www.energy.siemens.com,]

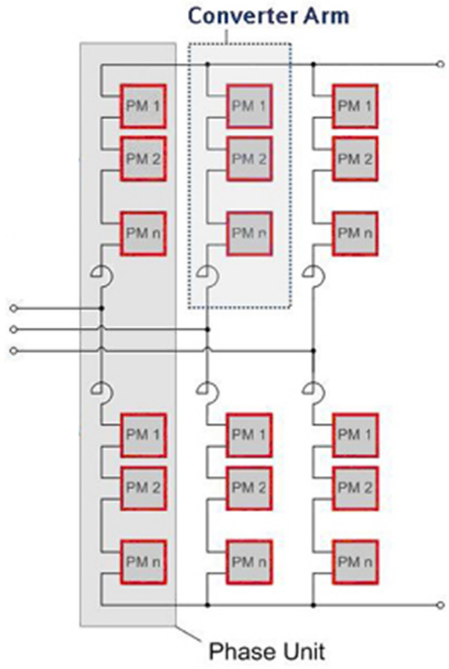

Figure 1.13: MMC converter scheme, [http://www.energy.siemens.com,]

For a multi-level application, each output wave step results in the operation of only one sub-module in each arm. The averaged commutation frequency by semiconductor can be significantly reduced compared to 2 or 3-level technologies. Also, the harmonic content of the produced wave is very small, which reduces the required filter size.

Those technology are relatively new. Variants exist depending on the manufacturers, and are known as M2C for Siemens and CTL (Cascaded Two Level converter) for ABB. Alstom Grid proposes a M2C variant where the half-bridges are replaced by full-bridges. This topology offers the possibility to reverse the DC voltage polarity, allowing the connection of a VSC to a LCC. They also permit the blocking of the current coming from the DC side, which might be particularly useful in case of DC fault event. Nevertheless, a full-bridge converter would lead to an extremely voluminous and very expensive device. The fault management method will still be shortly discussed in Chapter 2.

M2C by Siemens is the conversion technology that were chosen for the INEFLE (standing for *INterconnexion ÉLectrique France Espagne*), under development. Main

features of the INELFE link are described in Tab.1.3.

Characteristic	Value
Voltage	±320kV
Active power	2x1000MW
Distance	64km
Conductor	Underground cables
Converter	Siemens M2C
Commissioning date	2014

Table 1.3: INELFE main features, source: http://www.inelfe.eu

As any electrical system, those links are subjected to faults, that can be due to several phenomena, and must be protected in order to ensure the material and people safety. This will be developed in Chapter 2.

CHAPTER 2

Research view on MTDC grid protection

Chapter 2

Research review on MTDC grids protection

In this chapter, the behavior of the HVDC grid under fault condition is investigated. The most important features of the protection system are given, and the possible protection philosophies are detailed. The chosen one uses DC breakers, so their technologies are presented. Finally, the protection principles found in the literature are summarized, and the thesis objectives are clarified.

1 HVDC link behiavior under fault conditions

1.1 Fault phenomenon

In HVDC links, the faults that can happen are mostly line-to-ground or line-to-line. They are mainly caused by the degradation of the insulation material. For overhead lines, the insulation material is the air, and the degradation might be caused by pollution or lightning strike, arcing with vegetation, and are usually fugitive (non-permanent). At the opposite, cable faults are permanent faults since they are most often due to external mechanical constraint, or, if the insulation is deteriorated, this results also in a permanent fault since the material (XLPE, impregnated paper) is damaged for ever.

Internal converter faults can also occur, but are not considered in this thesis. Also, since underground or undersea cable are considered, only permanent faults will be assumed.

1.2 Protection system components

The protection system aims to detect the presence of an eventual fault, to identify the faulty device and then to control the breakers, whose tripping leads to the insulation of the faulty component from the rest of the grid.

A protection system is thus the arrangement of three main components:

- the sensors, that are measuring the electrical variables required for the fault detection and faulty component identification,
- the computation interfaces, including the algorithms that process the data measured by the sensors, in order to compare them to some predefined criteria,
- the breakers, that enable the opening of the circuit and hence the insulation of the faulty material.

In real applications, the protection system usually consists of the association of several elements for the protection of a considered system. By this way, in the case of the failure of the main protection system, one or several backup principles enable the fault detection and clearance. Several protective zones are considered, each one protected by a protection system. They must cover the whole grid. Therefore, the transmission cables, the converters, the busbars, the filters, and all the other elements are protected by several systems. On this thesis, the considered protective zone is limited to the cables and the busbar. Also, AC protections will not be treated, and it is assumed that they are able to clear faults that happen in the AC grid sides.

The protection system has to be able to detect and to clear faults with variable types. The magnitude of the currents to break can largely differ. Furthermore, the protections must not limit the normal operation of the grid. Therefore, they need to remain stable during perturbations due to healthy variation in the grid structure or power flow.

One of the main difficulties resides in the identification of the faulty component. Indeed, the overcurrent generated by a short-circuit will propagate all along the grid,

implying a perturbation everywhere. The strategy has thus to be defined such that it enables the fault localization, in order to insulate only a minor part of the grid, and not to shut down the whole zone. This is even more important in meshed or looped grids since the contribution to the fault comes from each sources connected to it, and all the cables composing the grid.

2 Overall behavior of a HVDC link under fault conditions

HVDC grid protection presents particular difficulties compared to traditional AC system because of the non-existence of current zero-crossing and the low line impedance, that does not limit the fault current. As a consequence, the DC current will rise much faster and interrupting the fault current is significantly more difficult in meshed DC than it is in AC networks.

The shape of a current measured during a fault even can be sketched as illustrated on Fig.2.1.

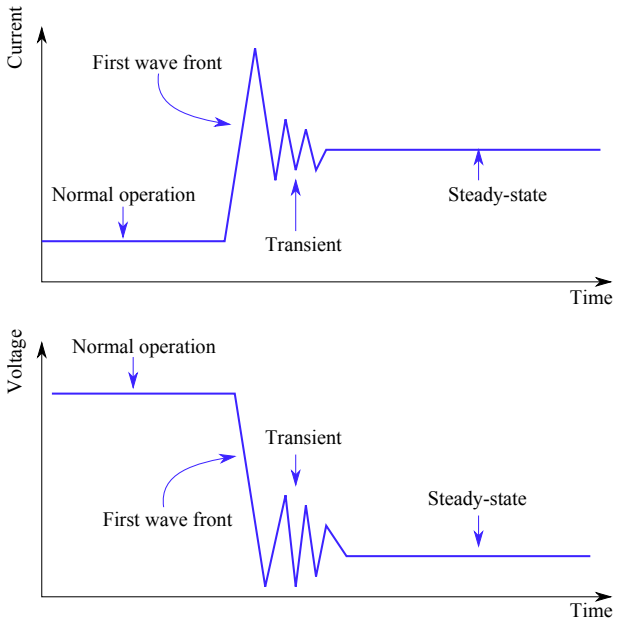

Figure 2.1: DC current and voltage behavior under fault conditions

Three main steps can be defined in those shapes:

- the first wave front,
- the transient phase,
- and the steady-state.

The first current wave front is due to the cables capacitor discharge, and can reach very large value (in the range of 50 kiloAmps). The transient that follows corresponds to the propagation of the perturbation generated by the fault in the whole grid. Finally, the signals stabilize in a steady-state, which corresponds to the AC side contributions. The MTDC grid components, and especially the converters, cannot withstand those large current values, which restricts the protection system to operate in a very small time (in the range of 5ms). This notion will be detailed in Chapter 5, but this time range needs to be kept in mind. Indeed, this implies that the protections cannot wait for the steady-state, since this one occurs several tens of milliseconds after the fault. Furthermore, note that today, the fastest AC mechanical breakers open in 40ms, and re-close in about 100 - 120ms. This later fact adds another constraint related to the DC current breaking speed of the breakers.

2.1 Traveling wave propagation

A fault occurring on a cable generates current and voltage waves, which are propagating along the cable until they reach a discontinuity, such as the fault point itself, a source, or a busbar. At this location, a reflected wave and a refracted wave appear, which propagate as well. This phenomenon is illustrated on Fig.2.2 by the Bewley-Lattice diagram [Datta and Chatterjee, 2012].

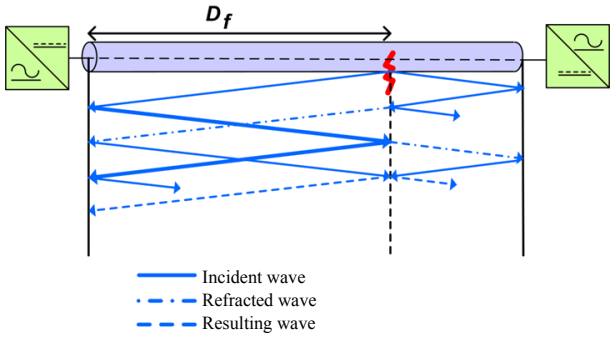

Figure 2.2: Bewley Lattice diagram

These reflections are visible on the current and voltage measurements.

2.2 MTDC grid protection difficulties

The fact that the low cable reactance does not limit the fault current leads to another difficulty for MTDC grids. Indeed, there is only a very small difference between the measurements of two different points, one located on the faulty area and the other one in a healthy part. This get the identification of the faulty device even harder. This phenomenon is developed in Chapter 5.

The protection strategy will be discussed in this current chapter.

3 Possible protection strategies

Several philosophies [Tang, 2003] can be possible for the DC grid protection system, and are summarized in this section.

3.1 Philosophy 1: Without recourse of DC breakers

The first philosophy avoids the problem of the DC current breaking due to the non-zero crossing. It is illustrated on Fig.2.3 for a MTDC grid example. No DC breakers are placed on the DC grid, but disconnectors are located at each cable end, and AC breakers are connected to each VSC on the AC side.

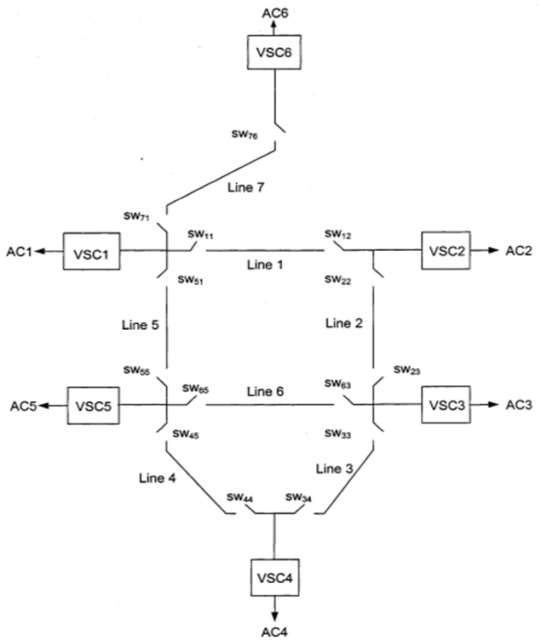

Figure 2.3: Protection philosophy without recourse to DC breakers, [Tang, 2003]

In this case, when a fault is detected in the DC grid zone, every AC breaker connected to the VSC composing the DC grid trips. Then, the disconnectors surrounding the faulty cable are opened, which is possible since no current is flowing anymore through the DC grid. The AC breakers are then closed, and the DC grid restores its operation.

The advantage of this philosophy is that there is no need of DC breakers. However, it supposes the total shut down of the DC grid, and even though this is done only for few milliseconds, it would lead to an interruption of the power transfer. It is highly probable that such a blackout of the DC grid would be prohibited by the concerned TSO. Besides, this philosophy does not avoid the transient current due to the cable capacitor discharge of the cables, that are destructive for the converters. Nonetheless, this transient would not happen for overhead lines.

3.2 Philosophy 2: With moderated recourse of DC breakers

This philosophy uses a moderated amount of DC breakers, at each VSC connection point in the DC grid, as it is illustrated on Fig.2.4 for the same MTDC grid example. Disconnectors are once again located at each cable end.

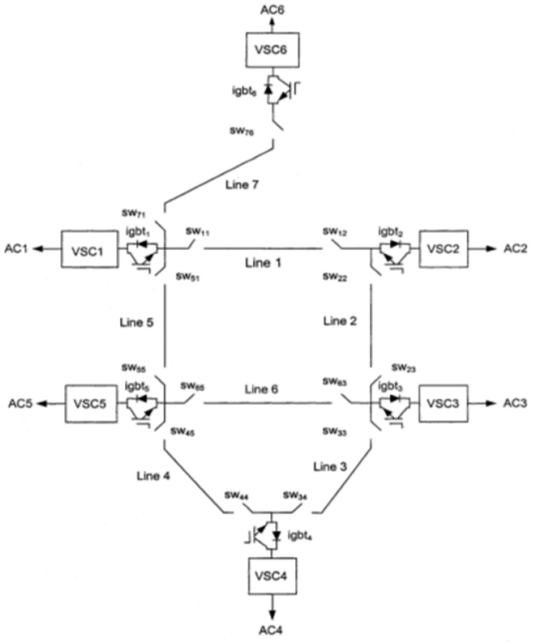

Figure 2.4: Protection philosophy with moderated recourse to DC breakers, [Tang, 2003]

The process is similar to the previous philosophy. If a DC fault is detected, the entire DC grid is shut down, but this time by the DC breakers. The advantage is that it keeps the components of the VSC charged. The next steps are the same as for philosophy 1, meaning that the disconnectors surrounding the faulty element are opened and then the DC breakers re-closed. Once again, it supposes a blackout of the DC grid, which makes this solution not viable. The operation recovery would however happen quicker than for philosophy 1.

3.3 Philosophy 3: With full use of DC breakers

This philosophy is similar to the one used for AC grid protection. A DC breaker is located at each cable end and at each station connection point (Fig.2.5). In case of a fault event, only the breakers surrounding the faulty element are opened.

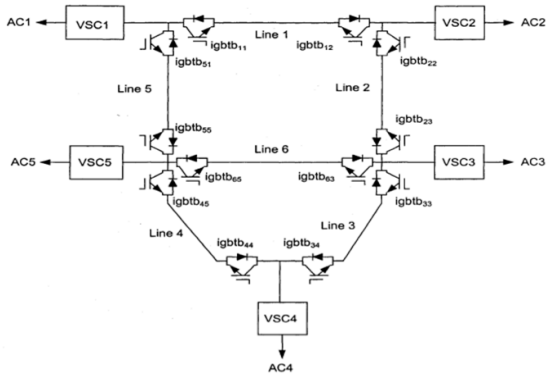

Figure 2.5: Protection philosophy with full recourse to DC breakers,[Tang, 2003]

This principle does not imply a shutting down of the whole DC grid, which can remains in operation at a N-1 level. This strategy has been chosen in this thesis, since this one is already in use in AC application and already proved its worth in real operation.

Before discussing the algorithms required for the control the DC breakers, and that were found in the literature, the DC breaker technologies are presented in the next section.

4 Current breaking technology

Special attention needs to be paid on the breakers, since they are the components that are responsible for the fault clearance once the tripping order is sent. In fault conditions, the contact separation where flows a short-circuit current cannot be performed instantaneously. Indeed, the area located between the two ends that aimed to be separated, but initially connected one to another, becomes ionized and hence is conducting [Vacquié, 1986]. This results in an arc, which implies the dissipation of the energy in a certain time, and avoids severe overvoltages that would happen in the case of an instantaneous dissipation, not withstandable for the grid. Nevertheless, it is easier to interrupt a lower power arc. This is why in AC grids the tripping is done when the current is at a zero-crossing instant, which occurs each half-period.

A technological lock is hence inherent to the DC case, since their is no zero-crossing in the current shape, at least naturally. This results in a high quantity of energy to dissipate, which corresponds to the electromagnetic energy stored in the proper inductance of the circuit, equivalent to $\frac{1}{2}LI^2$ [Pelenc, 2002]. Available breakers used for AC applications are thus non-adapted to break DC currents.

During current breaking process, once the contact is separated, the voltage at the initial contact terminals is re-established, and increases in a transient way. The rising speed of this Transient Recovery Voltage (TRV) can take very high values. If the electrical field did not recover its dielectric rigidity, this high voltage can lead to another arcing phenomenon, which would lead to a breaking failure [Schoenemann et al., 2004].

4.1 Electrical arc phenomenon

Electrical arcs can occur for many reasons. For example, in transmission lines, an arc is created when the voltage overpasses the breakdown voltage. The breakdown voltage depends on the distance between the electrodes and the dielectric rigidity of the field. The temperature, the pressure and the hydrometry are influencing factors [Andrea et al., 2010b]. If the source does not limit the current, this one is irreversible. Arcs can also appear in breakers when two conductors initially conducting

a current are separated. The arc is extinguished when the current is reduced to zero and when the field recovers its dielectric rigidity [Vacquié, 1986].

4.2 Research state on DC breaker

Breakers are manufactured such that the arc time constant (noted Θ, which is defined in [Andrea et al., 2010b]) is as low as possible. By this way, mechanical breakers using gases such as SF6 or vacuum were developed in order to improve their breaking capability.

Several kinds of breakers were developed for DC application purposes. Some of the methods consist in combining the mechanical breakers used in AC systems with other elements able to break large DC currents. Other methods are based on power electronics. This section summarizes those techniques.

4.2.1 Mechanical breakers

Mechanical breakers used in AC applications are not sized to break large DC currents, because of the huge energy that need to be dissipated. To enable such a breaking process, they can be combined with other elements that would create an artificial current zero-crossing.

Two methods exist to force the DC current to cross zero at the breaker level. The first one consist of the addition of a branch in parallel of the breaker. The created commutation can thus be either passive or active. The second way is to use a pyrotechnic method.

a) Passive commutation process

In this case, the current zero-crossing is obtained thanks to the superposition of two currents: the fault current, that needs to be extinguished, and the current coming from another branch, added to that purpose. This second branch is composed of an inductor L and a capacitor C in series, as illustrated on Fig.2.6.

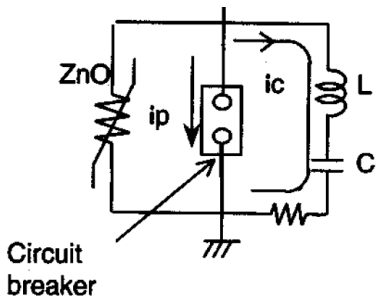

Figure 2.6: Passive commutation principle, [Nakao et al., 2001]

When a fault is detected, the switch is open which creates an arc. As explained in subsection 4.1, the voltage gradient of the arc tends to decrease when the current increases. This phenomenon leads to the self-excitation of the loop $L-C$, that results in current oscillations which, if the frequency of the oscillating circuit is properly set regarding the arc characteristics, will enables the current to oscillate at high frequencies with a increasing magnitude [Nakao et al., 2001]. This phenomenon will hence create a current zero-crossing point. During this zero-crossing phase, the current is really broken, and the varistor element Z_nO deletes the overvoltages that follow this interruption. A similar principle proposed in [Meyer et al., 2005] is to use thyristors in the parallel branch instead.

b) Active commutation process

This kind of technology is sketched on Fig.2.7.

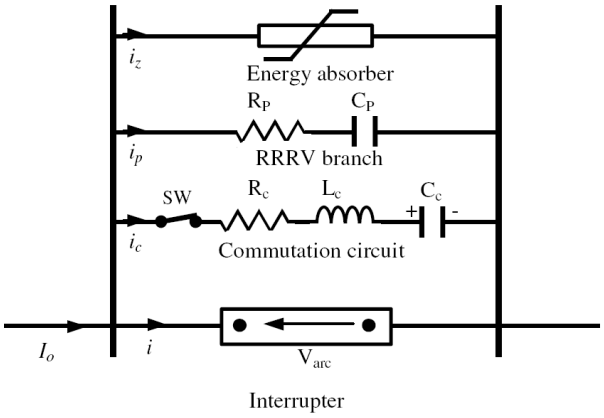

Figure 2.7: Active commutation principle, [Darwish et al., 2006]

Here, pre-charged capacitor and inductor in series are connected to the mechanical switch. During the opening of this mechanical switch, the auxiliary switch SW is closed, leading the capacitor to discharge. This creates an oscillating current,

superposed to the DC current, implying a zero-crossing [Darwish et al., 2006].

When the arc is totally shut down, the DC current does not flow through the main branch but through the commutation branch, and keeps the same value, which can lead to a large overcurrent and the re-arcing process. In order to limit the rising speed of the TRV, a $R-C$ branch (RRRV branch) is connected to the breaker, which allows the control of the TRV rate of rise during the period preceding the zero-crossing. The varistor is connected in parallel in order to limit the TRV magnitude. The energy stored in the DC system is dissipated through this non-linear element.

c) Pyrotechnic method

In [Jadidian, 2009], Jadidian suggests to use high power pulsed generators based on explosives to break huge current on HVDC links. The proposed method consist of the coupling of a vacuum mechanical breaker and two other devices:

- Magneto-cumulative generators (HFCG: Helical Flux Compression Generator) to create an inverse current which enables to delete the DC current,

- An intense Axial Magnetic Field (AMF), fed by a second HFCG, to control the arc generated by the opening of the breaker.

The principle has the advantage of being less voluminous than the previous method (based on a pre-charged capacitor). Also, it is less costly and its withstand capability does not depend on the shape of the current to break but on the HFCG's properties.

4.2.2 Power-electronic breakers

These devices are based on semi-conductor and varistors only, as shown on Fig.2.8. During normal operation, the current flows through the semi-conductors. When a fault is detected, they block the current and the voltage increases very fast, until the varistor becomes conducting. The varistor is sized to limit the voltage to a certain value, higher than the grid voltage value, enabling the demagnetization of the line inductance and the real current extinction [Meyer et al., 2005].

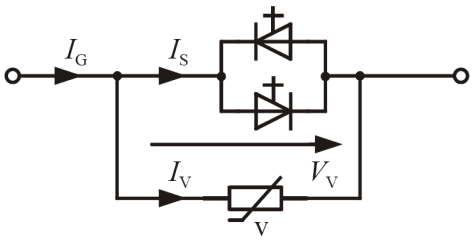

Figure 2.8: Semi-conductor based breaker, [Meyer et al., 2005]

Compared to all other technologies presented previously, this solution offers the best performances, since no mechanical part is considered and since no parallel connection is required. Therefore, the current clearing process is very fast and hence the maximal current is reduced significantly. Besides, it is the less costly device. Nevertheless, the main disadvantage is the on-state losses inherent of the power electronics, since the current flows through the thyristors during normal operation. This is why a new technology is considered, namely hybrid DC breakers.

4.3 Hybrid breakers

Traditional hybrid breakers are composed of a classic mechanical system and a semi-conductor based breaking device, as illustrated on Fig.2.9. When a fault is detected, the switch S related to the mechanical part opens and the current is transferred to the semi-conductor branch. Consequently, the mechanical part can extinguish the arc. The current flows through the semi-conductor branch until the dielectric rigidity in the mechanical breaker recovers. At this time, the semi-conductors block the current, and the same process as explained previously is performed thanks to the varistors. The voltage is limited once again at a level higher than the grid voltage to demagnetized the system.

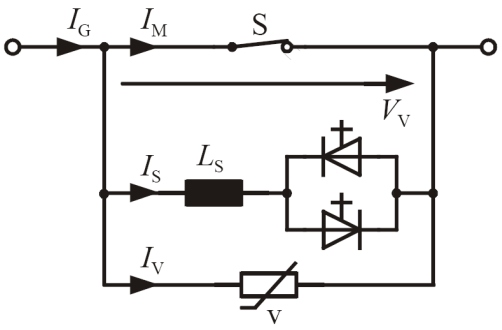

Figure 2.9: Conventional hybrid method, [Meyer et al., 2005]

On this system again, the current is broken independently of a zero-crossing. However, the elimination time is highly dependent on the mechanical part. Even though the opening of the switch can be performed very quickly, it is required to wait for the complete de-ionization of the field to block the semi-conductors. Hence, during this time, the current will continue to rise significantly. Another method is proposed to deal with this problem.

The objective is to reduce the delay before the blocking of the semi-conductors, since this delay is responsible for the high current values. The idea is to avoid the arcing at the mechanical breaker level, which requires a forced commutation of the current before the opening of the mechanical circuit. The contacts can then be separated without any arc development since no current is flowing through them at this time [Meyer et al., 2005]. The device is shown on Fig.2.10.

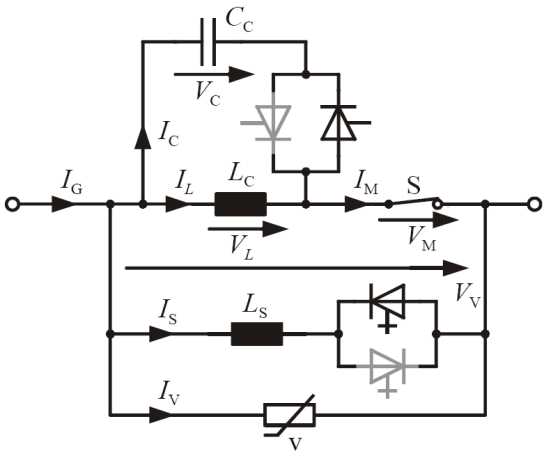

Figure 2.10: Hybrid method with forced commutation, source: [Meyer et al., 2005]

The elements that are added compared to the previous conventional breaker technology are required to force the commutation. The parallel semi-conductors are started and the circuit is demagnetized thanks to the capacitor discharge. The current flowing through the mechanical part is constant until the capacitor voltage polarity reverses, creating the commutation. The commutation time is set by the charge level of the capacitor.

Hybrid DC breakers were under investigation by main manufacturers, such as ABB and Alstom grid. They are becoming commercially available, but they still have limitations in fault current magnitude [Hafner and Jacobson, 2011].

The research is still ongoing, and as a partner of the TWENTIES project, Alstom grid made a prototype of their breakthrough. They have recourse to a clever shrewdness in the process, which cannot be communicated yet since this new technology is under patent process. The press release delivered on May, 25th 2013[1] told that the prototype was able to break currents exceeding 3kA current in less than 2.5ms.

The DC breakers can also be helped by the converters. Indeed, a full-bridge multi-level converter retains full control during faults. It can thus limit the current to break, by adapting the control methods for such events or adding new devices such as DC - DC converters [Jovcic et al., 2013]. Once again, those full-bridge technologies suffer from excessive number of switches, and thus are not considered in this thesis.

5 Review of protection principles found in anterior works

This part aims to present the protection algorithms that were investigated in the literature.

5.1 Use of DC breakers

This method is the closest to the one used for AC systems, and is based on the principle explained in section 1.2, which is reminded below:

- the sensors, that are measuring the electrical variables required for the fault detection and faulty component identification,
- the computation interfaces includes protection algorithms that process the data measured by the sensor, detect the fault and identify the DC breaker that needs to trip,
- the breakers are controlled and the chosen ones clear the fault.

The protection algorithms that were found in the literature are commented in the next part.

[1]The press release can be found on the TWENTIES website at: http://www.twenties-project.eu/node/21

5.2 Review of protection principles found in anterior works

5.2.1 Overcurrent and undervoltage protections

These are the simplest protection algorithms, and detect the overcurrent (or the undervoltage for the undervotage protection) that follows the fault occurrence. They enable the detection of high currents that are flowing in the DC link. If the measured current exceeds a set threshold, or if the measured voltage is below a set threshold, the tripping order is sent.

This principle is relevant for HVDC links, but the selectivity is limited by the low impedance of the lines in MTDC cases.

5.2.2 Differential current protection

The principle is based on the Kirchhoff law that states that the sum of the currents arriving at one node is equal to zero. Hence, the system measures the current at each cable end, and compares them. Depending on the sensors orientation, the algorithm computes the sum or the difference of the two measurements. The result is called the differential current. In the case illustrated on Fig.2.11, the differential current I_d would be defined by $I_d = I_A + I_B$. When the HVDC link is in healthy operation, this current I_d is not equal to zero, because of the losses in the cables, but remains at a very low value. Also, in case a fault occurs in the grid, this differential current stays at a low value for a healthy link, since the value of the current flowing to feed the fault are similar at both cable ends. At the opposite, for a faulty cable, the differential current takes large values, that can be detected by a set threshold [Aimin et al., 2009]. The tripping order can thus be set.

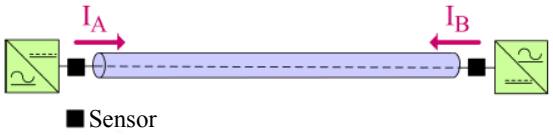

Figure 2.11: Differential current

This method is quite simple if the parameters are set properly. It offers very good selectivity since the faulty link can be discriminated easily, and does not depend on

the line impedance. However, the inconvenient is that the previous statements are valid only in steady-state, which happens too late compared to the required protection speed.

5.2.3 Current and voltage derivatives

The principle is the same than the overcurrent or undervoltage principle, but uses the derivative of the measurements instead. More recent schemes adopt principles that are based on traveling wave theory.

For those principles, the currents (or voltages) are measured, and their derivatives $\frac{dI}{dt}$ (or $\frac{dV}{dt}$) are computed, and using a threshold, the detection is done and the tripping orders are sent. A pondered sum of $\frac{dI}{dt}$ and $\frac{dV}{dt}$ can also be used in order to have a more reliable system.

This method has the advantage of using the first incident wave, which allows a quick detection [Naidoo and Ijumba, 2005]. However, as well as the overcurrent and the undervoltage protection principles, the selectivity is limited by the low cable impedance.

5.2.4 Distance protection using traveling wave propagation theory

According to traveling wave propagation theory, when a fault occurs, progressive current and voltage waves imply fast variations over the whole cable length. The waves generated by the fault contain enough information to detect and eliminate it [K. and N., 2005].

For AC applications, the magnitude of the generated waves depends on the voltage phase at the fault occurrence time. High difficulties reside in the detection of a fault that happens at a voltage zero-crossing point. Nevertheless, this problem does not exist for DC applications [Shang et al., 2001].

The waves are propagating at a speed that depends on the cable geometry and on the relative permittivity of the field where it is wired. For long overhead lines, this speed is in the range of the speed of light, but for cables, this speed is about 3 times lower [Thomas et al., 2009].

Wave front detection

The protection principle is to detect the wave front. To do so, currents and voltages are measured continuously, with a high sampling frequency (in the range of tens of kHz). The difference between two samples is computed, and if it exceeds a set threshold, then a series of measured is stated in order to determine if the wave magnitude is high enough in a predefined time interval [Naidoo and Ijumba, 2004]. If all the measures are higher than the set thresholds, then the fault is detected. Those measurements may vary depending on the methods, but are generally based on differences between currents or voltages on different time intervals, as illustrated on Fig.2.12.

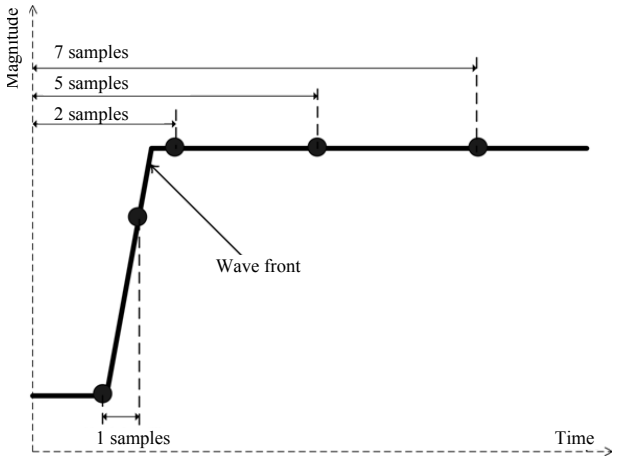

Figure 2.12: Examples of samples

This algorithm is robust since the current and voltage both contribute to the fault detection. However, for long links, the magnitude of the waves is largely damped so the detection becomes much harder to perform.

Several methods proposed to improve the reliability of this principle, and are generally based on wavelet transform. Numerous studies were found on this aspect: [Naidoo and Ijumba, 2005], [Liu et al., 2007], [You et al., 2009], [Gang et al., 2005], [Zhen-Qiang and Lv, 2008], [Liu et al., 2009]. The wavelet transform and its applications are well explained in [Mallat, 2008].

Its advantage is that it allows to detect very precisely the first wave front, and enables to detect a certain shape that can be predefined [Borghetti et al., 2008].

However, the wavelet transforms are very complex signal processing methods, so the methods require a large computation time which is prohibited for DC protection purposes. Furthermore, it assumes a very accurate knowledge of the grid structure and parameters, which makes the real application of those principles questionable. Nevertheless, the idea was investigated for a backup protection application, and is summarized in Appendix A2.

6 Thesis objectives

The thesis objective is to implement and test a complete protection system for MTDC grids. As the DC breakers, able to clear high DC currents, are investigated by Alstom grid as a partner of the Twenties European project, this present work focuses only on the protection algorithms, and not on the breaking technology. To ensure the selectivity using the philosophy chosen in section 1, a protection relay needs to be installed at each end of cable, on each pole, and on both sides of the busbars composing the DC grid. Each protection relay is associated with a DC circuit breaker, sensors and a relay.

To assess the possible algorithms, the precise behavior of the MTDC grid in fault conditions has to be investigated first, in order to deal with very accurate signals. To do so, a DC grid model needs to be implemented, since no MTDC grid exists so no real records can be used. The aim of Chapter 3 is to present the models that were used.

Then, based on the chosen philosophy of the protection plan, and on the principles found in the literature, a protection system proposal will be addressed in Chapter 5.

CHAPTER 3

MTDC NETWORK COMPONENTS AND GRID TEST MODELING

Chapter 3

MTDC network components and grid test modeling

To study the protection of DC grids, the transients following a fault occurrence have to be investigated. As no real application records of such transients were available, simulation studies were considered, and the development of a real mock-up has been conducted (the mock-up configuration and its results will be described in Chapter 6).

Several software can perform this task, such as PSCAD, MATLAB - SIMPOWERSYSTEM. Those softwares provide a lot of features, as well as the powerful tool EMTP-rv. This later one can perform either time-domain and frequency-domain simulations, and is often used worldwide by TSO for transient studies. The simulation software was chosen in order to simulate fault transients as accurately as possible. For such transients, cables behavior are a key components. Thus, EMTP-rv was chosen by RTE as its library provides the most complex cable models.

This chapter presents the models that were used for each components of the grid, namely the conducting cables, the AC grid and the substations, the fault and the protection relays components, excluding the protection algorithms, since they will be investigated in Chapter 5.

Topology (mentioned in Chapter 1) $\pm U$ link with grounded middle point is considered, and were chosen by RTE for both L2EP and G2Elab researches on the

control and protection topics.

1 Conducting cables

Transmission cables are one of the most important components in a HVDC model, especially when the aim is the study of fault transients, since cables have a huge impact on the fault signal transients and traveling wave propagation phenomenon. A precise cable modeling is therefore absolutely necessary to observe signals as close as possible to reality.

1.1 Cable composition

Power cables, and particularly the submarine ones, have to keep up hard pressure when they are in deep water. They are subject to a certain amount of threat, both human (drifted anchors, fishing machines, ...) and marine vegetation related [Nexans, 2013].

This section will be limited to coaxial cables, which can be applied generally.

A cable is built of several layers [PAYS, 2013b], as illustrated on Fig.3.1.

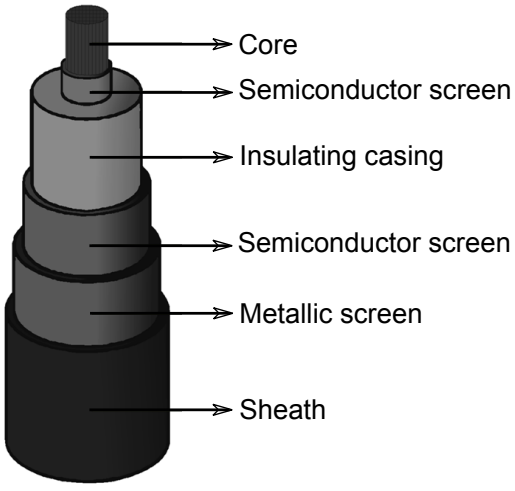

Figure 3.1: Cable layers arrangement example

The layers that are part of a cable can vary depending on its conditions of use. The most often used layers will be presented below.

The conducting core can be made up of copper, aluminum or aluminum alloy. It can be solid or cabled rounded. In submarine links applications, the cable is subjected to major stresses (in particular due to the water mass) whose core can support up to 60 % of the overall stresses applied to the cable [PAYS, 2013a]. Its maximal elongation under traction as well as its mechanical withstand capability at the junction-level are important factors to consider.

The electrical properties of the material that composes the insulating casing goes with the cable use. Impregnated and pre-impregnated papers are favored for submarine HVDC links [PAYS, 2013a]. Indeed, impregnated paper insulation sustains voltage polarity reversal. However, the VSC conversion technology does not require the voltage polarity reversal to inverse the power flow. Thus, polyethylene can be used instead [Nee and Angquist, 2010b].

Then, screens composed by conducting materials are placed on the core and on the external part of the insulating casing in order to ensure the internal magnetic field repartition of the cable, to block external electrostatic fields and to discharge capacitive currents. Furthermore, the grounding mode of the screen can lead to different phenomena and hence have an effect on the core dimensioning and operation conditions.

The sheath is the easiest protection. It is traditionally made up of lead for very high voltage cables. A polyethylene sheath could also be added as a protection against corrosion in case of a sea current return. It guarantees the waterproof property and serves as a shock absorber.

Finally, the role of the armor is to support stresses that are transmitted to the cable during its wiring, and to ensure the external mechanical protection. It is in most cases constituted by galvanized steel threads, and can have several structures (single threads layer or double, crossed or not).

Cables are thus characterized by their geometry and by the material properties they are made up of (permeability, permittivity, ...).

1.2 Line theory reminder

A transmission line always includes two routes. A line is most likely constituted by a pair of threads (parallel or coiled) or by a coaxial cable. The electrical signal propagates along the line from the source to the load, and goes back. If there is only one cable, then the return path is the ground.

The electrical behavior of a portion of a line, which is Δx long, can be expressed by the differential elements as displayed on Fig. 3.2.

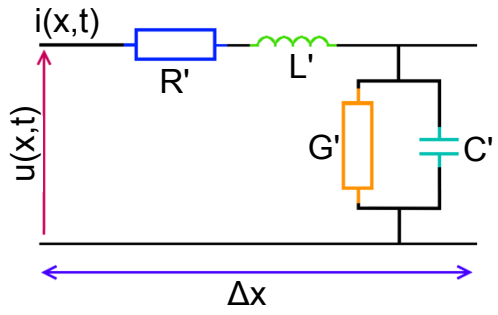

Figure 3.2: Line portion

Variables R', L', C' and G' represent respectively the per-unit length resistance of the line, the per-unit length inductance, the per-unit length capacity and the per-unit length shunt capacitance. Δx is the length of the line, and $\frac{\Delta u}{\Delta x}$ and $\frac{\Delta i}{\Delta x}$ the relative variations of voltage and current along the line.

In this representation, the series resistance R', in Ω/m, describes the ohmic losses of the conductor. It is proportional to the length, in this way $R'\Delta x$ expresses the longitudinal losses of the portion of the line.

At low frequencies, this resistance can be written by (3.1):

$$R' = \frac{4}{\pi\sigma d^2} \tag{3.1}$$

where σ is the conductivity (in S/m) and d the conductor diameter.

Formula (3.1) is no longer valid for high frequencies, because of the skin effect which decreases the section crossed by the current and like this, increases the

resistance. Thus, for frequencies higher than 100kHz, the formula becomes :

$$R' = \sqrt{\frac{\mu_0 \mu_r}{\pi \sigma}} \frac{\sqrt{f}}{dl} \tag{3.2}$$

where μ_0 is the vacuum permeability, μ_r the metal relative permeability, f the frequency and l the line length.

The currents flowing through the line lead to a magnetic flux which is represented by a series inductance $L'\Delta x$. This inductance varies depending on the structure of the line, and is defined by (3.4) in the case of a coaxial line.

$$L' = \frac{\mu_0 \mu_r}{2\pi} ln \frac{D}{d} \tag{3.3}$$

where D is the external diameter.

The parameters R' and L' vary with the frequency, and especially when the current returns from the earth. Indeed, the earth impedance is strongly frequency dependent [Dommel and Meyer, 1974]. In this way, the parameters R' and L' of the cable composing a DC link will not have the same value depending on the system is in steady state (DC, meaning frequency zero or very low frequency) or in fault conditions (where other frequencies appear).

Then, the two face to face conductors separated by an insulating material behave like a capacitor whose capacity value is proportional to the area of the face to face electrodes. This fact introduces the per unit length capacity C' (in F/m). In case of a coaxial line, this capacity is equal to:

$$C' = \frac{2\pi \epsilon_0 \epsilon_r}{ln\left(\frac{D}{d}\right)} \tag{3.4}$$

where ϵ_0 is the vacuum permittivity and ϵ_r the metal relative permittivity.

The losses between the two threads are proportional to the length and are modeled by the per unit length shunt conductance G' (in S/m). For cable applications, they depend on the losses angle of the insulating material which takes part in the losses factor of the dielectric field. Those notions are detailed in [NEY, 2013].

Now, the behavior of a line can be expressed by the simultaneous equations (3.5,3.6):

$$v(x) - v(x + \Delta x) = (R' + jL'\omega)\, i\Delta x \tag{3.5}$$

$$i(x) - i(x + \Delta x) = (G' + jC'\omega)\, v\Delta x \tag{3.6}$$

where v and i are respectively the voltage and the current, j is the complex number such that $j^2 = -1$, and $\omega = 2\pi f$.

The well-known Telegrapher's equation 3.7 is obtained by derivation of the system (3.5,3.6).

$$\frac{d^2v}{dx^2} = (R' + jL'\omega)\,(G' + jC'\omega)\, v \tag{3.7}$$

The solution of (3.7) is given by (3.8) assuming (3.9) and the characteristic impedance Z_C given by (3.10).

$$v(x,t) = V.e^{j\omega t}e^{-\gamma x} + V.e^{j(\omega t+\Phi)}e^{\gamma x} \tag{3.8}$$

$$\gamma^2 = (\alpha + j\beta)^2 = (R' + jL'\omega)\,(G' + jC'\omega) \tag{3.9}$$

$$Z_C = \frac{R' + jL'\omega}{G' + jC'\omega} \tag{3.10}$$

where Φ represents a phase difference.

The solution (3.8) can now be decomposed in two parts, that match with the incident wave V_i and the reflected wave V_r :

$$V_i = V.e^{-\gamma x} \tag{3.11}$$

$$V_r = V.e^{j(\Phi+\gamma x)} \tag{3.12}$$

The existence of the term $e^{\gamma x} = e^{\alpha x}e^{j\beta x}$ allows to deduce some characteristics of

the line:

- The pulsation ω describes the time-related frequency, and the propagation constant β characterizes the spacial-related frequency.

- The signal is mitigated due to power losses. The attenuation by unit length is given by the α coefficient (in m^{-1}). For a given distance, the attenuation increases with the frequency.

Several assumptions can be made in order to simplify the line representation. For example, a lossless line ($R' = G' = 0$), or a line where the parameters are no longer distributed along the whole length but localized in a given point could be considered to downsize the complexity of the model and to reduce the computation time. Several methods are used to model those transmission lines, and will be explained in the following subsections. Nevertheless, even though these simplifications enable an easier representation, they do not transcribe all the phenomena that really exist. Indeed, the more simplified the model is, the more inaccurate the results will be.

Numerous line and cable models exist, and can be dispatched into two wide groups depending on the resolution techniques used in the simulation software [Marti, 1988]: the time-relative models and the frequency-relative ones.

1.3 Frequency domain models

When the cable is modeled in the frequency domain, the time domain solution is obtained thanks to inverse transformation algorithms such as the Fast Fourier Transform (FFT). Therefore, the frequency dependence phenomenon of the line or cable parameters is taken into account. Nevertheless, abrupt changes in the system configuration (such as faults occurrence and breaker switching) as well as the modeling of non linear elements become very complex when frequency-based methods of analysis are used. Consequently, time domain modeling are preferred.

However, accurate computation of electromagnetic transients for underground cables (as well as for overhead lines) requires the frequency domain characterization of two matrix functions, namely the propagation and the characteristic admittance, generally noted H and respectively Y_C. This frequency domain characterization can

be then used to create a time domain model with better accuracy.

As explained in [Kocar et al., 2010], the general description of a line can be given by equations (3.13), (3.14) and (3.15) in the frequency domain.

$$\mathbf{I}_k = \mathbf{Y_C}\mathbf{V}_k - \mathbf{H}\left(\mathbf{Y_C}\mathbf{V}_m + \mathbf{I}_m\right) \tag{3.13}$$

where k and m are the line terminals.

The bold vectors $\mathbf{I}_k$ and $\mathbf{V}_k$ represent the currents and voltages. The size n of the vectors corresponds to the number of conductors.

The n-by-n propagation matrix $\mathbf{H}$ and n-by-n characteristic admittance matrix $\mathbf{Y_C}$ are given by (3.14) and (3.15):

$$\mathbf{H} = e^{\left(-\sqrt{\mathbf{Y}_S\mathbf{Z}_S}l\right)} \tag{3.14}$$

$$\mathbf{Y}_C = \sqrt{\mathbf{Y}_S\mathbf{Z}_S^{-1}} \tag{3.15}$$

where l is the length of the line, $\mathbf{Y_S}$ is the shunt admittance per-unit length, and $\mathbf{Z_S}$ the series impedance matrix per-unit length. These two matrices can be found from the geometry and electrical parameters of the line or cable. This task is performed thanks to the Cable Data block of EMTP-rv library.

The exact representation of a line in the frequency domain is given by the EMTP-rv model Exact Π, defined by equation (3.13). This is not a time domain model, and it can only be used for a steady state solution exciting a unique frequency or to compute a frequency scan [Marti, 1993]. This model is interesting since it enables the comparison of other models with theoretically exact values, but only in the frequency domain.

The time domain solution of (3.13) is obtained thanks to the convolution (3.16):

$$\mathbf{i}_k = \mathbf{y}_c * \mathbf{v}_k - \mathbf{h} * \mathbf{u}_m \tag{3.16}$$

where $\mathbf{u_m}$ is given by:

$$\mathbf{u}_m = \mathbf{y}_c * \mathbf{v}_m + \mathbf{i}_m \tag{3.17}$$

The propagation function constitutes a high order wide-band system with inherent time delays, and the frequency dependency problems are even more complex for underground cables [Kocar et al., 2008]. In order to solve (3.16), assumptions are made depending on the models. Those assumptions are described for each model, in the following subsections.

Besides, for a multi-phase cable or line, the matrix **H** contains several propagation modes with different velocities. The **H** matrix can be decomposed into decoupled propagation modes, thanks to a transformation. Thus, the solution of **H** is easier to get the in the mode domain. Then, the inverse transformation is done to obtain **H** in phase domain. The transformation matrix between modes and phases, named **Q**, is also subjected to assumptions depending on the models.

The assumptions made on these functions will be explained for each model.

1.4 Time-domain models

Several types of line and cable models draw attention: localized parameters models and distributed parameters models, frequency-dependent or not. Those different models already exist in EMTP-rv libraries and will be developed below.

1.4.1 Localized-parameters models

a) Π Line

The model is represented by an association of coupled Π circuits, as shown on Fig.3.3. The G parameter is most often neglected. The parameters are localised in a certain number of points along the line or the cable, depending on the number of Π sections used. The parameters R', L', and C' are evaluated at a given frequency, and the propagation phenomenon is not taken into account.

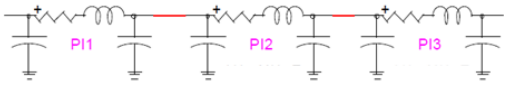

Figure 3.3: Π line model with 3 sections

As a result, the response of the model is only valid in the neighborhood of the frequency at which the parameters are evaluated, and is almost always used to represent relatively short lines [Marti, 1988]. Thus, this model does not suit for the application study of this thesis.

1.4.2 Distributed-parameters models

a) CP model

This model is also called the Bergeron model, or traveling wave model, and assumes a lossless line. The losses are included at a later stage.

The distributed nature of the parameters alongside the line with the propagation phenomenon are taken into account. Indeed, the inductance and capacitance are distributed. Two Norton equivalent generators represent the voltage and current values history, that are required at each line end in order to compute the actual value of the opposite end of the line.

The losses are modeled by separating the line into two separate lossless lines of halved equal propagation time. The total line resistance is re-injected in the model, lumped in three points: at the terminals and at the middle of the line. This approach remains acceptable for most transmission lines, it may however becomes invalid for some cable cases [EMTPWorks, 2005].

CP stands for Constant Parameters, meaning that as well as the Π model, constant parameters are evaluated at a given frequency leading to a frequency-independent model.

For a multi-phase line, the modal transformation is performed, based on matrix **Q**, as explained in the previous part. This matrix **Q** is assumed to be constant and real in the CP line case.

Simulation results of a CP model are faster and more precise than the Π circuit case. Nonetheless, the model generally shows very low damping effects at high frequencies, and the validity of the results is limited to a short frequency range. Therefore, a CP line evaluated at a given frequency could give valid responses for the representation of a system in normal operation, but can no longer transcribe the fast transients generated by a short-circuit for example.

In order to improve the validity of cable models on a large frequency range, frequency dependent models were investigated in order to take the frequency dependency problem into account. The three frequency dependent models that can be found in EMTP-rv library are described below.

b) FD model

The FD model is the first one to take the frequency dependency of the parameters into account.

For multi-phase cases, the modal transformation matrix **Q** is, alike the CP model, assumed to be constant and real. However, the model represents the frequency dependency of the resistance R and the inductance L by approximating with rational transfer functions the characteristic impedance and the propagation function for each mode [Marti, 1982].

The model is valid for a relatively large frequency range (from direct current conditions up to 1MHz [Marti, 1982]) for overhead lines. Nevertheless, problems exist for underground cables since the **Q** elements are strongly frequency dependent. Hence, the model is no longer valid for such applications.

c) FDQ model

This model is also well known as the LMarti model [Marti, 1993], and as well as the FD model, the characteristic admittance and the propagation function are decomposed into modes and they are approximating with rational functions for each mode.

The FDQ model overcomes the limitations of the FD line thanks to a frequency dependent matrix **Q**, also approximated using rational functions. It enables an accurate representation of both low and high frequencies phenomena in the same simulation, even for underground or undersea cables where frequency dependency problems are more complex than in overhead lines.

d) FDQ model limitations

In the FDQ model, rational transfer functions approximation over a range of frequencies are used. They are preferred since they enable an efficient computation of convolution integrals in time domain with a recursive scheme.

The estimation of the rational transfer functions in the frequency domain is based on identification techniques, and can be performed thanks to least-square techniques. Nevertheless, these techniques often introduce errors, especially for the propagation matrix **H** and **Q** when underground cables are considered. These techniques often result in poor fits and ill-conditioned equations [Kocar et al., 2008].

As FDQ has several problems and fails very often, new methods were introduced, resulting in the so-called WideBand cable model. This model will replace the FDQ model, which will be removed in further EMTP-rv versions[1].

e) WideBand model

The line or cable WideBand (WB) is the most sophisticated EMTP-rv model available, and is detailed in [Morched et al., 1999].

The characteristic admittance matrix $\mathbf{Y_C}$ is fitted directly in the phase domain.

The propagation matrix **H** is first fitted in the modal domain, and the results are then used for fitting **H** in the phase domain. The identification of the propagation function as a rational transfer function is done using a weighted vector fitting technique, detailed in [Kocar et al., 2008], and which avoid a lot of errors and numerical

[1]Information originated from EMTP-rv developers

instabilities.

The WB model responses are valid for a wide frequency range, for both overhead lines and underground cables, and is the most appropriate and accurate to study fault transients in DC grids. Tab.3.1 sums up the key characteristics of all the models explained previously.

Model	Parameters	Frequency dependence of the parameters	Transformation matrix Q	Applications
Π	Localised	No	Constant and real for the three-phase case	Short lines
Exact Π	Localised	No	Constant and real	Frequency scan
CP	Distributed	No	Constant and real	Lines and cables, very short frequency range
FD	Distributed	Yes	Constant and real	Overhead lines, large frequency range
FDQ	Distributed	Yes	Frequency dependent	Underground cables, large frequency range, old fitting method
WB	Distributed	Yes	Frequency dependent	Any kind, wide frequency range, most sophisticated fitting method

Table 3.1: EMTP-rv cable models

1.4.3 Cable structure modeling

Since the previously mentioned cable models are available in multi-phase version, it is possible to represent several structures, depending on the level of detail of the

model. Those structures are displayed on Fig.3.4a, 3.4b and 3.4c. The easiest way is to represent only the core of the cable (Fig.3.4a). However, screens have an important influence in the system and wise to model (Fig.3.4b). Furthermore, the coupling effect between the two cables (positive pole and negative pole), especially when the two cables are closed, is mandatory to consider (Fig.3.4c). As accurate dynamics of the signals are required to study a MTDC grid under fault conditions, the most precise structure will be modeled, meaning the one represented on Fig.3.4c.

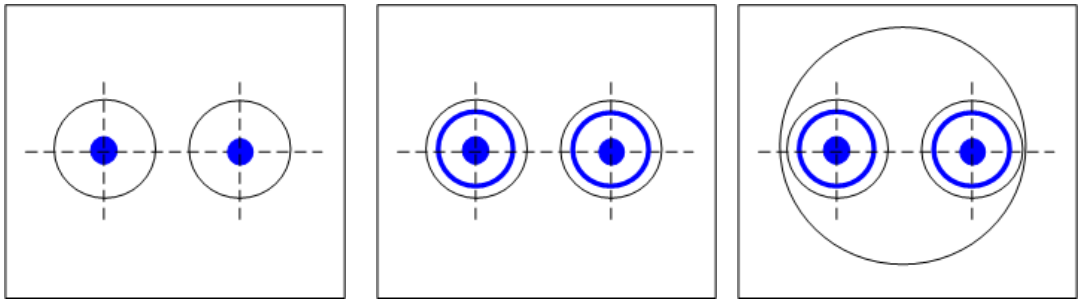

(a) Core

(b) Core + screen

(c) Core + screen with coupling effet beween the two cables

Figure 3.4: Cable structures

1.4.4 Cable parameters choice

As it was explained before, the PI model cannot be used in the study of transients since the propagation effects are not represented. Thus, only CP, FDQ and WideBand models responses will be compared, since the FD model was done to represent overhead lines only. Those models are computed in EMTP-rv thanks to the geometrical and dielectric properties of their components. They are given on Fig.3.5, Tab.3.2 and Tab.3.3, and were provided by RTE as they correspond to XLPE cables used for the INELFE link. ρ is the resistivity of the material, μ_{rc} is the relative permeability of the concerned conductor, μ_{ri} is the relative permeability of the insulation layer next to the conductor, and LF_i is the insulation loss factor.

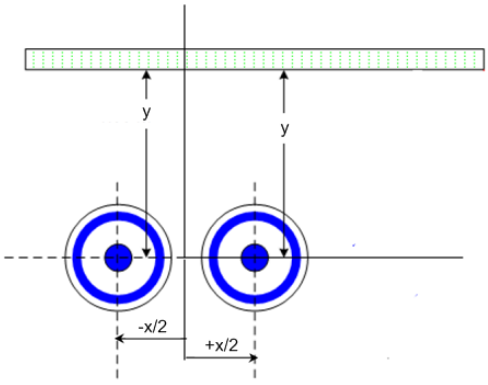

Figure 3.5: Layout of the cables

Conductor	Core	Screen
x [m]	0.5	
y [m]	1.33	
r_{int} [mm]	0	56.9
r_{out} [mm]	32.0	58.2
$r_{ext \quad insulation}$ [mm]	63.9	

Table 3.2: Cable geometrical properties

Conductor	ρ [Ω m]	$\mu_r c$	$\mu_r i$	ϵ_i	LF_i
Core	$1.72e^{-8}$	1	1	2.5	0.004
screen	$2.83e^{-8}$	1	1	2.5	0.004

Table 3.3: Cable components dielectric properties

Those values are used to compute the cable models in EMTP-rv. However, some assumptions are made by the software during the calculation of the model parameters [Gustavsen, 2001]. In particular, EMTP-rv assumes that the relative permittivity of each insulation layer does not depend on the frequency, that the core of the cables is composed of a homogeneous material and that the current distribution is symmetrical and cylinder-shaped in each conductor, which is not always the case in reality. Furthermore, the values given by cable manufacturers

can be imprecise. Those errors, even very low, can have an impact on the responses of the models, and particularly on the damping effects and on the propagation speed. It is thus suitable to do some conversions explained in [Gustavsen, 2001] to take those effects into account. However, a cable specimen would be required to do so, but was not available in the lab.

1.4.5 Cable model behavior

As mentioned in the previous paragraph, CP, FDQ and WideBand models will be compared. The Exact Π model can only be used for a frequency domain simulation, and gives the exact representation. Thus, the closer to the Exact Π the frequency response of a model is, the more precise it is.

a) Frequency domain analysis

Five models will be compared in this part, thanks to a frequency scan done by EMTP-rv :

- a CP model evaluated for the frequency 1kHz (default frequency in EMTP-rv)
- a CP model evaluated for the frequency 50Hz
- a FDQ model
- a WideBand model
- an Exact Π model

Their length is 100km. The frequency scan is done from 1Hz to 10kHz, with a frequency step of 1Hz. An other one is done from 10μHz to 1Hz with a frequency step of 10μHz, to look precisely at the DC response. The corresponding curves are given on Fig.3.6a and Fig.3.6b.

Looking at the magnitude as a function of the frequency, the CP models show a very low attenuation at high frequencies, whereas the FDQ and WideBand models attenuation is much more clear, which matches the Exact Π model response. At low frequencies, the CP model responses are higher and the FDQ, WideBand and Exact Π ones are really close.

The frequency domain analysis show that FDQ and WideBand models, even using simplifying assumptions, are really accurate since they give the same response

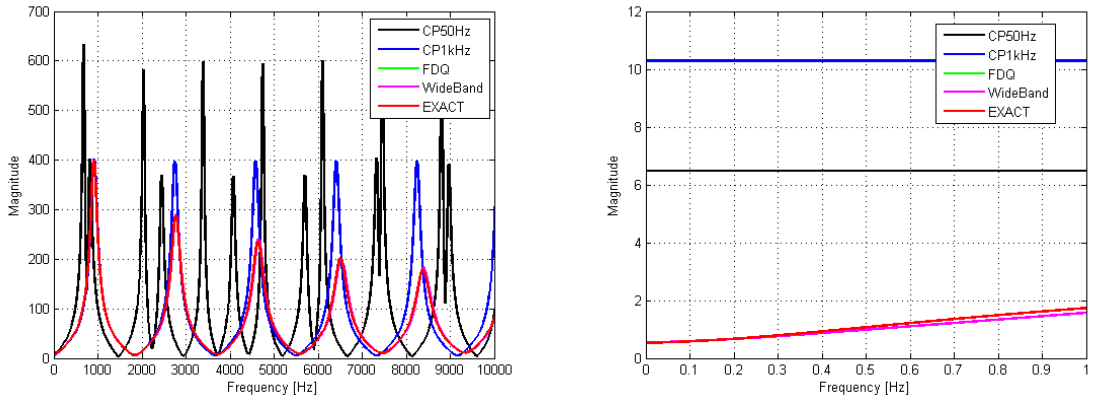

(a) High frequencies (b) Low frequencies

Figure 3.6: Frequency scan response of the different structure models

than the theoretical result (EXACT Π model). Furthermore, the model of a 100km cable gives the same results as two 50km cable models in series, so for a given cable length, no matter the number of sections are used, the frequency domain results would be the same as long as the total length is the same.

Besides, as shown on Fig.3.7 where the structures of the cable are compared using three WideBand models, the representation of the screen is significant. The coupling effect of the two cables does not appear clearly in the frequency domain analysis, but will still be investigated in a time domain analysis.

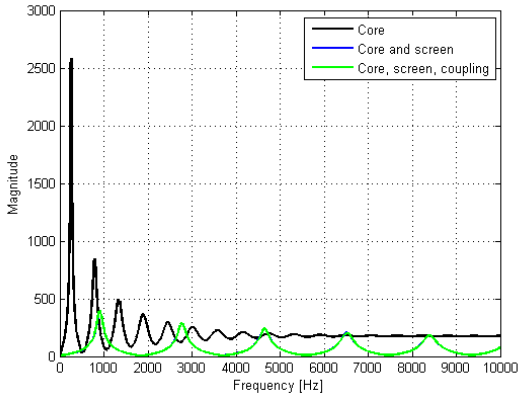

Figure 3.7: Frequency scan response of the cable models

b) Time domain analysis

Steady-state behavior

The behavior of the models is now compared in the time domain. A HVDC link is simulated (displayed on Fig.3.8), and as only the effects of the cables are wanted, the system is represented by really simple source models, meaning ideal DC voltage sources with infinite short-circuit power. A current flowing through the cables is created by a voltage difference between the two ends of the link. The 100km DC link is represented by two cables in series, one of 30km and one of 70km. The core current and the core to ground voltage are measured at the cable junction.

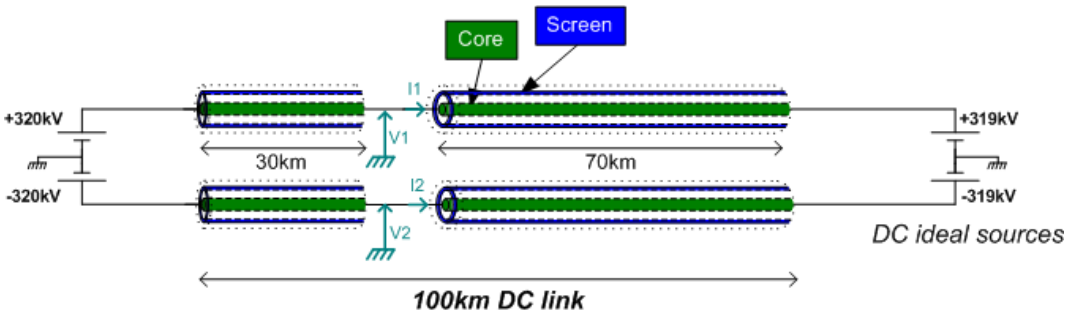

Figure 3.8: HVDC link simulation

The measured currents I1 and voltages V1 are shown on Fig.3.9a and Fig.3.9b. They are constant values in steady-state. The difference in the models is explained by the parameters values, and especially the resistance value, which depends on the frequency value at which the cable models are computed. In fact, the CP models are evaluated at 50Hz and 1kHz, which is not the signal frequency, and the FDQ and WB models are valid for any frequency. The error between the two last ones is due to the differences in the resolution techniques explained previously. As well, the voltages values are not the same, except for the two CP models.

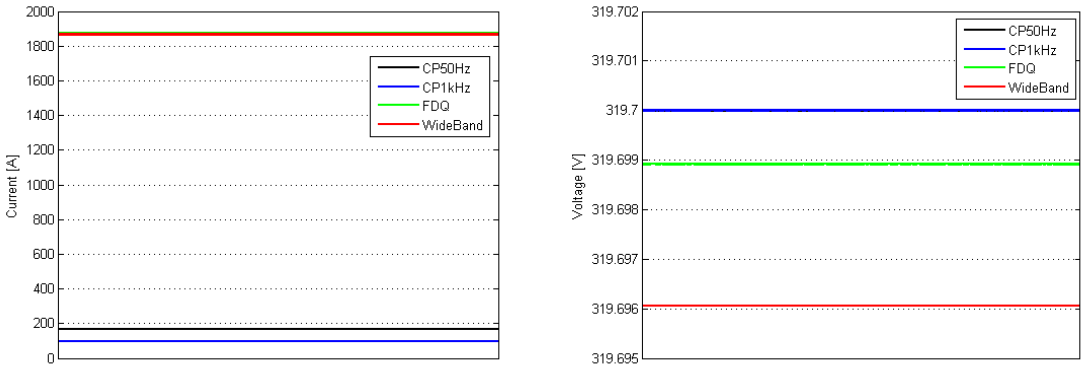

(a) Currents (b) Voltages

Figure 3.9: Steady state simulation results

Transient behavior

In this paragraph, the transient response of the models is evaluated. As the fault transients are the object of the study, the same system will be tested under the core-to-screen fault condition presented in Fig.3.10 and Fig.3.11. Only the positive pole is faulty, and the fault is created by an ideal switch closing at t = 500ms.

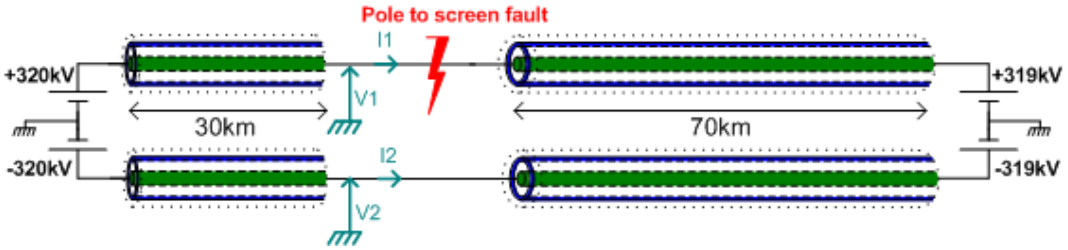

Figure 3.10: HVDC link simulation

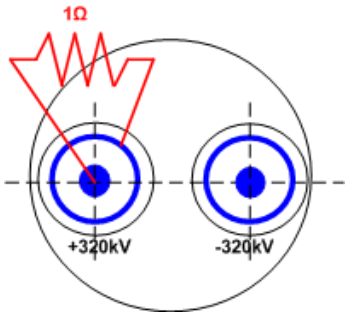

Figure 3.11: Pole-to-screen fault on the positive pole

The signals measured on the positive pole are shown on Fig.3.12a, 3.12b, 3.12c and 3.12d. The first thing to notice is the fault steady state is not the same,

even considering the offset already present in the healthy steady state shown in the previous paragraph, but the cause is the parameter frequency dependence as well. The error between the FDQ and WideBand models is lower than 1 % for both signals. On the other hand, the CP models give a very far response, especially for the voltages. The same conclusion can be done for the dynamic behavior during the first milliseconds after the fault. The response time of the models and the voltages shapes are different, except for the FDQ and WideBand model again.

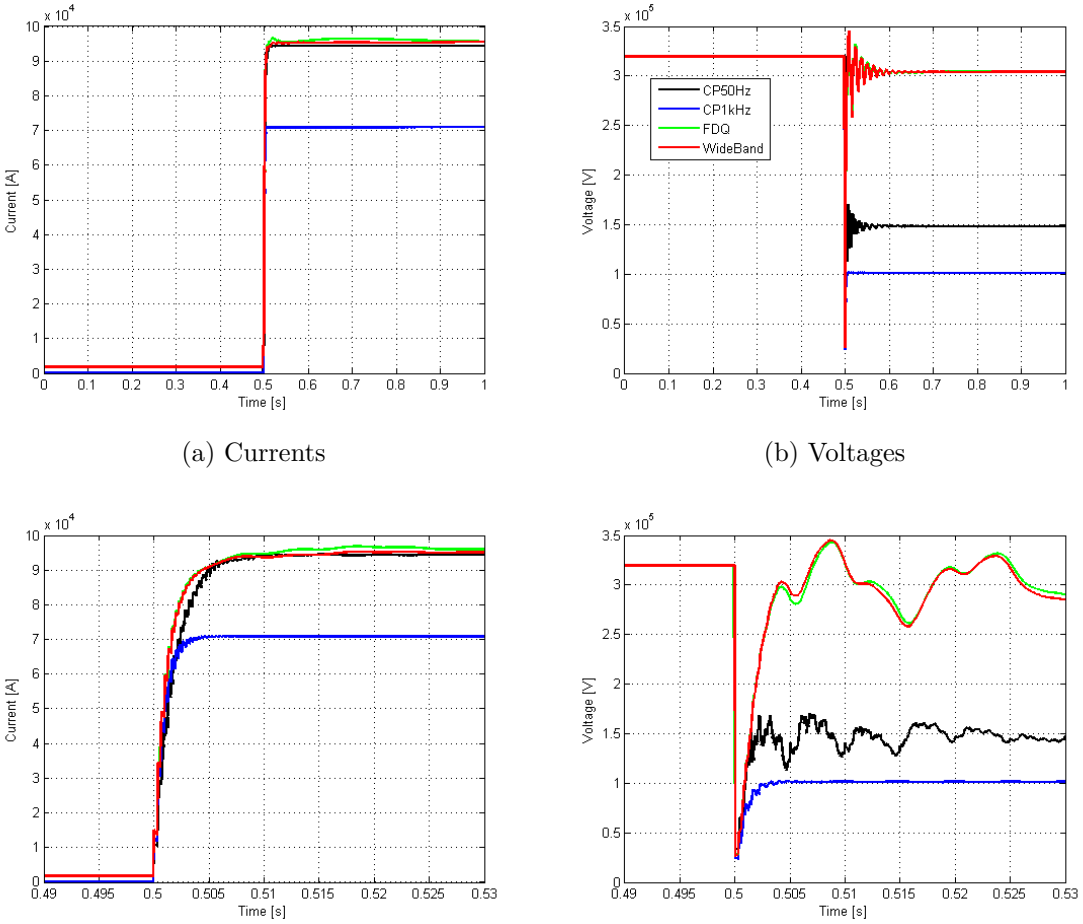

(a) Currents

(b) Voltages

(c) Zoom on the currents

(d) Zoom on the voltages

Figure 3.12: Fault simulation results

Furthermore, since the parameters are not computed at the same frequencies, the propagation speed of the traveling wave generated by the fault is not the same. Tab.3.4 gives the time at which the traveling wave generated by the fault reaches the left cable end, meaning 30km away from the fault. Remain that the fault occurred at t = 500ms.

Note that it is not possible to evaluate precisely the propagation speed of the

Cable model	Time [ms]
CP 50Hz	500.185
CP 1kHz	500.164
FDQ	500.158
WideBand	500.154

Table 3.4: Arrival time of the travelling wave

signals for FDQ and WideBand cable models since this one is frequency dependent, because the frequency of the signal propagating alongside the cable changes as it propagates and is attenuated.

Finally, the coupling effect between the two poles is highlighted. Indeed, the healthy pole is affected by the fault, but the attenuation is higher for the FDQ and WideBand cable models, as displayed on Fig.3.13a and Fig.3.13b.

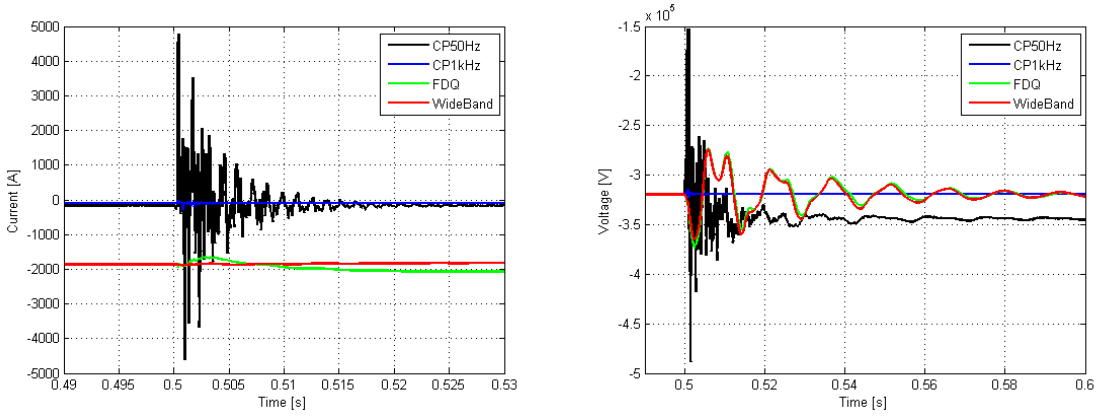

(a) Currents (b) Voltages

Figure 3.13: Coupling effect simulation results

To conclude on the cable modeling, the CP models are not precise enough to study fault transients as they are frequency-independent. WideBand and FDQ give sensitively close answers, and the frequency scan simulations proved their accuracy thanks to the Exact Π model.

The WideBand model was chosen since it was personally recommended by EMTP-rv developers and authors of the references of used fitting techniques. The FDQ model gives similar answers, meaning that in these cases, there is no numerical problems. The WideBand model will thus be used for all the next simulations,

except other mention.

2 AC side and substations

2.1 AC/DC conversion

As mentioned in Chapter 1, the AC/DC conversion can be done thanks to two kinds of power electronics elements: LCC or VSC. Since the voltage polarity remains constant irrespectively to the power flow transfer direction when VSC are used, it is easier to implement multi-terminal HVDC systems. Thus, only VSC will be treated in this section. The study focuses on two-level VSC, but the MTDC system behavior based on MMC will be discussed in the conclusion of the thesis. Indeed, MMC modeling is currently the topic of a whole Ph.D work done by Hani Saad and conducted at the *École Polytechnique de Montreal*. The EMTP-rv averaged and detailed models of MMC are available [Saad et al., 2013], [Peralta et al., 2012], but the detailed models are for now too slow to compute, and thus were not appropriate for fault transient studies at this time. This is why 2-level VSC were consider for this thesis. As the model of the two-level VSC and its control was done in the framework of another Ph.D thesis[2], this part only gives the headlines of this work.

2.1.1 EMTP-rv VSC components model

The converter itself is represented by a detailed model, meaning that each IGBT shown in Fig.3.14 is modeled. The hundreds IGBT normally disposed in series in each arm are simplified and represented by only one per arm. Those IGBT are controlled by an intersective Pulse Width Modulation (PWM) whose carrying frequency typically range between $1 - 2$kHz depending on the converter topology, system frequency and specific objectives of the considered application [Bahrman et al., 2003]. The EMTP-rv model uses a triangle PWM pattern with a carrying frequency of 1350Hz.

The VSC is associated with a DC filter, composed of capacitors C_{DC} and series inductors L_{DC}, commonly called smoothing reactors.

[2]Pierre Rault L2EP and RTE - CNER

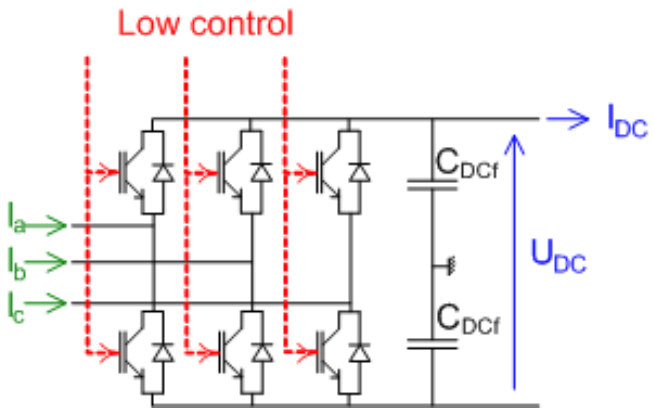

Figure 3.14: VSC structure model

2.1.2 VSC control strategy

A simplified line diagram of the substation and its associated controllers are presented in Fig.3.15. The role of the low level is to convert voltage references into transistor switching orders, so it depends on the converter unit topology. It is achieved by the PWM. The AC current control is done by a decoupled controller in the dq frame. Controllers are standard PI controllers and are tuned for a desired dynamic performance. For further information, refer to [Nguefeu et al., 2011] and [Andersen and al., 2005].

The converter goes with AC and DC filters. The DC filter is composed of the two capacities represented on Fig.3.14 to maintain the voltage level, and a smoothing reactor (one on each pole) to attenuate the current oscillations. The value of the smoothing reactor and the capacities has an impact on the fault transient since it modifies the dI/dt, and will be investigated in Chapter 4. The default values taken for the next simulations are depicted in Tab.3.5 and come from [Nguefeu et al., 2011]. The AC filter is shown on Fig.3.15.

AC and DC filters parameters are given in Tab.3.5.

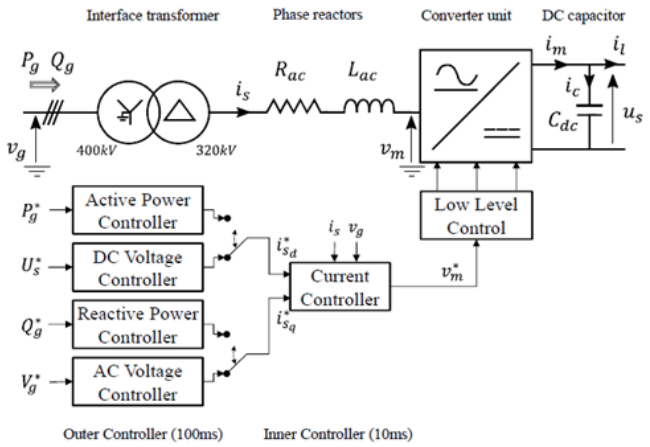

Figure 3.15: Substation topology, [Nguefeu et al., 2011]

Paramter	Value
R_{AC}	2.5mΩ
L_{AC}	76.4mH
C_{DC}	100μF
L_{DC}	10mH

Table 3.5: AC and DC filter parameters

The standard control of individual converter is well known, however an additional control layer is required in the case of MTDC grids. It acts as a primary control, and several methods exist to achieve this. The main property of the control is that there is no communication between the different substations of the MTDC grid. Three methods exist to do so: the Master Slave Method, the Voltage Margin Method and the Voltage Droop Method. They both adjust the DC power flow of the considered substation as a function of the voltage level, in real time, with a response time varying from 100ms up to several seconds. There also might be a supervisor that have access to the substation measures (with a lower sampling frequency) in order to readjust the power flow to more appropriate references.

The Master Slave Method has the inconvenience to lead to the DC voltage collapse in case the voltage-controlled substation is lost (as a result of a fault for example). The two other methods have the ability to operate in N-1 conditions. However, the Voltage Droop Method provides a better sharing of power variations than the Voltage Margin Method. The Voltage Droop Method was investigated and modeled in EMTP-rv by Pierre Rault. The reader can refer to [Nguefeu et al., 2011] for more details. However, the response time of the control is much higher than the

response time required for the protection plan (see Chapter 5 for more further information about the protection plan response time), and thus the control method does not impact the study of the system under fault conditions. The control strategy model is hence used to set an operating point only in the framework of this thesis.

2.2 AC producers and AC grid

In the MTDC grid application of this thesis, the AC side can be either the AC onshore grid or an offshore wind farm. Since the intermittent characteristic is not crucial in this study, both AC grid and wind farms are represented by ideal AC voltage sources associated with a short-circuit power. The respective short-circuit power are scaled to match the real one of the chosen application. For an AC grid application case, the short-circuit power can vary from 5 to 50GVA, and for an aggregation model of a wind park, the taken value is 200MVA [Nguefeu et al., 2011]. Their impact will be highlighted in Chapter 4. In order to match the DC side voltage, they are associated in series with a voltage transformer, and a LCL filter (Fig.3.16). The parameters are given in Tab.3.6 for an AC grid application case, and were chosen by Pierre Rault.

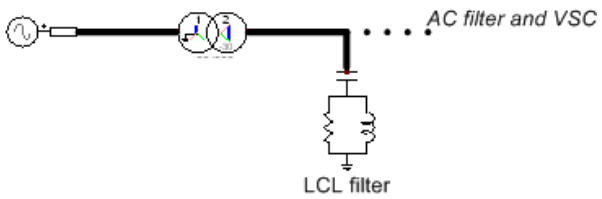

(a) AC side

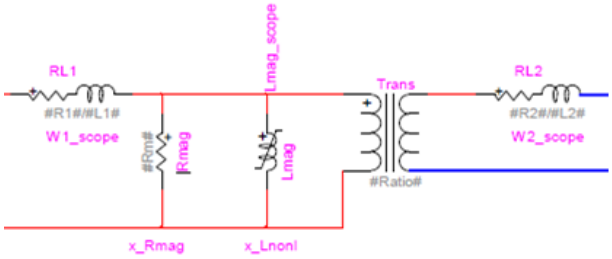

(b) Transformer model

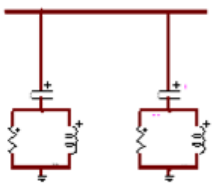

(c) LCL filter

Figure 3.16: AC side model

Paramter	Value
V_{AC}	400kV
S_{sc}	50GVA
LCL cutting frequency	500Hz
Transformer nominal power	1000MVA
Winding 1 voltage	400kV
Winding 2 voltage	320kV
Winding R	0.005pu
Winding X	0.15pu

Table 3.6: Parameters [Nguefeu et al., 2011]

3 Faults and protection relative components

By joining all the elements already detailed in this part, the grid can be modeled and simulated in healthy conditions. The last components to inspect are related to the simulation of fault conditions. The protection strategy and algorithms are not treated in this part, but their inputs (meaning current and voltage measurements) and their eventual action (opening of circuit breakers) are dealt with. Note that the current and voltage sensors used by the VSC's control system cannot be used for protection purpose, since the dynamic requirements are not the same.

3.1 Fault

The first element to model is the fault itself. As mentioned in Chapter 2, only permanent faults will be studied in this thesis. Thus, no self-extinguishing faults are considered and no arcing effects are modeled, even though they exist in the literature (such as Cassie [Andrea et al., 2010a], Mayr [Andrea et al., 2010b], Habedank [Darwish and Elkalashy, 2005] or Kizilcay [Idarraga Ospina et al., 2008]). This solves a huge work which would evaluate the large amount of arc model parameters. The fault can be easily represented by a constant resistance in series with an ideal switch. The location of the ideal switch depends on the nature of the fault: pole-to-ground (PG) or pole-to-pole (PP).

3.2 Sensors

Sensors are keys components in this study, since they give all the inputs that are used by the protection algorithms. A difference has to be performed between the

real values of the currents and voltages in the grid, even if that grid is a model, and the values given by sensors and which can be used by other components. If ideal sensors with no signal degradation existed, the real values and the measured values would be the same. However, no such sensors can be manufactured and the signals deterioration has to be modeled since it might have an impact on the protection algorithms decision. Furthermore, the real values of the signals are required to verify the withstand capability of the other components. These values are obtained by the EMTP-rv ideal sensors library. The measured values correspond to the real values in the grid, and are then processed to take the degradation effects of the real sensors into account.

3.2.1 Current sensor

Many current measurement ways can be used. The concerned application determines the choice of the technology. In this study, the sensor has to be chosen to measure DC currents obviously at their nominal values, but especially to measure large overcurrents up to several kiloAmps when a fault occurs. Since the protections have to act very quickly, so the response of the sensor has to match the requested time constraints.

a) Technology

While a large number of technologies exist and theoretically fulfil the requirements of the application, only the ones based on the magnetic field detection are matured technologies or are not only at the university-research stage. Indeed, even if magneto-optic sensors based on the Faraday effect seem to have remarkable characteristics ([Petersen, 1995], [Rahmatian and Ortega, 2006], [Takahashi et al., 2010]) particularly in terms of band width, the Hall effect technologies appear to be more relevant, and namely the Hall effect with flux compensation shows the best performances in terms of band width, measuring range, response time and accuracy [Eric Favre, 2004]. The measurement principles are detailed in [Correvon, 2005].

b) Model

The goal was not to model the elements of a Hall effect sensor, but to modify the values of the current measured by the ideal EMTP-rv sensor to approach the values that would be produced by an Hall effect sensor. The corresponding representation

done in EMTP-rv consist of a first order low-pass filter as described by its transfer function (3.18),with a cutting frequency f_c of 50kHz, in series with a rate-of-rise limiter, a saturation and a gain (to represent the accuracy error). The parameters are taken from the constructor PUISSANCE ANALYSE [PuissanceAnalyse, 2012] and LEM [LEM, 2012], and are depicted in Tab.3.7.

$$H(j\omega) = \frac{1}{1 + j\frac{\omega}{\omega_c}} \tag{3.18}$$

where $w = 2\pi f$, with f the frequency and $w_c = 2\pi f_c$ with f_c the cutting frequency of the filter.

Paramter	Value
Band Width	$DC - 50kHz$
Saturation	50kA
Accuracy	99.04%

Table 3.7: Current sensor parameters

The impact on the current measurements is given on Fig.3.17 which is an example of the current measured at a cable end in case of a DC fault.

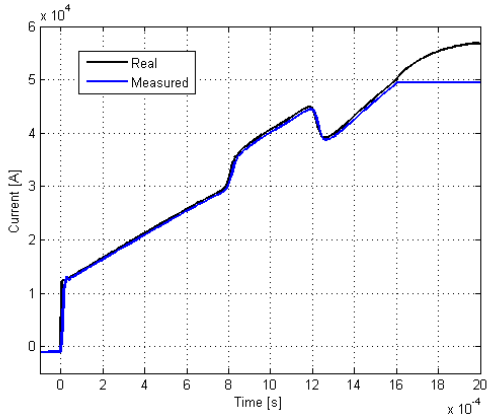

Figure 3.17: Current sensor influence on the measured signal

3.2.2 Voltage sensor

The voltage sensor related informations given below were provided by RTE, and were acquired from the voltage sensor manufacturer held up for the INELFE link. The voltage divider is elaborated using resistors and capacitors, and brings the 320kV DC voltage back to 100V. Then, an isolation amplifier drives down to 5V with galvanic insulation. The same model as the current sensor were used, with

a cutting frequency f_c of 10kHz for the low pass filter. The other parameters are depicted in Tab.3.8.

Paramter	Value
Measuring range	32kV − 640kV
Band Width	DC − 10kHz
Accuracy	99%

Table 3.8: Voltage sensor parameters

The impact on the voltage measures is given on Fig.3.18.

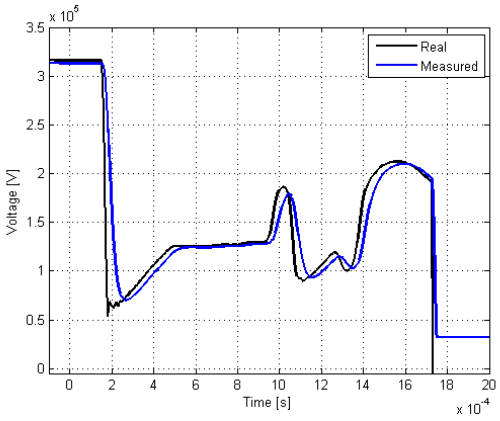

Figure 3.18: Voltage sensor influence on the measured signal

3.3 DC Circuit Breaker

As concluded in 2, hybrid DC Circuit Breakers are the best way to break large DC currents. Since the breaker technology was not the topic of the study, a simple model (Fig.3.19) is considered to represent the signals behavior during the extinction of the current after the fault detection. As well as the current sensor, the circuit breaker model do not represent the element of the considered breaker technology.

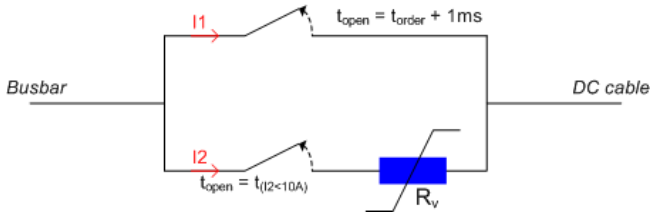

Figure 3.19: DC Circuit Breaker model

When the cable is healthy, the top ideal switch is closed and the bottom ideal switch is open. The protection detects and identifies that the considered breakers has

to open at t = t_{order}. The top switch opens one millisecond later to model a delay of communication between the protection and the breaker. The bottom breaker closes simultaneously and the current is switched to the bottom branch. Then, the variable resistance increases linearly until the current I2 is lower than 10A. At this instant, the bottom switch opens, and the whole current is cut.

4 Studied grid structures

From now on, the entire grid model components have been detailed. They are used to simulate two grid structures: a HVDC link and a MTDC grid. The values displayed in the figures are default values. The HVDC link will be used to investigate the influence of some relevant elements and component characteristics. Its advantage is the lower computation time required by EMTP-rv due to the reduction of the number of simulated parts. The MTDC grid will be used to test the protection plan that will be proposed in Chapter 5. Note that other grid structures might be simulated to highlight a particular phenomenon if those presented below are not demonstrative enough.

4.1 HVDC link

4.1.1 HVDC link characteristics

The HVDC link test model is exhibited on Fig.3.20. Several characteristics are displayed on the figure.

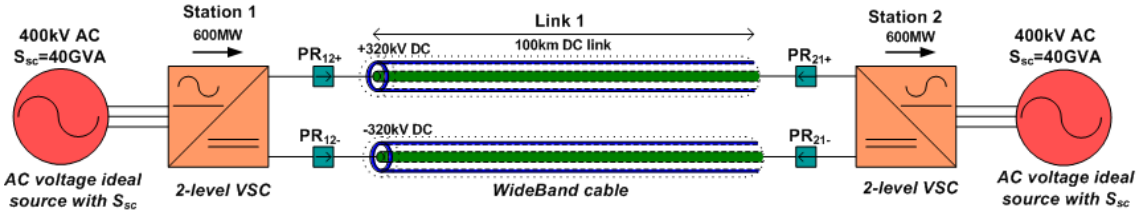

Figure 3.20: HVDC link test model

4.1.2 Protection elements and notations

The protection elements are the boxes named PR_{ijs}, where $i \neq j$, i represents the nearest station number, j is the station number that is connected to the opposite

cable end of the same link, and s is the sign of the polarity of the cable.

The protections are composed of a current sensor, a pole-to-ground voltage sensor and a DCCB assembled in the order shown on Fig.3.21. The calculation interface is not treated yet, and will be added in Chapter 5.

Real currents and voltages are written I^*_{ij} and V^*_{ij}, and the modified signals taking the sensors effects into account are written I_{ij} and V_{ij} respectively.

The current sensors are arbitrary oriented and set to measure a positive current when the current flows from a converter to a cable.

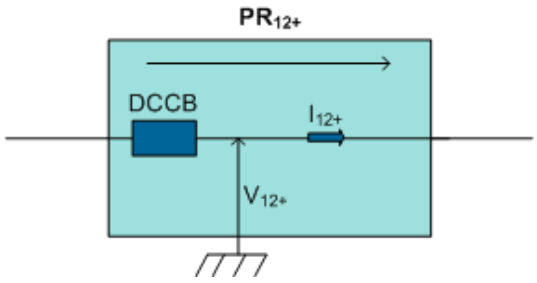

Figure 3.21: Protection elements arrangement

4.2 Twenties grid test

4.2.1 Twenties grid test model characteristics

Fig.3.22 below presents the multi-terminal grid test model, which was chosen during the redaction of TWENTIES deliverable 11.1 [Nguefeu et al., 2011]. For visual purposes, only the positive pole is represented on the figure, but the two poles are modeled.

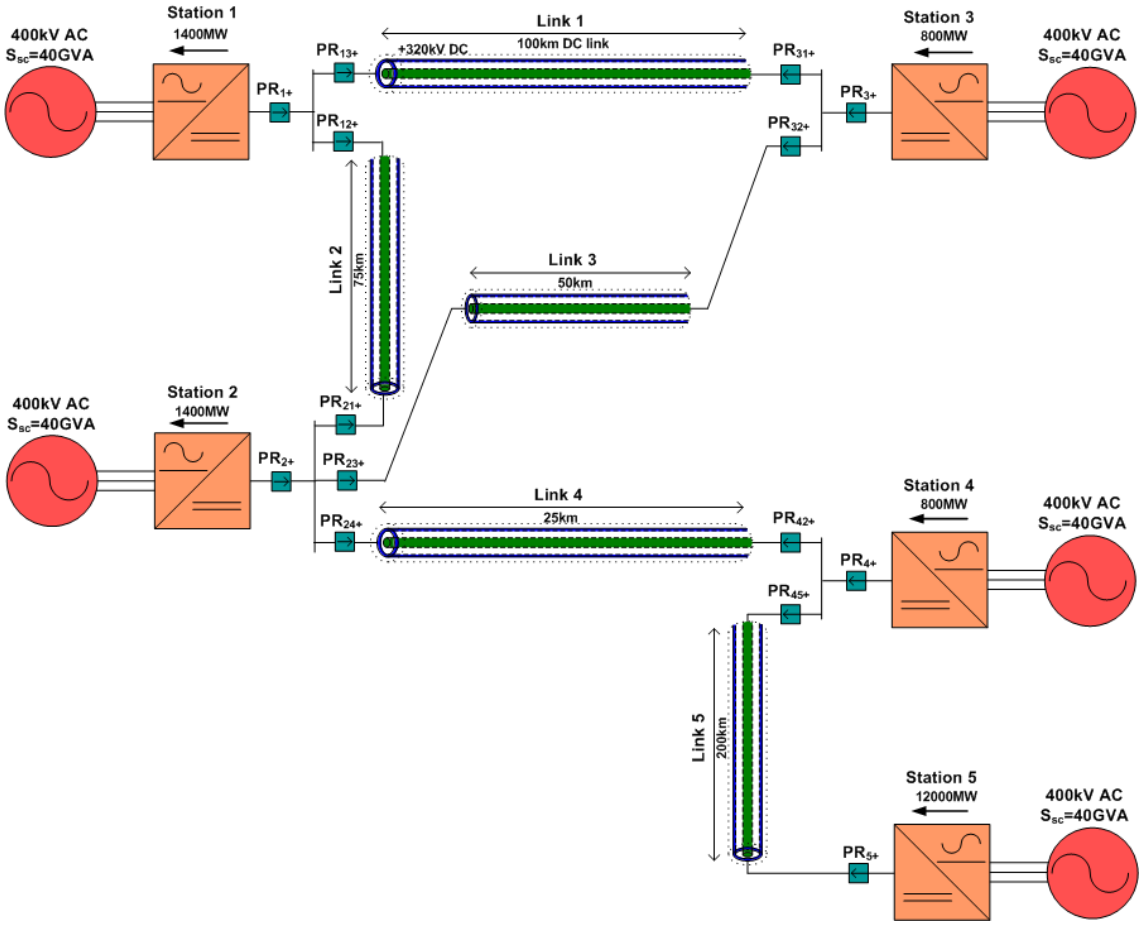

Figure 3.22: TWENTIES grid test model

4.2.2 Additional protection elements

The notations used are the one detailed in section 4.1.2, but other protection boxes are added at each station end to deal with busbar faults, as explained in Chapter 5. The corresponding notations are PR_{is}, where i represents the nearest station number and s is the sign of the polarity. The components arrangements are the same as the ones shown on Fig.3.21.

CHAPTER 4

Signals behavior under fault conditions

Chapter 4

Signals behavior under fault conditions

Now, the model of each element of the grid has been detailed. Accurate simulation of DC fault can therefore be made. This chapter constitutes a parametric study to highlight the components of the grid that have an influence on the signals that will be used by the protection system, which will be developed in Chapter 5. As mentioned in Chapter 2, the protection system needs to operate in a very short time (in the range of 5ms), that is why the results that follow will be focused on this small duration transients.

The impact of three kinds of parameters will be discussed: sources-related, grid-related and fault-related parameters. The effect of most of them on the currents and voltages will be argued thanks to the simulation of the HVDC test case model, others will be examined through the Twenties grid test model, and some other structures will be defined to highlight their influence. The parameters that will vary are listed in Tab.4.1. The simulation sampling frequency were set to 1MHz.

The default parameters of the grid were given in Chapter 3, and some of them are reminded on Fig.4.1. The default parameters for the fault are mentioned in Tab.4.2. In each section of this chapter, the influence of one parameter will be presented by varying only this one parameter, and keeping the others at their default value. Thus, only the value of the parameter that changes will be provided.

Kind-related	Parameter	Grid test
Fault	Type	HVDC
	Location	HVDC
	Impedance	HVDC
Sources	AC and DC filters	HVDC
	Scc of AC sources	HVDC
Grid	Link length	HVDC
	Topology	Other
	Feeder junction	TWENTIES

Table 4.1: Parameters influencing the signals behavior

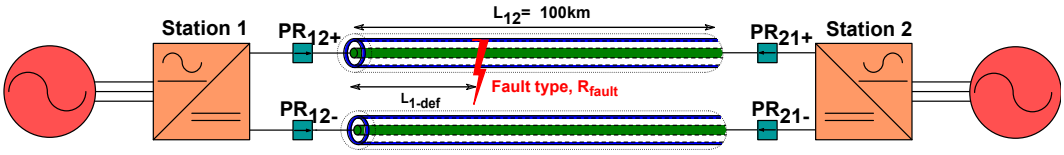

Figure 4.1: HVDC link test case

Fault	Parameter name	Parameter value
Type	—	Pole-to-ground
Location	L_{1-def}	30km
Impedance	R_{fault}	1Ω
Fault occurrence time	t_{fault}	0s

Table 4.2: Default parameters of the fault

Since the grid response under fault condition is the aim of the chapter, we will focus only on the real current and voltages (I^*_{ij} and V^*_{ij}). The sensors effects are not relevant to study the effects of those parameters since they would eventually hide some of them.

At the moment of the fault, the line will discharge its capacitors which results in a voltage and current wave front propagating away from the fault location. This is shown on Fig.4.2, for the simulation of the fault described in Tab.4.2 on the HVDC link. The signals measured more than 100ms after the fault should not be observed

since the converters are supposed to be uncontrollable, but the model assumes they are still commanded by the modeled control loops. The current measured at the cable end is shown, as well as the current flowing through the screen of this cable and the current resulting of the DC filter capacitor discharge.

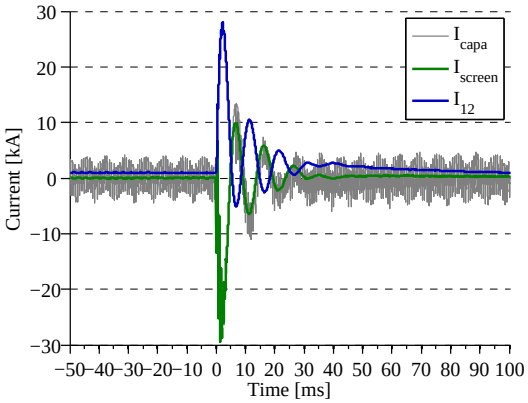

Figure 4.2: Behavior of the grid in fault conditions

1 Fault-related parameters

First of all, the influence of the fault parameters is explored on the HVDC link test model. These parameters are namely the fault type, the fault location and the fault impedance.

1.1 Fault type

Four fault types cases can be tested, and are shown in Fig.4.4.

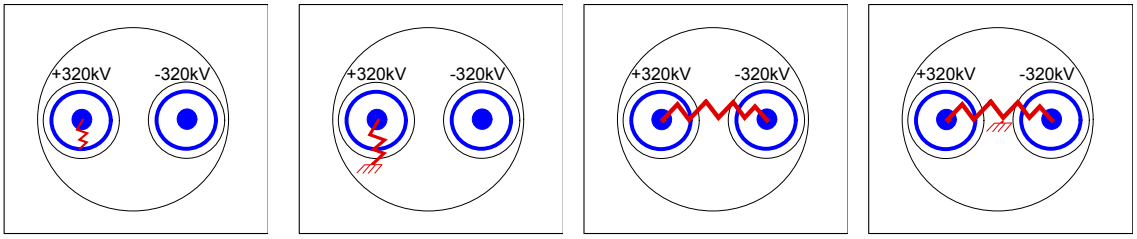

(a) Core-to-screen fault (b) Pole-to-ground fault (c) Pole-to-pole (d) Pole-to-pole-to-ground

Figure 4.3: Fault types

The most probable cable insulation fault is the pole-to-ground fault. Since the screens are grounded, as mentioned in Chapter 3, there is no difference between

a pole-to-screen fault and a pole-to-ground fault. Also, it is not probable that a fault links the core and the ground of a cable, without passing through the screen. Therefore, two types of faults are considered in the rest of this thesis, namely pole-to-ground fault and pole-to-pole faults, that both include the grounding effect. They correspond respectively to tested case $\mathscr{C}_{\text{type-pg}}$ and $\mathscr{C}_{\text{type-pp}}$. Pole-to-pole faults are very unlikely along a cable, but can still happen and thus need to be investigated. However, pole-to-pole fault can occur at the substation connection point. The resulting currents and voltages few milliseconds after the fault instant are shown on Fig.4.4.

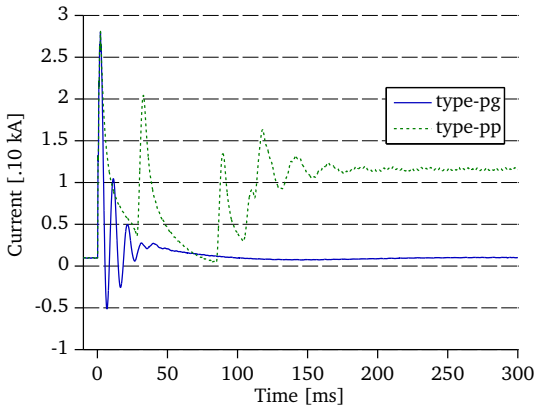

(a) Currents I_{12}^{+}

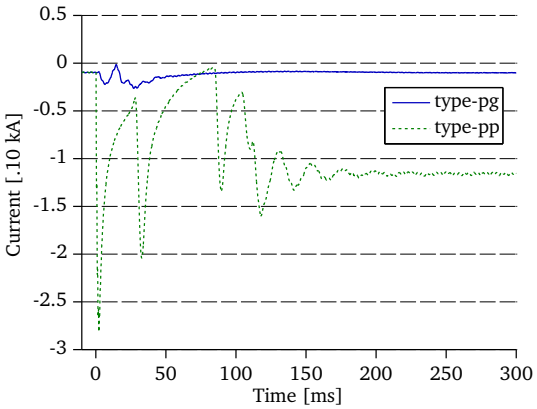

(b) Currents I_{12}^{-}

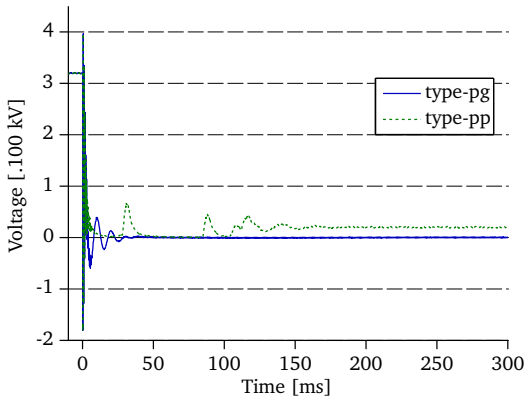

(c) Voltages V_{12}^{+}

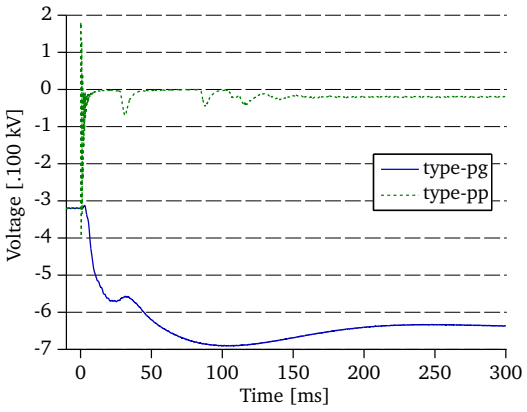

(d) Voltages V_{12}^{-}

Figure 4.4: Fault types

Two differences can be noticed on those figures: one related to the steady-state after the fault, and one related to the transient phase of the signals.

The steady-state signals after the fault occurrence are not meaningful since the

converters IGBT are not controllable in real applications considering the loss of voltage at the converter terminals, which is not the case in our simulations.

However, some observations can be made. The voltages V_{12}^{+} are close to zero for both cases (Fig.4.4c), since the positive pole is faulty for the two fault types. This is also the case for the voltage V_{12}^{-} concerning the pole-to-pole fault. However, in pole-to-ground conditions, the voltage of the healthy link decreases to twice the nominal voltage value (Fig.4.4d), making the pole-to-pole voltage keeping the nominal value. Since the controllability of the VSC is kept after the fault in our models, that implies that the current related to the case $\mathscr{C}_{\text{type-pg}}$ is reduced to zero after a few milliseconds after the fault.

The transient behavior of the fault depends on the cable length and sources characteristics and will be investigated later in this chapter. However, the difference between a pole-to-ground fault and a pole-to-pole is obviously due to the fact that the solicited passive components are not the same.

1.2 Fault location

Five locations are tested through the simulation of a pole-to-ground fault. The lengths are defined in Fig.4.5 and the values are provided in Tab.4.3.

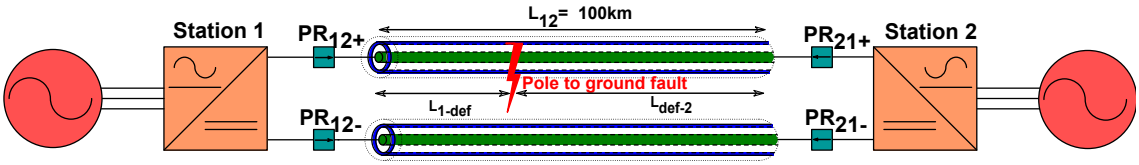

Figure 4.5: Fault location parameter on the HVDC link test model

Case name	L_{1-def}	L_{def-2}
$\mathscr{C}_{\text{pos}-1}$	0	100
$\mathscr{C}_{\text{pos}-2}$	30	70
$\mathscr{C}_{\text{pos}-3}$	50	50
$\mathscr{C}_{\text{pos}-4}$	70	30
$\mathscr{C}_{\text{pos}-5}$	100	0

Table 4.3: Cases parameters for position influence study

Several important effects can be observed on Fig.4.11.

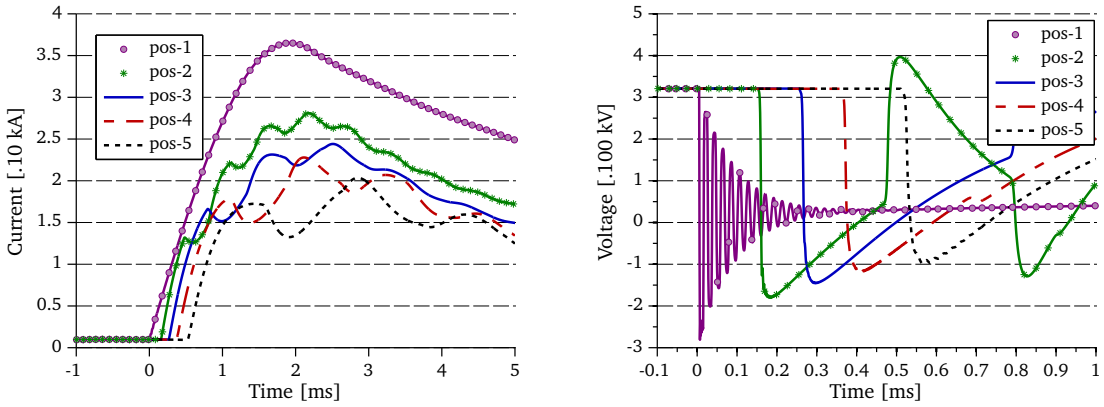

(a) Currents I_{12}^{+}

(b) Voltages V_{12}^{+}

Figure 4.6: Signals measured at left cable end for several fault locations

The first one is the arrival time of the first front transient (currents and voltages) at the sensors located at the cable ends. The measurements obtained by sensors I_{12}^{+} and V_{12}^{+} are shown on Fig.4.6a and Fig.4.6b respectively. The first front arrives $\Delta t_{L1-fault}$ after the fault occurrence ($t_{fault} = 0$), and is defined by (4.1) were v_{cable} is the propagation speed of a signal in the cable.

$$\Delta t_{L1-fault} = \frac{L_{1-fault}}{v_{cable}} \tag{4.1}$$

The second effect is the reflections seen after the arrival of the first front transient. The influence of the reflected wave, reaching the fault point after two times the propagation time corresponding to the cable length $L_{1-fault}$, is obvious due to the reflection factor $r = -1$ at the fault location. This explains the high frequency oscillations seen on the voltage for the case $\mathscr{C}_{pos-1}$. For that particular case, the reflections on the current wave form exist but are tough to see on the Fig.4.6a due to the high rate of rise of the current. The characteristic times are highlighted on Fig.4.7, which corresponds to the case $\mathscr{C}_{pos-2}$.

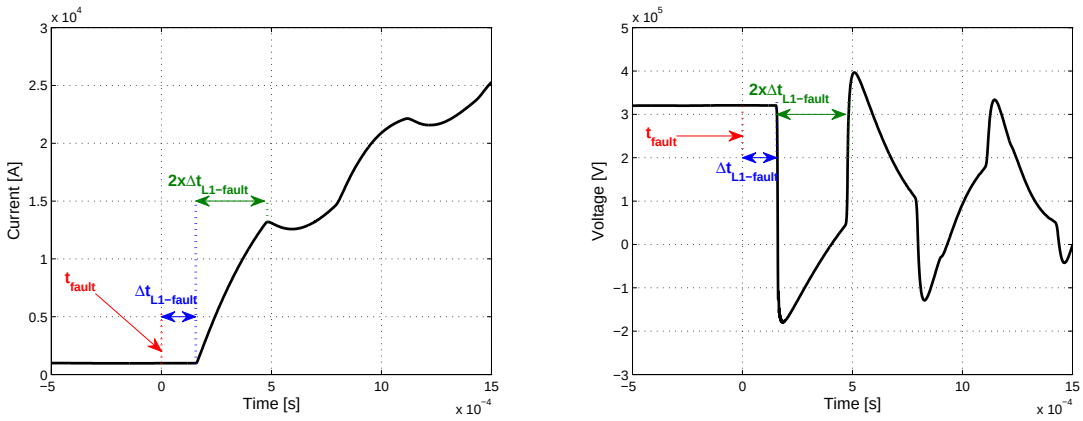

(a) Currents I_{12}^{+} (b) Voltages V_{12}^{+}

Figure 4.7: Zoom on the reflections for the case $\mathscr{C}_{\text{pos}-2}$

Then, the magnitude of the first current pic decreases when $L_{1-\text{fault}}$ increases, due to the attenuation of the wave through the cable length. The rate of rise of the first wave front is maximal at its arrival time, and also decreases for the same reason when $L_{1-\text{fault}}$ increases, as shown on Tab.4.4.

Case	$I_{12\text{MAX}}^{+}\,[kA]$	$\Delta t_{\text{L1}-\text{fault}}\,[\mu s]$	$\frac{dI_{12}^{+}}{dt}\,(\Delta t_{\text{L1}-\text{fault}})\,[kA/ms]$
$\mathscr{C}_{\text{pos}-1}$	36.507	8	57.877
$\mathscr{C}_{\text{pos}-2}$	28.098	163	49.878
$\mathscr{C}_{\text{pos}-3}$	24.409	270	46.462
$\mathscr{C}_{\text{pos}-4}$	22.787	377	43.689
$\mathscr{C}_{\text{pos}-5}$	20.346	533	41.781

Table 4.4: Characteristic times, pole-to-ground fault, several locations

1.3 Fault impedance

The fault resistance has two noticeable effects on the wave forms. First, the current derivative is decreased when the impedance is higher, and secondly the maximal current is smaller. The transient shape is similar for each fault resistances (each case is detailed in Tab.4.5) and are shown on Fig.4.8. The small oscillations on the currents, due to traveling wave reflections at each cable end, are however more attenuated if the resistance is higher. The phenomenon is emphasized on the voltage measurements shown on Fig.4.8b. Finally, the waves arrive at the same time at the cable end.

Case name	R_{fault}
$\mathscr{C}_{res-1}$	1Ω
$\mathscr{C}_{res-2}$	5Ω
$\mathscr{C}_{res-3}$	10Ω
$\mathscr{C}_{res-4}$	20Ω
$\mathscr{C}_{res-5}$	30Ω
$\mathscr{C}_{res-6}$	40Ω
$\mathscr{C}_{res-7}$	50Ω
$\mathscr{C}_{res-8}$	100Ω

Table 4.5: Cases parameters for resistance influence study

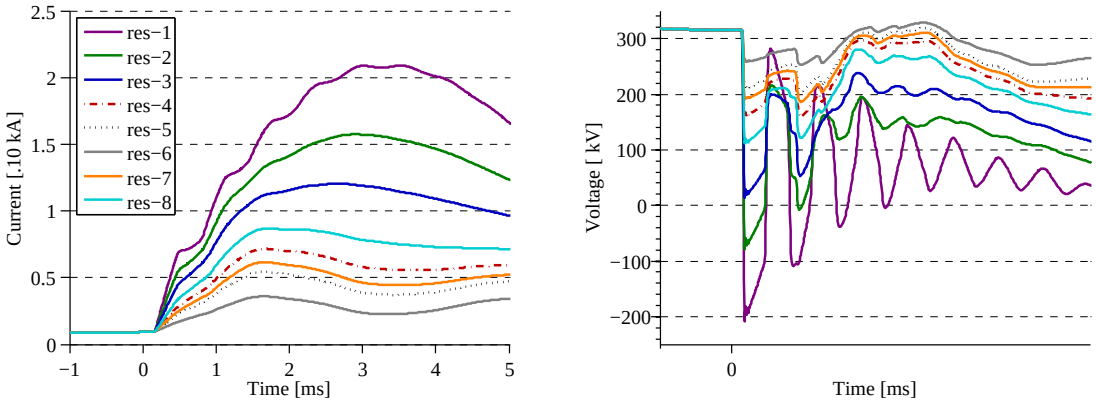

(a) Currents I_{12}^{+} (b) Voltages V_{12}^{+}

Figure 4.8: Signals measured at left cable end for several fault impedances

2 Source-related parameters

2.1 Short-circuit power of AC sources

Even though the short-circuit power of the AC side grid should impact the contribution of the sources, this phenomenon appears largely after the first transients, and can be seen only on the steady state value for few cases. During the first milliseconds, the overcurrents are due to cable capacitor discharge, and thus the S_{SC} of the AC source model do not impact the values used by the protection system.

2.2 AC and DC filter

This last remark stands for the AC filters (LCL), which do not impact the transients during the first milliseconds after the faults, but changes the source contribution to the fault. Nonetheless, the DC filter component values have an important impact on the current and voltages.

The DC filter is composed of smoothing reactors and capacitors, as shown on Fig.4.9. The influence of those two components is described in this subsection. Again, the values C_s and L_s are the same for each converter station. Default values are $C_s = 100\mu F$ and $L_s = 10mH$. Those values were chosen with RTE, in order to have the same MTDC model for both Grenoble and Lille works.

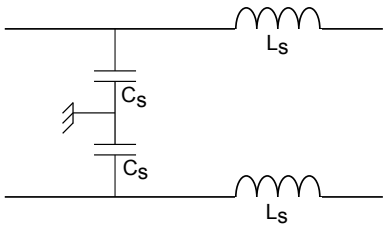

Figure 4.9: DC filter and parameters

2.2.1 DC capacitor

The five cases are presented in Tab.4.6.

Case name	C_s [μF]
$\mathscr{C}_{Cs-1}$	100
$\mathscr{C}_{Cs-2}$	200
$\mathscr{C}_{Cs-3}$	300
$\mathscr{C}_{Cs-4}$	400
$\mathscr{C}_{Cs-5}$	500

Table 4.6: Cases parameters for DC capacitor influence study

The relevant information on the influence of the DC capacitor value are observable on the currents measured on the faulty pole and on the voltage measured on the healthy pole. They are presented on Fig.4.10a and Fig.4.10b respectively. When the capacitor value increases, the current starts to decrease later than it does for a

smaller value. This is due to the discharge of this capacitor, which maintains the voltage a little bit longer, implying a smaller voltage rate of fall. Note that the current derivative at the first front is not affected.

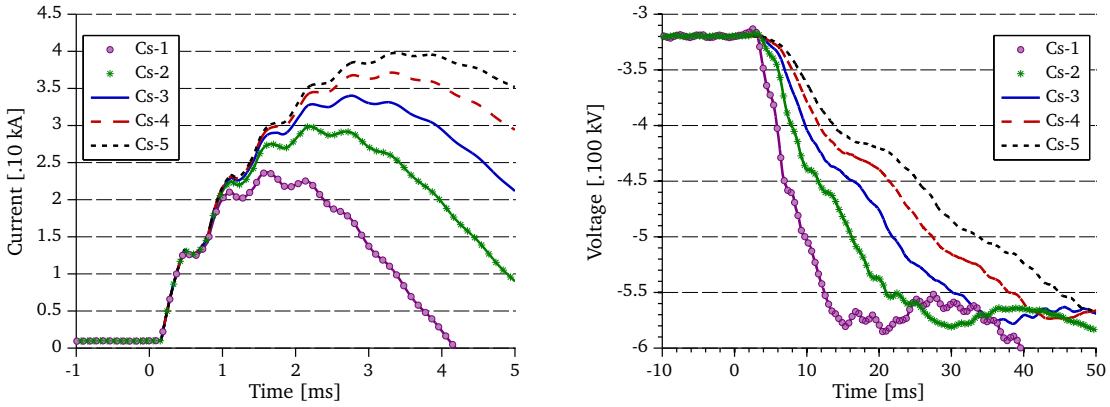

(a) Currents I_{12}^{+} (b) Voltages V_{12}^{-}

Figure 4.10: Signals measured at left cable end for several DC capacitor values

2.2.2 Smoothing reactor

Again, five cases are tested. The values of L_s are shown in Tab.4.7.

Case name	$L_s\,[mH]$
$\mathscr{C}_{Ls-1}$	10
$\mathscr{C}_{Ls-2}$	20
$\mathscr{C}_{Ls-3}$	30
$\mathscr{C}_{Ls-4}$	40
$\mathscr{C}_{Ls-5}$	50

Table 4.7: Cases parameters for smoothing reactor influence study

The smoothing reactor is a very interesting element for protection of DC links purposes. Indeed, as explicit as its name is, it smooths the current shape, leading to a smaller maximal current value. The current derivative decreases when the inductor value increases. Nevertheless, it adds to the grid a stored energy that has to be dissipated in case of current breaking process.

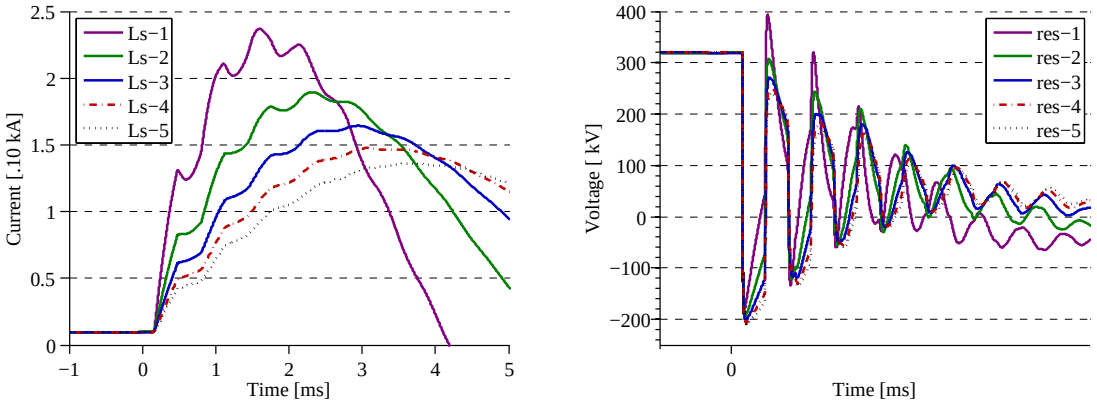

(a) Currents I_{12}^{+}

(b) Voltages V_{12}^{+}

Figure 4.11: Signals measured at left cable end for several DC inductor values

2.3 VSC control strategy

The VSC outer control strategy does not impact the transients since its response time to an event is in the range of 100ms. Several simulations were done using a master slave control, or droop control, and no variations were noticed on the fault signals.

Besides, a master slave control cannot be considered in real application since the loss of the voltage controlled station would lead to a whole DC grid black out. Those aspects are detailed in [Rault, 2013].

3 Grid-related parameters

3.1 Link length

First of all, the link length influence is assessed thanks to the simulation of the HVDC link for two different link lengths. The fault is always at 30% of the total length away station 1. Cases parameters are given in Tab.4.8.

Case name	Link length	$L_{1-fault}$
$\mathscr{C}_{length-1}$	100	30
$\mathscr{C}_{length-2}$	200	60

Table 4.8: Cases parameters for link length influence study

The resulting currents are shown on Fig.4.14b for the left hand side cable end, and on Fig.4.15a for the right hand side end. The wave front arrival time is higher for the 200km long cable since the fault is further for each ends. Also, the current is reduced at the two ends for the same reason, because of the attenuation through the cable length. The transient shape is modified because the reflections do not correspond to the same length, once again.

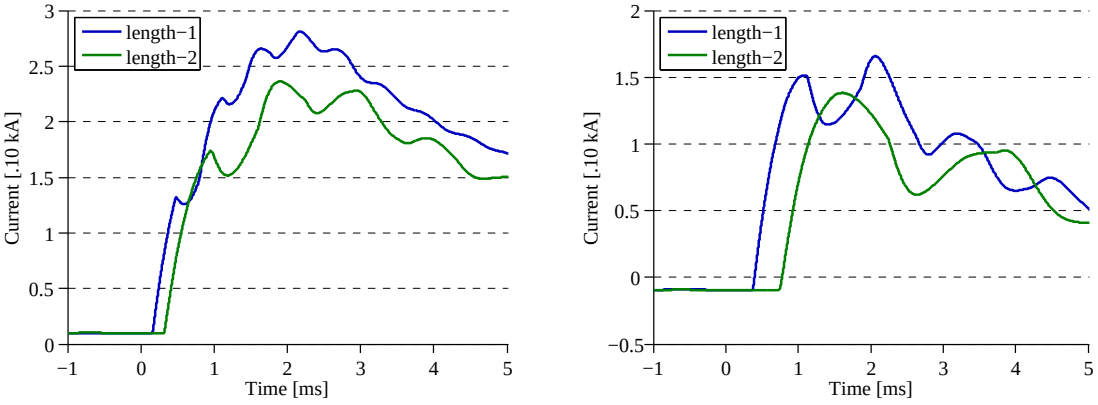

(a) I_{12}^{+} (b) I_{21}^{+}

Figure 4.12: Current measurements for several link lengths

3.2 Grid topology: number of feeders connected to a busbar

Only one feeder was considered from the beginning of the parametric study. The previous tendencies remain valid for any topology, but the number of feeders connected to a busbar has an impact on the signals. This is investigated thanks to the use of two new grid topologies, which are shown on Fig.4.13.

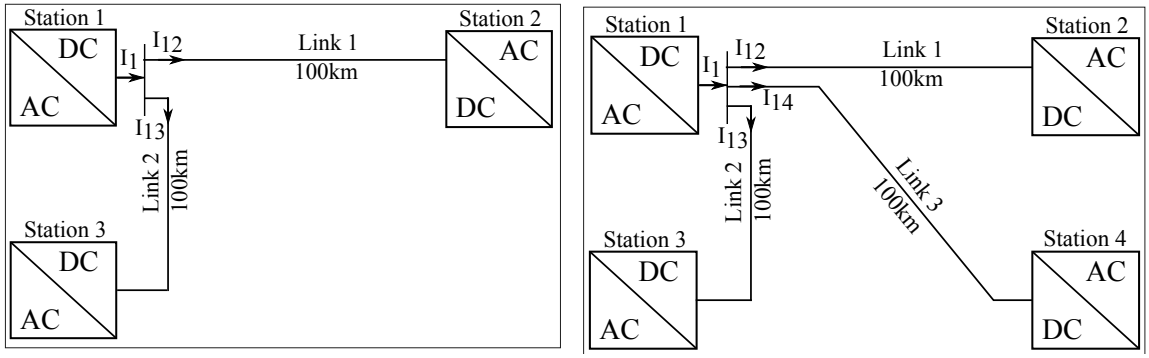

(a) $\mathscr{C}_{\text{topo}-1}$ (b) $\mathscr{C}_{\text{topo}-2}$

Figure 4.13: Grid topologies simulated to study the influence of the number of feeders connected to a busbar

The power reference of station 3 for both cases, as well as the one of station 4 for case $\mathscr{C}_{\text{topo}-1}$, are set to 0W. The results are shown on Fig.4.14, which represents the current flowing through the sensors I_1 and I_{12}, and Fig.4.18 which represents I_{13} and I_{14}.

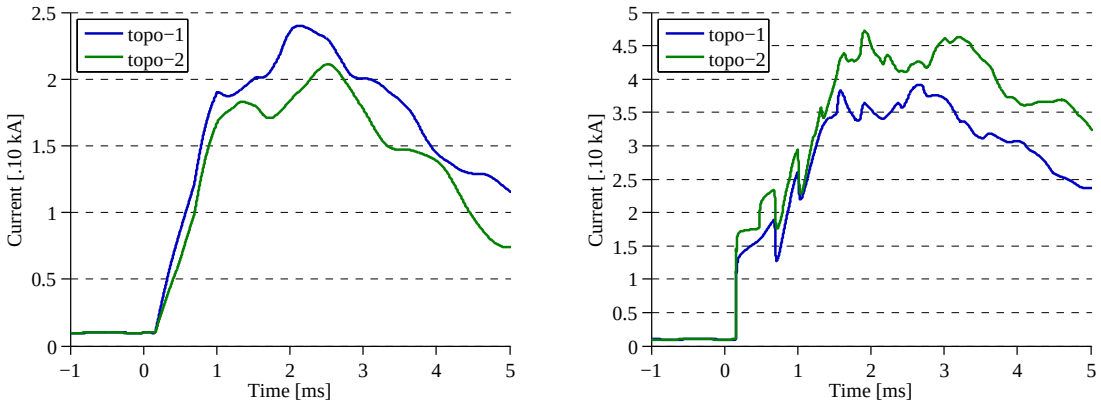

(a) Station connection point I_1 (b) Cable end I_{12}

Figure 4.14: Current measurements

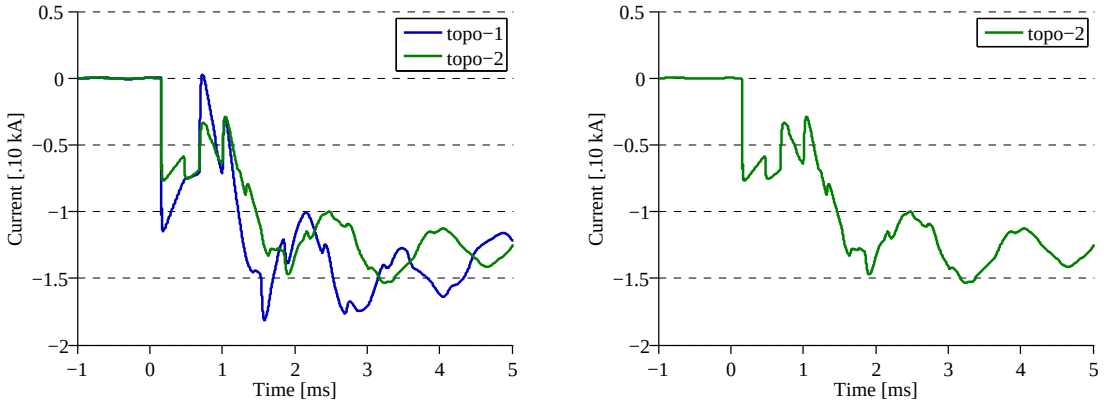

(a) Cable end I_{13} (b) Cable end I_{14}

Figure 4.15: Current measurements

The current measurements at the station connection point I_1 are smaller when 3 feeders are connected to the busbar. This is due to the contribution of station 4, which is not done by station 1. However, the current I_{12} is higher when 3 feeders are connected. That is because more cables are connected, and thus the capacitive discharge effect creates a higher current flowing to feed the fault.

Note that for the case $\mathscr{C}_{\text{topo}-2}$, since Link3 and Link4 are exactly the same cables (100km long, connected to a station of the same power reference), the currents I_{13} and I_{14} are exactly the same.

3.3 Feeder junction

The TWENTIES grid test case was used to test the feeder junction composition. The idea is to show the influence of the incorporation of inductors near each cable end relay, as shown on Fig.4.16.

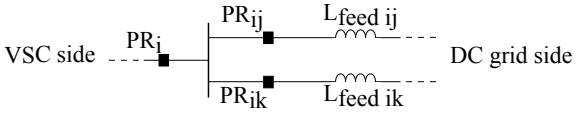

Figure 4.16: Feeder inductors location

A pole-to-pole fault was simulated near relay PR_{21}, as illustrated on Fig.4.17.

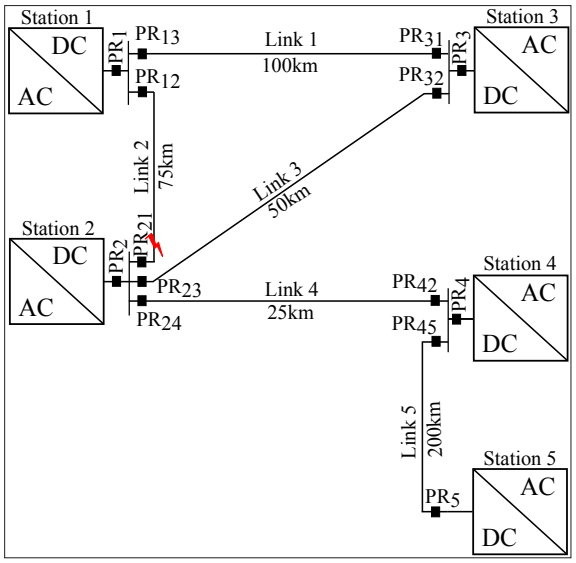

Figure 4.17: Simulation of a fault on the TWENTIES grid structure

The conclusions that were made about the smoothing reactor (cases $\mathscr{C}_{\mathrm{Ls-i}}$, $i = 1..5$) on the HVDC link are valid for the inductors L_{feed}, meaning that the current is smoothed (Fig.4.18). Moreover, this inductance has the advantage of reducing the current (due to cable capacitor discharge) arriving to the converter (like the DC filter smoothing reactor), but also to decrease the current created by the cable discharge, arriving to the relays.

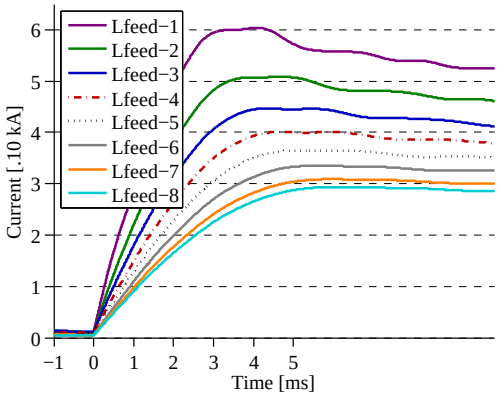

Figure 4.18: Current I_{21}

The parameters influence on the first current transients following the fault even are recapitulated in Tab.4.9.

Kind-related	Parameter	$t_{arrival}$	$\frac{dI}{dt}$	I_{max}
Fault	Location ↗	↗	↘	↘
	Impedance ↗	→	↘	↘
Sources	C_s ↗	→	→	↗
	L_s ↗	→	↘	↘
Grid	Link length ↗	↗	↘	↘
	Number of feeders ↗ - from station vue	→	↘	↘
	Number of feeders ↗ - from cable end vue	→	↗	↗
	Feeder inductor ↗	→	↘	↘

Table 4.9: Parameters influencing the signals behavior

The perturbation arrival time does not imply any modification, either for the protection algorithms, and for the converter station withstand capability, since the fault impacts an element only when this one already propagates to the considered element. At the opposite, if the current derivative increases, it implies that a given current value would be reached quicker, which lead to a smaller required protection operation speed. This will be detailed at the beginning of Chapter 5. Finally, when the maximal current takes larger values, that means that the breakers may have to break such large values. Thus, modifying the parameters in order to decrease the maximal current values might be a viable solution for some cases. This will be discussed at the end of Chapter 6.

Other phenomena were found, such as the different shape of the reflections depending on the fault location. This implies that the transient shape itself is influenced by the fault parameters, which implies that the protection plan, once proposed, needs to be validated by numerous fault cases simulations. This validation process will be presented in Chapter 6.

CHAPTER 5

Protection strategy

Chapter 5

Protection strategy

This part deals with the protection algorithms that are relevant for a MTDC grid, including main protection and backup algorithms in case of failure or non tripping of the protective relay.

This protection system is specifically designed for a MTDC grid and based on operational experience gained from protection practice of AC grids, meaning that the selectivity is ensured thanks to the use of DC circuit breakers located at each cable end and at each station connection point.

This work was conducted considering each converter of the grid as a two-level VSC. The generalization of the proposed protection plan for other conversion technologies will be discussed in the conclusion of this thesis.

First of all, the specification and the constraints related to the protection operation of a DC grid will be presented. Then, the protection plan will be developed. A busbar protection will be described, and two algorithms will be chosen for the cable protection, one with a communication assumption, and another one without any data exchange with other relays. Then, a backup principle in case of a breaker failure will be detailed, and the global protection system is summed-up at the end of the chapter.

1 Protection plan specification

A protection system is used to protect an electrical circuit and its users against damage. This thesis focuses on the protection against short-circuit faults, due to insulation breakdown. This phenomenon translates into a low or high impedance fault, and between pole and ground (PG) or pole and pole (PP). The protection plan has to handle all the possibilities, and must have the following properties defined in [Ghandhari et al., 2011]:

- **Sensitivity**: The protection system has to detect any fault occurring in the DC part of the grid, meaning either low impedance faults and high impedance faults. Following the example of the AC protection strategy, it is not necessarily the same algorithm which is used depending on the fault impedance.
- **Selectivity**: The protection system should only operate after a fault (not during normal operation), and only if the fault is in its own coverage domain. Several coverage domains can be defined depending on the level of the protection (main, backup).
- **Speed**: The protection system should be fast enough to interrupt faults before they may damage equipment or can no longer be interrupted by the breakers.
- **Reliability**: A good protection system is reliable and has a backup system in case the primary protection system or a breaker fails.
- **Robustness**: The protection system should have the ability to detect faults in normal mode as in degraded mode, and to discriminate faults from any other operation occurring (set-point changes, operations, ...).
- **Seamless**: After the fault clearance, the remaining part of the system should continue operating in a secure state. This means that the system itself can accept the transients generated by the fault and its clearing process, and that the protection system will remain stable during the transient implied by the clearing process.

The speed, the sensitivity and the selectivity constraints will be detailed in section 2.1, 2.2 and 2.3 respectively. The reliability is the subject of section 4 which defines the backup protection principle. The robustness to any operation point of

the grid is directly taken into account in the protection algorithms, since they use variables that do not depend on the set operation point. Finally, the seamless is verified in Chapter 6, section 2.

2 DC grid constraints

2.1 Grid components perturbation withstand capability

First of all, the aim of the protection scheme is to guarantee that no component of the grid (except for the faulty one) will be damaged by the overcurrent generated by the fault. This constrains the required operation speed of the protection system, which depends on the components withstand capability to perturbations. Indeed, the protection system needs to clear an eventual fault before the currents and voltages reach the withstand capability of the components.

As developed in chapter 4, a fault creates overcurrent and undervoltage waves, traveling through the whole DC grid. As the undervoltage is an issue for the control of the VSC (loss of controlability when the voltage is below 50 % of the nominal voltage), it does not damage the components of the grid. The controllability can be restored after the fault clearance. At the opposite, the huge overcurrent generated by the capacitive discharge of the cables and the DC filters to feed the fault is a problem for the converters, and especially for the anti-parallel diodes which cannot withstand this kind of current values. The current flowing through those diodes must not exceed twice the nominal current, as specified in the IGBT modules datasheet composing the converters of the INELFE link [Mitsubishi, 2009]. Fig.5.2 shows this constraint. The resulting measurement of the current flowing through the diodes, for the simulation of a fault on the HVDC link using default parameters (given in Chapter 4, Tab.4.2 page 82 and reminded on Fig.5.1) are shown on Fig.5.2b.

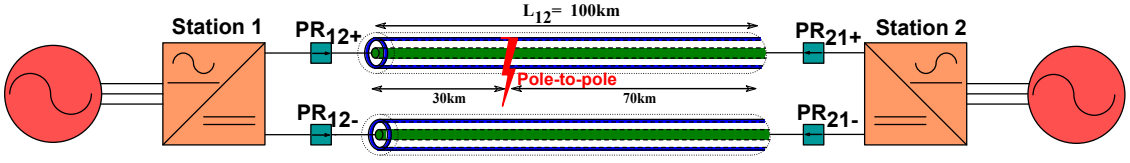

Figure 5.1: HVDC link simulation under default fault conditions

The current related to station 1 exceeds the critical value only 2.865ms after

the fault occurrence. This means that in this case, the fault has to be cleared in less than 2.865ms, which is an extremely small time value considering the usual AC protection clearing time (in the range of 100ms). Note that the IGBTs are not constrained since they are controlled and maintained open thanks to the internal VSC control during the fault.

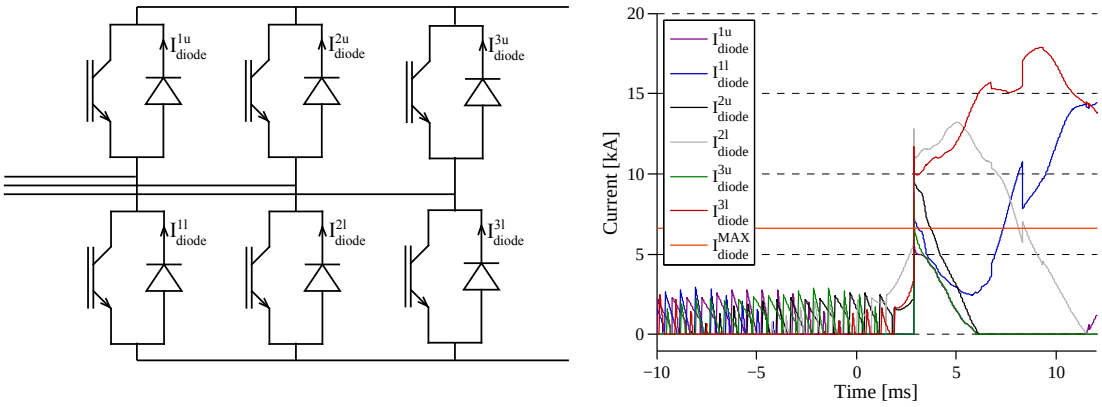

(a) Current sensors (b) Current measurements

Figure 5.2: Current flowing through the diodes of station 1

This time constraint, 2.865ms, is of course not a constant value. It depends on the grid structure, on the fault characteristics and on the operation point at the fault occurrence time. As an example, Fig.5.3 shows the time constraint as a function of the fault position, meaning the time when the current flowing through the diodes exceeds twice the nominal value for the cases $\mathscr{C}_{\text{pos}-\text{i}}$, with $i = 1..5$ defined in Chapter 4 page 85. The constraints related to the two converters are displayed.

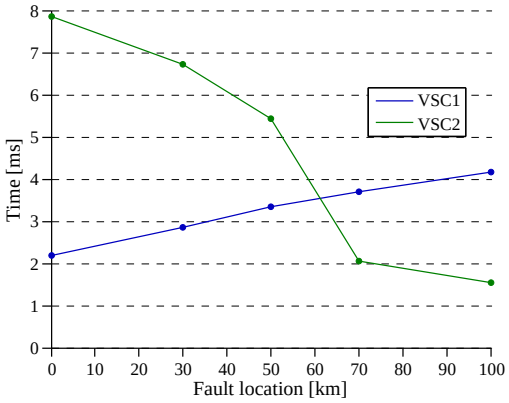

Figure 5.3: Diode constraint for several fault locations on HVDC link test case

The maximal allowed clearing time for each fault case is defined by the minimum

of the two values (minimum of the two curves). First, on Fig.5.3, the jump between 50 and 70km for the green curve corresponding to VSC2 is justified by the fact that the maximal diode current constraint is reached at the first front. This first front can be observed on Fig.5.3 for a particular case. For fault locations further than 50km, the first front was below 6kA, that is why the time values on Fig.5.3 are higher.

Then, the intuition would link to think that for a symmetrical system, the time constraint would be the same for the two sides of the grid. However, for the pole-to-pole fault at the middle of the link, which is the fault test case $\mathscr{C}_{\text{pos}-3}$, the time constraint is shorter for the converter of the right side, meaning VSC2. This is due to the fact that there is a current flowing through the link. Indeed, the current measurement at PR_{12+} before the fault occurrence is the opposite of the one measured at PR_{21+}, as shown on Fig.5.4. Thus, when the fault arrives at the current sensors of both ends, the current increases. The relative current rise is the same at both ends, but considering the current initially flowing through the link, the absolute maximal value is not the same. This explains why the constraint is reached earlier at the diodes of VSC2 for this particular case. This later phenomenon highlights the influence of the operation point before the fault on the maximal clearing time allowed to ensure the system reliability, since, the protection plan must be valid for an operation points range.

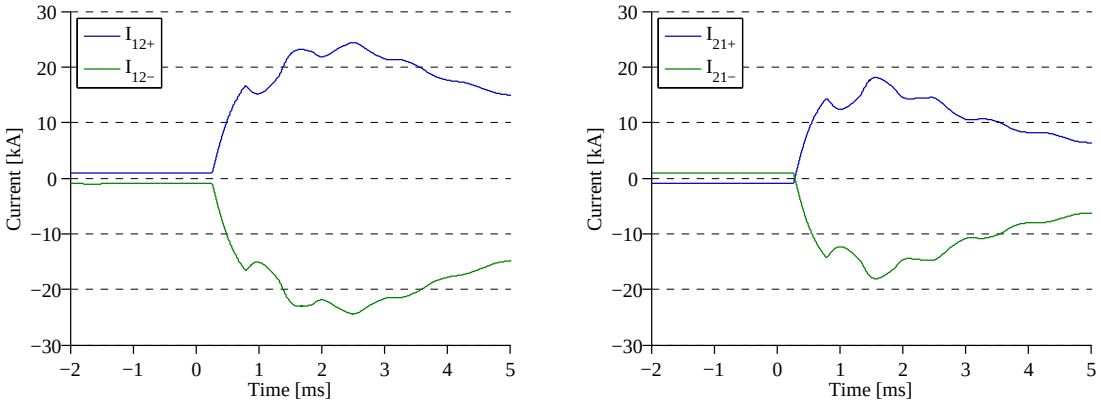

(a) At VSC1 terminals

(b) At VSC2 terminals

Figure 5.4: Current measurements at DC cables end for fault case $\mathscr{C}_{\text{pos}-3}$

To generalize, Tab.5.1 summarizes the influence of each component (the same as in Chapter 4) on the maximal allowed clearing time. For example, the time

constraint tends to increase (↗) when the parameter L_s increases. This means that there is more time to clear the fault if the DC filter inductance is higher. The fault location cannot be included in this table, since distance from a fault to a converter station increases, it means that this same fault becomes closer to another converter station.

Parameter	Tendency	Time constraint tendency
Fault type	PG → PP	↘
R_{fault}	↗	↗
S_{sc}	↗	→
C_s	↗	↘
L_s	↗	↗
L_{feed}	↗	↗
N_{feed}	↗	↗

Table 5.1: Parameters influence on the time constraint tendency

Considering this short time constraint, which is in the range of 5ms, the cables withstand capability to overcurrents does not limit the maximal clearing time. Indeed, XLPE cables can usually withstand short-circuit currents up to 60kA for half a second [Nexans, 2013], which is a lot higher than the diodes current withstand capability. The only thing to consider for the cables is the overloading case, namely when a fault in a meshed part of the grid is cleared and thus the power initially flowing in the faulty cable is re-dispatched to other links. The non-overload cable verification is not the responsibility of the protection plan but the dispatching center.

In this chapter, the current breaking capability of the breakers is not considered as a constraint. The protection system will be built in order to send a tripping order to the breakers as quickly as possible, and especially before the VSC diodes constraint is reached. Then, the required current breaking capability considering the proposed protection system will be assessed and discussed in Chapter 6.

2.2 Sensitivity constraint

A set protection principle is able to detect faults up to a certain impedance value. For a given protection principle, this maximal impedance value depends obviously

on the grid structure and the set thresholds associated to the protection principle. The proposed protection plan performances, in terms of maximal fault resistance detection, will be detailed in Chapter 6. However, the goal of this current chapter is to develop a protection system sensitive enough to cover faults with impedance included in the range $0 - 200\Omega$. This value was defined considering the TSO's experience feedback which points out that faults with a resistance higher than 200Ω are extremely rare in underground cables. However, the higher the maximal fault impedance detected by the protection plan is, the higher are its performances.

2.3 Selectivity constraint

Besides the diode current withstand capability constraint, the fault needs to be cleared before the internal protection of the VSC disconnect the station from the DC grid. Indeed, the substations are equipped with internal protective devices to ensure their safety. However, the protection plan must act before the internal VSC protection in order to guarantee the selectivity. These VSC internal protection principles were provided by RTE for the SIEMENS converters used in the INELFE HVDC link, but since they are confidential, they are not displayed in this thesis. However, both criteria are combined with a temporization delay, which is included in a range starting from 5ms up to 100ms, depending on the criterion. Hence, those internal protective principle would act after the main protection that will be proposed in this chapter.

Otherwise, the protection plan algorithms have to be selective (at least for the main protection algorithm), meaning that only the breakers located at the terminals of the fault element have to trip, and no unwanted trippings are allowed. This means also that the protection must not trip during an event resulting from a normal operation of the grid, such as a power transfer variation or a connection/disconnection of a cable. The robustness to power reference variation will be dealt with considering each protection principle on a case by case basis, when choosing the thresholds. The verification of the healthy state of a cable during the connection of a link process will be treated in section 5.

Moreover, the AC grid protection should not respond to a DC fault, if this later one is cleared by the DC protection systems. This last requirement is assumed to be checked given the large difference in the response time of both protection system.

2.4 Protection chain operation time

Based on these assumptions, the clearing process of a fault has to be performed in a very short time (in the range of 5ms), including the time to detect the fault, to discriminate between the faulty and healthy parts of the grid and the current breaking process time of the DC circuit breakers. This is illustrated on the time-line displayed on Fig.5.5.

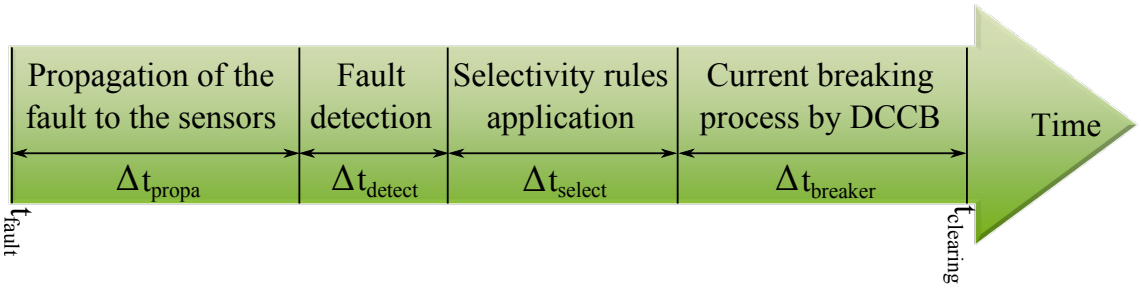

Figure 5.5: Time-line of the fault clearing process

Considering this time constraint, and the fact that the fault steady-state is reached much later, the conclusion is that the fault has to be cleared during the transient phase of the signals. This contributes to the fact that no AC grid protection principle can be duplicated without adapting it, and that traveling wave based protection principles have to be developed.

This chapter will investigate only the detection and the selectivity rules applications, since the propagation of the fault to the sensors is the response of the grid, so there is no element that can act on this, and since the DC breaker is not the scope of this Ph.D work, but under prototype process by Alstom Grid, in the framework of the TWENTIES project.

3 Main protection

In this part, the plausible principles for a main protection are investigated. They must fulfill the constraints explained in the previous part. In the rest of the chapter, the TWENTIES grid model (see Chapter 3 page 76 for grid structure) will be used for simulation examples, except other mention.

3.1 Preliminary signals analysis

As mentioned in Chapter 3 section 4.1.2, one protection relay is composed of a current sensor, a pole-to-ground voltage sensor and a DC breaker. The only information the relay has comes from those elements. The first intuition is to use overcurrent and undervoltage protection principles. Two fault types are used here, and are defined in Tab.5.2.

Case name	Type	Link	Location	R_{fault}
$\mathscr{C}_{int}$	Pole-to-ground	Link1, positive pole	30km away Station1	10Ω
$\mathscr{C}_{ext}$	Pole-to-ground	Link3, positive pole	Near Station3	1Ω

Table 5.2: Internal and external fault cases

Note that the current and voltages displayed here take into account the sensor effects.

3.1.1 Polarity selectivity

As mentioned in Chapter 1, a pole-to-ground fault may require the tripping of both healthy and faulty poles, which is the case considering the TWENTIES grid implementation used in this thesis. However, the polarity selectivity does not present any problem since the difference between the faulty pole and the healthy pole can be done using a simple overcurrent principle, as shown on Fig.5.6 for the fault case $\mathscr{C}_{int}$. The very low fluctuations on the healthy pole current are due to the coupling effect between the two poles.

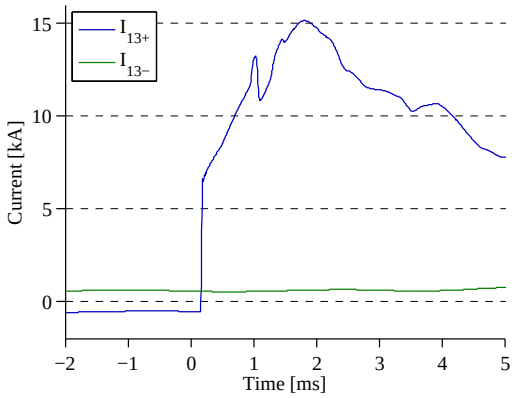

Figure 5.6: Current measurement at PR_{13+} and PR_{13-} for $\mathscr{C}_{\text{int}}$

3.1.2 Link selectivity

Fig.5.7 illustrates the information available at PR_{13} for the two fault types.

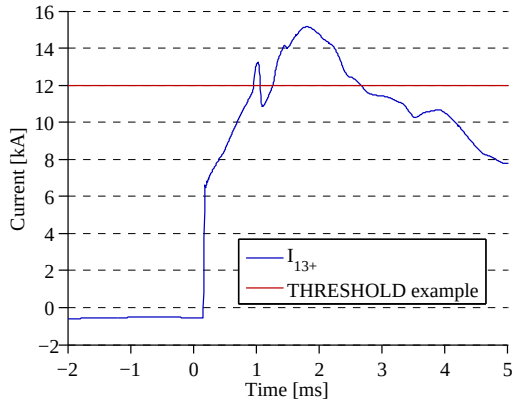

(a) $\mathscr{C}_{\text{int}}$ current

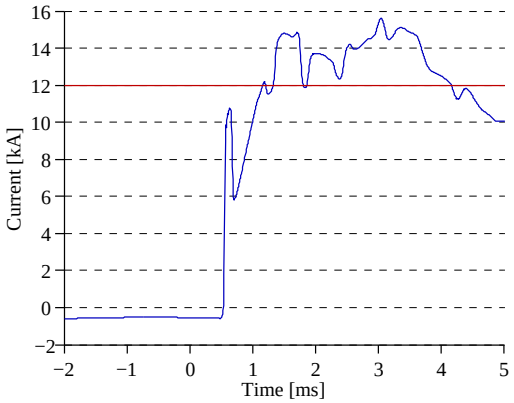

(b) $\mathscr{C}_{\text{ext}}$ current

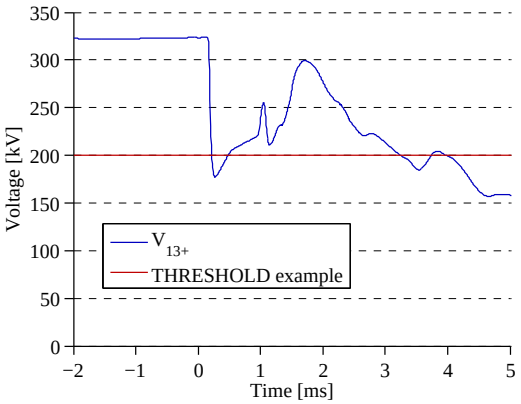

(c) $\mathscr{C}_{\text{int}}$ voltage

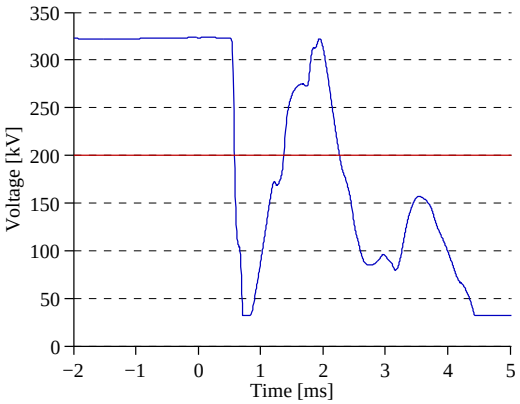

(d) $\mathscr{C}_{\text{ext}}$ voltage

Figure 5.7: Measurements at PR_{13+} for an internal and an external fault

Reminder

Fault $\mathscr{C}_{\text{int}}$ has to be cleared by PR_{13} and PR_{31}.
Fault $\mathscr{C}_{\text{ext}}$ has to be cleared by PR_{32} and PR_{23}.

This analysis shows that overcurrent and undervoltage principles cannot fulfill the selectivity requirement. Indeed, the protection relay PR_{13+} must trip only for the fault case $\mathscr{C}_{\text{int}}$. To do so, a current or voltage threshold has to be exceeded less than around 5ms after the fault (occurring at t = 0ms) to respect the converter diodes current withstand capability. Current and voltage thresholds examples are displayed on Fig.5.7a and 5.7c (12kA and 200kV respectively). They were chosen arbitrarily to fulfill the requirements. In $\mathscr{C}_{\text{int}}$ case, the protection would trip for a fault in its protective zone. However, using those threshold values in the case $\mathscr{C}_{\text{ext}}$, this same protection would trip for an external fault, as shown on Fig.5.7b and 5.7d. This is due to the fact that there is not enough mitigation between the current and voltages of two cables, due to the low resistivity of the DC links. The same conclusions can be made considering the current and voltage derivatives that are given in Fig.5.8. The derivatives are evaluated thanks to (5.1) with a sampling frequency $\Delta t = 10\mu s$.

$$\frac{dI_{13+}}{dt}(t) = \frac{I_{13+}(t) - I_{13+}(t - \Delta t)}{\Delta t} \tag{5.1}$$

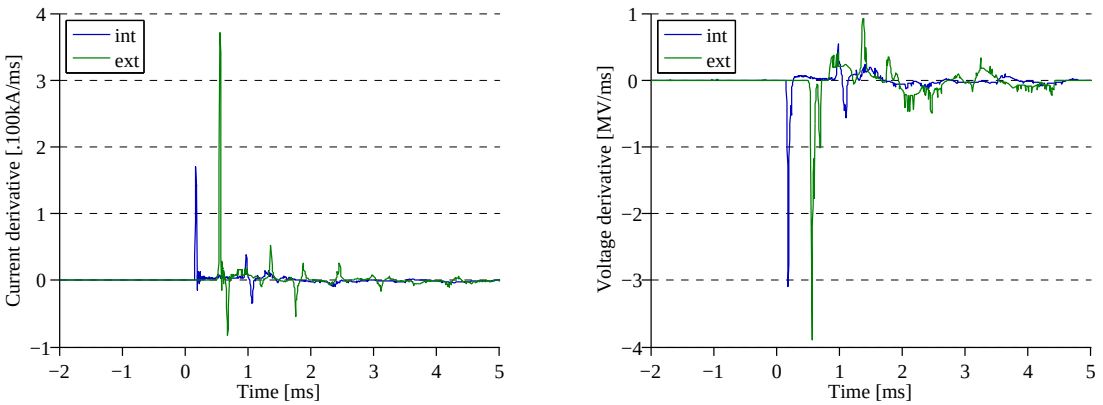

(a) Current derivative

(b) Voltage derivative

Figure 5.8: Current and voltage derivatives at PR_{13+} for $\mathscr{C}_{\text{int}}$ and $\mathscr{C}_{\text{ext}}$

Using simple principles, the only difference between the two cases resides in the

fault arrival time, which depends on the fault location. Even so, a protection relay does not have this kind of information since it does not know the exact fault occurrence time, but only has the time of arrival of the first front transient. Consequently, other trials has to be investigated.

3.2 Possible trails

Two possibilities can be investigated:

- the use of communication between some of the protection relays, or
- the recourse to more complex signal processing methods.

A more complex signal processing method could be considered, using the reflections that are in the signals or a wavelet-based principle. This kind of signal processing will not be investigated as a main protection principle as it requires a large computation time, which is prohibited by the required protection operation speed. Besides, it requires an exact knowledge of the grid and is highly influenced by the imperfections of the components. It however will be mentioned in appendix A2 as a possible backup principle since it has been studied during this Ph.D work.

The communication between some of the protection relays would allow a better knowledge of the situation since it enables a given relay to access to signals concerning several points of the grid. The variables that can be exchanged could be the current or voltage measurements, their sign, or the time when a criterion has been validated.

As it seems to be the most suitable lead, a communication is considered for the main protection principle. The communication can be at the busbar level or at the cable level, as shown on Fig5.9.

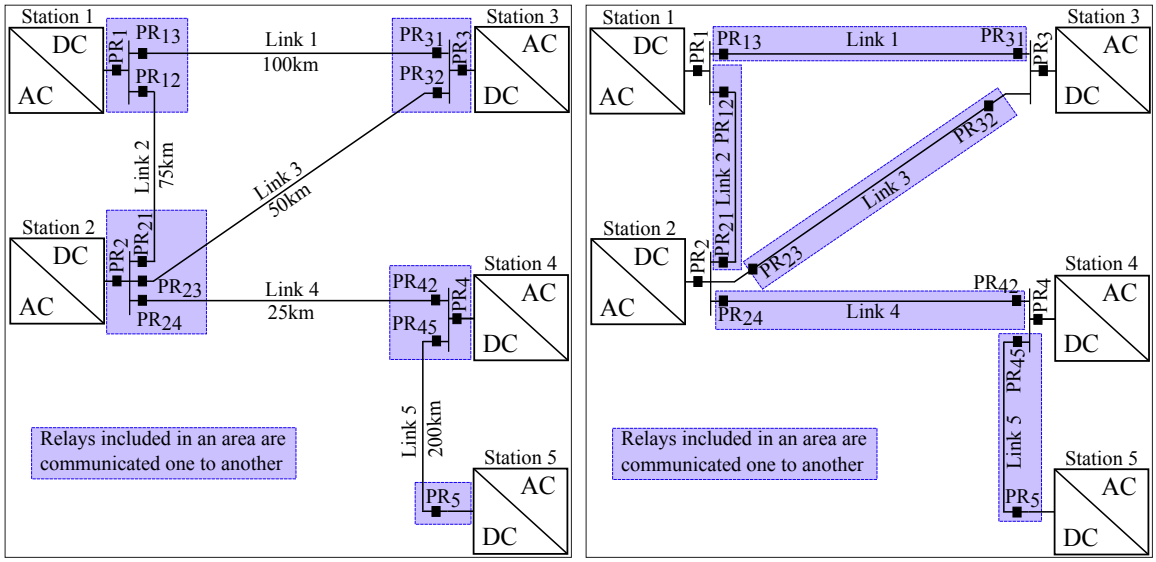

(a) Busbar level (b) Cable level

Figure 5.9: Communication strategies

As mentioned in section 3.1.1, the polarity selectivity can be ensured thanks to simple principles, but since the two poles of a given location need to trip, even for a pole-to-ground fault, the communication includes relays of both positive and negative poles of the considered area. So on Fig.5.9a, for busbar connected to Station 5, PR_{5+} and PR_{5-} are communicating together.

3.3 Busbar-level communication

3.3.1 Cable protection

If a busbar-level communication strategy is used for the protection of cables, this would lead to the following principle for a given cable end relay, named generically PR_{ij}.

PR_{ij} has the information of current and voltage measured at PR_i and PR_{ik} (if only 2 feeders are connected to the busbar). Given those information, the relay has two answer the following questions:

1. Is the fault located on a cable connected to the busbar i ?

2. If the answer is yes, is fault located to the cable connected to the feeder ij ?

For the same reasons than developed in section 3.1.2, namely the lack of mitigation between the signals of different geographical grid points, those questions were not solved using quite simple criteria. The corresponding curves showing the difficulty to discriminate between an internal and an external fault are displayed and commented in Appendix A1.

Consequently, a busbar-level communication strategy is not kept for the main cable protection. Nevertheless, it is suitable for protection against faults occurring inside the busbar zone. This is the aim of the next section.

3.3.2 Busbar protection

The busbar-level communication strategy is useful for busbar faults (Fig.5.10). It enables to take advantage of a really simple protection criterion, namely the busbar current differential, which is a direct application of the Kirchhoff node law.

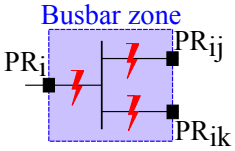

Figure 5.10: Busbar fault illustration

The busbar current differential variable is defined by (5.2), where nf is the number of feeders connected to the busbar.

$$I_{bus}(t) = \left| I_i - \sum_{j=1}^{nf} I_{ij}(t) \right| \tag{5.2}$$

The protection principle is given by equation (5.3), where I_{busTH} is a set threshold value.

$$\left.\begin{array}{rlcll} \text{If} & I_{bus}(t-2\Delta t) & > & I_{busTH} & \\ \text{AND if} & I_{bus}(t-\Delta t) & > & I_{busTH} & \\ \text{AND if} & I_{bus}(t) & > & I_{busTH} & \end{array}\right\} \; Trip$$
$$\text{Else} \qquad\qquad\qquad\qquad\qquad\qquad\qquad\qquad\qquad\qquad \text{Stand By} \tag{5.3}$$

The principle is applied on both positive and negative poles. As there is no element between the sensors, any purely positive threshold value I_{busTH} is theoretically

applicable. However, this threshold has to take into account the uncertainties of the sensors measurements. The numerical application will be addressed in Chapter 6.

3.4 Cable-level communication

The cable-level communication strategy was illustrated on Fig.5.9b. This is achieved by using a telecommunication link (optical fiber) set up in parallel of each power cable. The optical fiber way was chosen since it is the fastest way, with a propagation speed of the data of 200km/ms (this value was provided by RTE experts). A GPS synchronisation of the data is also assumed. Hence, each feeder relay exchanges its own information with the opposite cable end relay. Considering that fact, several algorithms can be implemented for the cable protection. Two of them are developed below.

3.4.1 Cable differential protection

This principle is the easiest one, in terms of computation time and robustness. It is based on the evaluation of the cable differential current, and is adapted to the dynamics of the signals under fault conditions in DC grids.

Given the current sensors orientation defined in Chapter 3 section 4 page 75, the cable differential current is easily evaluated thanks to equation (5.4). It is computed at each cable end relay, and its inputs are the current measured at the same time at each end of the considered cable. The differential current $\mathrm{I_{dij}}(t)$ evaluated by $\mathrm{PR_{ij}}$ takes into account the delay $\Delta \mathrm{t_{OFpropa}}$ the relay needs to wait until it receives the current data of the opposite cable end. Hence, when the relay $\mathrm{PR_{ij}}$ receives at time instant t the current measured at the opposite end, noted $\mathrm{I_{ji}}(t)$, it corresponds to the current flowing through the cable end ji at time instant $(t - \Delta t)$. The differential current is thus written as (5.4):

$$I_{dij}(t) = I_{dji}(t) = I_{ij}(t - \Delta t_{OFpropa}) + I_{ji}(t) \tag{5.4}$$

The delay $\Delta \mathrm{t_{OFpropa}}$ is the same at both cable ends since the relays are GPS synchronized and because the current measurements data are horodated. Thus, for a considered relay $\mathrm{PR_{ij}}$, the current value $\mathrm{I_{ij}(T_1)}$ is available at a time instant t. However, the current value $\mathrm{I_{ji}(T_1)}$ required to compute the differential current $\mathrm{I_{dij}(T_1)}$ is

received after the propagation delay, at $t + \Delta t_{OFpropa}$. Thus, the differential current $I_{ji}(T_1)$ can be evaluated only at $(t + \Delta t_{OFpropa})$, even though $I_{ij}(T_1)$ was available earlier.

As said earlier, the propagation speed of the data through the optical fiber is assumed to be 200km/ms. This gives a $\Delta t_{OFpropa}$ for each link of the TWENTIES grid structure detailed in Tab.5.3.

Link	Link length	$\Delta t_{OFpropa}$
Link1	100km	500µs
Link2	75km	375µs
Link3	50km	250µs
Link4	25km	125µs
Link5	200km	1ms

Table 5.3: Propagation delay of the data through the optical fiber

This later phenomenon is described on Fig.5.11 which represents the currents measurements at the faulty cable ends and the computed differential current for a the fault example $\mathscr{C}_{\text{int}}$ which is on Link1.

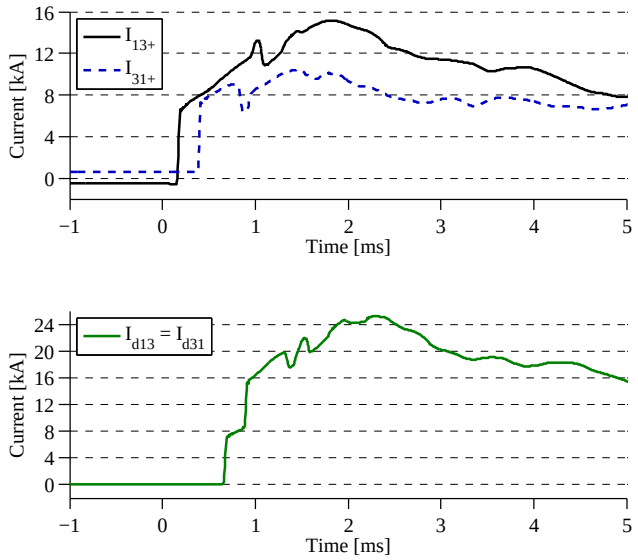

Figure 5.11: Data propagation delay on the differential current

The differential current acts as described chronologically in Tab.5.4 for a given relay.

Phenomenon	Faulty link	Healthy link
Fault occurence	$I_{dij} \approx 0$	$I_{dij} \approx 0$
Arrival of the first wave front to relay the closest from the fault	$I_{dij} > 0$	$I_{dij} < 0$
Propagation of the fault perturbation to the rest of the grid	Transient	Transient
Fault steady-state	$I_{dij} > 0$	$I_{dij} \approx 0$

Table 5.4: Differential current behavior under fault conditions

The selectivity of the cable differential current is obvious during the fault steady-state: the only link the differential current is not equal to zero is the faulty link. Otherwise, the differential current is positive. However, the protection operation time constraint does not permit to wait until this steady-state, as first mentioned in Chapter 2. The basic differential current principle is thus modified to become a traveling wave-based criterion, which takes into account the transient behavior of a DC grid under fault conditions. Fig.5.12 shows the transient behavior of the cable differential current for the fault case $\mathscr{C}_{\text{int}}$ defined in Tab.5.2 page 109. Both a faulty link (Fig.5.12a) and a healthy link (Fig.5.12b) are represented.

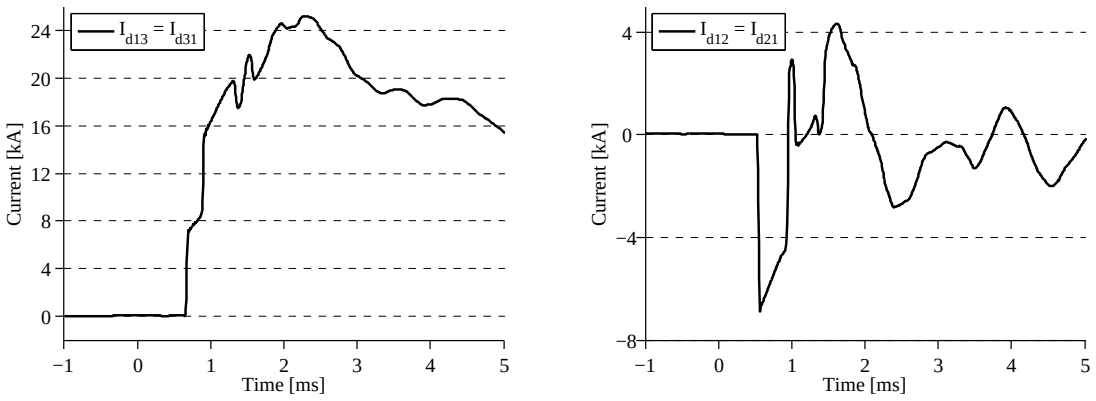

(a) Faulty link (b) Healthy link

Figure 5.12: Transient behavior of the cable differential current

The following observations has been noticed on the differential current records of all fault simulations:

- For a faulty link, the first front is always positive.

- For a healthy link, the first front is always negative.

This is due to the fact that for a given link, the traveling wave generated by the fault arrives by the exterior of the link, which discharges (cable capacitive effect), creating a current flowing from the link to the fault. During the short time the traveling wave reached the relay of one end but not the other one, and given the sensor orientation, this is traduced by a negative differential current.

A selective threshold enables the fault detection for the faulty link. If small enough, the threshold is exceeded at the front transient arrival. However, a set threshold could eventually be exceeded in the case of a healthy link, because of the oscillations during the transient part. Indeed, the threshold has to be set small enough to detect quickly faults with resistance up to 100Ω, so if a blank fault occurs, this threshold is smaller than the oscillation magnitude of the differential current.

To avoid unwanted trippings of healthy link protections, a negative threshold is added to detect the first negative front. This negative front defines the fact that the fault is exterior to the link. The over-passing of this threshold will imply the blocking of the tripping order, for a duration time corresponding to the fault clearing process time. Therefore, the selectivity is ensured. The cable differential current protection algorithm is thus defined by equation (5.5), where I_{dTH+} and I_{dTH-} are the positive and negative set thresholds, and Δt_{block} is the blocking time corresponding to the fault clearing time process.

To improve the robustness of the algorithm, a validation of the threshold over-passing of 3 consecutive samples, for both positive and negative threshold, is added.

$$\begin{array}{rlcll}
\text{IF} - -- & I_{dij}(t-2\Delta t) & > & I_{dTH+} & \left.\begin{array}{l}\\\\\end{array}\right\} \\
\text{and if} & I_{dij}(t-\Delta t) & > & I_{dTH+} & \left.\begin{array}{l}\\\\\end{array}\right\} \text{Trip} \\
\text{and if} & I_{dij}(t) & > & I_{dTH+} & \left.\begin{array}{l}\\\\\end{array}\right\} \\
\text{ELSE IF} & I_{dij}(t-2\Delta t) & < & I_{dTH-} & \left.\begin{array}{l}\\\\\end{array}\right\} \\
\text{and if} & I_{dij}(t-\Delta t) & < & I_{dTH-} & \left.\begin{array}{l}\\\\\end{array}\right\} \text{Block for } \Delta t_{block} \\
\text{and if} & I_{dij}(t) & < & I_{dTH-} & \left.\begin{array}{l}\\\\\end{array}\right\} \\
\text{ELSE} - - - - - - - - - - - - - - - - & & & & \text{Stand By}
\end{array} \tag{5.5}$$

This algorithm can be implemented in each protection relay, on both positive

and negative pole. The only difference between the positive and the negative pole algorithm resides in the thresholds sign that are inverted due to the polarity reversal. However, in the present case, if a pole is faulty, the protection of both positive and negative pole of the cable ends trip thanks to the communication as mentioned in section 3.2. For pole-to-pole faults, the differential current of both poles exceed the threshold.

The positive and negative thresholds do not necessarily have the same value. Theoretically, any positive threshold taking into account the sensors uncertainties enables the detection. The negative threshold need to be small enough to be overpassed to ensure the selectivity. The smallest the threshold are, the fastest is the protection clearing process. Thus, they were chosen to detect faults up to 200Ω anywhere in the grid. The numerical applications and validation will be developed in Chapter 6.

In order to be sure that the protection will record the negative front for healthy links, the sampling frequency needs to be at least three times smaller than the propagation time of the fault through the smallest cable. Indeed, if the sampling frequency is higher, the first front will be hidden between two samples, and unwanted trippings may occur. To ensure that the negative front will be validated by 3 samples, for the TWENTIES grid test case, the time step must be less or equal to 43µs (since the propagation of the fault in Link4 of 25km is 129µs). This corresponds to a sampling frequency of 23kHz.

This protection principle requires two different optical fiber links wired in parallel of each power cable to ensure the communication of the current measurement data in both ways.

3.4.2 Directional criterion protection

This principle is also based on the first current wave front. This directional principle takes advantage of the sign of the first current wave front. The physics beyond this criterion is the same than the one beyond the differential current criterion, namely the fact that the first current wave front is positive (considering the sensors orientation defined in this thesis) at each end of faulty link, and only for the

faulty link. The current wave starts with a negative front at one end for any healthy link, due to the propagation phenomenon of a signal through the cables.

The sign of the first wave front can be detected by several principles. In this thesis, the association of the current derivative with a positive or negative threshold is used as defined in equations (5.6), where dI_{TH+} and dI_{TH-} are positive and negative thresholds. The sign values are then exchanged between the relays of the two cable ends.

$$S_{ij}(t) = \begin{cases} 1 & \text{if } \dfrac{dI_{ij}}{dt}(t) > dI_{TH+} \\ -1 & \text{if } \dfrac{dI_{ij}}{dt}(t) < dI_{TH-} \\ 0 & \text{otherwise} \end{cases} \tag{5.6}$$

However, it is extremely necessary to be careful with the propagation phenomenon of the fault, and to only consider the first front, not the other ones following the fault arrival. The current derivative is shown on Fig.5.13 for a healthy link and a faulty link, that corresponds to the same fault condition and the same relays as the ones presented on Fig.5.12 for the differential current illustration.

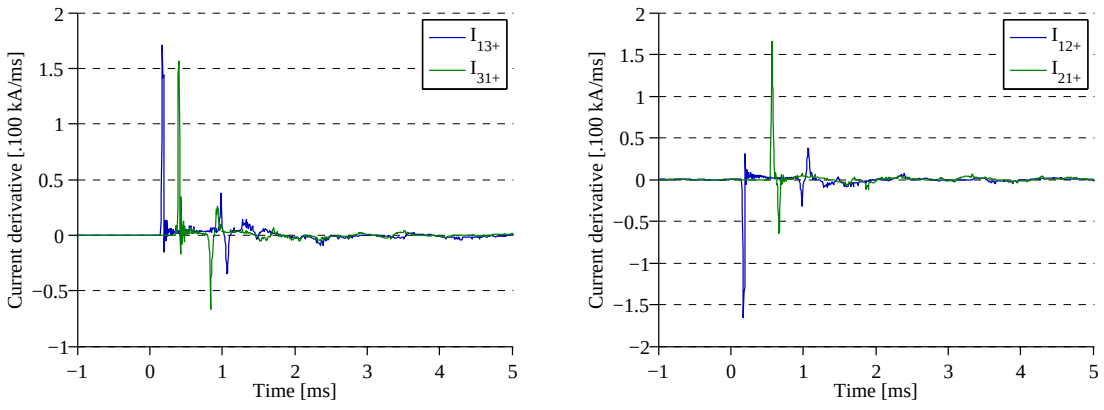

(a) Faulty link

(b) Healthy link

Figure 5.13: Transient behavior of the current derivatives at each end of a cable

As well as the differential current, the selectivity is based on the blocking of the tripping order in case a negative front is detected at one cable end. If not, the other peaks following the first front, related to the reflections of the fault along the cable ends, may exceed the set threshold, and imply unwanted trippings.

The implementation is however more complex than the differential criterion. Indeed, the first one uses only one variable to discriminate between a faulty and a healthy link. Even though this variable (the differential current) is evaluated thanks to several measurements coming from different geographical locations, the choice is done on one signal. At the opposite, the directional criterion requires that the relay verifies two criteria, that may be (in most cases) checked and received at different times. This is explained below on Fig.5.14 for a faulty link and on Fig.5.15 for a healthy link, for the same fault example that was shown on Fig.5.13. The value $\Delta t_{OFpropa}$ is the same than in the previous section, given in Tab.5.3 page 116, and S_{ij} is the sign of the first current wave front.

On the Fig.5.14 example, if the values $S_{13}(t)$ and $S_{31}(t)$ were continuously exchanged between the relays, PR_{13} would receive the information of the positive front, given by $S_{31} = 1$, at a time were S_{13} has already descended to zero. This would result in a non-tripping action of the relays, leading the non-clearance of the fault.

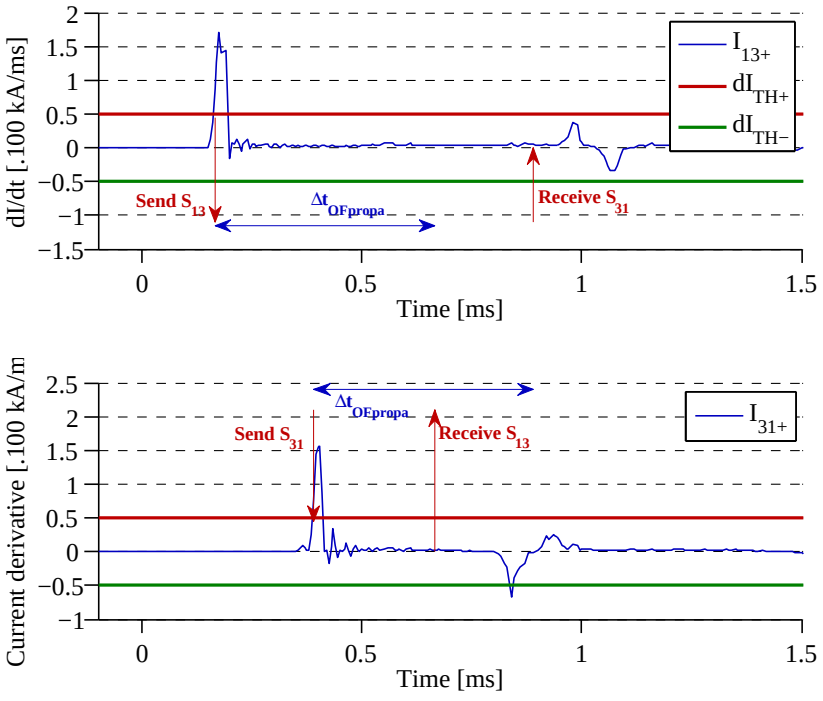

Figure 5.14: Current sign data exchange between two relays of a faulty link

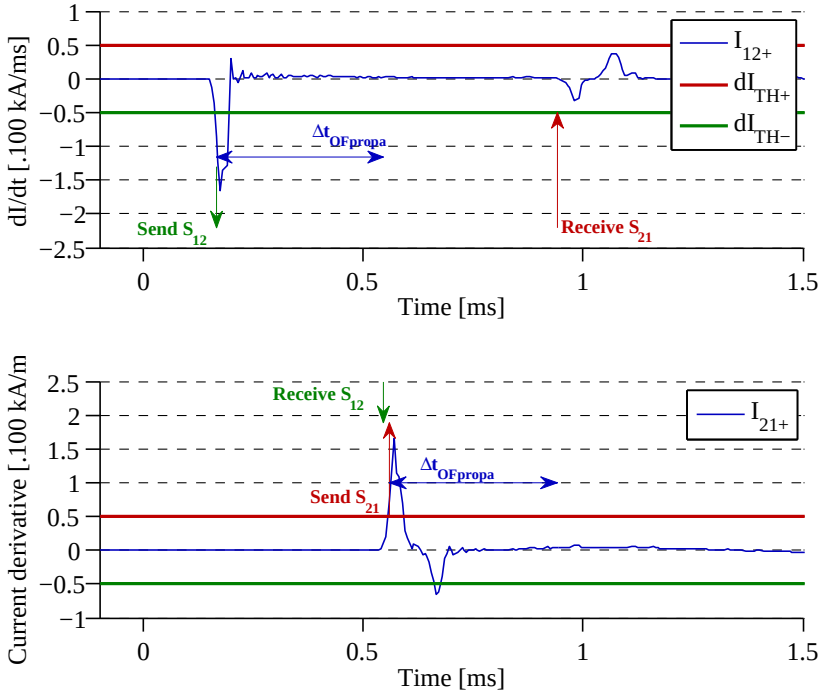

Figure 5.15: Current sign data exchange between two relays of a healthy link

To go beyond this limitation, when detected, the first current wave front sign has to be stored during a duration long enough to allow the comparison of the two cable ends first front signs. The value $S_{ij}(t)$ is consequently send only once, and only if the positive (in red) or negative (in green) threshold has been exceeded. Note that the thresholds shown on the curves are examples, and that the positive and negative ones are not necessarily balanced.

The storage duration should be also longer than the fault clearing process, to make sure that no unwanted trippings would happen in healthy links. The resulting algorithm is explained after defining the variables, thanks to the following equations, for one considered relay PR_{ij}.

Let t_{sign} be the time value corresponding to the detection of the first wave front, and defined such that:

$$t_{sign} = \min_{t} \begin{pmatrix} S_{ij}(t) & = & 1 \\ & or & \\ S_{ij}(t) & = & -1 \end{pmatrix} \tag{5.7}$$

The criterion C_{ij} is evaluated at protection PR_{ij} only if S_{ij} takes the value 1 or -1,

and can then be defined such that:

$$\forall t \in [t_{sign}; t_{sign} + \Delta t_{stop}]\,,\, C_{ij}(t) = \begin{cases} 1 & \text{if } S_{ij}(t_{sign}) = 1 \\ -1 & \text{if } S_{ij}(t_{sign}) = -1 \end{cases} \tag{5.8}$$

where Δt_{stop} is set to correspond to the fault clearing process duration, taken the data propagation delay through the optical fiber into consideration.

The directional cable protection algorithm becomes:

$$\begin{array}{ll} \left.\begin{array}{ll} \text{IF} - - & C_{ij} = 1 \\ \text{and if} & C_{ji} = 1 \end{array}\right\} & \text{Trip} \\ \text{ELSE} - - - - - - & \text{Stand By} \end{array} \tag{5.9}$$

Several cases are included in the ELSE. First, if $C_{ij} = 1$ and $C_{ji} = -1$, or vice-versa, then the link is healthy but a fault is present in the grid. In the differential current protection, the relay was blocked for a duration corresponding to the fault clearing process time. Here, this temporization delay is included in the value of the sign, as defined in equation (5.6). The resulting blocking time is thus equal to the delay Δt_{stop}. Then, there is a low probability to have $C_{ij} = -1$ and $C_{ji} = -1$. This would correspond to the case of a long healthy cable, were the traveling wave generated by the fault arrives to the considered healthy link by both ways, leading the cable to discharge in both directions. Furthermore, the case where $C_{ij} = -1$ and $C_{ji} = 0$ corresponds to a healthy link, remote from the fault location. The current wave front is attenuated along the healthy cable so the threshold is reached for only one end (the closest to the fault). Finally, the case where $C_{ij} = 1$ and $C_{ji} = 0$ cannot happen if the thresholds are set properly (meaning $dI_{TH+} > |dI_{TH-}|$).

Thresholds choice, for both positive and negative ones, have to be set small enough to be exceeded for the maximal fault resistance to detect, but as well as the differential current, it does not need to be higher than a certain value since the selectivity is ensured thanks to the blocking of the protection in case of a negative threshold exceeding.

The required frequency sampling is similar to the differential current protection since it depends once again on the shortest link length, in order to get the negative front.

For this protection principle, as well as for the differential current principle, two optical fiber links are required to guarantee the data exchange in both ways.

3.5 Communicant principles comparison

For both principles, the threshold value is exceeded as soon as the first fault wave front arrives at the faulty cable ends. The detection is thus done after the data propagation delay and is similar for the two principles.

Besides, the differential current seems to be more relevant since the information of the two ends of a considered cable are included in one variable. Also, this variable does not vary during power transfer variation, which is not the case for the current derivative.

The directional current has the advantage of requiring only the exchange of the sign value, with corresponds to a smaller size compared to the current measurement values. The horodated patch has to be considered for both cases. However, since the differential current principle assumes a continuous communication of the data, this later can be monitored and thus a loss of communication can be detected. In the case of the directional criterion, a loss of communication can be detected only during the fault conditions, except if a monitoring is set up in parallel of the protection-related data exchange. Note that this is always the case for communicant protections.

Note that both differential and directional principles are based on the current measurements and not on the voltage ones, which is due to the orientation information included in the current value. Indeed, the pole-to-pole or pole-to-ground voltages does not give a directional information, since a fault implies an undervoltage anywhere in the grid.

3.6 Non-communicative protection principle

The differential current principle seems to be very consistent for the cable protection. Even though it has some limits in terms of maximal link length and maximal resistance, which will be detailed in Chapter 6, the use of such a communicant principle is the only way that was found to ensure full selectivity, considering the grid structure and components arrangements given in Chapter 3. Nevertheless, the loss of the communication has to be considered. Indeed, it is possible that a fault would damage also the optical fiber. Consequently, another protection principle, this time without recourse to any communication between the relays, has to be investigated.

As said above, no selective principle were found considering those components arrangements, and thus the only way to find a non-communicant principle is to add a new element. Inductors were thus set up at each feeder relay, as shown on Fig.6.60. They are additional to the inductors that are included in the DC filter, at the terminal of the VSC.

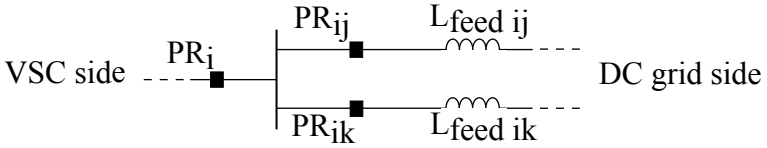

Figure 5.16: Feeder inductors arrangement

The idea of the feeder inductors came from another study aiming to solve a totally different technical problem which was found during the validation of the differential current protection, and which will be explained in Chapter 6.

The assumption of those feeders inductors leads to several possible selective protection principles, that will be explained in the following subsections.

3.6.1 Voltage differential protection

Even though the time constraint given by the diodes is increased by those inductors, the protection principle still has to be very quick, which is why the criterion must once again be traveling wave based.

As the sign of the first front transient is kept (giving the information of the

fault direction), the inductors attenuate the traveling waves when they circulate through them. Given these considerations, several variables can be used as a selective criterion, and the chosen one was the voltage measurement at the inductor terminals, as shown on Fig.5.17.

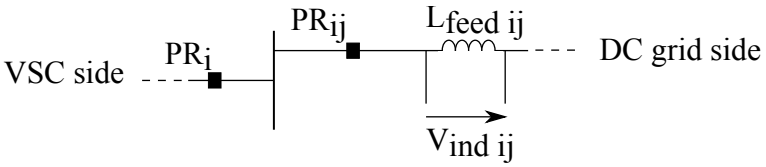

Figure 5.17: Voltage measurement at the inductor terminals

Fig.5.18 shows the voltage measurements for both a faulty and a healthy link. As well as the differential current, the first voltage wave front is positive at both ends of the faulty link (Fig.5.18a). For a healthy link, the closest end to the fault corresponds to a negative wave front, and the opposite end to a positive wave front (Fig.5.18b). This is due to the fact that the voltage at the inductor terminals is proportional to the current derivative, given by the behavior law of inductors reminded in equation (5.10).

$$V_{ind\,ij} = L_{feed\,ij}\frac{dI}{dt} \tag{5.10}$$

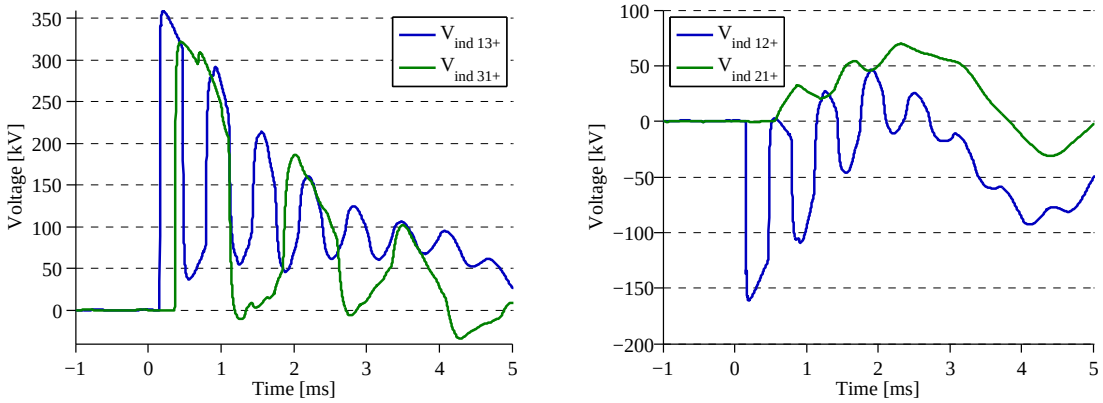

(a) Faulty link

(b) Healthy link

Figure 5.18: Current sign data exchange between two relays of a faulty link

The similar action can thus be applied on the end corresponding to the negative front, meaning that the protection can be blocked if this negative peak is detected. However, the difference with the differential current principle is that the healthy ca-

ble end corresponding to the positive first wave front does not have the information that its opposite end has seen a negative one, since no communication is assumed. However, this healthy cable end corresponds to the most remote end from the fault, and thus meaning that the traveling wave went through at least two inductors before arriving to this cable end. The relay related to this healthy cable end can thus discriminate between a internal fault thanks to the attenuation and properly set threshold, meaning a positive threshold small enough to detect high resistance internal faults but high enough to discriminate with small resistance external faults.

Thus, the new principle, which was named voltage differential principle, is based on the two phenomena:

- the attenuation given by the inductors, and
- the sign of the first front transient, giving the direction of the fault.

The resulting algorithm is developed in equation (5.11).

$$\begin{array}{llcll} \text{IF} & V_{\text{ind}ij}(t) & > & dV_{\text{indTH+}} & ; \text{ Trip} \\ \text{ELSE IF} & V_{\text{ind}ij}(t) & < & dV_{\text{indTH-}} & ; \text{ Block for } \Delta t_{block} \\ \text{ELSE} & & & & ; \text{ Stand By} \end{array} \tag{5.11}$$

where $dV_{\text{indTH+}}$ and $dV_{\text{indTH}-}$ are thresholds, and Δt_{block} a delay corresponding to the fault clearing process time, alike for the differential current principle.

Note that the relevance and the selectivity of this algorithm is extremely dependent on the inductors value. This phenomenon will be quantified in Chapter 6.

This protection principle is seen as a main protection because of its full selectivity and its rapidity, but it can act as a backup in case the communication is lost.

3.6.2 Other possible trail

The presence of inductors at the feeders protection relays also enables to use overcurrent or undervoltage principles, due to the filtering effect that attenuates the signals related to healthy links. However, those principles do not add any advantages

compared to the voltage differential principle, and thus are not developed in this thesis.

3.7 Conclusion on the main protection

Three possible principles were found for the main cable protection:

- the differential current protection,
- the directional protection,
- the voltage differential protection.

The directional protection do not add any advantages regarding the differential current. Thus, only the two other principles are kept for the protection plan. The busbar protection is performed thanks to the busbar differential current principle.

4 Backup protection

4.1 Purpose of the backup protection

Any transmission grid requires a backup protection system in case of the failure of any component of the main system. The main concern is a breaker failure. The lost of the optical fiber was already solved thanks to the voltage differential principle. Additionally, the monitoring of the communication can be done at the dispatching center level.

If a breaker failure happens during a fault clearing process, all the relays connected to the same busbar need to trip to avoid the fault feeding by the rest of the grid. This is shown on Fig5.19, in case of the breaker located on the right hand side of the faulty cable failed. Thus, when the backup protection triggers, the tripping order is sent to all DC breakers of the busbar, so the short-circuit current cannot flow through the other lines of the grid.

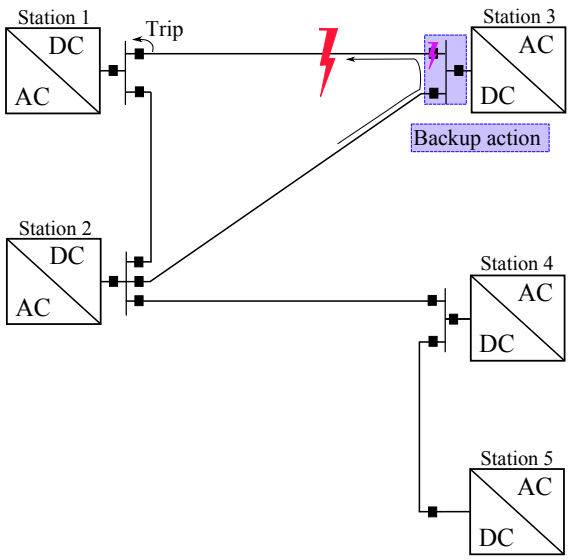

Figure 5.19: Backup action in case of breaker failure

This results in a less selective principle than the one of section 3, in the way that a station will be disconnected, even for a fault occurring on a cable of a meshed part of the grid. There is however still a selectivity since only the busbar connected to the faulty cable will trip and not the entire grid.

Several trails were investigated but real cases seem difficult to be implemented. They are however summarized in appendix A2. The best candidate for the backup protection is developed below.

4.2 Multi-criterion protection

A multi-criterion protection principle is considered as the best backup protection. This principle is based on a busbar-level communication, as previously shown on Fig.5.9a page 113.

This backup principle is based on the validation of three different criteria. Each one of them needs to be verified to validate the tripping order. The backup principle uses the values of the currents measured on the converter station side and on each feeder. The resulting algorithm will be detailed further. First of all, the aim of each criterion is explained.

- Criterion C1

  It defines the time range when the backup protection is active in case of a

fault. First, it detects the presence of the fault, without selectivity, meaning that it detects the presence of a fault anywhere in the DC part of the grid, but the fault can be either on the considered busbar protective zone, or external to this zone. Given this detection time, a time range is set, and the criterion is validated for this whole time range. The interval starts after a delay once the fault is detected, in order to wait for the main protection to act. The delay corresponds to the maximal clearing time of a fault if the main protection trips. Thus, the backup would not trip before, if there is no failure in the process of the main protection. The time range ends after a few milliseconds, so only the detected fault is taken into account.

- Criterion C2

  It is responsible for the selectivity of the backup protection. In fact, this criterion ensures that the backup of this particular busbar has to trip, and that the fault is in its protective zone. This criterion can be checked before the main protection action, but will be inhibited by criterion C1 and C3 if main protection trips, alike C1 can be inhibited by C2 or C3, and so on for C3.

- Criterion C3

  It ensures that the backup would trip only if the breaker solicited by the main protection fails. It verifies whether or not a feeder relay connected to this busbar tripped because of an order given by the main protection.

Several variables can be used for the validation of the criteria C1 and C2. They are generically named, $\mathrm{G_d}$ and $\mathrm{G_s}$ for the detection criterion C1 and the selectivity criterion C2 respectively. Therefore, C1 and C2 can be defined by the following equations, for a given busbar connected to station k.

Let $\mathrm{t_d}$ be the detection time, defined such that:

$$t_d = \min_t \left(\mathrm{G_d^k}(t) > \mathrm{G}^k_{dTH} \right) \tag{5.12}$$

where $\mathrm{G_d^k}$ is the detection variable evaluated at station k, and $\mathrm{G_{dTH}^k}$ a set threshold.

Criterion C1 becomes:

$$C1(t) = \begin{cases} 1 & \forall t \in [t_d + \Delta t_{main}; t_d + \Delta t_{stop}] \\ 0 & \text{elsewhere} \end{cases} \tag{5.13}$$

where Δt_{main} is a delay corresponding to the maximal clearing process time of the main protection, and Δt_{stop} is set to end the criteria comparison process.

Let t_s be the selection time, defined such that:

$$t_s = \min_t \left(G_s^k(t) > G_{sTH}^k \right) \tag{5.14}$$

Criterion C2 becomes:

$$C2(t) = \begin{cases} 1 & \forall t \in [t_s; t_s + \Delta t_{main}] \\ 0 & \text{elsewhere} \end{cases} \tag{5.15}$$

Criterion C3 is defined thanks to the current measurements of the feeders connected to the busbar. If there is one feeder where no current is flowing through it, that means that the breaker already tripped. Thus, C3 is defined such that:

$$C3(t) = \begin{cases} 0 & \text{if } \exists i \text{ such that } I_{ki}(t), I_{ki}(t - \Delta t), I_{ki}(t - 2\Delta t) < I_{feedTH} \\ 1 & \text{otherwise} \end{cases} \tag{5.16}$$

where I_{feedTH} is a threshold, and Δt is the time step of the protection.

The criterion C1, C2 and C3 are continuously evaluated, and the protection algorithm can now be defined thanks to equation (5.17).

$$\left.\begin{array}{rl} \text{If} & C1 = 1 \\ \text{AND if} & C2 = 1 \\ \text{AND if} & C3 = 1 \end{array}\right\} \text{ Trip}$$
$$\text{Else} \qquad \text{Stand By} \tag{5.17}$$

Fig.5.20 and Fig.5.21 illustrate the backup principle for two cases, each one corresponding to a busbar connected to the faulty cable, the first one is connected to the cable end that tripped thanks to the main protection, the other one connected to the cable end where a breaker failure occurred.

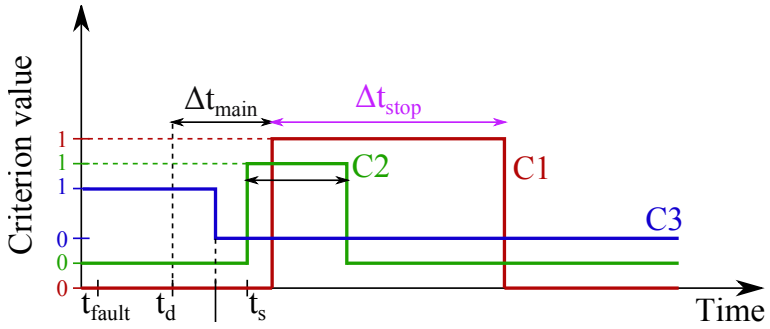

Figure 5.20: Backup does not trip because C3 is not verified

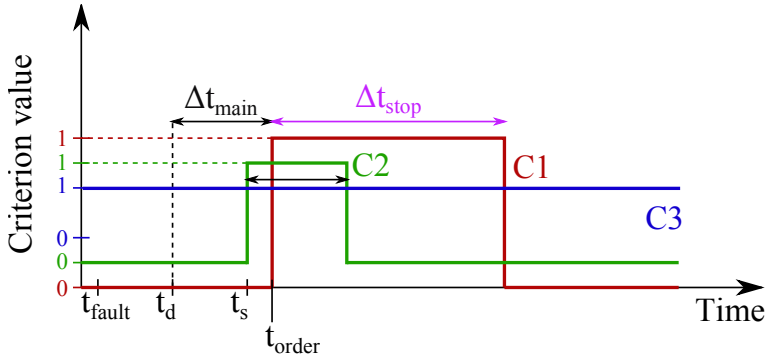

Figure 5.21: Backup fault clearing process principle

The algorithm (5.17) is computed at each protection relay of the station connection point PR_k and the tripping orders are sent to the feeders relay thanks to the busbar-level communication.

As mentioned previously, several variables can be used to evaluate G_d^k and G_s^k. The measurements of the whole busbar are available at the relay, so it can use any voltage or current measurements. Nevertheless, the chosen variables need to be independent on the operation point of the grid, to ensure the same theoretical performances, in terms of detection time of the backup principle, for any power flow configuration. This was the case for the differential current and the inductor voltage derivative. Indeed, the variable is around zero for any normal operation point.

The detection variable can be easily computed thanks to the use of the current or pole-to-ground voltage derivatives. The pole-to-ground voltage derivative was chosen since the voltage is the same for the whole busbar, because the same electrical node is considered. The voltage measurement is shown on Fig.5.22.

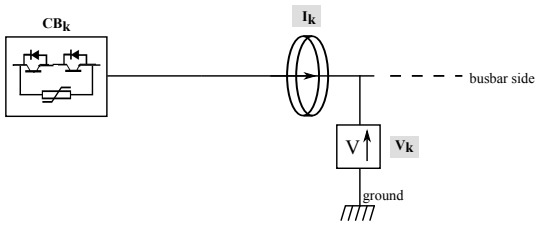

Figure 5.22: Protection relay of the VSC side of the busbar

The detection variable is thus defined by equation (5.18).

$$\mathrm{G}_d^k(t) = -\frac{dV_k}{dt}(t) \tag{5.18}$$

The -1 factor used with the voltage derivative aims to keep a positive threshold value to detect the undervoltage following the fault occurrence. This does not imply any changes but the threshold comparison orientation is kept and matches the description given in equation (5.12).

Concerning the selectivity, a new variable was chosen, as given in equation (5.19).

$$\mathrm{G}_s^k(t) = |I_k(t) - I_k(t - 20\mathrm{ms})| \tag{5.19}$$

The thresholds and delays setting will be detailed in Chapter 6 as well as the main protection ones.

Besides, it is possible to speed up the backup protection by adding an inverse time criterion on the detection variable. This will act on the delay $\Delta \mathrm{t}_{\mathrm{main}}$, which can vary as a function of the detection variable value, as shown on Fig.5.23. In the cased of a sever fault (very small impedance), the main protection would trip very quickly. The detection variable $\mathrm{G}_{\mathrm{d}}^{\mathrm{k}}$ would also take a very high value, and as a consequence, the highest threshold will be exceeded. The backup principle will thus wait for a smaller delay $\Delta \mathrm{t}_{\mathrm{main}}$ before checking the criterion C1.

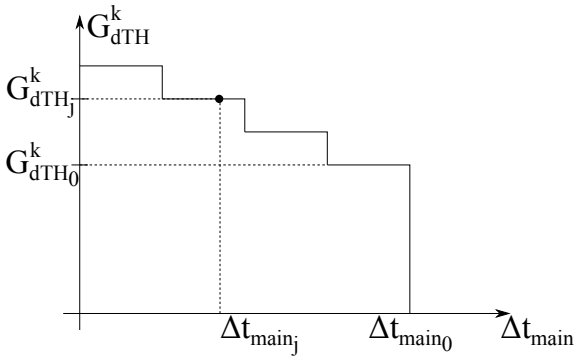

Figure 5.23: Inverse time principle to speed up the backup clearing process

5 Safety of connection manoeuvres of links

As mentioned earlier, the protection system must remain stable during normal operation of the grid, such as a power transfer variation, a connection or a disconnection of a link. These aspects are treated in this section.

5.1 Power transfer variation

A power transfer variation does not impact much the variables used for the detection, since the response time of the control loops are higher (in the range of 100ms). The inherent small variations are taken into account in the thresholds choice, which is explained in Chapter 6 section 1.

5.2 Disconnection of a link

In case of the disconnection of a link because of a fault, the healthy part of the grid stays in operation. Unwanted trippings could be caused by the transients related to the tripping process of the breakers. This phenomenon is directly taken into account in the protection algorithms, and the fact that no unwanted tripping occurs is validated in Chapter 6 section 2.

5.3 Connection of a link

In case of the connection of a link, a huge current transient flows through the cable due to the cable capacity loading. This large amount of current measured at each end of the cable leads the variables used by protection system to reach their respective threshold value. Since the transient current (in the range of tens

of kiloAmps) is destructive for the system, even if the transient is very short, the connection has to be done progressively thanks to inserted resistive elements that will be gradually short-circuited in steady state. The resulting device is sketched on Fig.5.24, and is placed at each feeder protection relay.

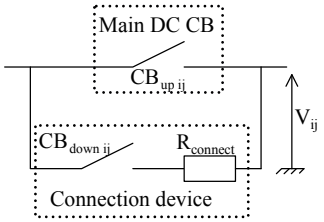

Figure 5.24: Progressive connection device

The resistive element $R_{connect}$ can be either a variable resistance or several series resistances that can be shunted progressively.

$CB_{up}{}_{ij}$ and $CB_{down}{}_{ij}$ are open or closed according to the state of the link. The link state can take the value 0, 1 or 2. State = 0 means that the link is disconnected, state = 1 means that the link is in the connection operation process ($CB_{up}{}_{ij}$ open and $CB_{down}{}_{ij}$ closed), and state = 2 means that the link is connected ($CB_{up}{}_{ij}$ closed and $CB_{down}{}_{ij}$ open).

Note that $CB_{down}{}_{ij}$ does not break a current when it trips, but orientates the current to flow in the other branch. Thus, the complex and costly technology of hybrid DC breaker is not required here.

With those definitions, the states are succeeding each other as shown in the diagram of Fig.5.25.

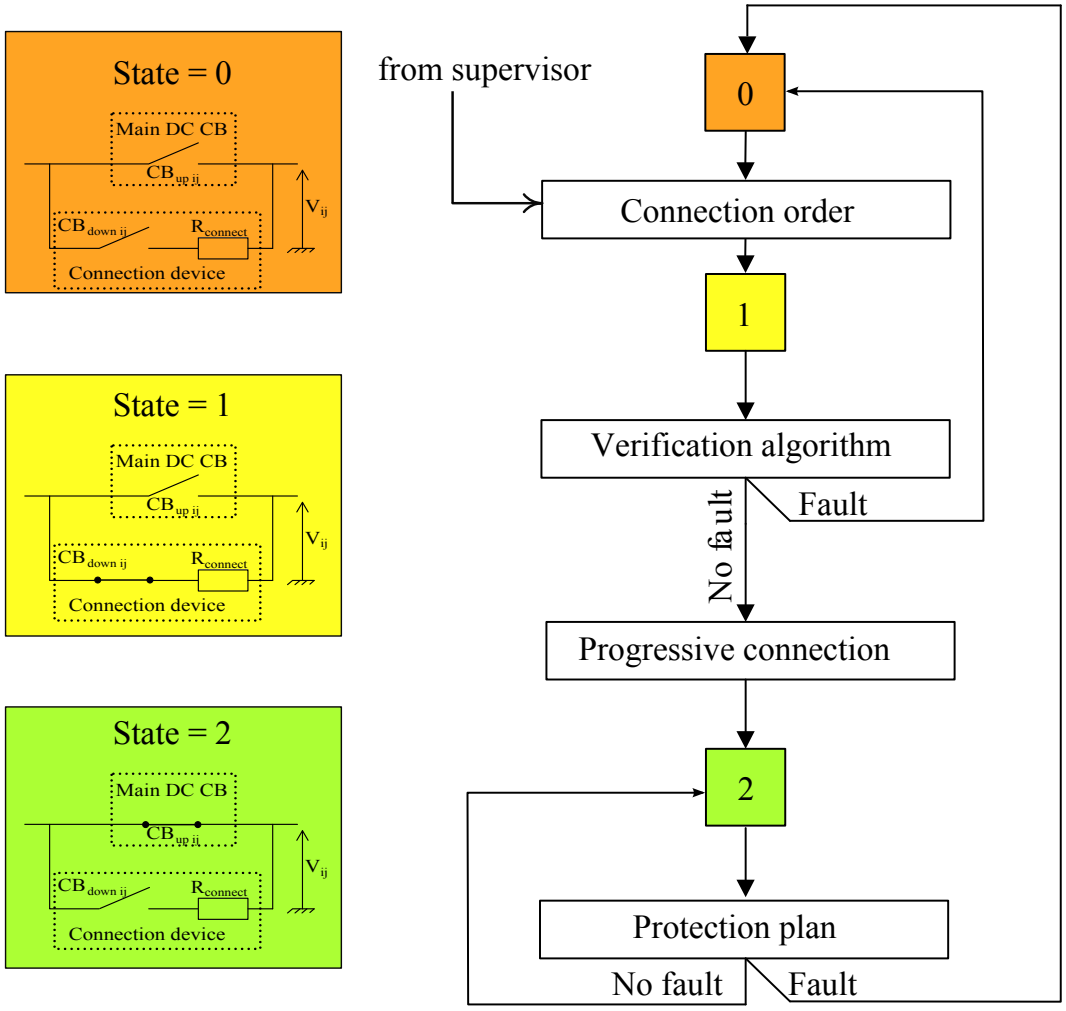

Figure 5.25: Progressive connection implementation

In addition of that, a verification of the condition of the cable has to be done before the full connection of the link is completed, in order to be sure to connect a healthy cable and not a faulty one, for safety purposes. This verification can be done at the first step of the connection, meaning when resistive elements are still connected in series with the cable. Nevertheless, the differential current and the voltage differential principles cannot complete this task since the variables magnitude is largely decreased by the resistive component (which is included for that purpose). Hence, another algorithm will check the voltage of the cable. The chosen principle to achieve that task is explained by equation (5.20) below.

Let $t_{connect}$ be the time when the relay PR_{ij} receives the connection order.

$$\begin{array}{lll} \text{IF } \exists t \in [\mathrm{t_{connect}}; \mathrm{t_{connect}} + \Delta \mathrm{t_{verif}}] \text{ such that} \mathrm{V}_{ij} > \mathrm{V_{connectTH}} & & \\ \text{then decrease } \mathrm{R_{connect}} \quad \text{and} & \text{State} = 2 & (5.20) \\ \text{ELSE} & \text{State} = 0 & \end{array}$$

where $\Delta \mathrm{t_{verif}}$ is a delay corresponding to the loading process of the cables, and $\mathrm{V_{connectTH}}$ is a threshold.

Simulation examples will be shown in Chapter 6.

6 Proposed protection system

The protection system implementation is summarized in this section. Two cases are treated: a relay connected to a station (Fig.5.26) and a relay connected to a feeder (Fig.5.27).

As mentioned earlier, the voltage differential algorithm was found in a later stage of the work, thanks to the incorporation of the feeders inductors. Thus, the protection plan was validated (in Chapter 6 section 2) at first stage considering the optical fiber communication link and no feeder inductors. Then, the feeders inductors were incorporated for another purpose, as it will be developed in Chapter 6 section 4. Hence, the validation process of the voltage differential protection will be done at the end of Chapter 6. It is still included in the protection system as a backup against the loss of the optical fiber, as shown on Fig.5.27.

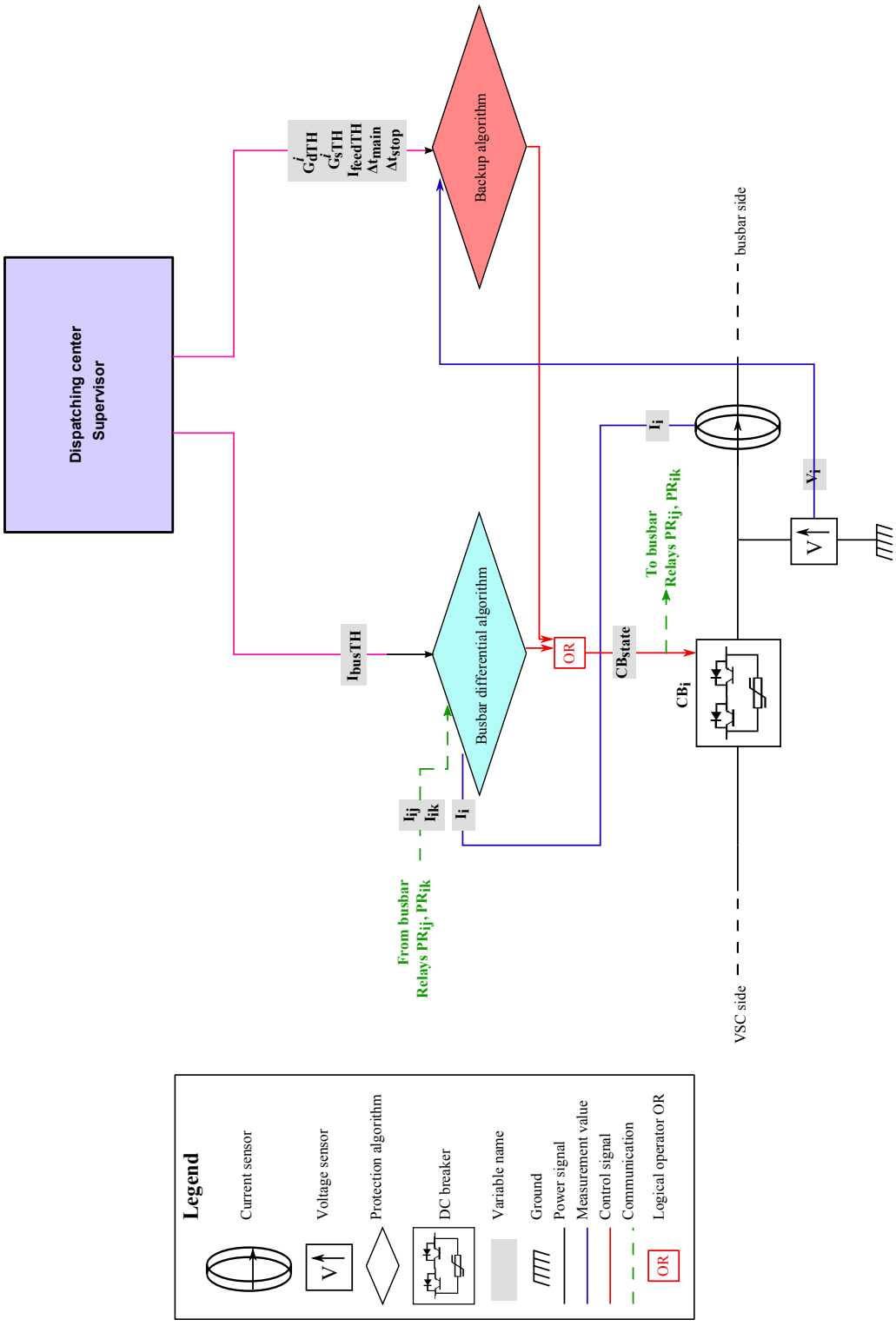

Figure 5.26: Protection system implementation for a station relay PR_{ij}

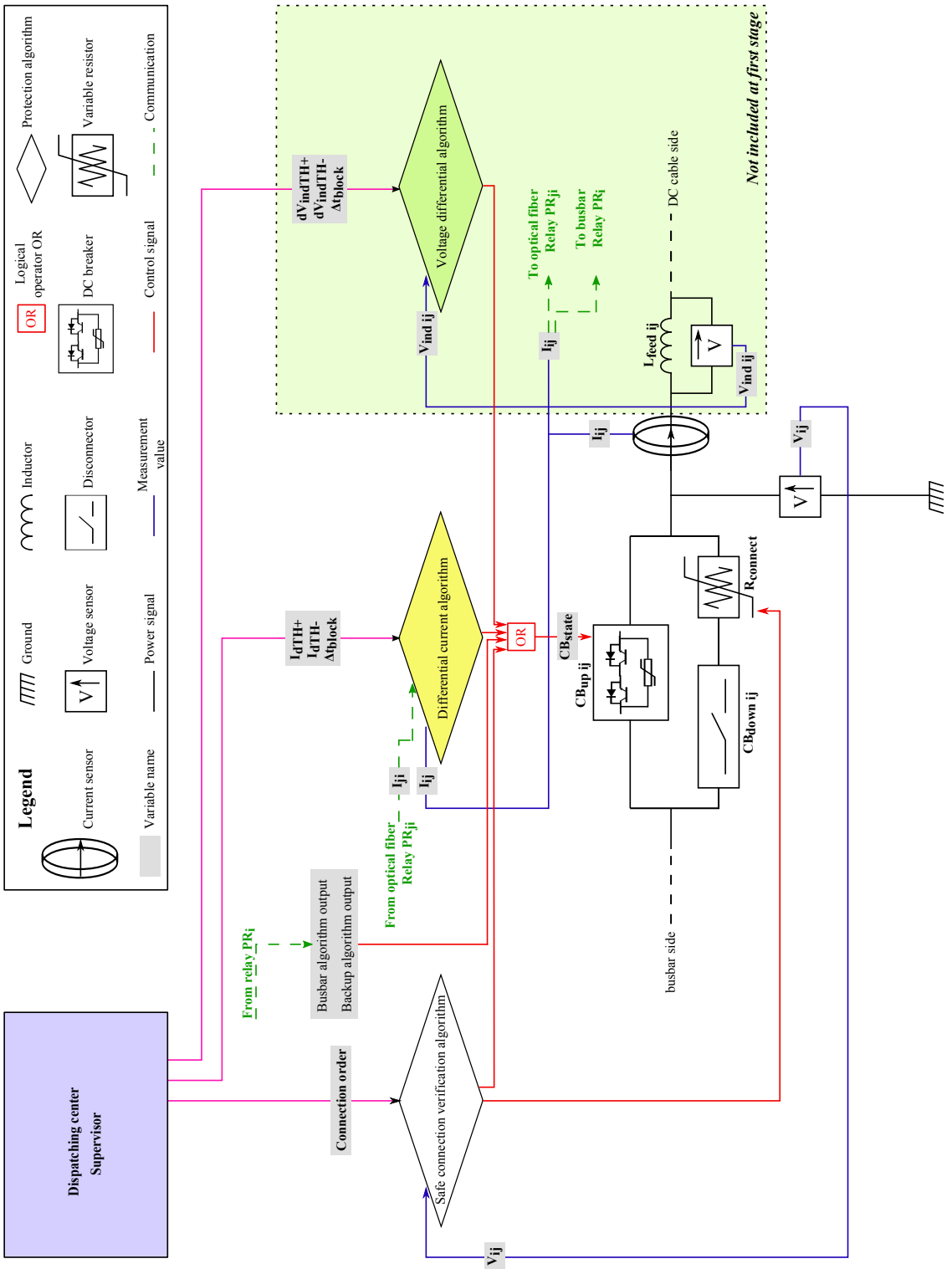

Figure 5.27: Protection system implementation for a feeder relay PR_i

CHAPTER 6

Protection plan validation

Chapter 6

Protection plan validation

The protection system proposed at the end of Chapter 5 will now be validated in this current chapter. First, the theoretical performances will be assessed thanks to EMTP-rv simulations. Then, the real-time validation on a DC grid hybrid demonstrator will be presented. Investigations to improve the limits of the protection system will finally be developed at the end of the chapter.

The DC grid structure used for the validation is the TWENTIES grid test model, which is reminded below on Fig.6.1, with the characteristics defined in Chapter 3.

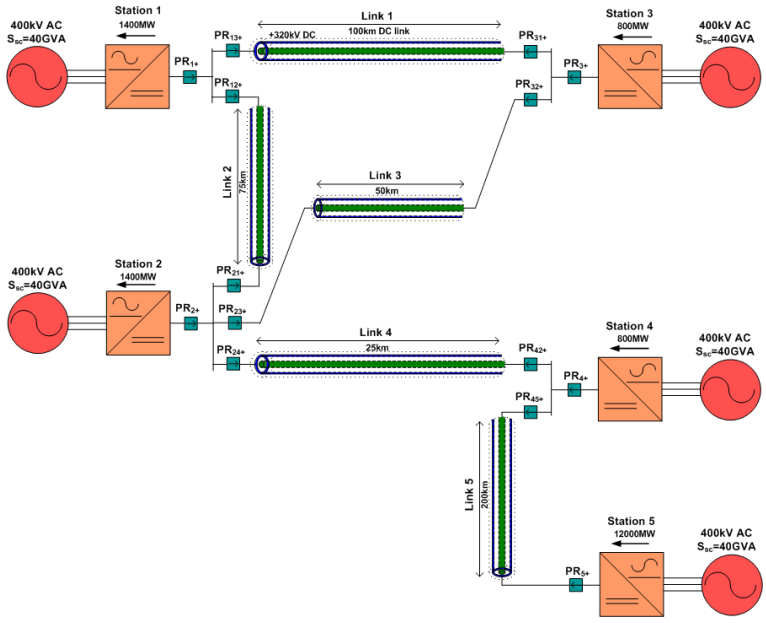

Figure 6.1: TWENTIES grid test used for the validation of the protection system

The protection algorithms are implemented in EMTP-rv, on the same model than the grid. All the protection algorithms are computed so their compatibility

can be tested.

1 Complete protection plan implementation in EMTP-rv

The inputs of the protection algorithms are the current and voltage computed by EMTP-rv, considering the sensors models developed in Chapter 3. Indeed, the protection system do not have access to the real current and voltages, and the inputs can only be the measurement outputs of the sensors. The signals that are shown for illustration in this chapter are the real current, and not the one issued by the sensors model, since the constraint in the grid depends on those real current.

As mentioned in Chapter 5, the busbar protection, the differential current protection and the backup protection will be treated in section 2. The voltage differential protection will be discussed when the feeder inductors will be considered, in section 4.

1.1 Data processing

The frequency sampling of the protection relays is set to 100kHz, meaning a time step of 10µs.

The delay resulting of the propagation delay of the data through the optical fiber link was given in Chapter 5 section 3.4.1 in Tab.5.3 for each link. Another delay was added to take into account the data conversion (analog - digital conversion and digital - analog), and was set to one time step for (10µs) each conversion. This gives the new delays in Tab.6.1, and these global delays are notated Δt_{OF}.

Link	Link length	Δt_{OF}
Link1	100km	520µs
Link2	75km	400µs
Link3	50km	270µs
Link4	25km	150µs
Link5	200km	1.020ms

Table 6.1: Differential current protection delay

Hence, at the time instant t, the differential current available at the protection relay PR_{ij} is $I_{dij}(t - \Delta t_{OF\,ij})$.

1.2 Thresholds setting determination process

1.2.1 Differential current

The algorithm governing the differential current protection is reminded in equation (6.1).

$$\begin{array}{rlcll} \text{IF} - -- & I_{dij}(t-2\Delta t) & > & I_{dTH+} & \left.\begin{array}{l}\\\\\end{array}\right\} \\ \text{and if} & I_{dij}(t-\Delta t) & > & I_{dTH+} & \left.\begin{array}{l}\\\\\end{array}\right\} \text{Trip} \\ \text{and if} & I_{dij}(t) & > & I_{dTH+} & \left.\begin{array}{l}\\\\\end{array}\right\} \\ \text{ELSE IF} & I_{dij}(t-2\Delta t) & < & I_{dTH-} & \left.\begin{array}{l}\\\\\end{array}\right\} \\ \text{and if} & I_{dij}(t-\Delta t) & < & I_{dTH-} & \left.\begin{array}{l}\\\\\end{array}\right\} \text{Block for } \Delta t_{block} \\ \text{and if} & I_{dij}(t) & < & I_{dTH-} & \left.\begin{array}{l}\\\\\end{array}\right\} \\ \text{ELSE} - - - - - - - - - - - - - - - - & & & & \text{Stand By} \end{array} \tag{6.1}$$

Thresholds were chosen as small as possible, but taking into account the fact that they must not be exceeded during normal operation of the grid, even during manoeuvres or power reference variation on the grid. The connection of a link was treated in Chapter 5 section 5, so only the cases of the disconnection of a link and a power reference variation will be discussed in this section.

a) Power reference variation

To avoid unwanted trippings during power reference variations, the positive threshold I_{dTH+} must not be exceeded. This remark stands also for the negative

threshold I_{dTH-}, since the protection relays should not be blocked during such operation, because they would not be able to protect the grid if a fault occurs shortly after this power variation.

An example is shown below. The initial power flow and its variations are given in Tab.6.2, where a positive power value corresponds to a power flowing from the AC side to the DC grid. On station 3, a power reference variation of 1000MW is done at t = 100ms. Fig.6.2 represents the power at each station in per-unit values.

Station	Power flow at $t = 0$	Variation done at t = 100ms
Station1		0W
Station2	-1400MW	0W
Station3	0W	+1000MW
Station4	+800MW	0W
Station5	+800MW	0W

Table 6.2: Power reference value for each station

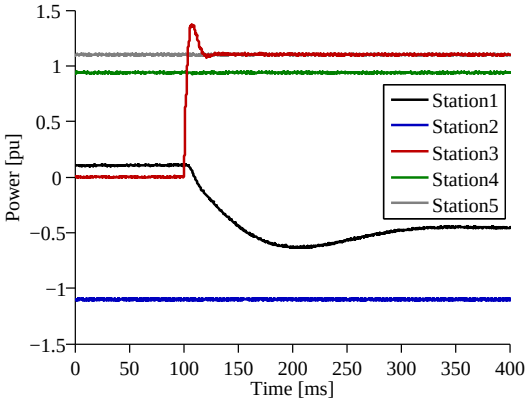

Figure 6.2: Power flowing through the stations

As it can be noticed on Fig.6.3, the differential current measured in each link do not exceed 250A. This small value is due to the response time of the control loops, which is much higher than the transients related to faults that has to be detected. When the current starts to increase at the cable end close to the station subjected to a power transfer variation, the other cable end current is still at a value corresponding to the previous power reference. Then, the current increases at this

later cable end after the propagation time related to the cable length. Since the control loops have a quite high response time (largely higher than the propagation time of a signal through the cable), the current difference between the two ends is sensitively small. Hence, the thresholds take into account the oscillations present in the signal, due to AC/DC conversion, and the transient that can appear in power variations.

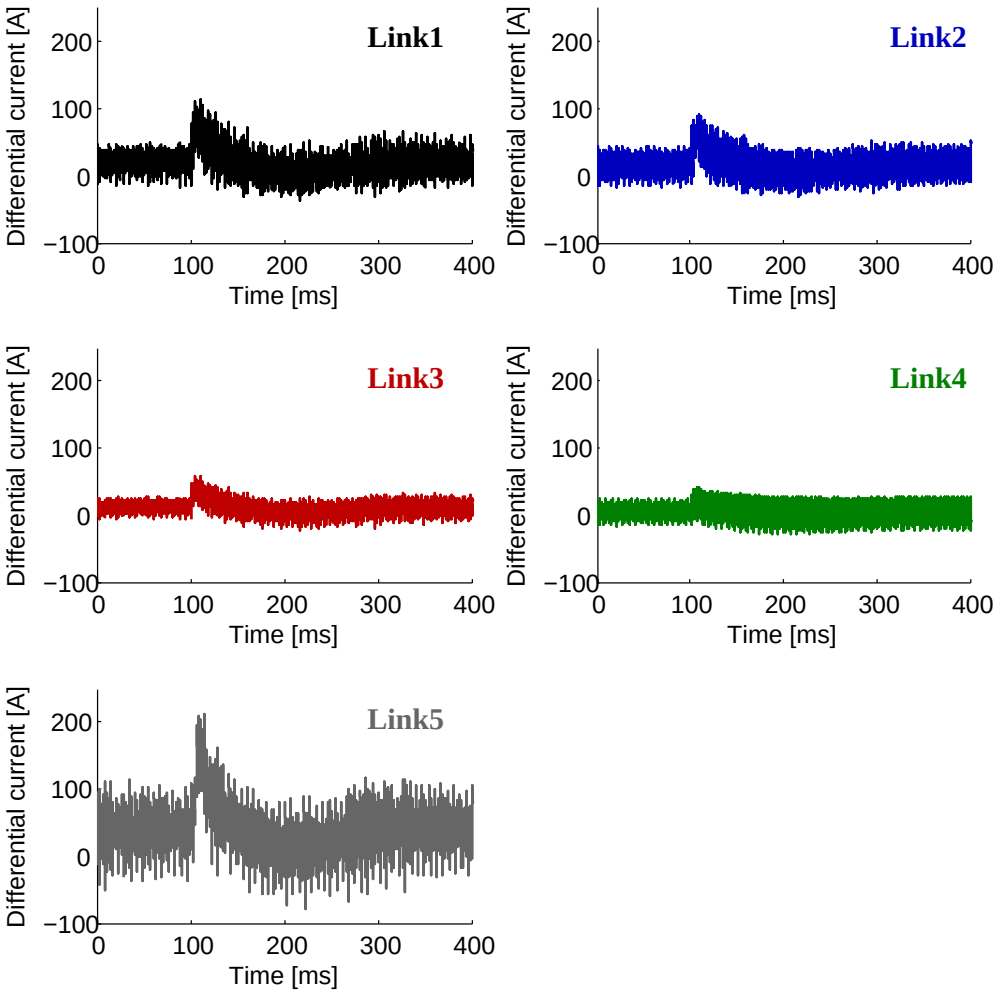

Figure 6.3: Differential current during a power flow variation

b) Disconnection of a link

When a fault occurs and is cleared by the breakers of the faulty cable ends, the differential current protection needs to remain stable. The transients following the tripping may imply unwanted trippings, which is also why the negative threshold

I_{dTH-} and the blocking time Δt_{block} were introduced. They are set in order to avoid such unwanted tripping events.

The thresholds for the differential current protection are chosen to match the constraints emphasized in this subsection, and are given in Tab.6.3.

Threshold name	Value
I_{dTH+}	500A
I_{dTH-}	-500A
Δt_{block}	30ms

Table 6.3: Thresholds setting for the differential current protection

Note that the threshold values could be different for any protection relay, but since the selectivity was guaranteed with those values, they were used for each relay. This is validated in section 2.1 where this principle was implemented and tested.

1.2.2 Busbar differential

The busbar differential current threshold can theoretically be any positive value, and the closest to zero it is, the fastest thee protection operates and the highest the maximal fault resistance that can be detected is. A margin needs however to be taken into account, and to avoid unwanted trippings due to other fault clearing process, a threshold value of $I_{busTH} = 500A$ were thus set for each station. The results related to the busbar protection are shown in section 2.3.

1.2.3 Backup

The backup thresholds were set in order to be selective in case of a breaker failure.

Three thresholds have to be set, and correspond to the values, G^k_{dTH} G^k_{sTH} and I_{feedTH} that were mentioned in Chapter 5. The value of G^k_{dTH} is responsible of the detection, without any selectivity purpose. It was chosen to be the same value for each station relay ($k = 1..5$), and is equal to 200kV/ms, which is reached even reached for faults with resistance of resΩ. Also, the threshold I_{feedTH} is used to verify if there is still a current flowing through the cable. It is thus set to 10A. Note

that the noise that are presented in the current measurements are in the range of 2A [PuissanceAnalyse, 2012].

The selectivity criterion is harder to parameter. To increase the selectivity, the threshold G^k_{sTH} is set independently for each station relay. Pole-to-pole faults occurring at cable ends imply the highest overcurrents, even at busbars connected to only healthy links. Those cases are thus used to find the minimum threshold values required to ensure the selectivity. Thus, the ten possible pole-to-pole faults occurring at each cable end were simulated considering the differential current as the main protection principle and a breaker failure at the cable end where the fault is located. First, only those faults are considered. The signals measured at each relay where the backup protection is implemented, meaning at each station connection point relay, are recorded and used for a post-treatment performed in Matlab. The strategy used to determined the threshold is described below.

The pole-to-pole faults are sorted in 5 fault groups, corresponding to the station connected to the feeder where they occur. The faults are named F_{ki}, where ki corresponds to the name of the relay near which it occurs (fault F_{13} is the pole-to-pole fault occurring near relay PR_{13}). The five fault groups are thus defined by:

$$\mathscr{F}_k = \{F_{ki}, i = 1..n\} \tag{6.2}$$

where n is the number of feeders connected to the corresponding busbar.

The thresholds G^k_{sTH}, for $k = 1..5$ are thus searched to verify (6.3) and (6.4).

$$\forall F_{ki} \in \mathscr{F}_k,\ \exists t \in [t_{fault}; t_{fault} + \Delta t_{stop}] \text{ such that } G^k_s(t) > G^k_{sTH} \tag{6.3}$$

$$\text{and } \forall j \neq k,\ \forall t \in [t_{fault}; t_{fault} + \Delta t_{stop}] \text{ then } G^j_s(t) < G^j_{sTH} \tag{6.4}$$

Equation (6.3) implies that for any breaker failure occurring at a cable end connected to a busbar, the backup implemented at the relay connected to this busbar needs to trip. Equation (6.4) means that for any other faults, it has to remain stable. If the inequalities occur after the time interval, then the criterion would be

inhibited by criterion 1 or 3.

Those two equations were used to find the thresholds using Matlab. The implementation of the algorithm is shown below.

$$\forall k,\ \forall \mathrm{F_{ki}} \in \mathscr{F}_k,\ \mathrm{G^k_{sTH-MAX}} = \min_{\mathrm{F_{ki}}} \left(\max_{\mathrm{t}\in[\mathrm{t_{fault}};\mathrm{t_{fault}}+\Delta\mathrm{t_{stop}}]} \left(\mathrm{G^k_s}(t) \right) \right) \tag{6.5}$$

$$\text{and}\ \ \forall j \neq k,\ \mathrm{G^j_{sTH-MIN}} = \max_{\mathrm{F_{ki}}} \left(\max_{\mathrm{t}\in[\mathrm{t_{fault}};\mathrm{t_{fault}}+\Delta\mathrm{t_{stop}}]} \left(\mathrm{G^j_s}(t) \right) \right) \tag{6.6}$$

The thresholds values are thus defined $\forall k = 1..5$ such that

$$\mathrm{G^k_{sTH-MIN}} < \mathrm{G^k_{sTH}} \leqslant \mathrm{G^k_{sTH-MAX}} \tag{6.7}$$

The temporization delay $\Delta \mathrm{t_{stop}}$ was arbitrarily set to 5ms. Indeed, if the algorithm does not stop thanks to this kind of temporization delay, the inequality (6.7) has sometimes no solution. The threshold values are thus given in Tab.6.4, and were chosen 10% higher than $\mathrm{G^k_{sTH-MIN}}$:

Threshold name	Value
$\mathrm{G^1_{sTH}}$	22.624kA
$\mathrm{G^2_{sTH}}$	23.219kA
$\mathrm{G^3_{sTH}}$	21.232kA
$\mathrm{G^4_{sTH}}$	20.436kA
$\mathrm{G^5_{sTH}}$	13.646kA

Table 6.4: Thresholds setting for the selectivity criterion of the backup protection

The time delay $\Delta \mathrm{t^k_{main}}$ are set at each station relay $k = 1..5$ to match the overall clearing time of the considered faults, meaning the time defined by equation (6.8). They are displayed in Tab.6.5.

$$\Delta \mathrm{t^k_{main}} = \max_{\mathrm{F_{ki}}\in\mathscr{F}_\mathrm{k}} \left(\Delta \mathrm{t^{F_{ki}}_{clear}} \right) \tag{6.8}$$

where $\Delta \mathrm{t^{F_{ki}}_{clear}}$ is the overall clearing time of fault $\mathrm{F_{ki}}$ by the main differential current protection, including a 1ms delay for the breaker, as it was developed in Chapter 3 section 3.3.

Δt^1_{main}	1.340ms
Δt^2_{main}	1.510ms
Δt^3_{main}	1.510ms
Δt^4_{main}	2.010ms
Δt^5_{main}	2.010ms

Table 6.5: Temporization setting for the backup protection

The validity domain of the backup protection will thus be assessed in section 2.2.

1.2.4 Safe connection verification

The thresholds were set to allow a safe progressive connection through a resistance of $R_{connect} = 10k\Omega$. The threshold $V_{connectTH} = 60kV$ and the temporization delay $\Delta t_{verif} = 100ms$ were chosen using simulations of faults up to 500Ω, as shown on Fig.6.4.

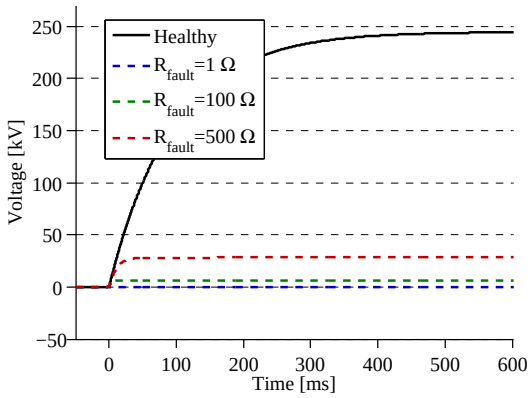

Figure 6.4: Voltage measurements during the connexion of cables either healthy or faulty, with different fault resistances

Once the verification process checked the good state of the cable, the resistance $R_{connect}$ can be decreased progressively. The solution that was chosen for the simulations that will be presented uses resistances that are short-circuited progressively after the connection order as described in Tab.6.6, if the verification process succeeded. This was chosen arbitrarily, and the two resistances were enough to have low magnitude transients. This is shown on a connection example below.

$R_{connect}value$	Time
10kΩ	$t_{connect}$
5kΩ	$t_{connect} + \Delta t_{verif}$
1kΩ	$t_{connect} + \Delta t_{verif} + 100ms$
500Ω	$t_{connect} + \Delta t_{verif} + 200ms$
100Ω	$t_{connect} + \Delta t_{verif} + 300ms$
0Ω	$t_{connect} + \Delta t_{verif} + 400ms$

Table 6.6: Progressive connection through $R_{connect}$

Link1 is supposed to be initially disconnected from the rest of the grid. A connection order is sent at $t_{connect} = 0$. The voltage measurements of the connected cable ends during the connection process as well as the differential current of the link are shown on Fig.6.5.

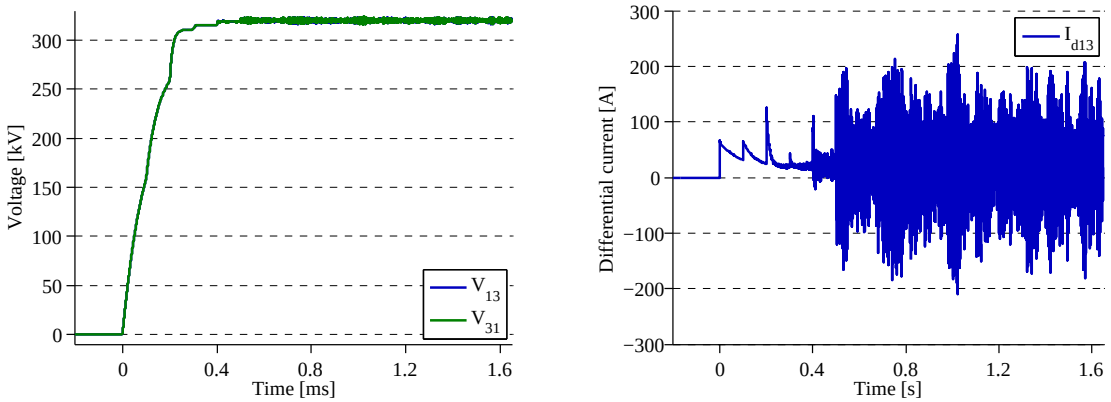

(a) Voltages

(b) Differential current

Figure 6.5: Connection process of Link1

The differential current of each link are both below the threshold value $I_{dTH} = 500A$, but this would not be the case if the 10kΩ resistance is fully short-circuited instantaneously.

The same example is shown this time for the connection of a faulty cable. The voltage measurements are shown on Fig.6.6. The voltage threshold $V_{connectTH} = 60kV$ is not reached, thus the cable is disconnected while it is still connected through the resistance.

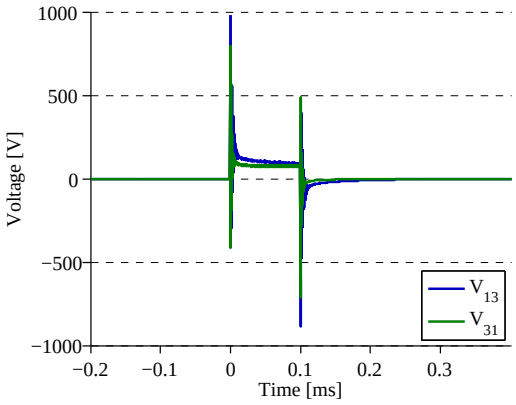

Figure 6.6: Voltage measurements for a connection of a faulty link

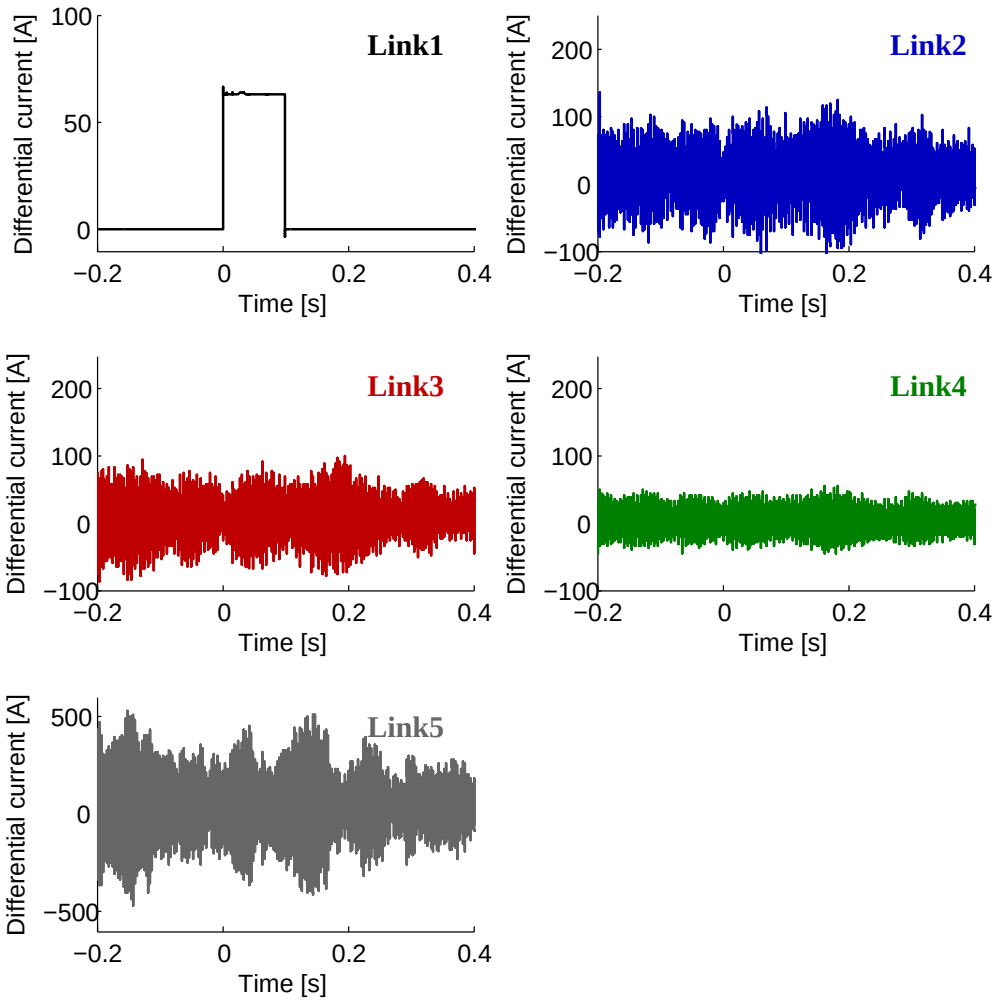

Figure 6.7: Differential current of each link during the connection-disconnection process of Link1

The differential currents of the healthy links are shown on Fig.6.7 for a duration including the whole connection - disconnection process. They remain below the threshold, so there is no unwanted trippings of healthy links, and the grid stays in a N-1 operation state.

This connection process is more likely related to the grid operation and no other results on this process will be provided in this thesis, since this the priority were given to the protections.

2 EMTP-rv results

In this section, the protection principle theoretical performances are assessed thanks to the simulation of the protection system implemented as detailed in the previous section. The differential current, the backup and the busbar protection will be treated.

2.1 Differential current protection

First of all, the fault clearing process responding to the main differential current algorithm is detailed through an example. A pole-to-ground fault is simulated on Link1, with the parameters defined in Tab.6.7.

Parameter	Value
Type	Pole-to-ground
Location	Link1
Position	30km away Station 1
Impedance	1Ω

Table 6.7: Parameters of the fault example

Fig.6.8 shows the fault clearing process. On Fig.6.9a the current measured at the faulty cable ends is presented. The fault is cleared 1.660ms after the fault occurrence, and the current to break are 32.263kA and 18.926kA for PR_{13} and PR_{31} respectively. The difference is due to the fault location, which is closer to PR_{13} than to PR_{31}.

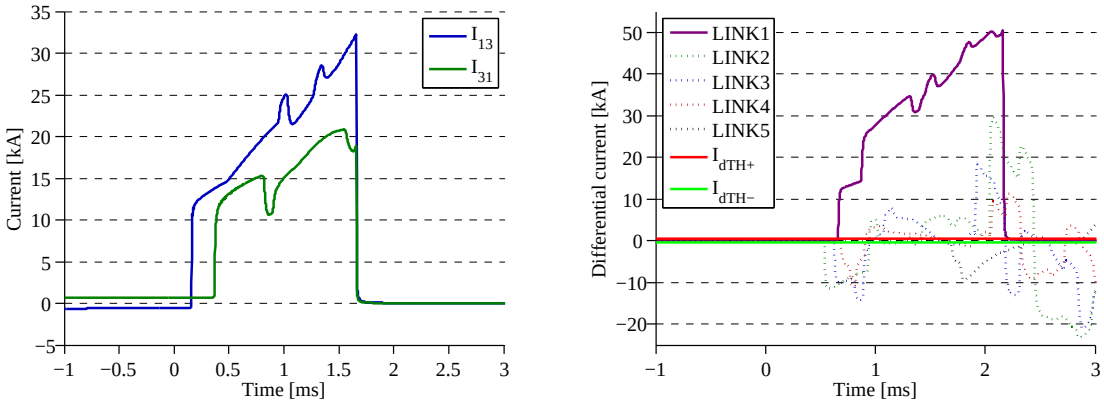

(a) Current at the faulty cable ends

(b) Differential current in each link

Figure 6.8: Fault clearance illustration

On Fig.6.9b, the differential current computed in each link is shown. The selectivity is thus obvious for this example, since all the differential currents of the healthy links exceed the negative threshold.

The global fault clearing time (1.660ms) is composed of several time intervals, explained in Tab.6.8.

Time interval	Value	Interval definition
Δt_{OF}	0.520ms	Data propagation through the optical fiber link and conversion delay.
Δt_{detect}	0.140ms	Required time for the differential current to exceed the threshold (including 3 consecutive samples validation delay).
$\Delta t_{breaker}$	1ms	Operation time of the breaker, representing by a delay of 1ms, as explained in Chapter 3.
$\Delta t_{clearing}$	1.660ms	Overall clearing time, from the time of arrival of the first front transient to the closest sensor until the current extinction time.

Table 6.8: Relevant operation times related to the fault clearing process example

The currents measured at the station connection points are shown on Fig6.9. It can be observed that after the transient related to the fault and its clearance, the

currents recover to their initial values. The current initially flowing through the faulty cable is now flowing through Link2 and Link3, meaning through the cables connected to the busbars where the faulty link were connected. Hence, the power reference is kept.

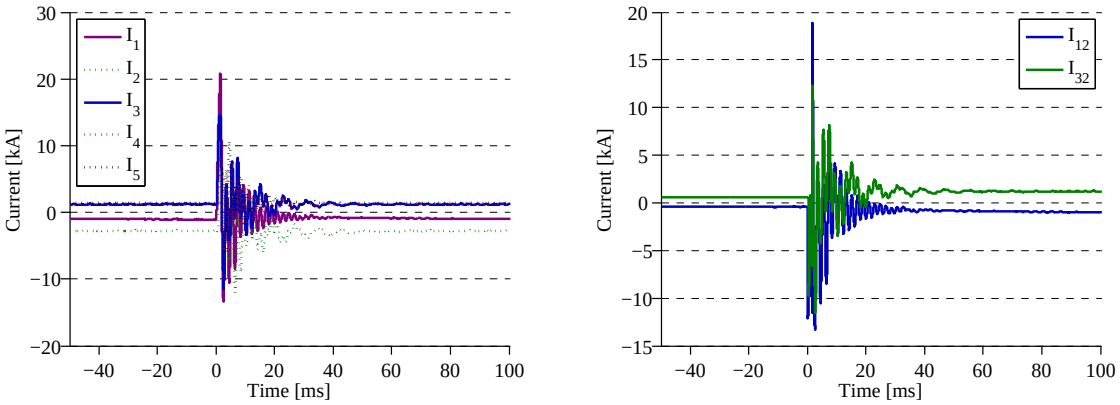

(a) Current at station connection point

(b) Current measured at the end of the healthy links

Figure 6.9: Fault clearance illustration

Several parameters can affect the tripping time and the currents to break. They are investigated in the following next subsections.

2.1.1 Fault resistance influence

The fault resistance impact on the protection system performances were assessed thanks to the simulation of 30 cases. This number of cases was chosen arbitrarily. The fault is always located on link 1 and 30km away station 1, and only the fault resistance changes compared to the fault detailed previously. Thus, fault resistances $R_{fault} = i \times 1, i \times 10$ and $i \times 100$, with i the integer $i = 1..10$, were simulated. The results are shown below.

a) Influence on the required operation speed of the protection

As it was detailed in Chapter 4 and reminded at the beginning of Chapter 5, a high fault resistance damped the signals, and thus decreases the current flowing through the diodes of the converters. This results in a higher acceptable clearing time for a considered fault.

For the first fault resistance $R_{fault} = 1\Omega$, the time constraint defined by the current flowing through the diodes, which cannot exceed 2 per unit, is exceeded 5.820ms after the fault occurrence. For resistances higher than 1Ω, and for those fault parameters (location, link, ...), the diode constraint is not exceeded, due to the damping effect and the fact that the diode is remote from the station.

b) Influence on the tripping time

The fault resistance variation cannot imply unwanted trippings considering the differential current principle. However, it influences the detection time, as shown on Fig.6.10.

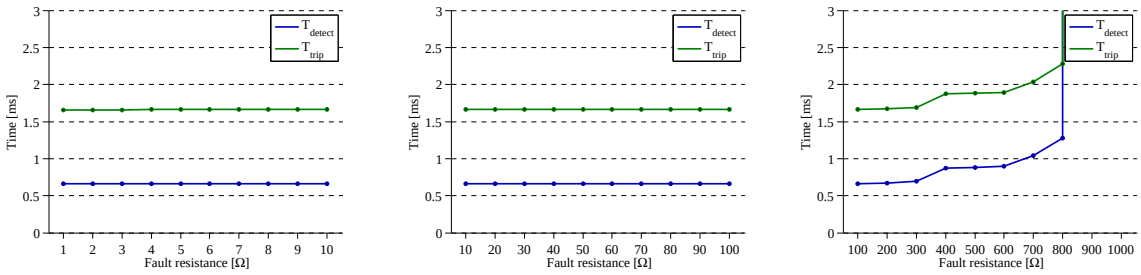

(a) $R_{fault} = 1..10\Omega$ (b) $R_{fault} = 10..100\Omega$ (c) $R_{fault} = 100..1000\Omega$

Figure 6.10: Detection time as a function of the fault resistance

As said in the previous paragraph, the diode constraint exists only for the first fault case $R_{fault} = 1\Omega$. This fault case is the example that was developed in section 2.1. The tripping time is 1.660ms, which is below the constraint. This tripping time is constant for all the resistances below 100Ω, because the differential current exceeds, for each case, the positive threshold at the same time. The tripping order is sent 0.660ms after the fault occurrence, and there is 1ms delay before the tripping action. In the duration of 0.660ms, there are 500µs corresponding to the propagation delay through the optical fiber, 20µs that correspond to the anolg - digital and digital - analog conversions, 20µs that correspond to the 3 samples verification included in the algorithm, and 120µs which is the propagation time of the fault to the sensor PR_{13}, which is the closest one. For each fault case below 100Ω, the differential current exceeds the threshold at this time, meaning that the first current wave front arriving to the closest sensor is responsible for the detection. For higher fault resistances, the detection time is higher, because the first current wave front is not enough to have a differential current that exceeds the threshold value. It thus

happens further, once the current rose enough to have a differential current over 500A.

For fault resistances over 900Ω, included this value, the threshold is never exceeded, meaning that the differential current protection does not cover these values. For Link1, this protection covers only faults up to 800Ω. Note that it might detect a resistance of 850Ω, but the fault resistance parametric study was performed with a step of 100Ω. This is valid for a fault located on Link1, 30km away station 1. The highest fault resistance value that can be detected changes with the location in the link. The influence on the fault location is shown in subsection 2.1.2, after what a global validity domain of the differential current protection will be given at the end of section 2.1.

c) Influence on the current to break

Since the current is damped by a high resistance, the current to break will also decrease when the fault resistance increases. It is shown on Fig.6.11.

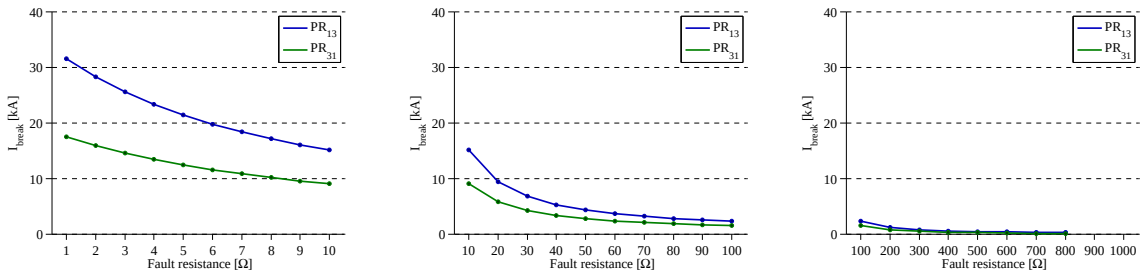

(a) $R_{fault} = 1..10\Omega$ (b) $R_{fault} = 10..100\Omega$ (c) $R_{fault} = 100..1000\Omega$

Figure 6.11: Current to break as a function of the fault resistance

There is no other comment to do on this phenomenon, and compatibility with the current breaking capability of the breakers will be discussed in section 2.1.3, after having determined the fault implying highest current to break.

2.1.2 Fault location influence

For a given fault resistance (here arbitrarily chosen to 1Ω), the fault location on one link impacts the detection time. Indeed, as is was shown in the parametric study of Chapter 4, the current magnitude are damped as they are propagating

along the cable. Even though the resistivity and internal inductance of the cables is low, but combined with the highest propagation time of the fault to the closest sensor, the impacts can still be observed on the detection times, that are illustrated on Fig.6.12a, which shows the detection and tripping time as a function of the fault distance from station 1. Once again, only link 1 is considered.

The highest detection time occurs for a fault located at the middle of the link. This is obviously due to the fact that if the fault is further 50km away station 1, it will thus be closer than station 3, so the current arriving at PR_{13} is thus responsible for the detection.

For higher resistances, the conclusions are the same as for a fault resistance of 1Ω.

Concerning the currents to break, the conclusions are easy to assess. First, for a given fault location, the current to break is higher for the closest relay. Then, the further the fault is from a considered relay, the smaller the value of the current to break is. This does not depend on the detection time, since the tripping is performed at the same time for both ends. However, it depends on the current value at the detection time. An example is discussed to justify this statement. For a fault located near station 1 (the point on the left of the figure), the current measured at the relay PR_{13} increases quicker than the current measured at the relay PR_{31}, since the fault is remote (see Chapter 4). This explains either a couple of points for a given fault location, and the shape of the curves of Fig.6.12b.

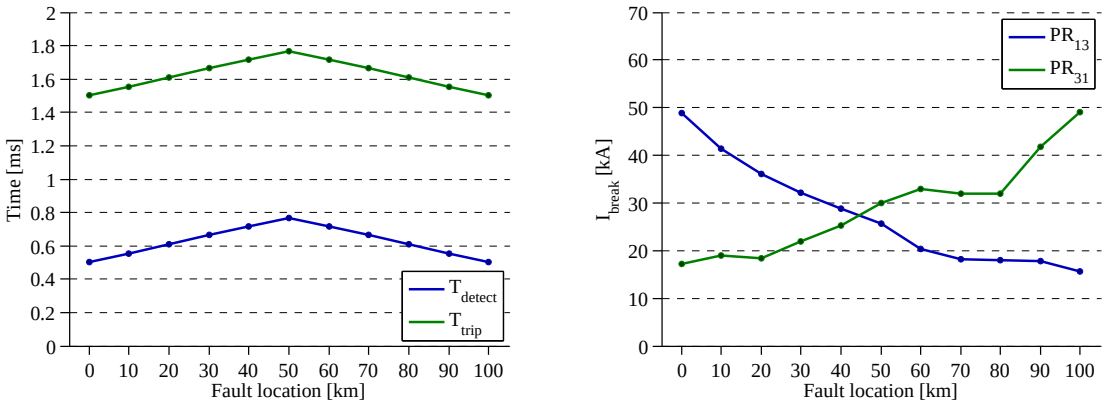

(a) Detection time

(b) Current to break

Figure 6.12: Fault location influence

Both the resistance and the location of the fault impact the detection time. Since the conclusions on the fault location are the same for another fault resistance, this implies that for some resistance values, the fault might be detected if it occurs near a relay, but will not be detected if it is located at the middle of the link. Thus, the validity domain of the differential current protection (Tab.6.9) will be provided for each link for the worst case in terms of detection, it means for faults occurring at the middle of the links. Therefore, it is possible that higher fault resistances can be detected if they happen somewhere else than at the middle of a cable. Once again, the constraint defined by the current flowing through the diodes of the converters is not exceeded for such high fault resistances.

Link	Maximal fault resistance detected at the middle of the link	Tripping time
LINK1	800Ω	3.300ms
LINK2	900Ω	2.930ms
LINK3	900Ω	2.810ms
LINK4	900Ω	1.350ms
LINK5	800Ω	2.900ms

Table 6.9: Validity domain of the differential current protection

2.1.3 Worst case scenarios

a) Worst case from the detection point of view

The differential current protection validity domain were assessed in the previous paragraph from the detection point of view, meaning in terms of tripping time. The worst case corresponds thus to faults occurring at the middle of Link1, with a resistance of 800Ω, for a maximal tripping time occurring 3.300ms after the fault occurrence.

b) Worst case in terms of current to break

The worst case in terms of current to break is now investigated. Given the conclusions of sections 2.1.1 and 2.1.2, the worst case would occur for a fault located

at a cable end. Hence, 10 faults were simulated, each one occurring at a cable end. The resulting currents to break are given in Tab.6.10. The value displayed corresponds to the highest value for the considered fault case, meaning the value that have to be broken at the closest relay to the fault (for fault located near relay 13, then the value is the one for relay PR_{13}).

Fault location cable end	Current to break
13	62.680kA
31	34.751kA
12	57.181kA
21	50.133kA
23	33.197kA
32	42.370kA
24	45.031kA
42	34.537kA
45	50.478kA
54	26.578kA

Table 6.10: Maximal current to break for faults located at cable ends

The worst case in terms of current to break corresponds to the fault occurring near relay PR_{13}, given this grid configuration, and exceeds 60kA. Such huge current values are too high considering the DC breakers that are under prototyping phase. Even though no maximal breaking current capability of future breakers is known at this time, it is very unlikely that they will be able to cut such current. Thus, solutions to decrease those current values need to be explored. Two of them were found. The first one uses fault current limiters and the other one consists in adding inductors at each feeder relay. The benefits of the incorporation of those new elements is one of the aims of section 4.

c) Worst case for the diode constraint

Those worst case scenarios, in terms of current to break, are also the worst case scenario for the protection operation time constraint. Fig.6.13 illustrates the tripping time and the diode constraint time for each fault. On this figure, a column

corresponds to a given fault occurring near the relay named in abscissa axis, the blue points corresponds to the detection time, the green point to the tripping time (1ms later), and the red point is the constraint given by the current flowing through the diodes.

The diode constraint is always verified, meaning that the tripping time is below the time when the current flowing through the diodes would exceed 2 per unit, except for Link5. Indeed, considering a delay of 1ms for the breaker, the diode constraint is exceeded. This is the case only for this link because it is the longest one (200km), which added another delay of 1ms due to the propagation of the data through the optical fiber. This put another limit on the validity domain of the differential current principle, in terms of maximal cable length that can be protected. For this grid structure and components, this maximal length is equal to 150ms. However, the incorporation of inductors at each feeder relay increases the maximal cable length that can be protected, since it reduces the current rate of rise that arrives at the converter station and thus the current that flows through the diodes. This will also be detailed in section 4.

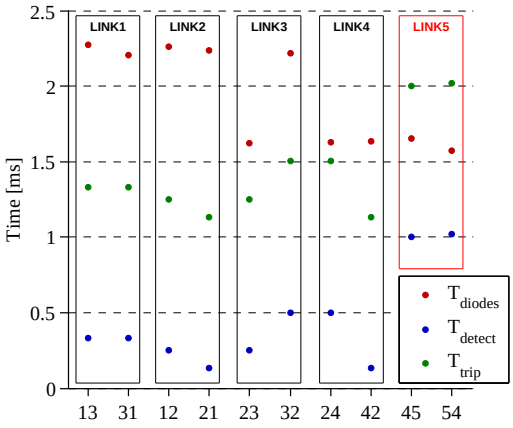

Figure 6.13: Detection time and diode constraint for faults occurring at cable ends

2.1.4 Frequency sampling requirements

The protection sampling frequency was assumed to be 100kHz, from the beginning. The influence of this parameter is investigated in this subsection.

Note that the simulations are computed with a frequency sampling of 1MHz. The fault is not necessarily synchronized with the sampling frequency of the protec-

tion system.

For a faulty link, the augmentation of the frequency sampling would not impact the detection phenomenon, but only the time of the detection. Indeed, the difference between two samples would still be positive, but the validation process using 3 consecutive samples would thus be longer. Also, the exact first time when the differential current exceeds the threshold becomes the knowledge of the protection at the first sample consecutive to the phenomenon. For example, with a sampling frequency of 100kHz, where samples are recorded at t = 10µs, t = 20µs, t = 30µs, ... if the prospective differential current exceeds the threshold at t = 12µs, the protection would know it only at t = 20µs, because the differential current is not computed at t = 12µs. Waiting then for 3 consecutive samples validation (samples at t = 20µs, t = 30µs, t = 40µs), the tripping order is sent after a total of t = 28µs once the differential current exceeded the threshold. If the sampling frequency is 10kHz (samples recorded at t = 100µs, t = 200µs, t = 300µs, ...), then the tripping order would this time be sent after t = 282µs. But still, the detection occurs.

At the opposite, the frequency sampling impacts the protection process. This was mentioned in Chapter 5. The algorithm is looking for a negative front in that case. The negative front duration corresponds to the propagation time of the wave through the cable. If no samples exist during this front, then the blocking of the protection does not occur, which can lead to unwanted trippings. Furthermore, since the protection uses once again 3 consecutive samples as a validation of the blocking process, 3 samples need to be present in this negative front. The required frequency sampling of the protection system is thus defined by the minimal cable length, in our case 25km. Thus, since the propagation time of a perturbation through the 25km cable is equal to 129µs, the frequency sampling has to be up than 23kHz.

However, using a frequency sampling of 23kHz and given the conclusion expressed concerning the faulty link case, this would result in a delay in the trippings leading to diode constraint exceeding for some cases. It is thus highly dangerous to decrease the frequency sampling, and 100kHz, meaning a time step of 10µs, should be conserved.

2.1.5 Impact of synchronization error

In the previous part, an ideal GPS synchronization of the protections was assumed. Hence, the differential current is evaluated at each step time thanks to the current measured at the exact same time, at each end of the cable. However, a synchronization error may occur and its influence needs to be investigated. Fig.6.14 displays the differential current for a faulty link (on the left) and a healthy link (on the right) for different synchronization errors. The two red lines are respectively the positive and the negative threshold examples I_{dTH+} and I_{dTH-} of the differential protection.

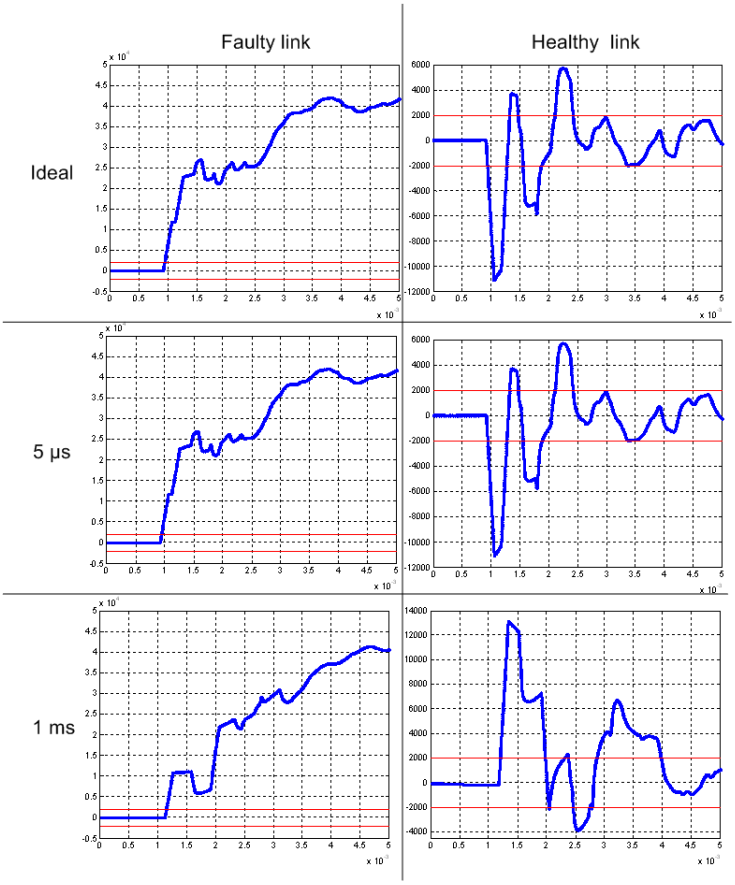

Figure 6.14: Differential current for several synchronization errors

The idea is the same than for the influence of the sampling frequency. For a faulty link, the synchronization error may delay the time when the differential current reaches the positive threshold. This results in a delay of the tripping order, but does not affect the protection principle and the selectivity if the delay stays beyond the time constraint given by the diodes. However, for a healthy link, the synchronization error may impact the shape of the differential current and hide the

negative front transient that is used by the protection algorithm to block the protection during Δt_{block}. This would result in an unwanted tripping of the protection.

Nevertheless, there is a maximum synchronization error that guaranties no unwanted tripping of the healthy links. In fact, the negative front transient would be hidden if the propagation time of the wave is equal or lower than the synchronization error. Thus, the maximum error allowed depends on the length of the link and is the value of the propagation time of the wave generated by the fault through the cable. For example, this value is equal to 515µs for a 100km long cable. Since the already installed GPS synchronization devices ensure a synchronization error lower than 5µs [Siemens, 2008], no unwanted tripping would occur on a link longer than 1km, which covers most of the cases of DC links in a transmission grid. For shorter links, other communication principles would require further investigations in order to avoid unwanted trippings.

2.2 Backup protection

Alike the differential current protection, the backup protection principle is illustrated through an fault example. This fault example parameters are provided in Tab.6.11.

Parameter	Value
Type	Pole-to-pole
Location	Link1
Position	neat relay PR_{13}
Impedance	1Ω
Fault occurrence time	t = 0

Table 6.11: Parameters of the fault example

The differential current protection detects this fault at t = 440µs. The DC breaker of relay PR_{31} thus trips at t = 1.440ms, and a breaker failure is simulated at the relay PR_{13}. The three criterion C1,C2 and C3 related to the backup principle of relay PR_1 and relay PR_3, meaning the stations connected to the faulty cable, are shown on Fig.6.15. On Fig.6.15a, it can be seen that the three criterion are both

equal to 1 after t = ms. The last criterion that takes the 1 value is C1, which waited for the temporization delay Δt^1_{main} after the fault was detected. The selectivity criterion C2 is validated at t = 864µs, and since no breaker of relay PR_{12} or PR_{13} tripped, the criterion C3 remains at the value 1. For the backup protection implemented on relay PR3, the selectivity criterion is not reached. Also, since the breaker of the relay PR_{31} tripped thanks to the order of the differential current protection, criterion C3 goes down to 0. The fault was however detected, but the tripping order from the backup is inhibited by criteria C2 and C3.

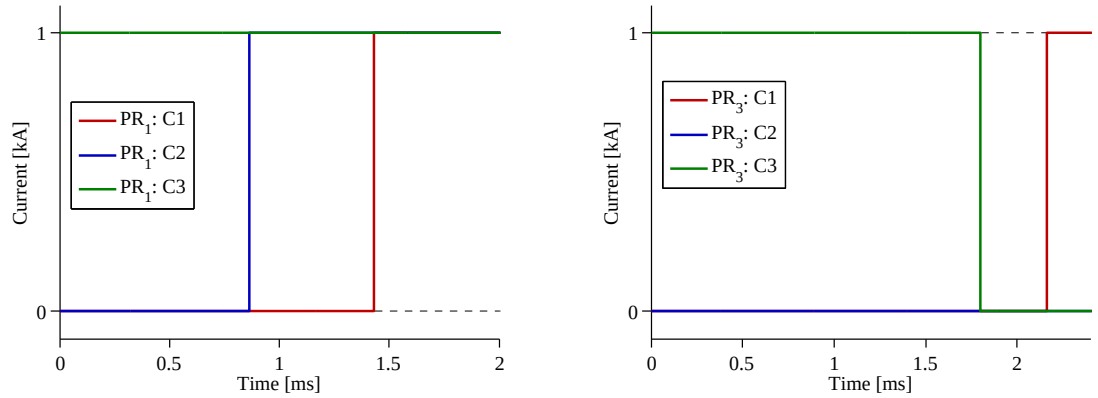

(a) C1, C2 and C3 evaluated at PR_1

(b) C1, C2 and C3 evaluated at PR_3

Figure 6.15: Criteria related to backup operation

For the backup protections implemented in relays PR_2, PR_4 and PR_5, the only criterion that takes the 1 value is C1 (the detection criterion).

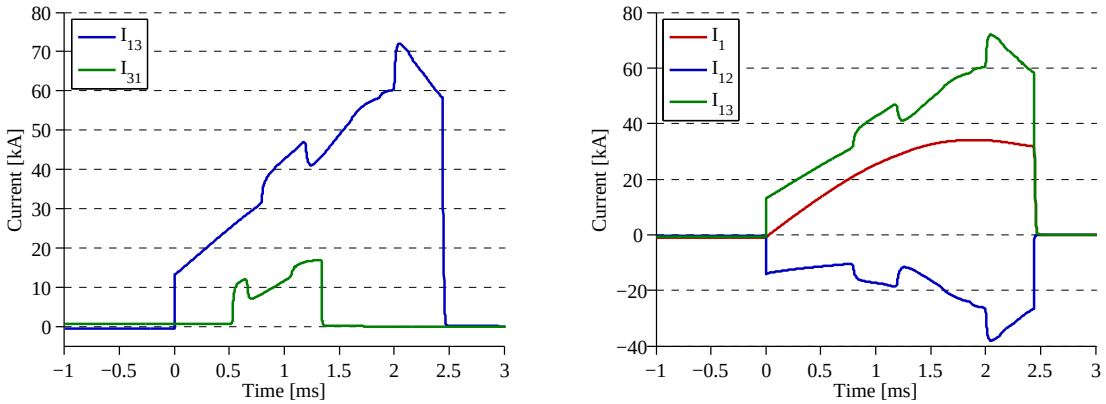

(a) Faulty cable ends

(b) Station 1 and its feeders

Figure 6.16: Current measurements for the fault clearing process

The fault is thus cleared by the differential protection at one faulty cable end ($PR_3$1), and by the backup protection thanks to the tripping of breakers related to PR_1 and PR_{12}, since the breaker of PR_{13} failed. The related operation times are summarized in Tab.6.12, and Fig.6.16 represents the relevant current measurements to illustrate this fault clearing process.

Protection principle	Relay	Selective detection	Tripping	Current to break
Differential current	PR_{13}	430µs	1.430ms	16.744kA
	PR_{13}	430µs	FAILED	prosp: 43.175kA
Backup	PR_1	1.440ms	2.440ms	31.751kA
	PR_{12}	1.440ms	2.440ms	26.654kA
	PR_{13}	1.440ms	FAILED	prosp: 58.416kA

Table 6.12: Relevant operation times related to the clearing process of the fault example, and current to break by the breakers (prosp means prospective current to break if the breaker did not failed

Even though the breaker of the relay PR_{13} failed, the fault is cleared and the grid remains in operation, as it is illustrated on Fig.6.17. The current to break are smaller at the cable end where the breaker failed since this current is separated in 2. The differential current (Fig.6.17b) of both healthy links are below the threshold value after the blocking time $\Delta t_{block} = 30$ms because the fault is cleared. The current measurements at the station relays (Fig.6.17a) show that the grid recovers.

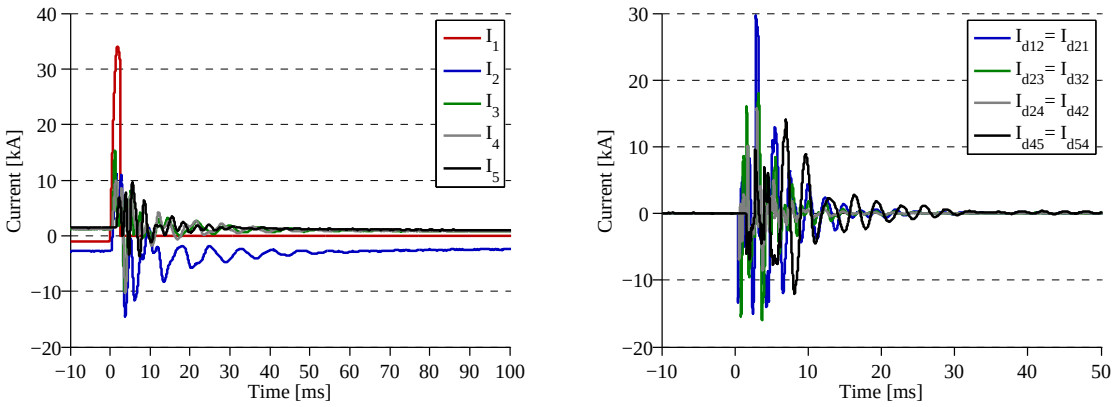

(a) Faulty cable ends

(b) Station 1 and its feeders

Figure 6.17: Current measurements for the fault clearing process

The relevant operation times and current to break for the worst case faults in

terms of current to break are the most likely ones subjected to imply a breaker failure. Since those times and current do not add any crucial information, they are given in Appendix B1.

2.2.1 Validity domain of the backup protection

a) In terms of detection

The selectivity criterion threshold setting were explained in section 1.2.3. They were chosen in order to be selective for the worst case fault scenarios. By doing so, the selectivity is ensured for each case, meaning that unwanted trippings cannot happen in relays related to busbar connected to healthy cables. However, the margin between the minimal value they must be (given by this selectivity principle) and the value the variable takes when the worst case fault is effectively in its protective zone was very low. This means that if the thresholds are chosen to ensure the selectivity, then the detection will be validated for a short range of faults. This is the case for the Twenties grid structure used here. Indeed, faults of 10Ω, or faults located at the middle of the links are not detected by the backup principle. This is due to the selectivity criterion C2. The detection criterion C1 and the criterion C3 are working though.

The backup principle hence covers a poor fault range, either in terms of resistance and in terms of location. It has to be improved. These improvements are mentioned in section 4.2.2, that is why a detailed covering range was not looked for before implementing those improvements.

b) In terms of DC grid constraint requirements

For most cases, the time constraint given by the current flowing through the diodes of the converter is not fulfill. Indeed, for the example shown in this section, the fault is cleared by the backup at $t = 2.440$ms, but the diode constraint is reached no later than $t = 2.272$ms. The proposed backup protection do not fulfill the specification of the protection plan expressed in Chapter 5. This is mostly due to the 1ms time delay related to the operation of the breaker, which is responsible for the large temporization delay Δt_{main}, and another delay before the tripping after the backup order.

There is no way this breaker operation speed would be decreased in a near future, which is why the solution of the backup operation time has to be investigated through modifying the grid structure. Indeed, as it was mentioned in Chapter 5, the addition of feeder inductors is considered for several reasons, that will be developed and tested in section 4. An impact of this inductors is that they relax the current flowing through the converter diodes, which increases the time constraint. This can thus give the time to the backup to operate in a safe time range. Those notions will be developed in section 4 page 211.

2.3 Busbar protection

As for all other protection principle, an fault clearance example is shown to illustrate the operation of the busbar protection. A pole-to-ground fault of 1Ω is simulated on the busbar connected to station 1. The current measurements at this busbar are depicted on Fig.6.18, and the relevant information are given in Tab.6.13.

$T_{I_{diode}>2pu}$	$T_{I_{bus1}>I_{busTH}}$	Relay	T_{trip}	Current to break
2.272ms	30µs	PR_1	1.030ms	33.522kA
		PR_{12}	1.030ms	23.899kA
		PR_{13}	1.030ms	18.789kA

Table 6.13: Busbar fault clearance operation information

The busbar differential exceeds the threshold instantaneously after the fault occurrence (meaning at the next protection sampling point, at t = 10µs). The delay in the detection time of 20µs is due to the data process assumption explained in section 1.1.

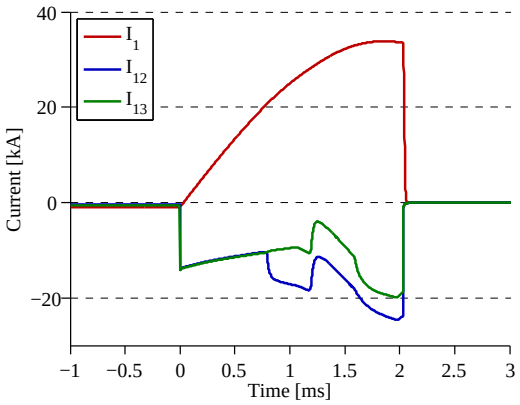

Figure 6.18: Busbar fault clearing process

The validity domain is expressed in terms of fault resistance only since the fault location on the busbar do not impact the variable I_{bus} used for the detection. The maximal fault resistance that can be detected is hence 600Ω.

Besides, the differential current protection and the backup protection as well do not imply unwanted trippings in case of busbar faults. For the differential current protection, this is due to the fact that a busbar fault will imply a first negative current wave front. For the backup protection, this is due to the temporization delay Δt_{main} which is larger than the operation time related to the backup operation. Indeed, the busbar protection operation time is much smaller than the cable differential current time since it is not based on long communication links. For this same reason, the grid constraint related to the current flowing through the diode is never reached for busbar faults.

2.4 Conclusion on the theoretical performances of the protection system

In this section, the proposed protection system was tested through the TWENTIES grid structure.

The busbar protection was validated, and covers faults with resistance up to 600Ω.

Concerning the main protection, the fault resistance range is higher, and depends

on the cable length. Note that for those two principles, the fault resistance covering range is largely acceptable since the experience feedback of TSO's points out that faults with a resistance higher than 200Ω are extremely rare in underground cables.

While the time constraint related to the current flowing through the diodes is never reached for faults occurring on busbars, it is exceeded for some faults in Link5. This is due to the 1ms delay related to the data communication through the optical fiber. The simulations points out that using this grid structure, a maximal allowed cable length of 150km is required to ensure the protection plan specification.

The main concern highlighted by those simulations is the dramatically huge currents to be broken by the DC breakers. Indeed, the DC breakers are still under prototyping process, and they do not have this kind of huge current breaking capability. Some solutions hence need to be found to decrease these large values, and the best one that was found was to add inductors at each feeder relay. This will be the topic of section 4

These modifications in the grid structure will also improve the backup protection, which has a poor validity domain. The improvements will be either on its fault detection range and on the compatibility with the DC grid constraint.

Before going through those grid modification, the validation of the whole protection chain on a real-time mock-up will be presented in the next section. This demonstrator is the TWENTIES DEMO 3 demonstrator, mentioned in the introduction of this manuscript.

3 Real Time HIL demonstrator

The purpose of this chapter is to validate the full protection chain principle including the sensors, the selective detection algorithms and the DC breakers. To go beyond theoretical simulation results, a real time hybrid low voltage mock-up was assembled in L2EP building, in Lille. The project was supported by RTE and the European Commission, since it is a part of TWENTIES WP11 objectives. It makes it possible to run tests on different control laws for DC grids and experiments on protection devices.

Since on-site tests cannot be conducted (because no multi-terminal HVDC grid using VSC technology exists) and since a unitary scale MTDC grid mock-up is impossible to achieve in a laboratory, for many reasons such as space, insulation, safety and cost issues, and because all the components constituting DC grids are not available yet (especially the DC breakers), a low-scale mock-up was designed with the aim to be as representative as possible of what would happen in real DC grid applications. Fig.6.19 gives a general overview of the mock-up configuration. It aims to represent the TWENTIES grid structure used in this thesis, with a DC grid voltage of 250V. Station 3, 4 and 5 are connected to wind farms, and station 1 and 2 are connected to AC grid.

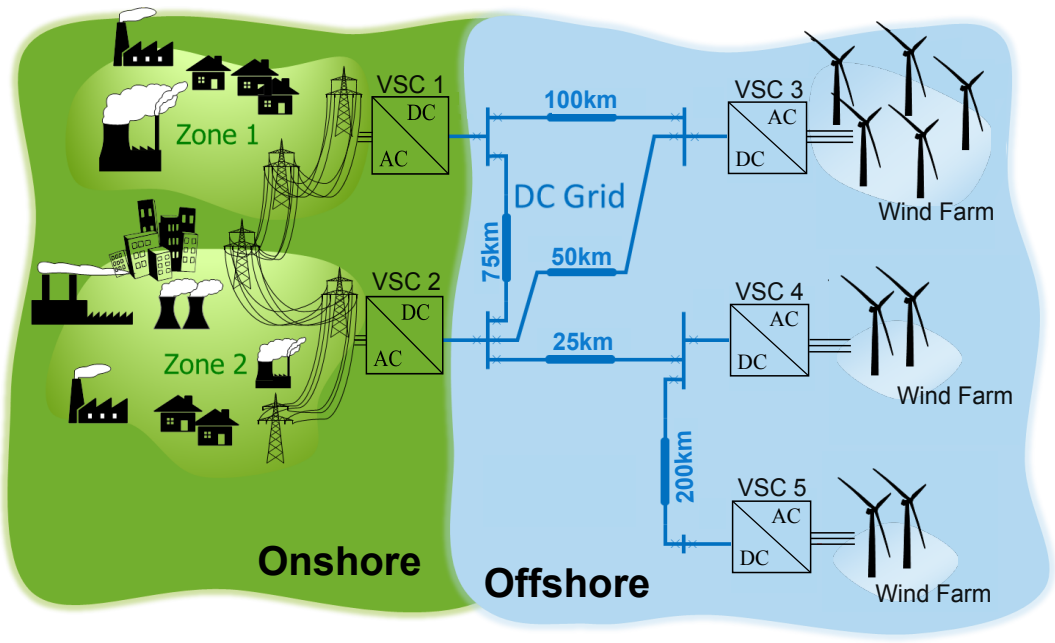

Figure 6.19: Mock-up overview

3.1 Overall mock-up design and description

The organization of the mock up is explained on Fig.6.20. Two main parts can be highlighted:

- Devices that are actually physical
- Devices that are real-time simulated (in the blue form)

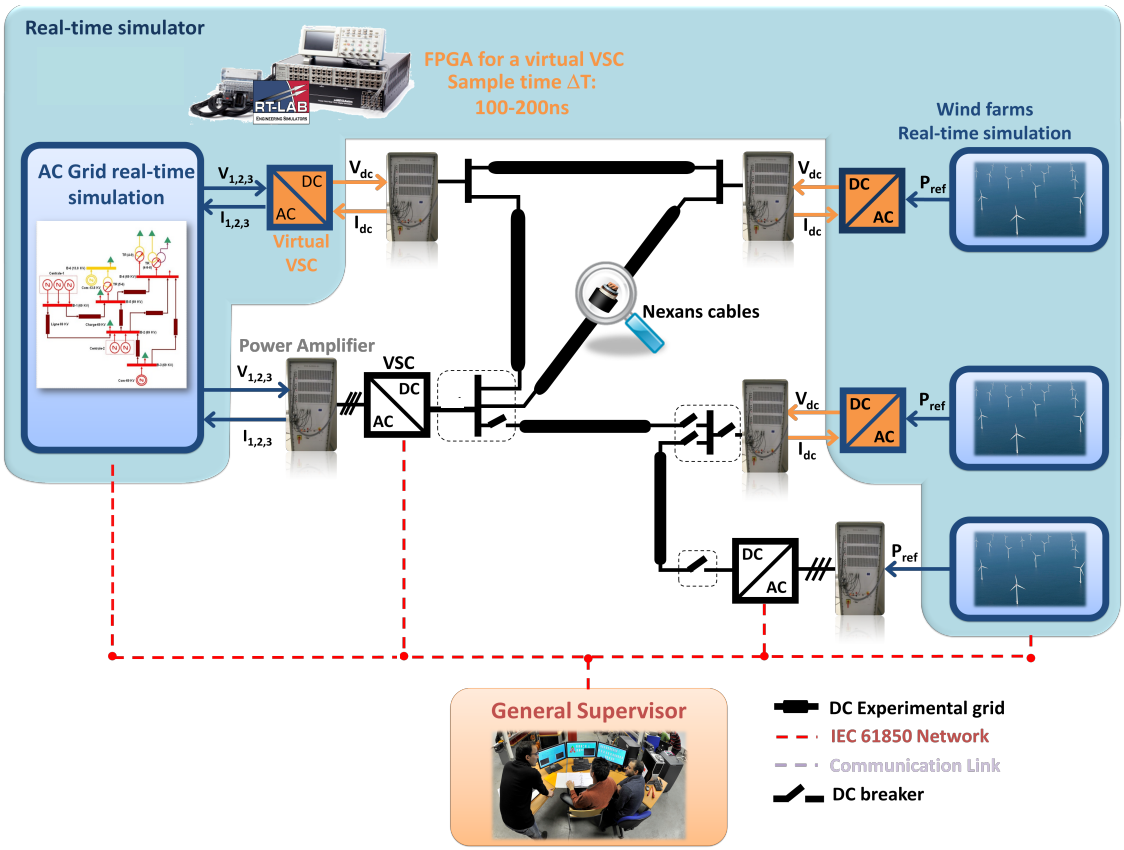

Figure 6.20: Mock-up configuration

The interface between the real-time simulator and the physical devices is achieved thanks to high bandwidth amplifiers.

Two out of the five VSC are actual converters, and are connected to the AC grid or offshore wind farms thanks to a power amplifier configured as a three-phase amplifier.The three other VSC are real-time simulated.

The control of the mock-up (converter engagement, control type, power reference, fault creation) is done thanks to a SCADA system.

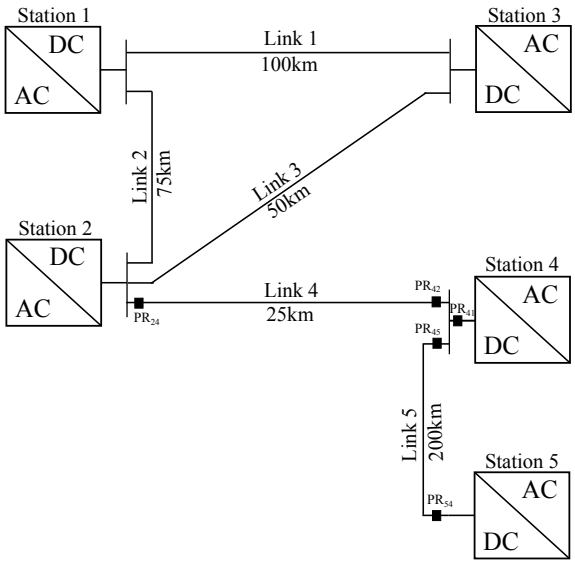

Figure 6.21: Notations used for the mock-up

3.1.1 Real-time simulator

A OPAL-RT real-time simulator is available in the L2EP lab. The simulator is made of two racks with 7 cores (i7 core) available for simulation. These cores may be used in different ways. For the mock-up application, one rack is used for the simulation of the AC system and the wind farms, the other for the simulation of the protection algorithms. The protection relays implementation will be treated in subsection 3.2. The AC grid and wind farms models are implemented on only one core since the computation time is quick. The main features (on each rack) are the following ones:

- 16 Analog Inputs
- 16 Analog Outputs
- 32 Digital I/O

Those features are used to link the real-time simulated parts and the amplifiers.

a) AC grid model

For power grid control purpose, the AC grid is represented thanks to a Kundur power system model [Kundur, 1994]. The structure and the value of the parameters are described in Fig.6.22. The AC grid is connected to VSC 1 and 2, which could be either master-controlled (voltage), slave-controlled (power) or droop-controlled.

Since this topic is not the purpose of this thesis, the fault tests were conducted with VSC 1 master-controlled, VSC 2 slave-controlled. Please refer to [Rault, 2013] for more details on the advantages of the use of a Kundur grid model.

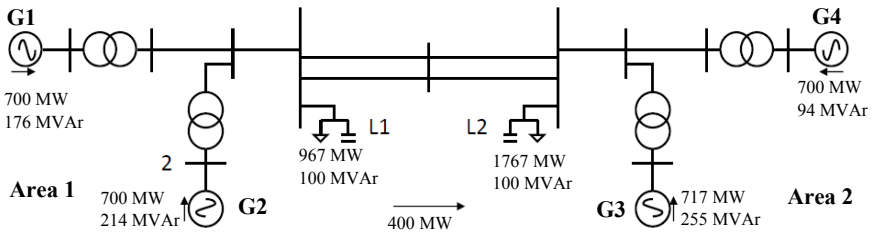

Figure 6.22: Kundur AC power grid model

b) VSC model and filters

The VSC are represented by an average model (which is also available in EMTP-rv) and this model controls the power amplifiers. Same parameter name notations than Chapter 3 are used. Their values are given in Tab.6.14. The only difference between the mock-up and the previously studied TWENTIES grid structure is that for the mock up, no transformer is used. A per unit approach was used to design the passive components, and only one AC per unit base needs to be defined.

The control of this VSC is implemented in the real-time simulator, and they are interfaced with the DC bus thanks to a power amplifier configured as a DC amplifier.

	Parameter	High power converter value	Per Unit value	Mock-up value
AC side	S_{base}	1077MVA		3kVA
	$U_{AC-base}$	320kV		125V
	$I_{AC-base}$	1943A		14A
	$Z_{AC-base}$	95.1Ω		5.2Ω
	LCL filter cut-off frequency	500Hz		1kHz
	R_s	0.48Ω	0.005	0.17Ω
	L_s	45mH	0.15	2.5mH
	R_t	0.48Ω	0.005	0.17Ω
	L_t	45mH	0.15	2.5mH
DC side	$U_{DC-base}$	640kV		250V
	$P_{DC-base}$	1000MW		2500W
	$I_{DC-base}$	1563A		10A
	C_s	50µF	0.0102	819µF
	L_s	10mH	1.10^{-5}	610mH

Table 6.14: Per unit approach for passive components design

c) Wind farms model

The power reference of VSC 3, 4 and 5 is calculated thanks to the historic of actual wind turbine production data provided by L2EP lab. The amplitude of the power generated can be chosen by multiplying it by a ratio, but the intermittent effect is kept. VSC 3 and 4 are thus modeled as a power controlled VSC, and physical VSC 5 is in slave mode (power-controlled). The power reference is equal to the power generated by the wind farms.

3.1.2 Digital-analog interconnection

The linear power amplifiers are the interface between the simulated model and the physical devices. The connection between simulated and actual environment is based on Power Hardware in the Loop (PHIL) principle ([Craciun et al., 2011]) which is described on Fig.6.23 and operated as it follows:

- The simulated model of VSC computes the DC voltage for the capacitor.

- The DC voltage signal is applied on the input of the linear amplifier as a voltage reference (us_{ref}).
- The linear amplifier applies a voltage on the DC bus.
- The current in the DC bus (i_{DC}) is measured and then converted into a digital signal.

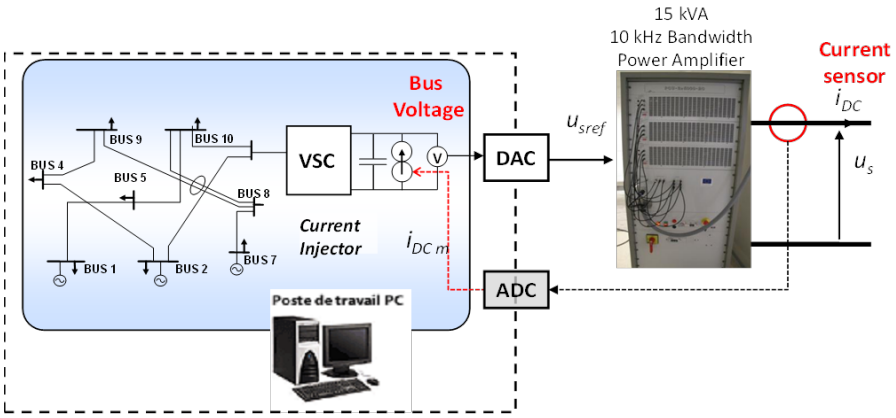

Figure 6.23: PHIL concept

To mimic as closely as possible the actual analog behavior of the VSC, its real-time model was implemented in a field-programmable gate array (FPGA) board with a very low time step (150ns).

Note that intensive off-line simulations obviously preceded real time tests in order to quantify all physical parameters of the mock-up.

3.1.3 Physical devices

a) VSC

Two-level VSC assembling and control development were done by engineers from the L2EP lab in Lille. Fig.6.24 illustrates the devices composing it. The control of these two VSC is implemented on an external digital signal processor (DSP) specially devoted to this application. Even if the principle of both VSC controllers is the same, the implementation is rather different since the external control on DSP supposes the development of a specific hardware.

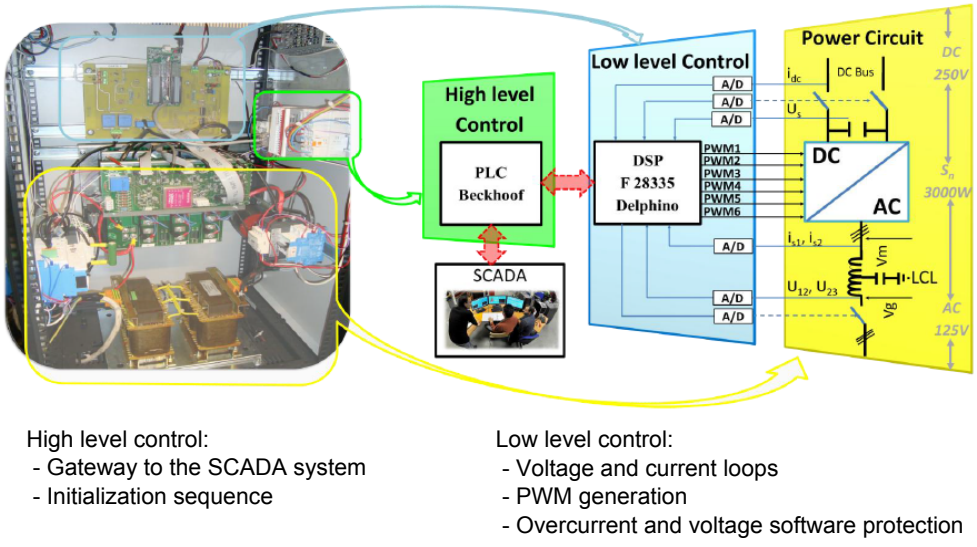

Figure 6.24: Physical VSC and control

b) DC cables

As developed in Chapter 3, DC cables are key components since the signals behavior under fault conditions is highly correlated to the cable model used in simulations. This is why the use of physical cables as representative as possible to high voltage XLPE cables was chosen. However, considering the difficulty to make coincide both high and low voltage families, and because the behavior of control regulation loops is sensitive to link resistance and to the magnetic and electrostatic energy stored in the cable, adding the fact that protection algorithms are dependent on the waves propagation speed in the cable, the idea was to use a cable which would have characteristics that are homotetic to the ones of a real XLPE 320kV 2500mm^2 Cu cable. Please refer to Ta.3.3 and Tab.3.2 in Chapter 3 page 59 for real XLPE cable parameters value.

Regarding the impossibility to store very long length cables in the L2EP laboratory, the choice was limited to a total length of 15km per pole for the whole DC grid. Nexans proposed to use cables with copper sections of 10mm^2 or 25mm^2, with a structure shown on Fig.6.25, and characteristics depicted in Tab.6.15 and Tab.6.16. The 10mm^2 cable is used for Link5 and the 25mm^2 cable for the other links. The cables are a reduced scale technology of the real DC cables, and the sections were chosen to obtain a maximal voltage drop of 10% for a current of 10A and a nominal voltage of 250V.

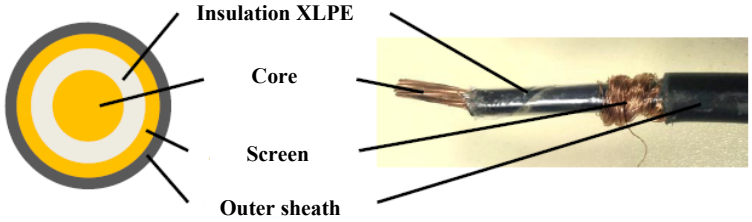

Figure 6.25: Nexans cable structure

10mm^2 Nexans cable		
Conductor	Core	Screen
r_{int} [mm]	0	2.55
r_{out} [mm]	1.85	2.72
$r_{ext\,insulation}$ [mm]	4.3	

25mm^2 Nexans cable		
Conductor	Core	Screen
r_{int} [mm]	0	3.05
r_{out} [mm]	3.95	4.10
$r_{ext\,insulation}$ [mm]	5.8	

Table 6.15: Nexans cable geometrical properties

Cable section	ρ_c	ϵ_i	L'[mH/m]	C'[µF/m]
10mm^2	$1.72e^{-8}$	2.3	$4.8e^{-1}$	$3.22e^{-4}$
25mm^2	$1.72e^{-8}$	2.3	$3.79e^{-2}$	$4.15e^{-4}$

Table 6.16: Nexans cable dielectric properties

Assuming that, the DC cable configuration in the mock-up is given on Tab.6.17.

Link	Number of drums per pole	Drum length [m]	Total cable length [km]
Link1	10	227	2.270
Link2	8	227	1.816
Link3	5	227	1.135
Link4	2	227	0.454
Link5	9	161	1.449

Table 6.17: DC cable configuration on the mock-up

This kind of cable has the same propagation speed than the real high power DC cables. However as the total length is smaller, the propagation time has to

be increased. The idea was to keep cable on their cable drums to increase their linear inductance and thus the propagation time ($t_{propa} = \sqrt{LC}$). As illustrated on Fig.6.26, the cables were installed on their cable drums, and they were connected to each other with shielded junction box.

Figure 6.26: Nexans cable on their drums

In this configuration, the linear inductance and capacitance for each cable was measured and new propagation speeds were calculated. Tab.6.18 summarizes the characteristics. Note that the parameters identification were done at a frequency of 1kHz.

Cable number	R′[Ω/km]	L′[mH/km]	C′[µF/km]	Mock-up cable t_{propa}[µs]
Link1	0.6806	38.106	0.409	285
Link2	0.6806	38.106	0.409	228
Link3	0.6806	38.106	0.409	142
Link4	0.6806	38.106	0.409	57
Link5	1.6977	40.511	0.320	570

Table 6.18: DC cables on their drums parameters identification

3.2 Protection system components

Each protection relay is composed of a voltage and a current sensors, a DC breaker and is organized as shown on Fig.6.27.

Protections implementation will be described in subsection 3.2.3, but the breaker state of one feeder or one station connection point is the same for both positive

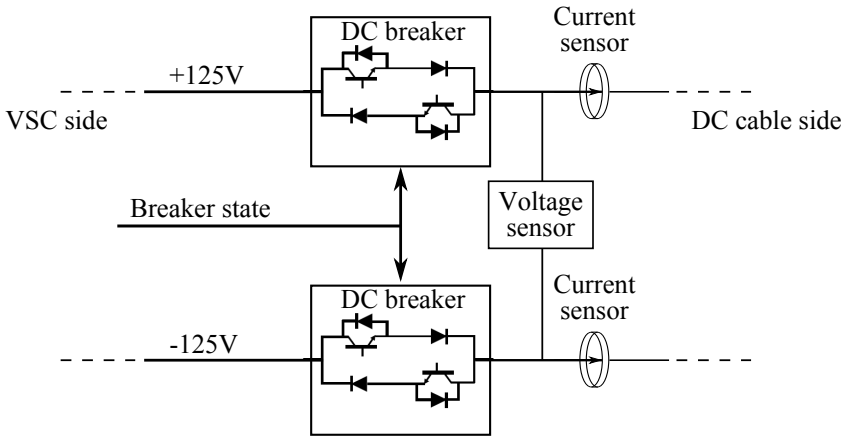

Figure 6.27: Protection relay organization

and negative poles, because they are controlled by the same protection algorithm. Indeed, only pole-to-pole fault will be generated so there is no need to implement the selectivity regarding the faulty pole. The breaker control will be detailed further.

3.2.1 Protection-related physical devices

a) DC breaker

DC breaker devices, that are associated to protection relays and to the fault generator device, are composed of IGBT and diodes in order to create a 4 quadrants switch (Fig.6.28). They are associated with surge arresters (placed at each IGBT terminals) so the overvoltages created during the current breaking process are limited. The surge arrester is a varistor with characteristics given in Tab.6.19.

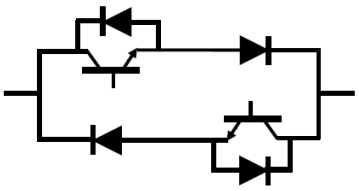

Figure 6.28: DC breaker device

Name	Value
V_{DC}[V]	615
i_{max}[8/20µs]	40000
W_{max}[2ms]	1000
P_{max}[W]	1.4

Table 6.19: Varistance characteristics

b) Sensors

Voltage and current sensors main characteristics are given in Tab.6.20. The current sensor technology is a closed loop (compensated) current transducer using the Hall effect. Pole-to-pole voltage is measured.

Voltage sensor	
Reference	LEM CV3-500
Nominal voltage	350V
Bandwidth	DC-300kHz
Saturation	500V

Current sensor	
Reference	LEM LA 100-P/SP13
Nominal current	100A
Bandwidth	DC-200kHz
Saturation	160A

Table 6.20: Sensors characteristics

c) Fault generator device

The fault device is composed of parallel resistances, that are connected or not, so as faults with resistance from 1 to 10Ω can be generated (Fig.6.29). The fault resistance is equal to $\frac{10}{N_R}$, where N_R is the number of connected 10Ω resistances. The fault is placed in order to create a pole-to-pole fault, either at the middle of Link4 or at the middle of Link5. The choice between those two locations is done through the SCADA system, on which it is possible to select the fault resistance. The connection of the fault is done by a FAULT START button on the SCADA system which commands the 4 quadrants IGBT switch. A pole-to-ground fault was unlikely to be tested because of the uncertainties of the ground network of the laboratory and safety issues. The fault generator device can eventually be located to some other places in the DC grid, but requires additional cabling work so it was not done before the writing of this thesis.

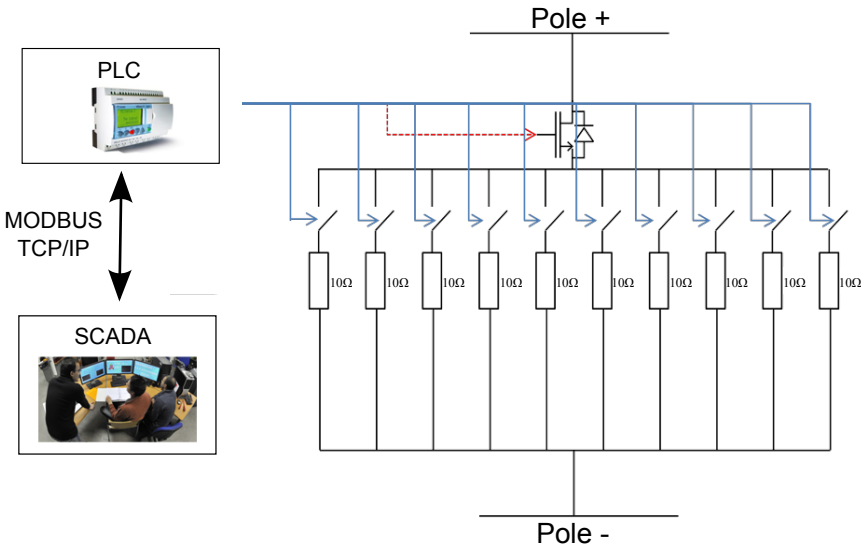

Figure 6.29: Fault generator device

3.2.2 Physical devices positioning

Due to cost issues, only 10 breakers could be bought and their location on the mock-up is displayed on Fig.6.20 page 173, where only the positive pole is represented, but the two poles are equally equipped. Each breaker is associated with a current and a voltage sensor, as illustrated on Fig.6.27 page 181. The voltage sensor however is not used for protection purposes.

This implementation was used for the first test series, and was then modified in order to conduct other tests that will be explained in subsection 3.4.

3.2.3 Protection relays implementation

a) Tested protection principles

The protection algorithms related to the following principles are implemented on the mock-up.

- Cable differential protection
- Busbar protection
- Backup

Indeed, the protection using the voltage measurement between the feeders inductance terminals cannot be implemented since those inductances were not placed on

the mock-up. This is due to the fact that this protection algorithm was investigated only after the mock-up development.

A protection relay is associated with each breaker located on the positive pole, and controls the breakers of both positive and negative pole. As mentioned in 3.1.1, the protection principles are real-time simulated in a totally independent simulator, with a frequency sampling of 100kHz. The inputs are the current measurements provided by the sensors, and the outputs are the breaker states.

Giving this configuration, the cable differential protection are implemented in each relay they can be, meaning only at PR_{24}, PR_{42}, PR_{45} and PR_{54}. Note that PR_{54} and PR_5 that have been defined in the previous parts of this chapter are here the same protection, since no component is placed between them. This protection is named PR_5 for the mock-up study. Busbar protection is implemented at PR_4. Only the busbars connected to station 4 and station 5 are equipped with backup protection, since station 2 is not equipped with enough breaker and sensors. However, since station 4 is not composed of a physical converter, the current shape I_4 under fault conditions does not correspond to what it would be in real applications. Indeed, I_4 remains constant, and makes it impossible to apply the backup protection principle at this node. Protection algorithms related to each relay are implemented, as shown on Fig.6.30, which represents the model which is real-time simulated.

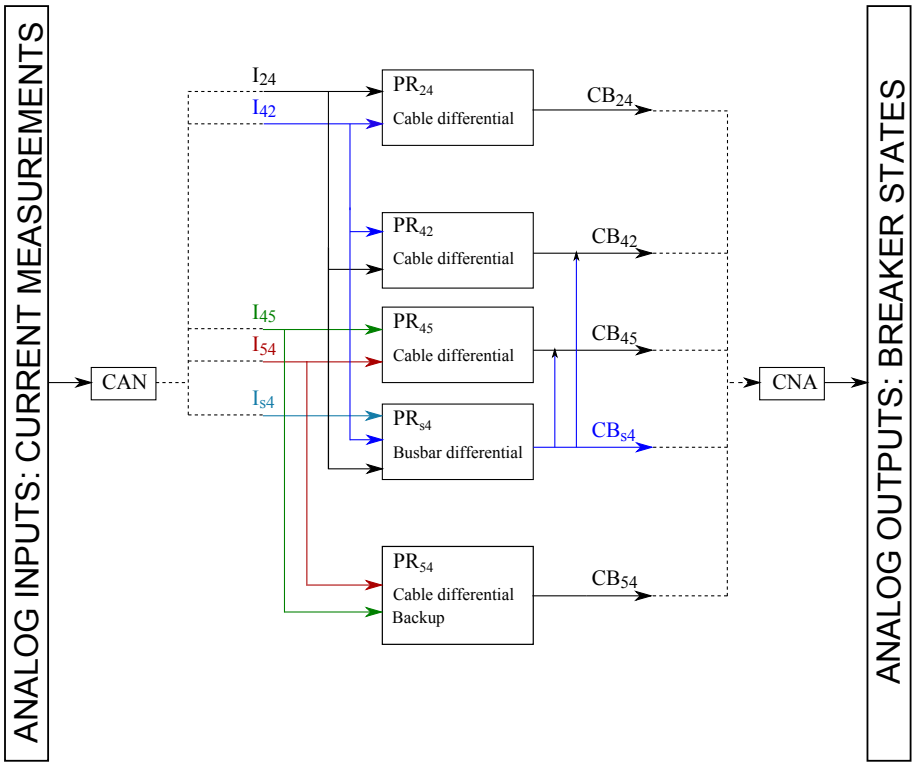

Figure 6.30: Protection relays implementation

b) Other information related to the algorithms

For the cable differential protection, the optical fiber link is modeled using a delay corresponding to the propagation time of the data (200km/ms). The considered length is the one of the grid that was aimed to be represented by the mock-up, and not the real cable length, meaning 25, 50, 75, 100 and 200km. The numerical values for those delays are the same than the one used in the EMTP-rv study in section 1, and are reminded in Tab.6.21. The time delays are approximated to the upper value in order to fit the sampling frequency of the simulation. The different protection algorithms are not reminded here, as they are described in Chapter 5.

Link number	Length [km]	Propagation time [µs]	Simulation delay [µs]
Link1	100	500	500
Link2	75	375	380
Link3	50	250	250
Link4	25	125	130
Link5	200	1000	1000

Table 6.21: Data propagation delay in the optical fiber

The backup is implemented using the same variable for the detection and the selectivity criterion. These variables, used by the backup protection algorithm as explained in 1, are named G_d^i and G_s^i, where i corresponds to the station number connected to the concerned busbar. It is evaluated thanks to equation (6.9).

$$G_d^i = G_s^i = |I_i(t) - I_i(t - 20\text{ms})| \tag{6.9}$$

c) Threshold scaling

The mock-up purpose was to represent the behavior of a DC grid as close as possible to what it would be in real application. Even though, it cannot pretend to behave exactly the same way with a scaling factor, for several reasons such as the fact that some of the converters are not physical, or because the cables drummed. As a scaling process cannot be done to define the threshold applied on the protection algorithms, they were adjusted thanks to EMTP-rv simulations of the mock-up. The model uses CP cable models, and will be described further in 3.4.5.

The effects to be observed on the mock-up are the transient behavior in the signals and the protection relays functioning (selective detection, no unwanted trippings). This is to highlight the fact that the threshold values (as long as they allow a selective detection) are not very important here, since they will only affect the operation time related to Δt_{detect}, which was defined in 2. Indeed, the effect of the reduction or increase of the threshold values is known, and can be assessed thanks to the results with a given threshold value. The numerical values will be given at the beginning each paragraph related to a test series, since they are set for the whole series and do not change.

d) Signal processing chain

The real-time simulated protection plan and its interactions with the mock-up are illustrated on Fig.6.31. For clarity of illustration purposes, only the main cable differential protection is represented on the scheme.

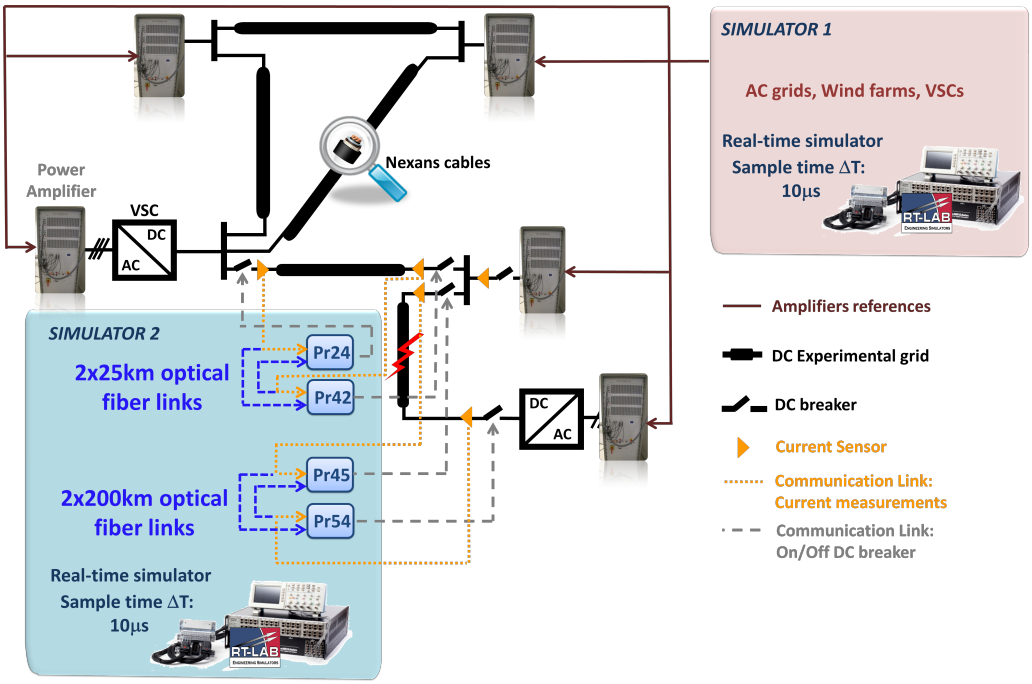

Figure 6.31: Protection interactions

3.3 Demonstrator control

The mock-up is controlled thanks to a SCADA system (Fig.6.32). It enables to control manually the connection of the VSC, the power references, and the creation of a fault. The protection plan can also be controlled by the console related to the simulator. It is possible to activate, disactivate a protection relay, or to simulate a breaker failure by forcing the breaker state to a 0 constant value.

Figure 6.32: SCADA system to control the mock-up

3.4 Real Time HIL tests results

The tests regarding DC faults and protections plan validation are presented in this subsection. Other tests related to substation control had been conducted, such

as power dispatch identification, drop control dynamics observation, on so on. About this topic, please refer to [Rault, 2013] and deliverable twenties 11.3 for details about configurations and conclusions.

3.4.1 Tests description

As said earlier in this chapter, the cable differential protection and the backup protection have been tested through several tests that will be presented further. One test series was done on the TWENTIES grid DEMO3 implementation presented earlier in the current section, and a second test series has been conducted for another configuration of the mock-up. A complete list of the tests that have been conducted on the mock-up can be found in appendix B2. Only the relevant cases will be addressed in this subsection.

3.4.2 Test series 1 results

Three of the tests that were conducted on the TWENTIES configuration are highlighted here. They are described in Tab.B.3. The notations used are the same as in Fig.6.21.

Test	Faulty link	R_{fault}	VSC 2	VSC 5	Operation point	Comments
T1	Link5	5Ω	–	Ph	VSC5 +100W	—
T2	Link4	10Ω	Ph	Ph	VSC5 +300W	—
T3	Link5	5Ω	–	Ph	VSC5 +100W	Cable differential protection disconnected at PR_{54}

Table 6.22: Test series 1 description, Ph: physical VSC, –: not connected, +100W: injects 100W to the DC grid

The threshold values set for this test series is given in Tab.6.23.

Protection	Threshold name	Threshold value
Main cable differential	I_{dTH+}	12A
	I_{dTH-}	−10A
Main busbar differential	I_{busTH}	10A
Backup	G^5_{dTH}	3A
	G^5_{sTH}	10A
	I_{feedTH}	1A
	ΔT_{main}	2ms

Table 6.23: Test series 1: Threshold values

During the tests, protections are activated after the voltage reaches its nominal value and before any operation point variation. Thus, the robustness of the algorithms to normal operation events is guaranteed since no unwanted tripping has been observed.

Note that the fault always occurs at the middle of the cable, as said earlier in this chapter. Also, the fault instant in unknown since it is controlled by the SCADA system. This reinforces the fact that the algorithms are not biased.

a) Current signal processing for illustrations

For clarity purposes, the currents are filtered before they are displayed in some of the figures presented further. Indeed, current measurements present oscillations with large magnitude, especially when the two physical VSC are connected. This problem, due to the PWM frequency, is not supposed to happen in real application and is currently under investigation in order to be solved. However, oscillations remained during the tests. Thus, current post-processing was done under Matlab software, using the function $filt1$ to create a band-pass filter cutting the PWM frequency. The filtered current is noted $I_{ij}f$ and is translated 5ms earlier to correct the resulting delay. Fig.6.33 illustrates the filter effects.

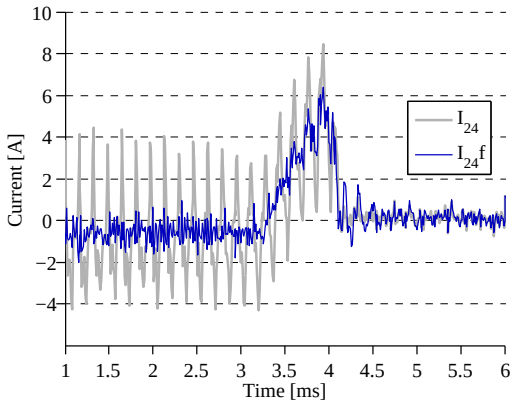

Figure 6.33: Current signal filtering effects

It is important to highlight that the protection principles use currents that are not filtered (the filtering process was done for clarity purposes of the illustrations only). The high magnitude oscillations enable to emphasize the robustness of the algorithms to noise. Furthermore, in real application, the magnitude rate of those oscillations compared to nominal currents would be lower, which makes our tests more constrained.

b) Highlight on cable differential protection operation

Test T1 results are shown below, and aims to validate the main cable differential protection developed in Chapter 5 section 3.4.1. Fig.6.34a represents the differential current calculated by the protection PR_{24} and PR_{54} (please refer to Fig.6.21 page 174 for notations). The differential current calculated by PR_{42} and PR_{45} are the same as PR_{24} and PR_{54} respectively, since they are calculated with the exact same values of current measurements. The selectivity between the two cables is obvious on Fig.6.34a, since only I_d^{45} (and thus I_d^{54} as well) exceeds the threshold value. However, the differential current I_d^{24} does not present a negative front. This is due to the very small propagation time of the signal in the cable (only 57µs between PR_{42} and PR_{24}) and the low rate of rise of the current. This phenomenon is illustrated on Fig.6.34b. Also, there is no notable difference in the current values used to calculate the differential current of the healthy link during this propagation delay.

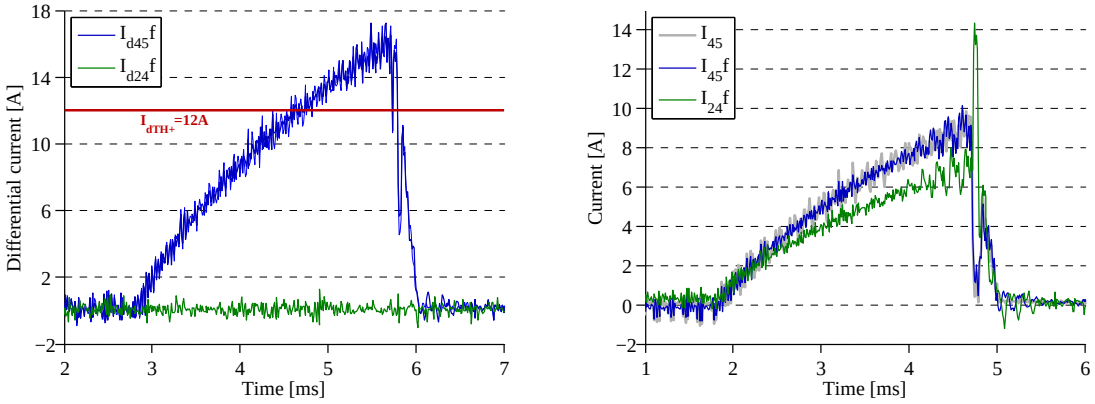

(a) Differential current of the 2 protected cables (b) Current measurements given by the most remote sensors

Figure 6.34: Test T1 results, calculated differential current and current sensor measurements

Furthermore, those figures show that the unfiltered currents do not present as much oscillations as the one presented in Fig.6.33. This is due to the fact that only one physical converter is turned on for this particular test.

The relevant times related to the protection operation are provided on Fig.6.35. Their numerical values are given in Tab.6.24, where their definition is reminded. The values are the same for both ends, since the differential current is calculated thanks to the same current measurements at both cable ends, and since the current values at the breaking instant are similar.

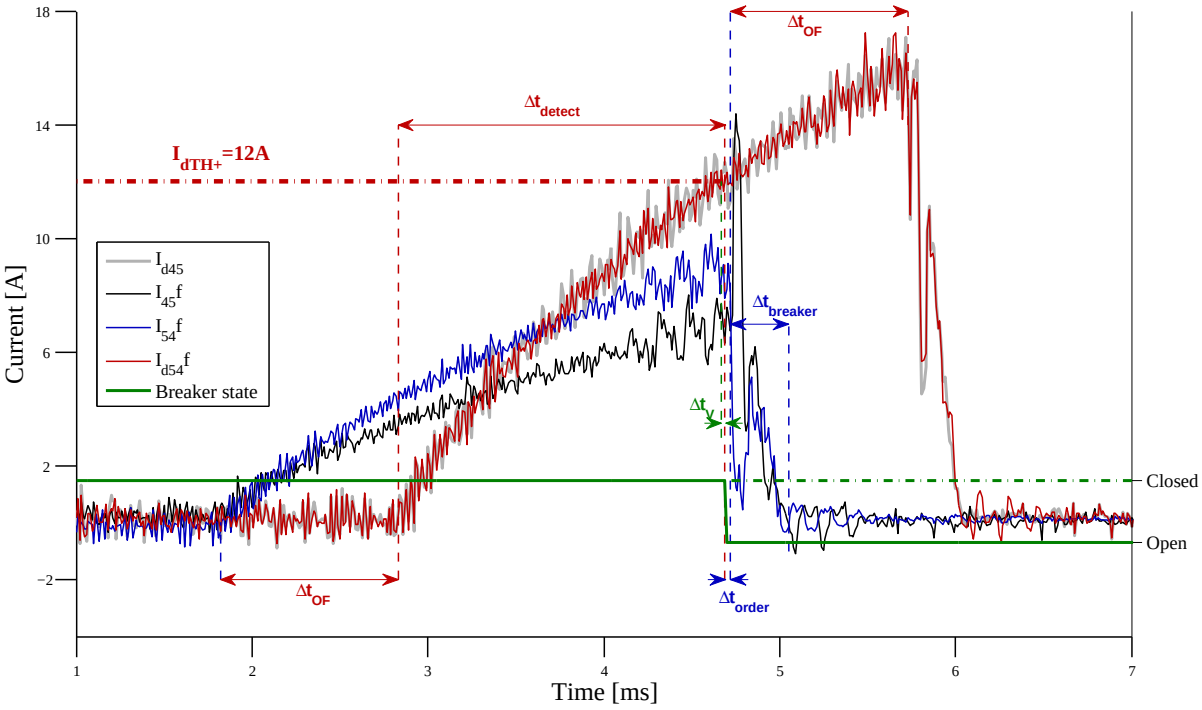

Figure 6.35: Test T1: Protection operation times related to PR_{45} and PR_{54}

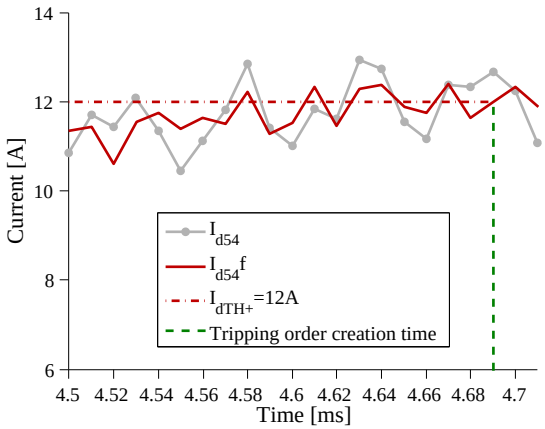

Figure 6.36: Zoom on the detection time for test T1

Time interval	Value	Interval definition
Δt_{OF}	1.010ms	Data propagation through the optical fiber link and conversion delay.
Δt_{detect}	1.770ms	Required time for the differential current to exceed the threshold (including 3 consecutive samples validation delay).
Δt_{V}	20µs	Validation of the detection criterion (waiting for 3 consecutive samples). A zoom is shown on Fig.6.36.
Δt_{order}	30µs	Time interval between the creation of the tripping order and the time when the breaker starts to trip.
$\Delta t_{breaker}$	330µs	Operation time of the breaker, meaning the time to break the whole current.
$\Delta t_{clearing}$	3.140ms	Overall clearing time, from the time of arrival of the first front transient to the closest sensor until the current extinction time.

Table 6.24: Relevant operation times related to test T1

The voltage measurements at the two ends of the faulty cable are shown on Fig.6.37. The undervoltage due to the fault can be observed. At the tripping time, the voltage reduction is followed by overvoltages caused by the dissipation of the energy stored in the grid. The sensors saturation below 500V is obvious on those curves, which makes impossible to see the surge arrester effects.

The overall clearing time is evaluated thanks to (6.10), and its value for this test is 3.140ms. Note that the equation (6.10) does not include the 20µs validation time since this one is already included in Δt_{detect}. The $\Delta t_{clearing}$ value could be reduced by decreasing the threshold, which will be done in the next mock-up configuration presented in 3.4.3. Nevertheless, Δt_{detect} is the only time interval that can be reduced. Δt_{OF}, Δt_{V}, Δt_{order} and $\Delta t_{breaker}$ are incompressible time intervals.

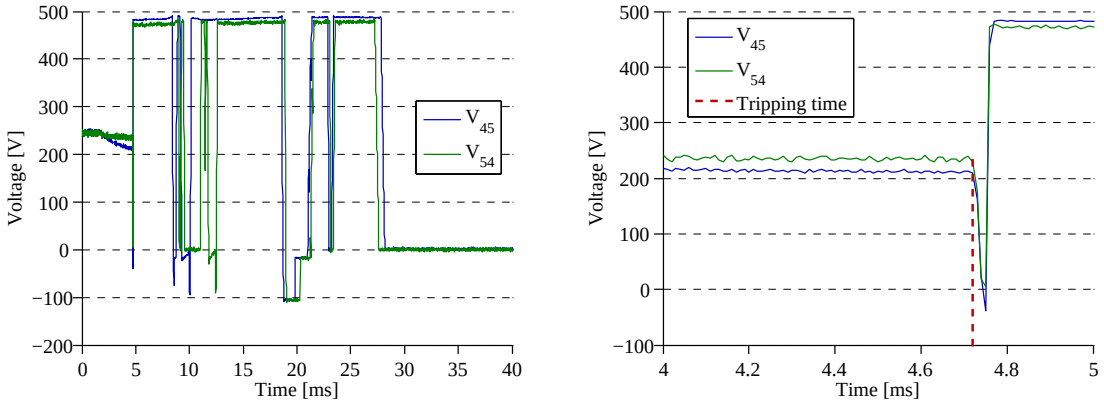

(a) Voltage measurements (b) Zoom on the fault instant

Figure 6.37: Test T1 results, voltage sensor measurements

$$\Delta t_{clearing} = \Delta t_{OF} + \Delta t_{detect} + \Delta t_{order} + \Delta t_{breaker} \tag{6.10}$$

Tab.6.25 summarizes the results of test T2. Since all the corresponding curves are not essential here, only the two differential currents and the current measurements at the faulty cable ends are shown on Fig.6.38.

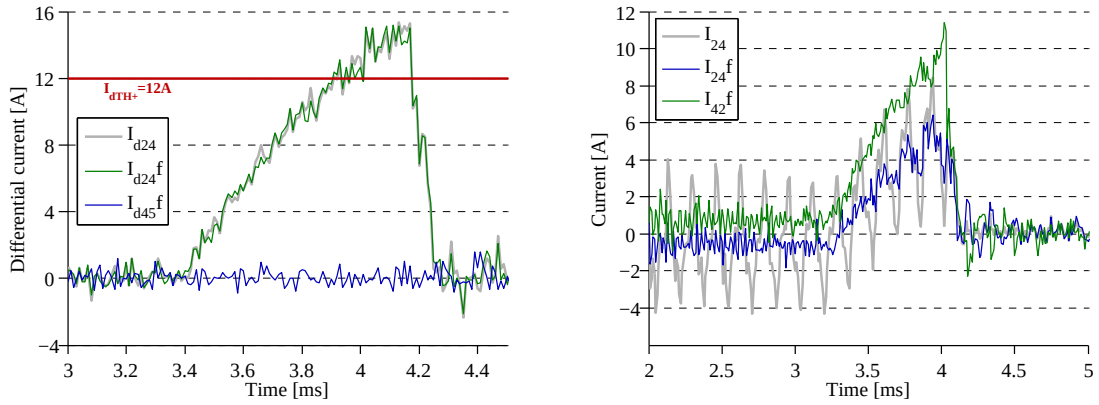

(a) Differential current of the 2 protected cables (b) Current measurements at the faulty cable ends

Figure 6.38: Test T2 results, calculated differential current and current sensor measurements

Again, the selectivity is obvious on Fig.6.38a. The oscillations are higher than in the previous test (Fig.6.38b) since this time, two physical converters are turned on.

This fault was cleared in less than 1ms, due to the low Δt_{detect} and Δt_{OF}. The low value of Δt_{OF} is due to the short length of Link4. The value of Δt_{detect} is lower

Time interval	Value
Δt_{OF}	140µs
Δt_{detect}	580µs
Δt_{V}	20µs
Δt_{order}	30µs
$\Delta t_{breaker}$	180µs
$\Delta t_{clearing}$	910µs

Table 6.25: Relevant operation times related to test T2

than the one for the test T1 value for the same reason. Indeed, the attenuation of the signals along the cable decreases with the cable length. The high linear resistance of the cables explains the fact that the detection time is lower for test T2, even if the fault resistance is higher for that case (the total resistance of Link4 and Link5 are respectively R = 0.3090Ω = and R = 2.4600Ω).

Note also that the backup protection remained stable, and that no unwanted tripping occurred, even during the process of power transfer variations from 0W to 100W or 300W. The selectivity and the relevance of the cable differential protection was highlighted in this part for a radial structure. To prove the robustness of the algorithms, the mock-up has been reconfigured so the various protection algorithms can be tested in a meshed structure. This will be presented in section 3.4.3.

c) Emphasize of backup protection operation

As mentioned earlier in this chapter, only the busbar connected to station 5 is equipped with backup protection, since station 4 is not composed of a physical converter. Indeed, the current shape I_{41} under fault conditions does not correspond to what it would be in real applications, and makes it impossible to apply the backup protection principle at this node. However, it still can be applied at node 5, and the corresponding results are presented in this section.

Therefore, the backup protection operation is emphasized here by simulating a failure of the differential protection at PR_{54} (test T3). This fault test is cleared by the main cable differential protection at PR_{45}, and by the backup at PR_{54}. This can be observed on Fig.6.40. The relevant times are illustrated on Fig.6.39, and their numerical values are given in Tab.6.26. Note that as the temporization delay

ΔT_{main} is reached before the selection criterion $G_s^5 > G_{sTH}^5$ is checked, the backup sends the tripping order as it is validated.

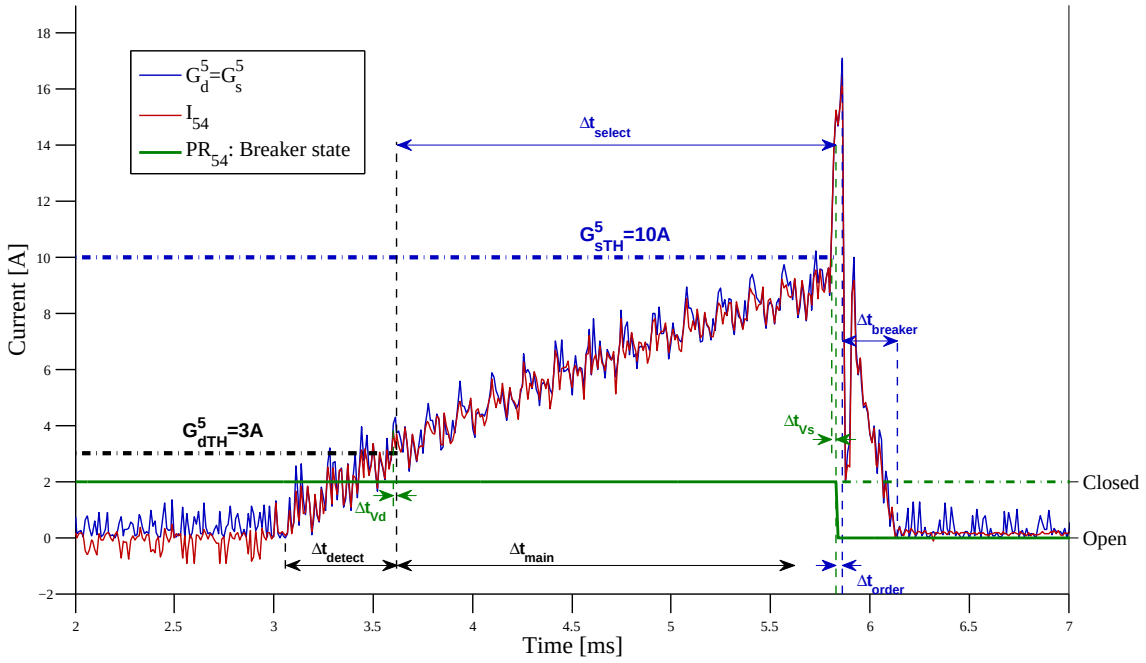

Figure 6.39: Test T3: Protection operation times related to the backup at PR_{54}

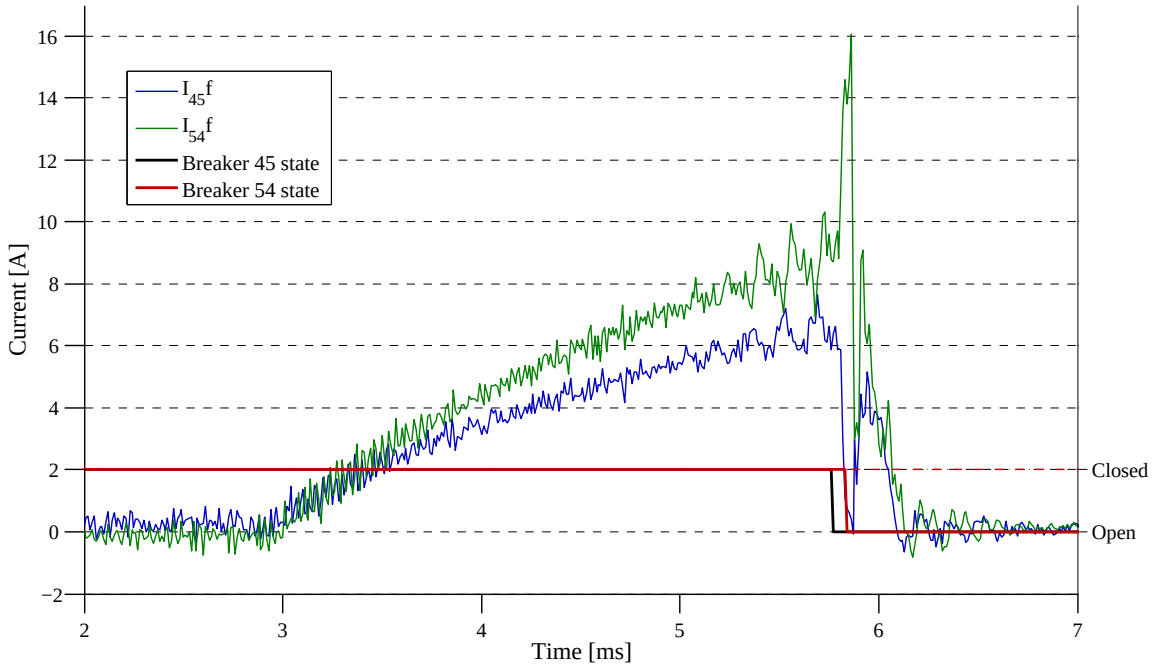

Figure 6.40: Test T3: Current measurements and breaker state

Time interval	Value	Interval definition
Δt_{detect}	560µs	Required time for the detection variable G_d to exceed the threshold value (including 3 consecutive samples validation delay).
Δt_{Vd}	20µs	Validation of the detection criterion (waiting for 3 consecutive samples).
Δt_{select}	2.220ms	Required time for the selectivity variable G_d to exceed the threshold value (including 3 consecutive samples validation delay).
Δt_{Vs}	20µs	Validation of the selectivity criterion (waiting for 3 consecutive samples).
Δt_{order}	30µs	Time interval between the creation of the opening order and the time when the breaker starts to trip.
$\Delta t_{breaker}$	280µs	Operation time of the breaker, meaning the time to break the whole current.
$\Delta t_{clearing}$	3.090ms	Overall clearing time, from the time of arrival of the first front transient to the closest sensor until the current extinction time.

Table 6.26: Relevant operation times related to test T3

The overall clearing time here ($\Delta t_{clearing} = 3.090$ms) is lower than the one for test T1 (3.140ms), which was the exactly same fault test but cleared with the main cable differential protection at both faulty cable ends. However, the order is well and truly sent later for test T3, as shown on Fig.6.41 which represents the current I_{54} and the breaker CB_{54} state for both tests T1 and T3. Thus, the tripping of the breaker is not done simultaneously, which implies a higher current to break at PR_{54} for case T3. This is why, $\Delta t_{breaker}$ is higher for test T1 than for test T3. This is illustrated on Fig.6.41, where the time was rearranged in order to make the first front transient arrive at $t = 0$ at PR_{54}.

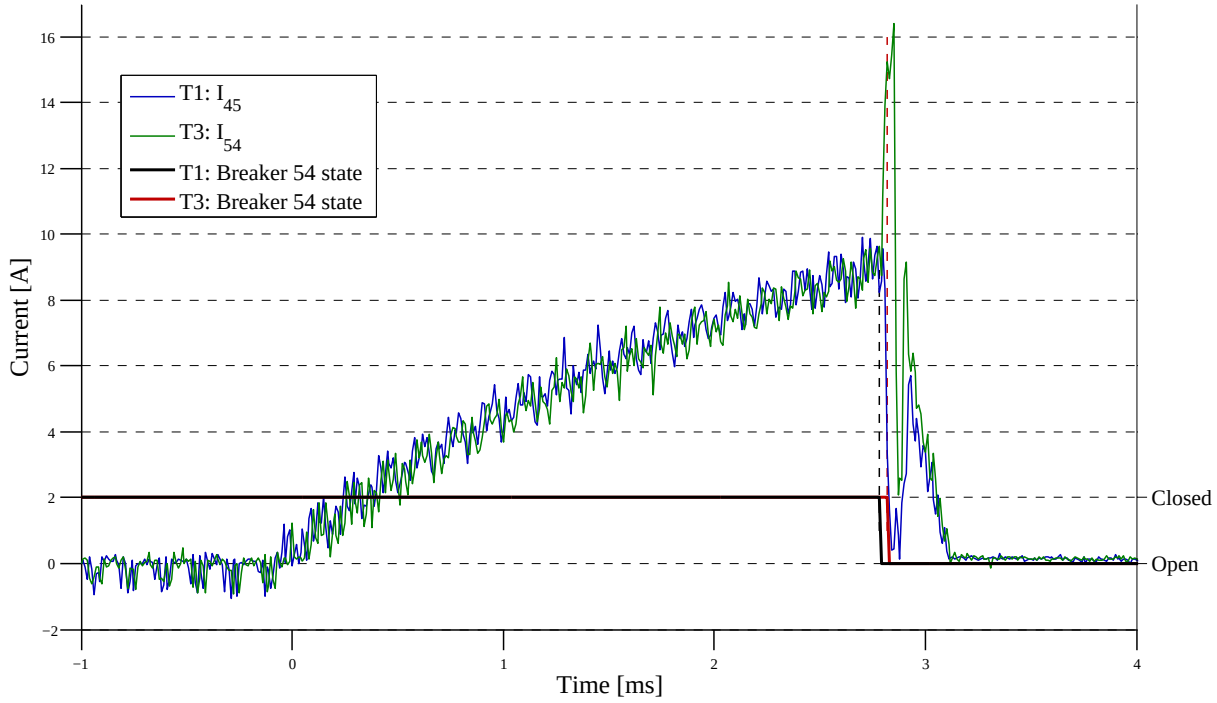

Figure 6.41: Tests T1 and T3: Current I_{54} and breaker CB_{54} state

In order to test the backup for a busbar with more than one feeder, the mock-up was reconfigured. The purpose of the following parts is to describe the new configuration and to show the related tests results.

3.4.3 Mock-up reconfiguration

The mock-up reconfiguration aims to test both main protection and backup protection in a meshed grid structure. To do so, station 3 was replaced by station 5, as shown on Fig.6.42, where old notations are written in black, and the new notations used in this section are written in blue. On this new configuration, VSC 2 and VSC 3 are physical VSC.

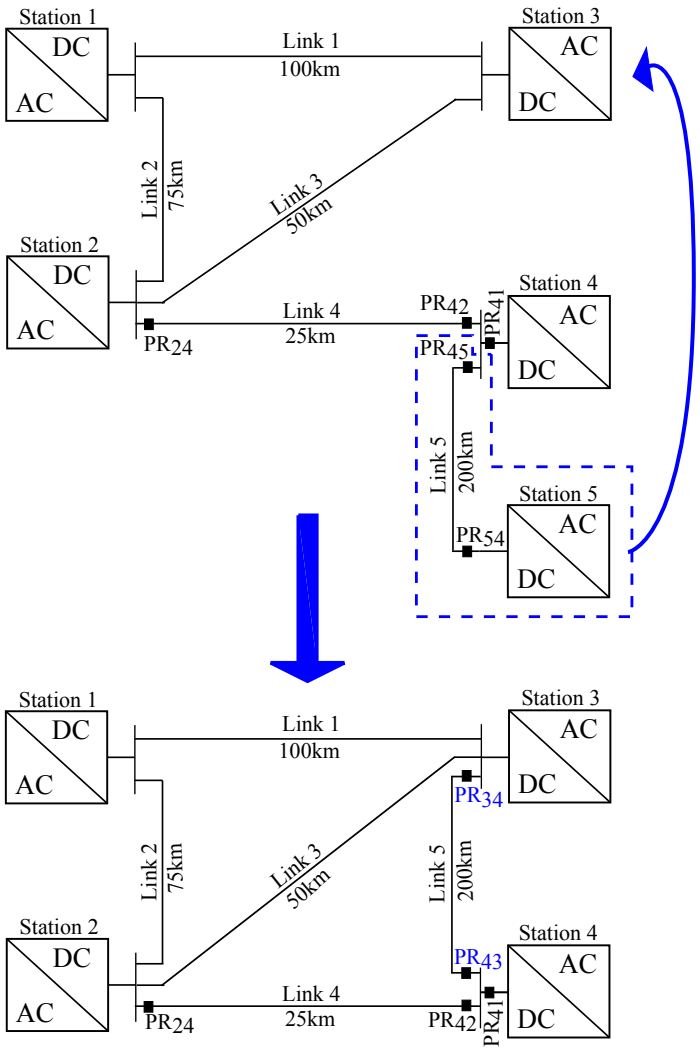

Figure 6.42: Mock-up reconfiguration

Thus, the main cable differential protection can be implemented on both Link4 and Link5, and the backup protection is implemented on busbar connected to station 4. This will enable the simulation of a breaker failure (meaning that it does not open even though the tripping order was sent).

The threshold values used are given in Tab.6.27 The main cable differential threshold value was voluntarily decreased in order to emphasize the rapidity of the protection algorithm.

Protection	Threshold name	Threshold value
Main cable differential	I_{dTH+}	4A
	I_{dTH-}	−4A
Main busbar differential	I_{busTH}	10A
Backup	G^5_{dTH}	3A
	G^4_{sTH}	18A
	I_{feedTH}	1A
	ΔT_{main}	3ms

Table 6.27: Test series 2: Threshold values

3.4.4 Test series 2 results

As well as the first test series, 3 cases were treated, and are described in Tab.6.28.

Test	Faulty link	R_{fault}	VSC 2	VSC 5	Operation point	Comments
T4	Link5	5Ω	–	Ph	VSC3 +100W	—
T5	Link4	10Ω	Ph	Ph	VSC3 +300W	—
T6	Link5	5Ω	–	Ph	VSC3 +100W	Cable differential protection disconnected at PR_{43}

Table 6.28: Test series 2 description, Ph: physical VSC, –: not connected, +100W: injects 100W to the DC grid

a) Highlight on the cable differential protection selectivity

In this paragraph, the selectivity of the main cable differential protection in a meshed grid structure is highlighted thanks to tests T4 and T5. Differential currents are provided in Fig.6.43. Once again, the selectivity is clear on those figures for both tests. The time intervals related to test T4 are shown on Fig.6.44, and the numerical values are provided on Tab.6.29 for both T4 and T5 cases.

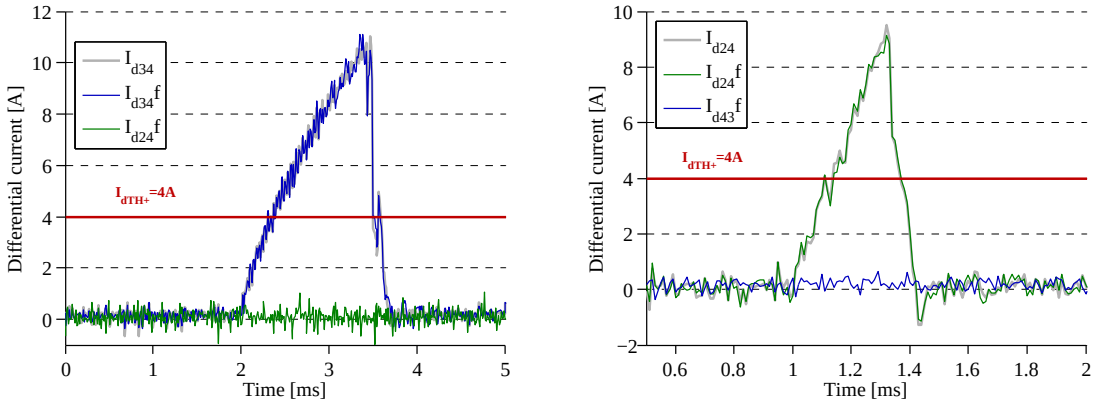

(a) Test T4 results

(b) Test T5 results

Figure 6.43: Test T4 and T5 results: Differential current of the 2 protected cables

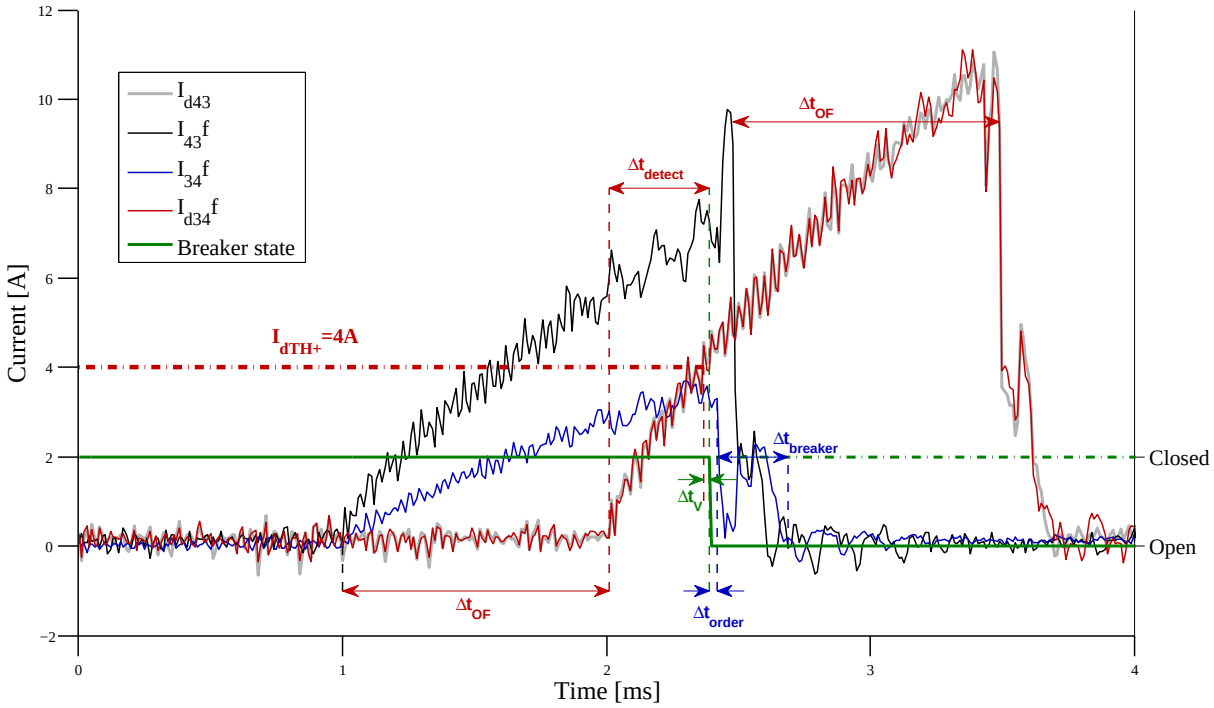

Figure 6.44: Test T4: Protection operation times

The clearing times are extremely low for those cases, due to the reduction of the differential current threshold. The backup protection remained stable during the clearing process of the faults by the main protection algorithms.

Time interval	Value
Δt_{OF}	1.010ms
Δt_{detect}	380µs
Δt_{V}	20µs
Δt_{order}	30µs
$\Delta t_{breaker}$	270µs
$\Delta t_{clearing}$	1.690ms

Time interval	Value
Δt_{OF}	140µs
Δt_{detect}	160µs
Δt_{V}	20µs
Δt_{order}	30µs
$\Delta t_{breaker}$	110µs
$\Delta t_{clearing}$	440µs

Table 6.29: Protection operation time for test T4 (left) and T5 (right)

b) Highlight on the backup protection

Test T6 simulates the failure of breaker at PR_{43} location, meaning that it does not trip. This case is different compared to test T3 since 2 feeders are connected to busbar 4. Fig.6.45 shows the backup operation times related to this test, and Fig.6.46 shows the current measurements at each end of the faulty cable. The breaker of PR_{34} trips around 1.5ms after the fault due to the main cable differential protection. The effect can be noticed on the current measured at the opposite end I_{43} on Fig.6.46, where an overcurrent can be seen at this particular time. Indeed, the current shape presents a discontinuity at this time due to the tripping of only one end, which implies an augmentation of the current of the opposite end.

The backup variable G_s^4 exceed the selectivity threshold G_{sTH}^4around 5ms later, and since the current of both feeders is not close to zero, the tripping order is sent to breakers of PR_4 and PR_{42}, as expected. Once again, the selectivity threshold is exceeded later after the time out ΔT_{main}.

An overcurrent can be observed in I_{34} during the current breaking process of the opposite cable end. This can be explained by Fig.6.47 which represents the voltages of the two faulty cable ends. Indeed, when breakers of PR_4 and PR_{42} trip, an overvoltage occurs and thus the surge arresters located at the breakers terminals of PR_{34} become conducting, and makes a current flowing to the fault, which becomes temporarily alimented, until the energy is dissipated.

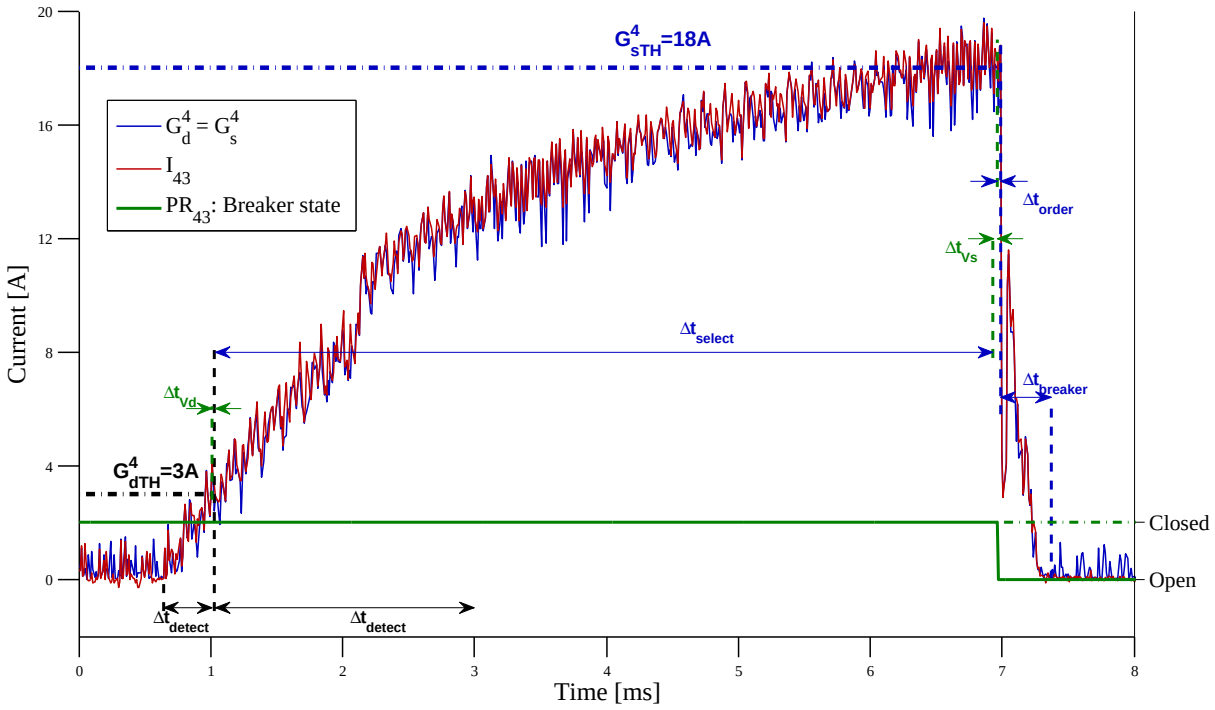

Figure 6.45: Test T6: Protection operation times

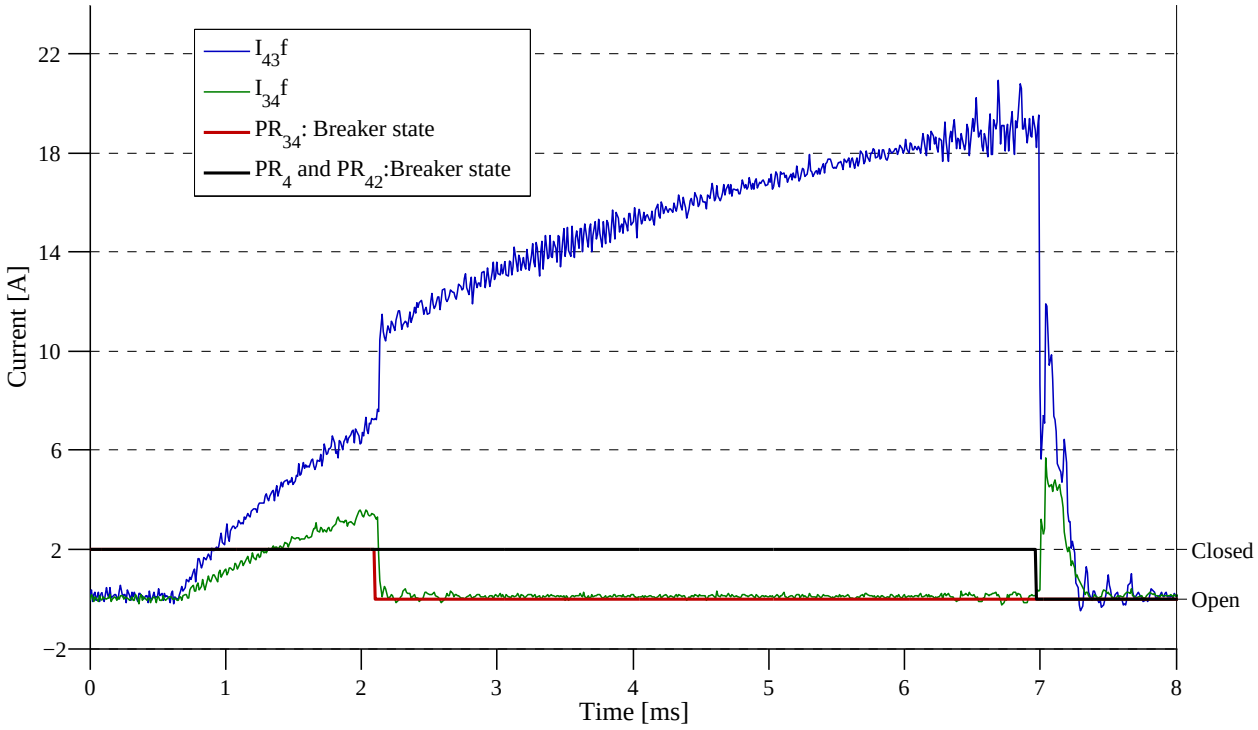

Figure 6.46: Test T6: Current measurements

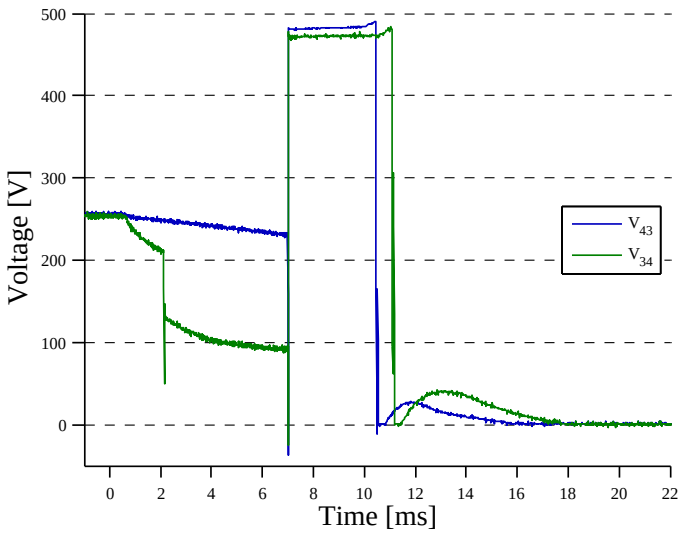

Figure 6.47: Test T6: Voltages measurements

c) Comments on the busbar differential protection

The busbar differential protection has not been tested on the mock-up, because to do so, the fault generator device would have to be displaced and the agenda did not allow it. Nevertheless, its robustness against cable faults was proved since it was implemented on busbar 4 during both test series 1 and 2. Also, it depends on a simple Kirchhoff low with no cable effects, which makes think it would act as expected.

3.4.5 EMTP-rv study validation

The mock-up was modeled in EMTP-rv in order to compare the results and to validate the cable models used.

a) EMTP-rv mock-up model

The VSC models are the same than the ones used in section 1, but the values are the ones given in Tab.6.14 page 176. DC breakers are modeled with ideal switches. For each simulation that will be compared to the mock-up tests results, the protections threshold values were set to the exact same value than during the mock-up tests.

Three cable models were created in order to compare the results. The first one

is a CP model using parameters that were identified at 1kHz. The second one uses geometrical and dielectric parameters of the cables to create a WideBand model (those parameters were provided in subsection 3.1.3 b)). This model claims to be the most accurate one, but since the cables are on their drums, the coupling effect is minimized so another model was created. This later one aims to represent the drum effect by representing the winding constituted by the cable. A WideBand cable model was therefore created, composed of N cable sections (Fig.6.48a), but with a length decreased N times and connected on to another, as shown on Fig.6.48b. However, a complete drum model cannot be done because EMTP-rv cable data generation block is limited to a certain number of conductors. Thus, several assumptions were made:

- The number of windings composing one drum is reduced to 5.
- The windings are configured as shown on Fig.6.48c.
- The length of the winding is constant.

Thus, the length of one winding L_w has been evaluated by $L_w = L_d/5$, where L_d is the length of the cable winded around one drum (227m for the 25mm^2 section and 161m for the 10mm^2 section).

The geometrical parameters and dielectric properties are the same as the ones used in the previous model.

Therefore, 5 cables were created (5 cores and 5 screens), representing 5 winding ($N = 5$) configured as shown on Fig.6.48c. Thus, 2 types of drum were modeled: one for the 10mm^2 cable and one for 25mm^2, and are connected in series to match the number of drums constituting the links, as mentioned in Tab.6.17.

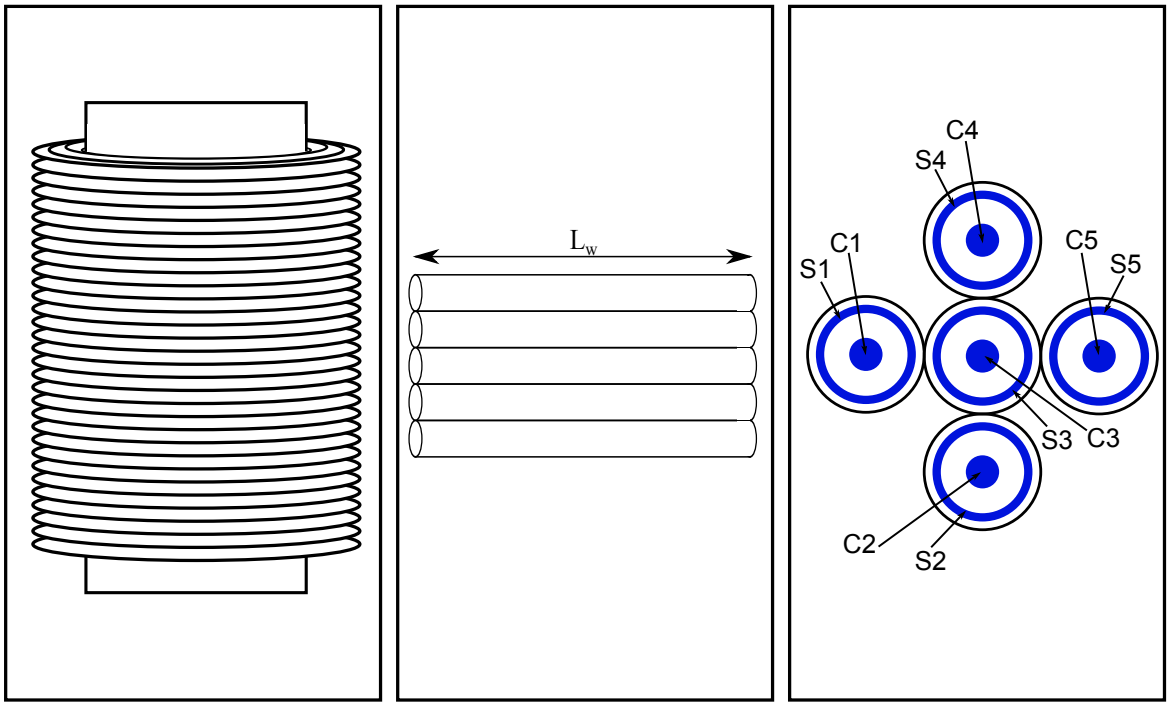

(a) Drum (b) Cables (c) Configuration

Figure 6.48: WideBand model of the cables on their drums

The core parameters of those 3 cable models are given Tab.6.30 for a frequency of 1kHz. The values corresponding to the CP model are the ones that have been identified, and the ones related to the two other models were calculated by EMTP-rv. For each one of those 3 models, the positive pole and the negative pole are represented separately. The two cable types (sections $10mm^2$ and $25mm^2$) are presented.

Model		CP	WideBand	WideBand on the drum
Structure		Core	Core and screen	5 cables, core and screen
$25mm^2$	R′[Ω/km]	$0.6806e^{-0}$	$1.6275e^{-0}$	$1.62751e^{-0}$
	L′[H/km]	$3.8106e^{-2}$	$2.2742e^{-3}$	$2.2742e^{-3}$
	C′[F/km]	$4.0969e^{-7}$	$4.9485e^{-7}$	$4.9485e^{-7}$
$10mm^2$	R′[Ω/km]	1.6977	2.6070	2.6072
	L′[H/km]	$4.0511e^{-2}$	$2.3760e^{-3}$	$2.3760e^{-3}$
	C′[F/km]	$3.2022e^{-7}$	$3.9873e^{-7}$	$3.9873e^{-7}$

Table 6.30: Cable models: core parameters at 1kHz

The parameters are the same for the two WideBand models. Indeed, the cable

layers geometry and the dielectric constants are the same. However, the core linear inductance is very different than the CP value. This is due to the coupling effect, which is taken into account in the CP model since the parameters were measured, and not computed. This increases the global inductance. This later one is partly taken into account in the drum WideBand model thanks to the mutual inductance between the winding. The inductance matrix is given in Tab.6.31.

	C1	S1	C2	S2	C3	S3	C4	S4	C5	S5
C1	2.2742									
S1	2.1709	2.1696								
C2	1.8697	1.8697	2.2742							
S2	1.8697	1.8697	2.1709	2.1696						
C3	1.7675	1.7675	1.9507	1.9507	2.2741					
S3	1.7675	1.7675	1.9597	1.9507	2.1708	2.1696				
C4	1.8003	1.8003	1.8696	1.8696	1.8329	1.8329	2.2742			
S4	1.8003	1.8003	1.8696	1.8696	1.8329	1.8329	2.1709	2.1696		
C5	1.8329	1.8329	1.9507	1.9507	1.8814	1.8814	1.7675	1.7675	2.2742	
S5	1.8329	1.8329	1.9507	1.9507	1.8814	1.8814	1.7675	1.7675	2.1709	2.1696

Table 6.31: Inductance matrix L′[mH/km], C: core, S: screen

However, this inductance only represents a part of the real global inductance since only 5 winding per drum, which is more than 10 times less than the real number.

b) Results comparison

The objective in this part is to compare the behavior of the system under fault conditions, and not to validate the protection plan, since this was the aim of section 2. To do so, the signals taken from the mock-up will be compared to EMTP simulation results, for test T1. In the EMTP-rv model, the protections are implemented using the same thresholds. The mock-up signals illustrated in this paragraph are the one that have been filtered as mentioned in 3.4.2 a).

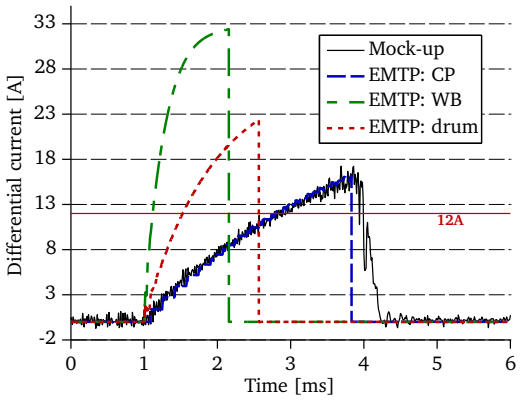

Figure 6.49: Differential current calculated by PR_{54}

On Fig.6.49 which represents the differential current evaluated at PR_{54} (which is equal to the one calculated at PR_{45}), some differences can be observed on three of the curves characteristics:

- The rate of rise of the differential current
- The time when the differential current is reduced to zero
- The decreasing part, corresponding the breaking instant

As the first item is directly due to the current shape, it will be explained using the next illustration.

The rate of rise of the differential current is higher in the case of the WideBand and drum models. This implies that the threshold $I_{dTH} = 12A$ is exceeded earlier. Nevertheless, the differential current is cut after a time delay corresponding to Δt_{OF} once the differential current exceeded the threshold value, for both cases.
However, since the DC breakers are represented by ideal switches in EMTP-rv, the delays defined earlier by Δt_{order} and $\Delta t_{breaker}$ are not simulated. This explains why the curve corresponding to the CP model takes a zero value before the mock-up curve, and this in spite of the two curves are very close.

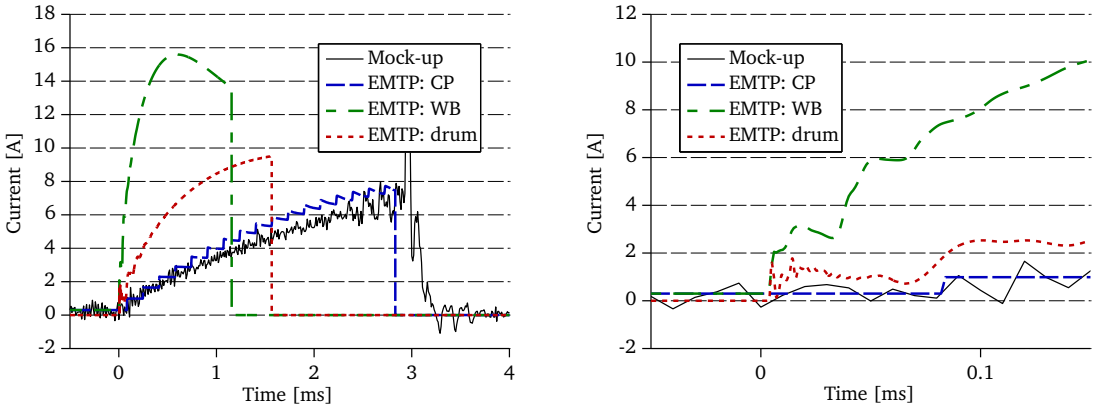

(a) I_{45} (b) Zoom

Figure 6.50: Current measurements I_{45} and zoom at the first front arrival time

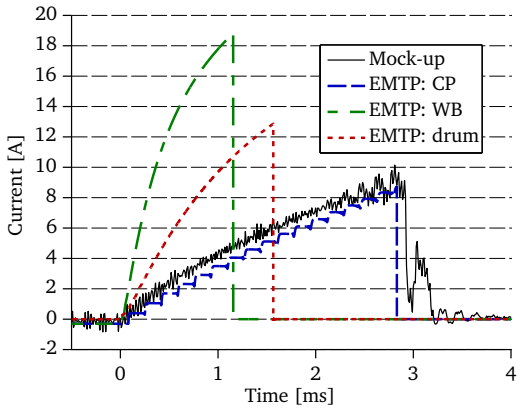

Figure 6.51: Current measurement: PR_{54}

Fig.6.50 and Fig.6.51, which are the current measurements at the faulty link end, show that the CP model is the one which fits the best with the mock-up results. This is due to the fact that this model takes into account all the winding effects thanks to a high inductance value. Furthermore, the WideBand model presents a very high current derivative at the first front arrival time, which is also in that sense. The winding representation in the drum model shows results that tend to the CP model. The difference can be justified by the insufficient number of represented winding, due to the software limitations.

Also, the propagation speed is not the same for both models since it depends on the inductance value. This can be noticed on Fig.6.50b. On this figure, the reflection effects are also emphasized, for which the explanations are the same as in

section 2. The short high frequency oscillations related to the drum model are the result of the use of very short cable lengths.

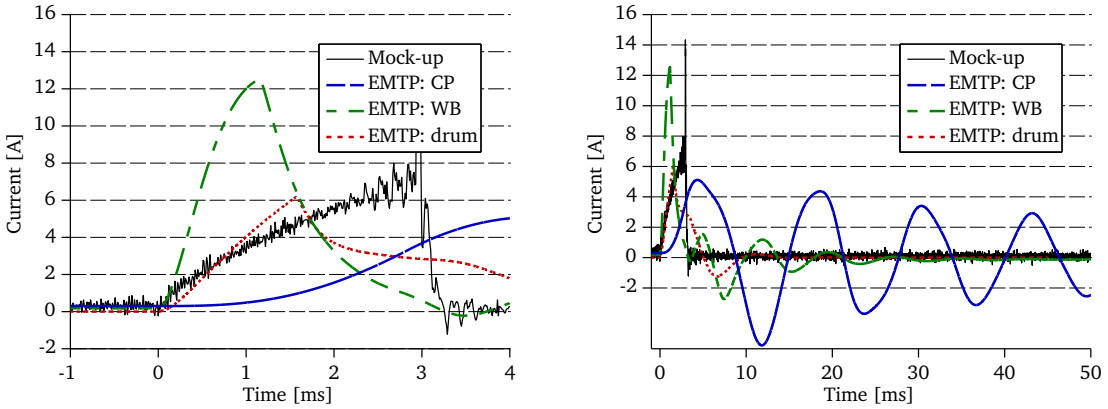

(a) I_{24} (b) Zoom

Figure 6.52: Current measurements I_{24} and zoom

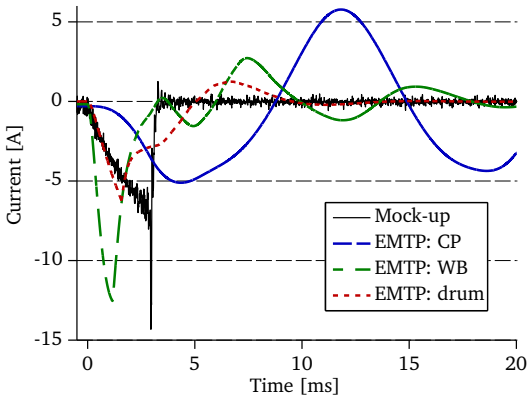

Figure 6.53: Current measurement: PR_{42}

Fig.6.52a and Fig.6.53 show this time that the drum models fits better with the mock-up results after the fault clearing process. In that case, the CP model results are totally wrong. This is due to the fact that there is no attenuation effect at high frequencies in the CP model, as it was explained in Chapter 3. Nevertheless, big errors are still present in the WideBand model.

Those simulation results show that in that case, the CP model gives the closest representation of the mock-up behavior. The drum model seems to tend to the CP results, but this affirmation would require the model of both windings, which was not possible due to the software limitations. Also, the length of the cables

considered here are quite short, which is another justification of the relevance of the CP model in this case. For larger length, the frequency dependence effect would be emphasized. Adding the fact that real cables are much less inductive than the drums, the mock-up did not allow to validate the cable transient response to faults, but this does not mean in any case that a CP model would be enough to study the transients in a 640kV grid application.

3.5 Real Time HIL demonstrator benefits

This mock-up allowed to justify the relevance of the protection plan on both radial and meshed grids, and the fact that it is robust to oscillations and transient shape variation. Indeed, the functioning of both principles was not degraded, even considering the huge difference in the transient of the EMTP-rv 640kV study.

This mock-up constitutes the intermediary step between full simulation and full-scale demonstrator. It enables the experimental validation of the behavior found in simulation, and a more realistic view on the communication between the different elements. The last tests presented in this section were achieved on May, 30th 2013, after a year and a half of development and thanks to the joined work of 2 professors, 3 engineers, another Ph.D student, and the support of RTE.

4 Current relaxation during breaker tripping action

This last part of the thesis comes back to EMTP-rv simulations, and investigates some trails to limit the extremely large current values estimated in section 2.

Simulation results of the protection system show that the current to break can, is some cases, reach values in the range of 60kA. Given those high current values, combined with the fact that DC breaker under prototyping process may not have this kind of huge current breaking capability, the conclusion is that some solutions need to be found to decrease these large values. Two methods were investigated. The first one was evoked several times in this thesis and consist in incorporating inductors at each feeder relay. The other one is base on superconducting fault

current limiters. They are detailed below, and they were studied in order to limit the current to break to an arbitrary value of 15kA.

4.1 Incorporation of superconducting fault current limiters

In this study was conducting in collaboration with the Ph.D research work of Camille Gandioli [Gandioli, 2013], which is supported by the European Commission under the ECCOFLOW project[1]. Superconducting fault current limiters (SCFCL), using high temperature superconducting tapes, are used to reduce the dramatically huge current to be broken by the DC breakers.

4.1.1 SCFCL introduction

There are various superconducting materials, they can be bulk and tape material [Tixador and Brunet, 2007]. In this study, the model used represents high temperature second generation superconducting tapes. These tapes are coated materials and are hence made of several layers. The superconducting material used is YBaCuO and this layer is about 1µm thick. The others layers of the superconducting tape are non superconducting. There are mechanical, chemical and electrical protections. The whole thickness of the tape is about 100µm and it is 12mm wide. This is illustrated on Fig.6.54.

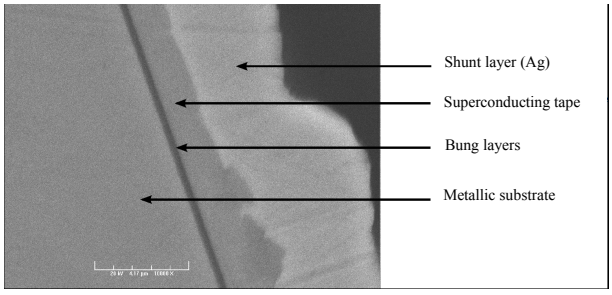

Figure 6.54: Layers

The length will depend on the design we wish to have for the SCFCL. Below the critical temperature and the critical current of the superconducting material, the tape is almost non resistive. Above the critical temperature and its critical current, the superconducting tape has the resistance of the non superconducting layers. In

[1]The study were done in the ECCOFLOW project framework: http://www.eccoflow.org/. The research leading to these results has received funding from the European Union Seventh Framework Programme (FP7/2007-2013) under Grant 241285.

the SCFCL application, the superconducting tape is plunged into a liquid nitrogen bath in order to keep the superconducting tape below its critical temperature, as shown on Fig.6.55.

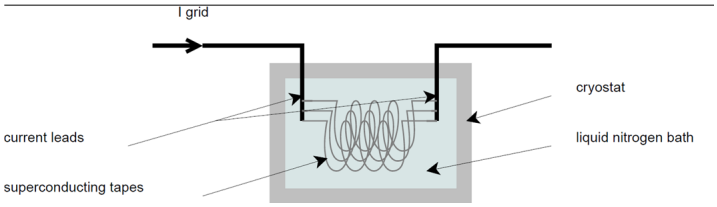

Figure 6.55: Scheme of the SCFCL

a) Resistive SCFCL

The SCFCL is then placed in series with the station and the busbar near the protection relay, and it is designed in order to be still superconducting for a nominal current. When a fault occurs in the grid, the current will increase suddenly and will exceed the critical current of the superconducting tape. Therefore, the tape will become resistive in a matter of milliseconds. Consequently, the SCFCL will limit the current flowing through it. The critical current of the superconducting tape is about 300A. In order to adapt the critical current of the tape to the nominal current of the grid, tapes can be connected in parallel. The length of the tape depends on the nominal voltage and on the temperature the tape reaches when it quenches. For the following simulations, three different designs have been done in order to adapt as much as possible the critical current of the SCFCL to the nominal one.

substation	1 and 2	3 and 4	5
critical current (A)	2700	1500	2400

Table 6.32: SCFCLs design

The model of resistive SCFCL used for the EMTP-rv study is presented in the next paragraph.

b) SCFCL model

A model of SCFCL had been developed previously in [Tixador et al., 2011]. This model enables to calculate the resistance of the superconductor and therefore

of the SCFCL. A brief model description is given in this paragraph. Above the critical temperature, the superconductor tape is considered as a resistance which depends only on the temperature of the material. Below the critical temperature, as the modeled tape is a coated tape, the superconductor tape is modeled by two parallel impedances: one superconducting and the other one non superconducting. The non-superconducting impedance is a resistance which symbolizes the non-superconducting layers of the tape. The superconducting impedance depends on the current flowing through the superconducting layer and its temperature, as shown on Fig.6.56. The tape is considered as an isotherm block.

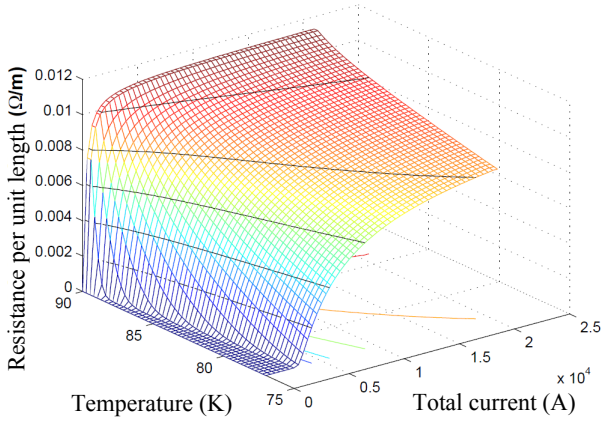

Figure 6.56: Scheme of the SCFCL

4.1.2 Simulation results

This part shows EMTP-rv simulation results conducted on the Twenties grid structure used for section 2. The objective is to assess if the incorporation of current limiters could ensure that the current to break by the DC breakers in case of fault is lower than 15kA at the fault clearing instant (meaning that the DC current has to be lower than 15kA at the time the beaker operates, but does not need to be lower than that value before, as long as the current flowing through the diodes does not exceed 2pu). The superconducting fault current limiter model detailed below is inserted in each station protection, meaning at PR_1, PR_2, PR_3, PR_4 and PR_5. Critical currents of each limiter are displayed in Tab.6.32, and the same length of 3000m is considered for each one.

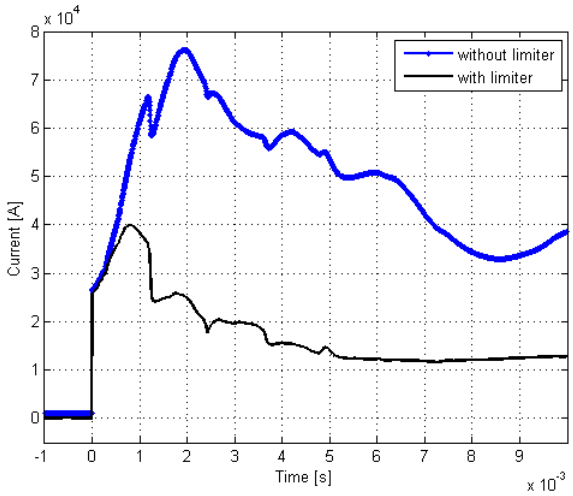

Figure 6.57: Currents measured at each end of the faulty cable

Fig.6.57 compares the current measured at PR_{21}, which is drastically reduced by the limiters. However, the current to cut remains very high (34kA). Nevertheless, the time constraint given by the diodes is released by the limiter. In that case, there is 4.95ms before the current flowing through the diodes exceeds 2pu, compared to 2.16ms when there is no limiter. Thus, the opening time of the breakers could be delayed in order to wait for the current to break to be lower than 15kA, meaning 4.36ms after the fault.

Several simulation tests were conducted in order to choose the length of the limiter as short as possible. 21 lengths were tested, from 1000m to 5000m. The curves of Fig.6.58 summarize the results of the simulations. The maximal time the breaker can wait to clear the fault, given by the diode constraints, is shown on the black curve, and the minimum time the breaker has to wait to ensure that the current to break is lower than 15kA is shown in blue. The jump of the blue curve between 2200 and 2400m is explained by the second part of the oscillations of the current which is higher 15kA depending on the case (see Fig.6.59).

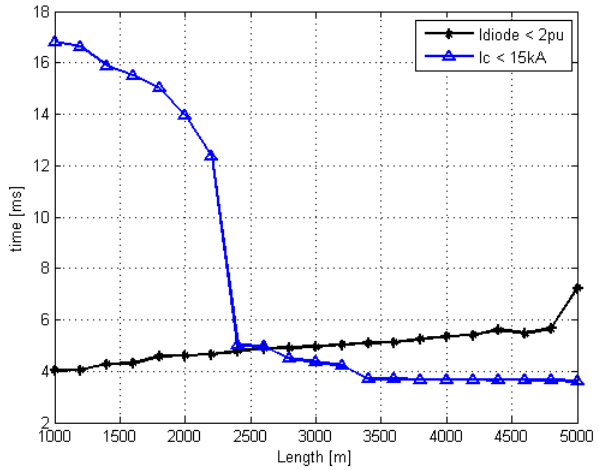

Figure 6.58: Time constraints

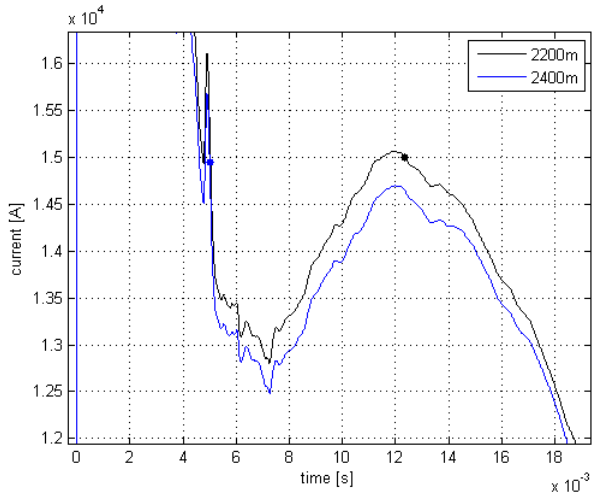

Figure 6.59: Oscillation responsible for the jump between 2200 and 2400m

The shortest length that satisfies the two conditions (6.11) and (6.12) is 2800m. For this length value, t ($I_{diodes} < 2pu$) = 4.91ms and t ($I_c > 15kA$) = 4.48ms.

$$t_{open} < t\,(I_{diode} < 2pu) \tag{6.11}$$

$$t_{open} > t\,(I_c > 15kA) \tag{6.12}$$

The protection algorithm becomes:

$$
\begin{array}{lllll}
\left.\begin{array}{lllll}
\text{IF} - - - & I_{dij}(t-2\Delta t) & > & I_{dTH+} & \\
\text{and if} & I_{dij}(t-\Delta t) & > & I_{dTH+} & \\
\text{and if} & I_{dij}(t) & > & I_{dTH+} & \\
\text{and if} & I_{ij}(t) & < & 15kA &
\end{array}\right\} & \text{Trip} \\
\left.\begin{array}{lllll}
\text{ELSE IF} & I_{dij}(t-2\Delta t) & < & I_{dTH-} & \\
\text{and if} & I_{dij}(t-\Delta t) & < & I_{dTH-} & \\
\text{and if} & I_{dij}(t) & < & I_{dTH-} &
\end{array}\right\} & \text{Block for } \Delta t_{block} \\
\text{ELSE} - - - - - - - - - - - - - - - - & \text{Stand By}
\end{array}
\tag{6.13}
$$

where Ifeed is the current measured at the protection. As mentioned earlier, the pole-to-pole fault case used for the simulation is the condition where the current is the highest at the opening time of the breaker. Thus, for any other fault, the current would still remain lower than this case.

The Twenties grid with the five current limiters were simulated for various fault cases. The current limiters do not affect the detection of high impedance faults by the main differential current protection since the current, even reduced, still increases enough to exceed the threshold value. The simulation results show that the limit is reached for a pole-to-ground fault of 500Ω (whereas 800Ω without limiters). However, the proposed backup protection cannot be implemented considering fault current limiters, since the signals measured at several points of the grid becomes to close one to another, which remove any discrimination possibility.

Another trail was thus investigated to limit the current to break without impacting the relevance of the protection principle. This is the aim of the next subsection.

4.2 Incorporation of feeder inductors

The idea developed here is to add inductors near each protection relay in order to limit the current rise, and consequently, its value at the tripping time.

Two inductors type are considered: the inductors that are already included in the DC filters (L_s), and the inductors that are added in each cable end relay, as shown on Fig.6.60.

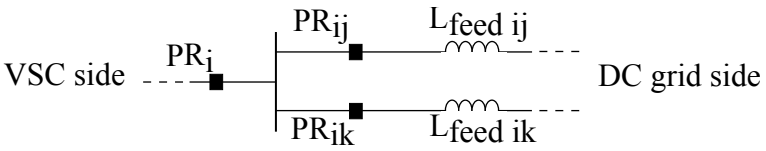

Figure 6.60: Inductors located at cable ends

There is thus 10 inductors L_s included in the DC filters of the 5 stations (positive and negative pole), and 20 feeder inductors (10 cable ends times 2 poles). The objective is to find the 30 inductors values that ensure a current to break lower than 15kA for any fault case.

4.2.1 Inductors value choice

The objective is to ensure that the current to break does not exceed 15kA, for any fault that can happen on the grid. Therefore, the worst case fault scenarios can be taken into account to perform the study. The worst case fault is defined by the fault leading to the highest current to break. It is a pole-to-pole fault occurring near a relay, and the location of this one was known thanks to the simulations of those 10 possible faults. The worst case fault scenario is thus the pole-to-pole fault occurring near the relay PR_{13}, with a current to break equal to 62.680kA. The worst case scenario for the busbar differential protection is also considered, and is a fault occurring on the busbar connected to station 5, with a current to break of 28.533kA.

The ideal method would be to set the inductor value one by one, in order to minimize it. Nevertheless, the modification of one inductor value has both a local influence and a global influence on the grid. Indeed, the modification of a single inductor value lead to a modification in the signal measured near this inductor, but also in the signals measured remotely in the grid. An exhaustive study would thus be the only solution to ensure an optimal inductor values set. Nevertheless, the required simulation number becomes too high when the number of inductor values that need to be chosen is consequent. In the Twenties grid case, if the inductor values are chosen among 8 values for example, then $8^{15} \approx 3.10^{13}$ simulations need to be performed to test all the cases, and this for each fault case.

Thus, the influence of the variation of the inductor values were first investigated, assuming that the DC filter inductors L_s both take the same values, and that the

feeder inductors L_{feed} of the two ends of a cable have the same value. There is thus only 6 inductor value to choose, one for L_s and five for L_{feed}. A study were done to choose those six inductors between a set of two values: 32mH and 48mH. Thus, only $2^6 = 64$ simulations were required for each fault case. The conclusion on the variation influence are the following ones:

- The solution $L_s = 32$mH and $L_{feed} = 32$mH for each feeder enables to limit the current to break below 15kA.

- If one inductor is increased, then it can imply a current to break higher than 15kA somewhere else in the grid.

Thus, a parametric study assuming that the feeder inductor take the same value everywhere in the grid were chosen. The two worst case faults were used to determine the smallest inductor values.

The inductor are chosen in a set of 8 values: 10mH, 15mH, 20mH, 25mH, 30mH, 35mH, 40mH and 45mH, which were chosen arbitrarily. There is thus 64 possible cases, that were simulated for both the cable and the busbar faults.

a) Cable fault occurring near relay PR_{13}

For this fault case, among the 64 possibilities, 28 inductor values set enables to limit the current to break below 15kA. Two solutions can be kept:

- Solution 1: minimizes the source inductors, then minimizes the feeder inductors: $L_s = 10$mH and $L_{feed} = 40$mH

- Solution 2: minimizes the feeder inductors, then minimizes the source inductors: $L_s = 25$mH and $L_{feed} = 30$mH

The curves presented in Fig.6.61 illustrate the influence of each inductor.

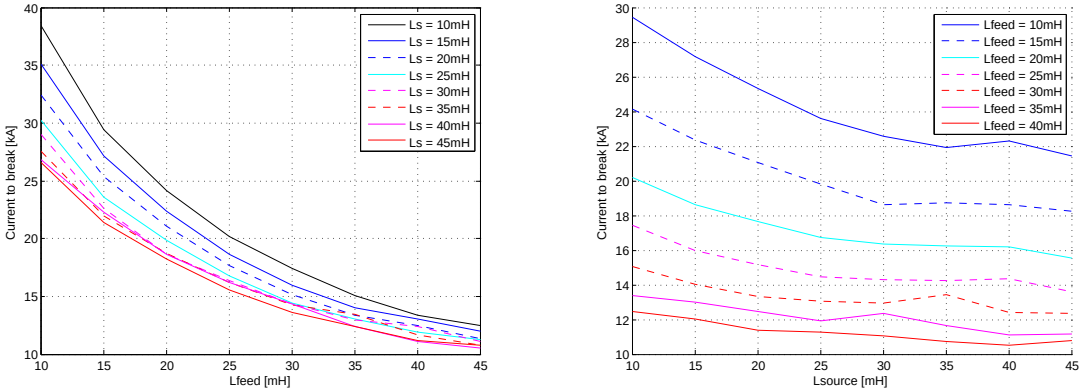

(a) as a function of the feeder inductor value (b) as a function of the source inductor value

Figure 6.61: Influence of the inductors on the current to break

On Fig.6.61a, each curve shows the current to break as a function of the feeder inductor value. It can be seen that the value of the source inductor L_s has a low impact, since the different curves are close one to another. At the opposite, the feeder inductor value impacts a lot the current to break, which can show a variation of 30kA depending on the cases.

The same observations can be done on Fig.6.61b which is another way to present the results. This time, the feeder inductor value is fixed for a given curve, and the current to break is shown as a function of the source inductors L_s. The conclusion is that for this fault kind (on the cable side), the feeder inductor has a higher impact than the source inductor. This is explained by the fact that the current rise is due to the cable capacitor discharge.

b) Busbar fault occurring on busbar connected to station 5

For this fault case, among the 64 possibilities, 40 inductor values set enables to limit the current to break below 15kA. For this fault, the solution is the same whether the minimization is done one the feeder inductor or on the source inductor first, and is $L_s = 25$mH and $L_{feed} = 10$mH.

Once again, the influence of the inductor values is illustrated, and the results are shown on Fig.6.62. This time, this is the source inductor L_s that has the highest impact.

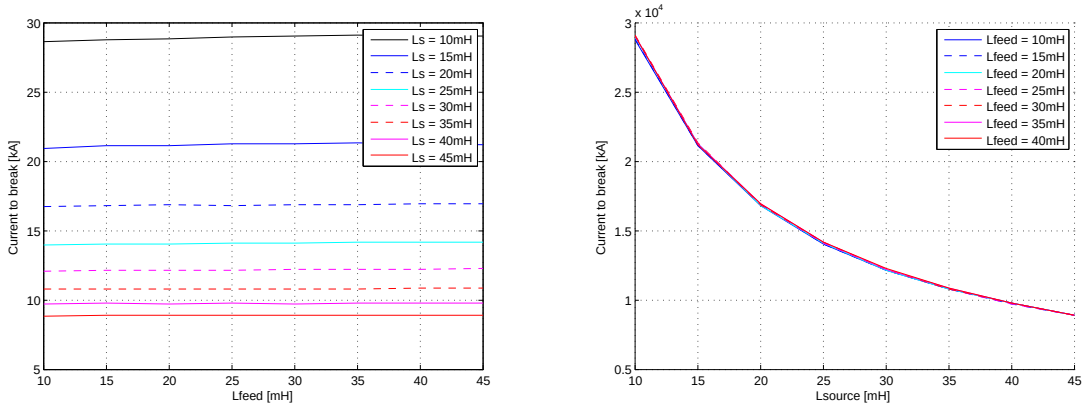

(a) as a function of the feeder inductor value (b) as a function of the source inductor value

Figure 6.62: Influence of the inductors on the current to break

When the two worst case faults are both considered, 20 possibilities exist to ensure a current to break below 15kA. As well as it is the case for the busbar fault, the minimization of one inductor before the other one do not change the result, which is $L_s = 25mH$ and $L_{feed} = 30mH$.

This are the values that are kept for the rest of this chapter.

4.2.2 Impact on the grid constraint and protections

The addition of the feeder inductors do not only impact the current to break by the DC breakers. Indeed, the current flowing through the diodes of the converter is also damped, which increases the maximal allowed time to clear the faults.

Using the previous TWENTIES grid structure, this time constraint was already respected for all cases when the differential current protection was considered, except for long cables. The maximal cable length, with no feeder inductors, was equal to 150km. Considering the modification explained in the previous subsection, the maximal cable length becomes 600km.

This also has an impact on the backup principle. The time constraint specification was not respected, but the inductor modification solves this problem. It also allows a better covering range in terms of fault resistance that can be detected, since the damping effect introduced by the inductors increases the mitigation be-

tween the signals, and thus enables a better discrimination between internal and external fault. Due to agenda limitation, the results on the backup considering this new grid structure could be shown in the thesis.

4.2.3 Voltage differential protection

As explained in Chapter 5 section 3.6, the incorporation of feeder inductors enables to use another protection principle, which does not require any communication along the cables. The algorithm is based on the voltage measurement at the inductor terminals, and is reminded in (6.14).

$$\begin{array}{llcll} \text{IF} & \mathrm{V_{ind}}_{ij}(t) & > & \mathrm{dV_{indTH+}} & ; \text{ Trip} \\ \text{ELSE IF} & \mathrm{V_{ind}}_{ij}(\mathrm{t}) & < & \mathrm{dV_{indTH\text{-}}} & ; \text{ Block for } \Delta t_{block} \\ \text{ELSE} & & & & ; \text{ Stand By} \end{array} \tag{6.14}$$

The theoretical performances were tested through EMTP-rv simulations, and are resumed in this subsection.

a) Threshold settings

The pole-to-pole faults occurring at each cable end are used to find the thresholds values guaranteeing the full selectivity of the criterion.

A negative threshold value of $\mathrm{dV_{indTH-}} = -40\mathrm{kV}$, set at each feeder protection relay, enables to discriminate the faults occurring close to the relay but external to their protective zone.

The positive threshold values were chosen to ensure the selectivity of the principle, similarly than it was performed for the backup protection, as explained below.

Let the fault groups $\mathscr{F}_{\mathrm{ki}}^{int}$ and $\mathscr{F}_{\mathrm{ki}}^{ext}$ being the groups of faults defined for each protection relay $\mathrm{PR_{ki}}$ by (6.15) and (6.16) respectively.

$$\mathscr{F}_{\mathrm{ki}}^{int} = \{\mathrm{F_{ki}}; \mathrm{F_{ik}}\} \tag{6.15}$$

$$\mathscr{F}_{\mathrm{ki}}^{ext} = \{\mathrm{F_{ij}}, i \neq k \text{ and } j \neq k\} \tag{6.16}$$

Let $\mathscr{F}_{\mathrm{ki}}^{ext-neg}$ the fault group now defined by (6.17), which represents the faults

that occurs in external links to PR_{ki} and which implies a negative voltage wave front detected by PR_{ki} in the time interval $I = [t_{fault}; t_{fault} + \Delta t_{stop}]$.

$$\mathscr{F}_{ki}^{ext-neg} = \left\{ F_{ij} \in \mathscr{F}_{ki}^{ext} \text{ such that } \exists t \in I / V_{ind ki}(t) < dV_{indTH-} \right\} \tag{6.17}$$

The new fault group $\mathscr{F}_{ki}^{ext-pos}$ is hence defined by (6.18), and contains all the faults in $\mathscr{F}_{ki}^{ext}$ that are not in $\mathscr{F}_{ki}^{ext-neg}$:

$$\mathscr{F}_{ki}^{ext-pos} = \mathscr{F}_{ki}^{ext} \setminus \mathscr{F}_{ki}^{ext-neg} \tag{6.18}$$

The threshold values V_{indTH+} are thus found for each relay PR_{ki} by resolving equation (6.19):

$$\max_{F_{ij} \in \mathscr{F}_{ki}^{ext-pos}} \left(\max_{t \in I} \left(V_{ind ij}(t) \right) \right) < dV_{indTH+} < \min_{F_{ki} \in \mathscr{F}_{ki}^{int}} \left(\max_{t \in I} \left(V_{ind ki}(t) \right) \right) \tag{6.19}$$

The thresholds were chosen % higher than the minimum value defined in the left hand side of equation (6.19), and are given in Tab.6.33 for each feeder protection. For information purpose, the maximum values, defined by the right hand side of (6.19), are displayed.

Relay	V_{indTH+}	$\min_{F_{ki} \in \mathscr{F}_{ki}^{int}} (\max_{t \in I} (V_{ind ki}(t)))$
PR_{13}	82.5770kV	209.1kV
PR_{31}	81.8620kV	210kV
PR_{12}	71.5990kV	208.8kV
PR_{21}	81.0920kV	231.1kV
PR_{23}	93.5330kV	231.6kV
PR_{32}	76.9230kV	209.5kV
PR_{24}	101.9590kV	231.8kV
PR_{42}	97.4820kV	210kV
PR_{45}	14.5200kV	210.2kV
PR_{54}	70.7300kV	168kV

Table 6.33: Thresholds setting for the voltage differential protection

b) Voltage differential protection validation

The fault clearing process of the worst case faults in terms of current to break are summarized in Tab.6.34. The tripping times and the current to break that are displayed correspond to the maximal values between the two ends of the faulty cable.

Relay near the fault	t_{trip}	Current to break
PR_{13}	1.550ms	9.322kA
PR_{31}	1.550ms	10.257kA
PR_{12}	1.400ms	7.801kA
PR_{21}	1.410ms	6.115kA
PR_{23}	1.270ms	8.581kA
PR_{32}	1.270ms	8.340kA
PR_{24}	1.140ms	9.691kA
PR_{42}	1.140ms	10.531kA
PR_{45}	2.080ms	9.725kA
PR_{54}	2.060ms	11.987kA

Table 6.34: Thresholds setting for the voltage differential protection

Note that since there is no communication between the relays, the trippings are not synchronized at the two cable ends. This could eventually lead to higher currents to break at the cable end which trips last. However, the time difference is small and considering those high feeder inductor values, the current remains below 15kA.

The pole-to-pole fault example occurring near PR_{13} is used to compare the differential current protection and the voltage differential principle, and the results are provided in Tab.6.35.

Relay	**t_{trip}**		**Current to break**	
	Current	Voltage	Current	Voltage
PR_{13}	1.590ms	1.010ms	8.957kA	8.799kA
PR_{31}	1.590ms	1.550ms	9.473kA	9.322kA

Table 6.35: Differential current and voltage differential principles for a fault example occurring near PR_{13}

The shortest detection time occurs for the cable end close to the fault, with the voltage differential principle. This is due to the fact that there is no delay due to communication. The highest detection time is though also for the voltage differential principle, at the other cable end. Indeed, there is a mitigation in the signal while it propagates through the cable, which damps the waves, which leads to a delay of the detection. This is not the case for the differential current. Indeed, the differential current is the same at both cable ends, and once the perturbation is seen at one end. For this fault case, the communication link enables a quicker detection of the fault.

The same comparison is done for a fault occurring on the longest cable, near PR_{54}. The results are given in Tab.6.36.

Relay	**t_{trip}**		**Current to break**	
	Current	Voltage	Current	Voltage
PR_{45}	2.120ms	2.060ms	5.252kA	12.208kA
PR_{54}	2.120ms	1.010ms	12.445kA	7.408kA

Table 6.36: Differential current and voltage differential principles for a fault example occurring near PR_{54}

In this case, the tripping time related to the differential current is sensitively higher than the one for the voltage differential criterion. This is due to the longer communication delay. Indeed, for short links smaller than 200km, the differential current is quicker than the voltage differential protection. However, for longer links, the voltage differential protection becomes faster.

Beside, the impact of the non-synchronization of the trippings of the two cable ends is highlighted on this example. This explains the fact that the current to break at PR_{45} is higher if the voltage differential principle is considered, since the tripping is done around 1ms before at the other cable end.

The two principle can thus be both implemented in the protection system. The voltage differential can thus be a backup in case of the communication loss for links smaller than 200km. For links higher than this value, it becomes the main cable protection.

Note that the validity domain of the voltage differential protection depends strongly on the feeder inductors value. Indeed, for smaller inductor values, the mitigation of the signals is reduced, and thus the maximal fault resistance that can be detected is also reduced. The inductor value choice can thus be chosen in order to ensure the detection of a given fault resistance. For the presented inductor values, the maximal fault resistance detected is $R_{fault} = 50\Omega$. For higher fault resistances, the differential current protection is responsible for the fault clearance.

5 Conclusion on the protection system

The theoretical performances of the protection system were assessed thanks to EMTP-rv study. The thresholds settings and the validity domain of the different protection principles strongly depends on the grid structure. Indeed, the thresholds might be subjected to change if the grid configuration changes. Other calculations would be required but can be performed similarly than explained in section 1, and new threshold values would be sent by the supervisor to the relays.

The proposed protection system thus includes inductors located near each feeder relay, and this way enables the recourse to a non-communicant protection principle. This later one can hence support the protection system in case of the loss of the optical fiber link. The differential current protection is however crucial in the system since it is the only one that can detect high impedance faults.

Even though the inductor values seems to be high (25mH and 30mH), they are

not prohibited. Indeed, the stability of the control loops under those conditions were validated in the L2EP. Furthermore, smoothing reactors up to 100mH are already considered for industrialized HVDC project by ABB.

Nevertheless, even though the addition of feeder inductors limits the current to break below a certain value, it also increases the energy store in the system and thus that needs to be dissipated. This means that other investigations are required on the current limitation during breaker tripping action.

General conclusion

General conclusion

In electricity transmission, the inherent qualities of alternative grids fade in front of the difficulty imposed by the reactive power transportation, when overhead lines or, particularly, underground or submarine cables reach critical lengths. In the frame of the thought aiming to operate at best renewable energy resources, coming from wind or hydro power stations, the creation of a high voltage direct current grid is assumed to dispatch those energies to the consumption centers. As mentioned in Chapter 1, from a certain amount of power to transmit, there is a critical length beyond which AC transmission is not viable anymore, and where DC links becomes both more efficient and less costly. The new conversion technologies, namely the voltage source converters, now enables the connection of several terminals and therefore the creation of a true grid, which can either have a looped, meshed, or radial structure. The advantages of such grid structure in relation to point-to-point links are obvious in terms of reliability of the transmission grid. Nevertheless, some technological locks remains, and the protection against faults of those grids is currently largely debated. This Ph.D thesis aims to propose a complete protection plan against insulation faults in cable or busbar, including a main protection and two backups in case of failure of a component, for a submarine DC grid. The target application would be a grid linking offshore wind farms and countries through the North Sea.

Even though several protection philosophies, detailed in Chapter 2, can be followed, the one used for the protection of AC grids was chosen since this one already proved its worth in operation. A given grid structure composed of five nodes and five links was chosen. This structure was subjected to EMTP-rv model and simulations to study the constraints related to the protection operation, and to investigate the grid behavior under fault conditions. A parametric study was presented in Chapter

4 to show this grid behavior. The protection system must respond to several specifications, that were detailed at the beginning of Chapter 5. The very restrictive constraint, in terms of operation time range of the protection system, is given by the current flowing through the diodes of the converters, and requires a maximal operation time of the protection in the range of few milliseconds. This implies that the selective detection has to be performed during the transient phase of the signals. In order to represent the transients phenomena following a fault occurrence, a very detailed model of the grid was created and was presented in Chapter 3. The main characteristics of undergrounds or submarine cables is that they present power damping in the signals due to their low resistivity. As it is explained in Chapter 5, selective criteria are thus harder to find, which forces the recourse to communicant protection principles. The differential current was found to be the most relevant solution. Even though it is already used in AC applications, it was modified to become a traveling wave based criterion adapted to fault transients related to DC grids. The EMTP-rv validation of the protection principles, presented at the beginning of Chapter 6, highlighted the dramatically huge current that would need to be broken by the DC breakers. Those DC breakers, still under prototyping phase as mentioned in Chapter 2, might not be able to cut those kind of large currents, in the range of several tens of kiloAmps. This is the reason why a solution to limit these currents was investigated. The best trail is to incorporate inductors at the cable ends. This results in a lower rate of rise of the current, and if the inductor values can be set in order to ensure that the current to break would be below a given value. This grid structure modification enables the discovery of a non-communicant principle, which cannot be implemented without the presence of those new inductors. This later principle, named voltage differential protection, can thus be combined with the differential current protection and act either as a backup in case of the loss of the communication link, or acts as a main protection since its operation is quicker for very long links. Besides, the addition of the inductors at the cable ends releases the constraint related to the current flowing through the diodes, and hence enables a larger validity domain of the differential current protection, in terms of maximal cable length that can be covered. A backup protection in case a breaker fails was also proposed. Once again, the presence of the inductors improves the validity domain of the protection principle.

To conclude, a protection plan composed of two main protections (one covering the cable zone and the other one the busbars), and two backups (one in case of communication loss and the other one in case of breaker failure) was proposed. Besides, an other algorithm was included in the protection system to ensure the safe connection manoeuvres of links, and checks the cable state before fully connecting it to the grid. This avoids the connection of faulty cables. The theoretical performances of the system were assessed thanks to EMTP-rv studies, taking into account the damping effects of the sensors on the inputs of the protection system. The robustness to noise and other perturbation related to physical devices of the principles were performed through the implementation and testing on a low-scale mock-up. The differential current and backup protection principles was verified on this demonstrator (Twenties Demo 3) which is a Real-Time Power Hardware In the Loop grid that was presented in Chapter 6. The demonstrator also showed that the protection system is robust to the modification of the grid topology, and requires only new thresholds settings.

The main conclusion of this thesis is that even though fast protection principles, reliable and robust, are feasible, the DC current breaking technology remains a major obstacle. Indeed, the hybrid DC breakers prototypes are for now only able to break around 10 kiloAmps. The incorporation of inductors can effectively relax the constraint and limit the current to break to this kind of value, but however increases largely the energy stored in the system and thus the energy to dissipate by those breakers. This phenomenon requires further investigations to verify if the inductor solution is viable. If not, some trails could be to combine the breakers with DC/DC converters that can limit the fault current, and will probably be studied at the University of Aberdeen. However, the impact on the backup protection could be too high, and then would require the investigation of new backup principles. This was the main disadvantage of the superconducting fault current limiters, beyond the fact that this technology is not mature and extremely costly. The only other trails on the backup protection that were found during this Ph.D work are presented in appendix but their application in real grids seems to be compromised.

The system was tested considering two-level voltage source converters. Some simulations were performed with averaged models of half-bridge multi-modular con-

verters, but the short transient study would require the use of detailed models. Considering the large number of components, the simulations are too long and were thus prohibited. Nevertheless, there is no reason that the differential current and the voltage differential criteria would become less relevant with those converter technologies, since the traveling wave principle remains. This is not the case for the backup protection, once again.

Full bridge converter types were not investigated since they suppose a totally different protection strategy, due to their ability to delete the fault current themselves.

The main question remains in the validity of the cable model. Indeed, the global work on the current to break evaluation is strongly dependent on the cable model response. The WideBand model was chosen since it is the most complex and most representative model, but no comparison with real DC cable tests were found in the literature. The mock-up could not validate the model since the physical cables were kept on their drums. Such physical tests and comparisons would be a huge step in the validation of the DC grid behavior of EMTP-rv models. Note however that the FDQ model response where sensitively close to the WideBand one. Adding to that, a full DC breaker model would enable the validation of the protection system.

In this thesis, the protection of DC grids was investigated based on a DC grid point of view only. The global transmission grid is composed at 99% of AC lines. Therefore, the impact of the DC system has to be investigated from the AC grid point of view, and that not only in terms of protection, but also considering the overall operation of such DC grids, considering the bulk power they are supposed to transmit.

Appendices

Appendix A

Protection principles

1 Difficulty to find non-communicant selective principles

As mentioned in Chapter 5, the selectivity (insulate only the faulty cable) cannot be achieved if only a busbar level communication is considered.

Fig.A.1 shows the current measurements for busbar 1 and 3 for the two fault cases $\mathscr{C}_{\text{int}}$ and $\mathscr{C}_{\text{ext}}$, defined in Chapter 5 and reminded in Tab.A.1. The idea here was to find a criterion based on a busbar-level communication that enables a selective detection.

Case name	Type	Link	Location	R_{fault}
$\mathscr{C}_{\text{int}}$	Pole-to-ground	Link1, positive pole	30km away Station1	10Ω
$\mathscr{C}_{\text{ext}}$	Pole-to-ground	Link3, positive pole	Near Station3	1Ω

Table A.1: Internal and external fault cases

Reminder

Fault $\mathscr{C}_{\text{int}}$ has to be cleared by PR_{13} and PR_{31}.
Fault $\mathscr{C}_{\text{ext}}$ has to be cleared by PR_{32} and PR_{23}.

On Fig.A.1a, it can be noticed that the protection that has to trip (PR_{13}) can be discriminated from the other ones, since this is the only current that is positive

and higher than the current of the station connection point protection PR_1. This is also the case for PR_{31} on Fig.A.1c and PR_{32} on Fig.A.1d. This criterion was thus tested.

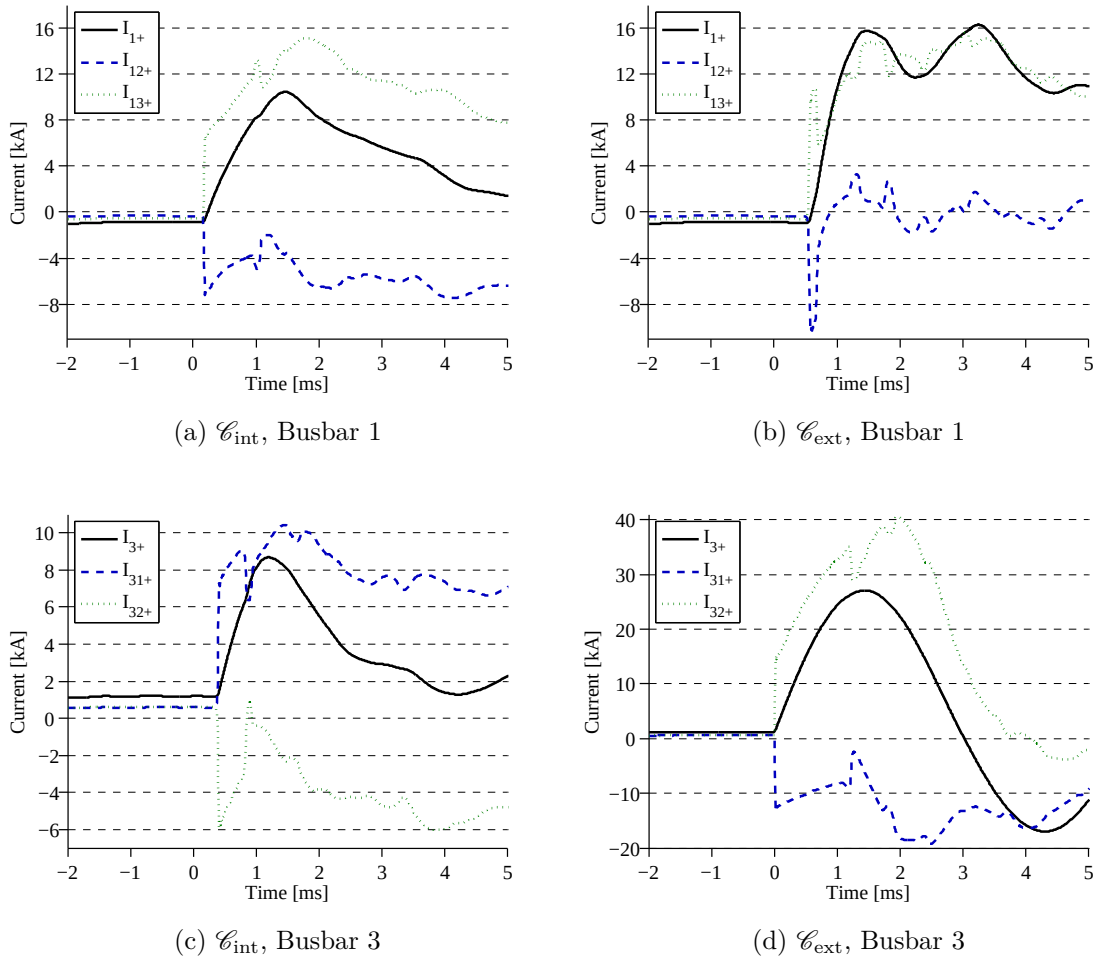

(a) $\mathscr{C}_{\text{int}}$, Busbar 1

(b) $\mathscr{C}_{\text{ext}}$, Busbar 1

(c) $\mathscr{C}_{\text{int}}$, Busbar 3

(d) $\mathscr{C}_{\text{ext}}$, Busbar 3

Figure A.1: Busbar-level measurements

However, on Fig.A.1b, there is also a positive current higher than the other ones (I_{13+}), but for this fault, PR_{13} must not trip since the fault is on another link. This phenomenon is also highlighted on Fig.A.2 for the measurements of busbar 2 and 4 for the fault $\mathscr{C}_{\text{int}}$. On Fig.A.2a, there would be an unwanted tripping from PR_{21}, and another one by PR_{42} on Fig.A.2b.

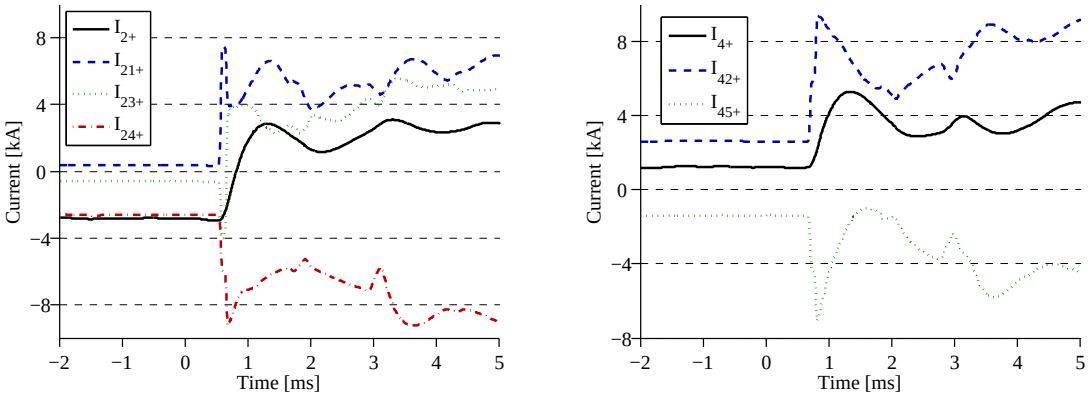

(a) $\mathscr{C}_{\text{int}}$, Busbar 2

(b) $\mathscr{C}_{\text{int}}$, Busbar 4

Figure A.2: Busbar-level other measurements

This is example was given to show that some simple criteria might be found but can result in unwanted trippings for some cases.

2 Backup protection: other trails

Other trails were investigated for the backup protection. They are all based on complex signal processing techniques and thus require large computation times. This is why they were investigated only considering high fault resistances, which avoid the time constraint given by the current flowing through the diodes.

At the time those principles were imagined, another grid structure was under used for EMTP-rv simulation. The examples will thus be illustrated using the grid shown on Fig.A.3.

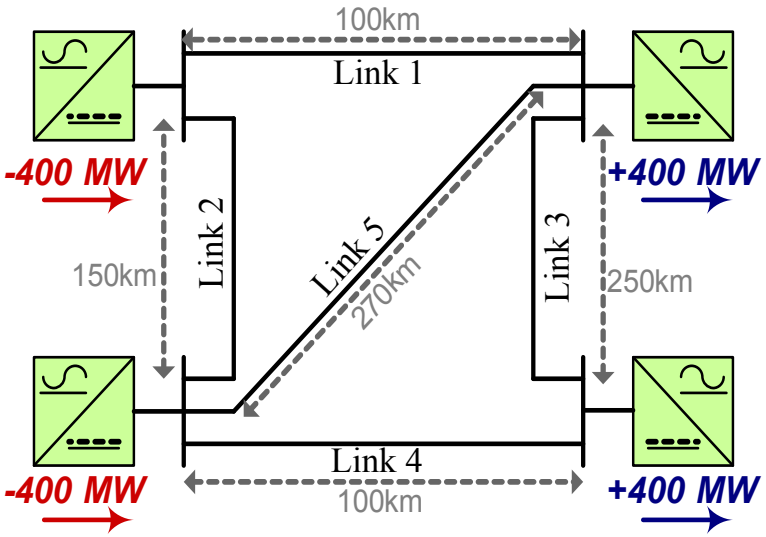

Figure A.3: EMTP-rv tests

2.1 Frequency domain analysis protection

The idea is to inject alternative signals in the DC grid and to monitor the phase of those signals. In normal operation, the phase would be constant. At the opposite, if there is a fault in a link, then the signal phase would change.

The principle works as it follows for a given link:

- A signal $sin\,(\omega t + \Theta)$ is injected by the VSC station
- A Phase Locked Loop (PLL) calculates the phase of the signal, which is monitored
- If a discontinuity is present in the measured phase signal, that means a fault occurred

For a HVDC line, the principle is illustrated on Fig.A.4. The station on the left injects a signal $sin\,(\omega 1t + \Theta 1)$. On the right station, the corresponding signals is $sin\,(\omega' 1t + \Theta 1)$, since their is a phase difference due to the propagation of the signal through the link. The phase $\Theta 1'$ is thus monitored, and if there is a discontinuity (due to a fault on the link), the tripping order is sent to the protection on the right (blue).

Since there is no communication, the same process needs to be done for the other protection. This results in the injection of an other signal $sin\,(\omega 2t + \Theta 2)$ by

the right station, and a PLL monitoring $\Theta 2'$ to command the protection of the left hand side (red).

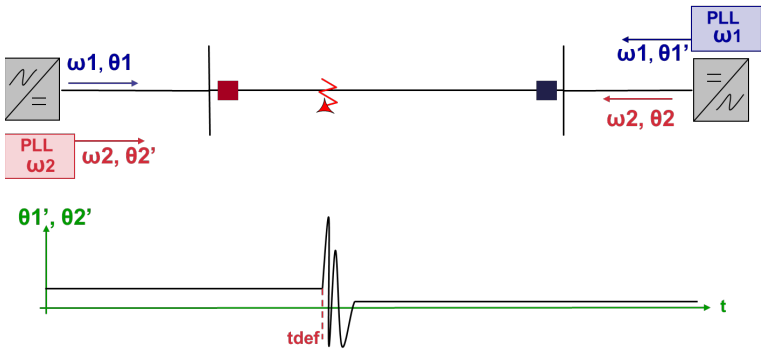

Figure A.4: Frequency domain based protection principle for a HVDC link

To ensure the selectivity, each cable end has to be associated with a given signal, with its own frequency and phase. This results in a lot of signals, as shown for a multi-terminal grid example on Fig.A.5.

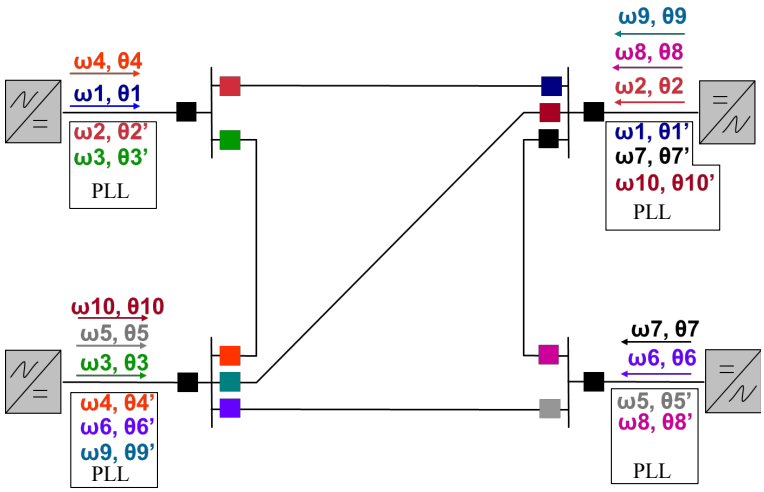

Figure A.5: Frequency domain based protection principle for a multi-terminal DC grid

This principle was tested for a HVDC link with classical PLL that can be found in EMTP-rv library. Simulations proved that faults can be detected by this method. However, for multi-terminal applications, numerous signals are required which leads to the superposition of several frequencies (n frequencies, where n is the number of DC cable ends, meaning 10 in the example of Fig.A.5). Those frequencies need to be chosen to be easily identified by the PLL, and also below the cutting frequency of the DC filters connected to the VSC.

In any case, the global signal is very complex and thus very efficient PLL need to be implemented. Hence, the principle was not investigate in further details, due to its complexity for a real implementation and operation.

2.2 Complex signal-processing methods

2.2.1 Traveling wave based protection using reflections

As mentioned in Chapter 2 section 2.1, the traveling wave implied by the fault reflects at any discontinuities, such as busbars or the fault itself. Such reflections can also be created on purpose by injecting a short current step. In that way, the absolute current step occurrence time is known, unlike the absolute fault time, and the resulting reflections can be analysed. The idea assumes a communication of all the protection with the dispatching center or a supervisor, and is explained below.

- The fault is detected by a simple non-selective principle in the grid, such as an overcurrent or undervoltage protection principle.

- One converter station injects a very short current step, which can be seen like a peak.

- The protection of each cable end analyses the reflections following the peak that are present in the current shape.

Indeed, if the network topology is well known, the normal reflections can be predicted. Indeed, from a protection point of view, the reflected wave coming from the same cable (for example the opposite end of the cable) will result in a positive front. At the opposite, the reflection coming from a discontinuity of an other cable will result in a negative front.

An example is shown on Fig.A.6. On this case, a fault occurred on the diagonal line. The values L1 and L2 are the lengths of the cables. The fault is considered to be more than $L1 + L2$ away from the rounded protection. The top left converters sends a current peak (I_{ref}). Each protection of the grid analyses the reflections, but the example is given for the rounded one.

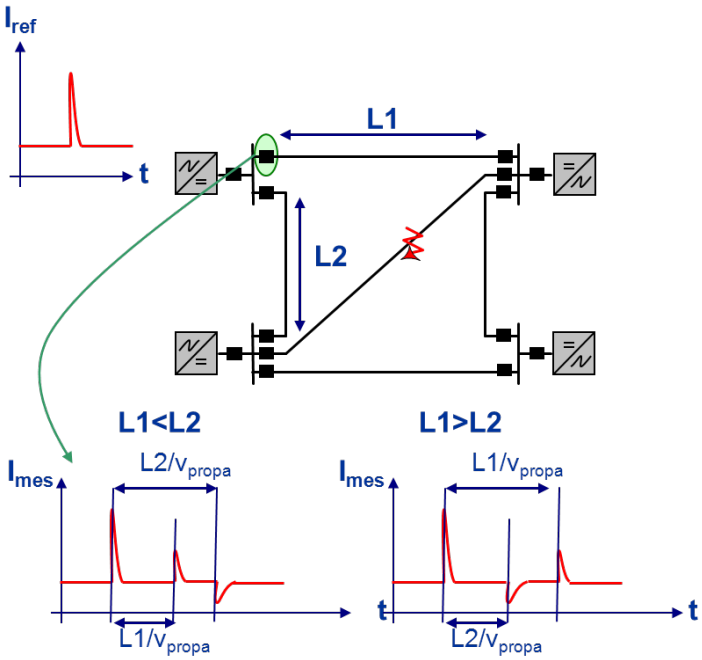

Figure A.6: Illustration of the protection principle based on a current step injection for a healthy link

In any cases (different lengths), the normal reflections can be predicted. Thus, if another reflection is seen, it corresponds to the fault. Furthermore, if this non-predicted reflection results in a positive front (Fig.A.7), then the fault is on the cable where the considered protection is connected, and the tripping order can be sent.

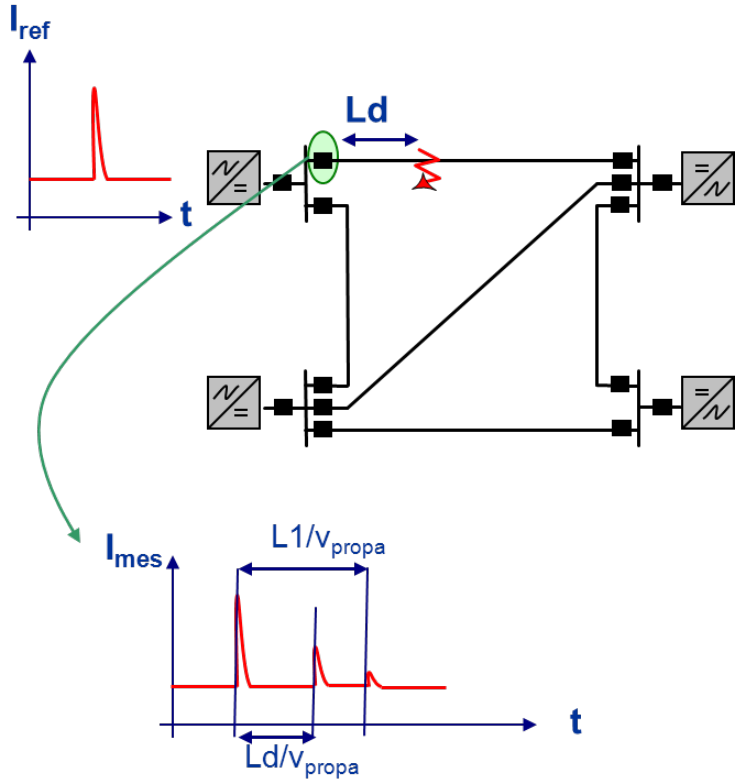

Figure A.7: Illustration of the protection principle based on a current step injection for a faulty link

The protection can thus follow the rules below:

1. Detection of the fault somewhere in the grid

2. Non response of the main protection algorithms

3. The converter stations send successively current peaks until the faulty link is identified.

A converter station send a current peak once the previous one is mitigated enough to ensure that the reflection analysis will not be altered by the previous reflections.

This principle was tested using EMTP-rv simulations on the MTDC grid of Fig.A.3. The current measurements for the faulty link are shown on Fig.A.8 for two fault cases with resistance of 100Ω and 200Ω.

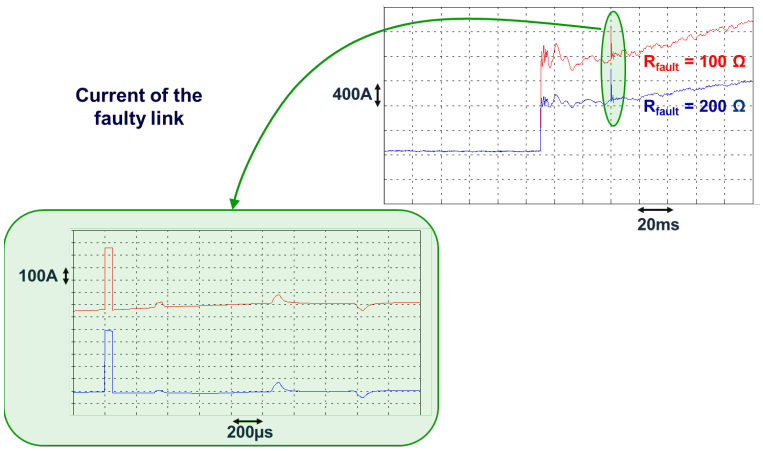

Figure A.8: EMTP-rv tests

The reflections that are seen on the zoomed currents are the expected ones, and the fault can effectively be detected. To do so, the measured current can be compared with a pre-defined current shape, using a correlation principle to assess if a non-predicted reflection is present. The sign of this reflection is then used to ensure the selectivity.

Once again, the real application of such principles seems to be compromised. First, the current peak injection is hard to achieve due to the DC filter which would damp the signal. Also, faults close to the cable ends are hard to discriminate with normal reflections and moreover, very accurate sensors are required.

2.2.2 Wavelet-based protection

Wavelet-based protections are widely found in the literature. They are mainly used for fault localization in AC distribution networks, but some trails were also found for the selective detection of faults occurring in DC grids. Wavelet based protections use the concept of traveling wave by applying a transformation, called the wavelet transform, to a signal, as it is explained below.

a) Generalities on wavelet transform

The wavelet transform is particularly adapted for the analysis of transient phenomena. Indeed, it enables the localization (both in the time and frequency domains) the signal simultaneously at the moment of the analysis. Furthermore, the analysed window can be automatically adjusted depending on the frequency. It is

possible to decompose the signal into several frequency ranges, which is suitable with the propagation of the waves whose characteristics vary with the frequency. This is why those aspects seem to be interesting for fault detection. The detail of wavelet transform is not detailed here but the reader can refer to [Mallat, 2008] for further information. In order to understand the global principle, a short description is presented.

Wavelet transform decomposes a signal based on a wavelet family, thanks to a scalar product. The resulting numbers are traditionally called *wavelet coefficients*. This wavelet family is composed of translations and dilatations of a mother wavelet ψ. The components of the family are defined by (A.1):

$$\psi_{u,s}(t) = \frac{1}{\sqrt{s}}\psi\left(\frac{t-u}{s}\right) \tag{A.1}$$

where u and s are reals which represent the translation parameter and the scaling factor of the decomposition respectively.

Hence, the continuous wavelet transform of a signal f is defined by (A.2):

$$Wf\,(u,s) = \langle f, \psi_{u,s}\rangle = \int_{-\infty}^{+\infty} f(t)\frac{1}{\sqrt{s}}\,\psi\left(\frac{t-u}{s}\right)dt \tag{A.2}$$

Several kinds of wavelet transform can be applied, and the principle has already been widely used for AC distribution grids. The discrete wavelet transform is the most appropriate since the signal to be transform is sampled, and the dyadic transform is usually employed [Evrenosoglu and Abur, 2005]. It consists in sampling the scaling factor s and the translation parameter u in powers of 2. Thus, they can be written $s = 2^j$ and $u = k.2^j$. This method is equivalent to treat the wavelet transform like a filter bank. For each decomposition level, two coefficients are evaluated: an approximation coefficient (A), that corresponds to low frequencies components, and a detail coefficient (D), which corresponds to high frequencies components. Each level corresponds to a time and frequency range. The global idea is represented on Fig.A.9.

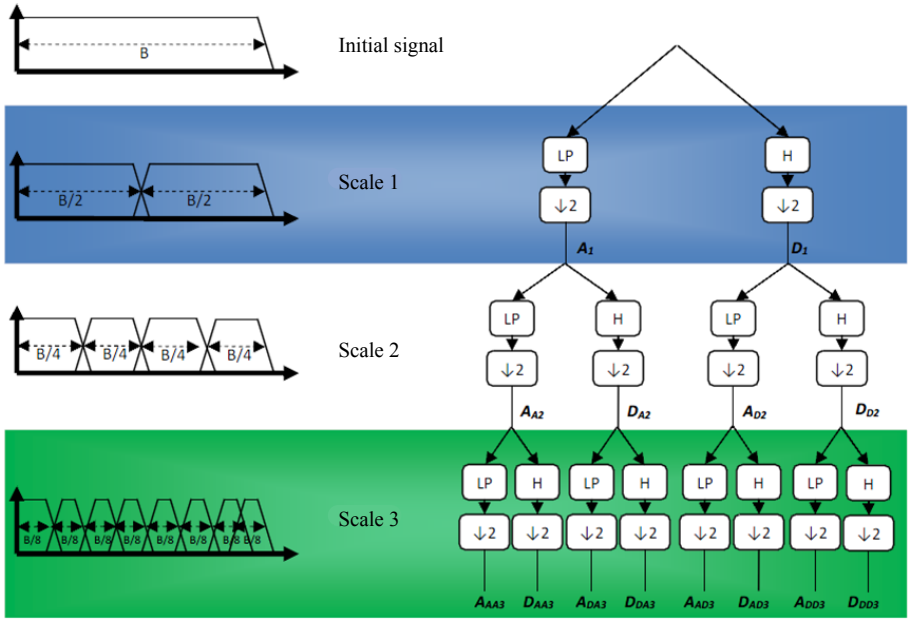

Figure A.9: Dyadic wavelet decomposition

As mentioned in Chapter 2, several studies were found concerning the application of the wavelet transform to protection of DC grids. The idea was investigated and is explained in the next paragraph.

b) Protection using wavelet transform

The wavelet decomposition of a measured DC current during fault conditions is illustrated on Fig.A.10. The approximation and detail coefficients are plotted as a function of the time. They are evaluated thanks to a Matlab algorithm using a Daubechies mother wavelet[1].

[1]Several mother wavelets can be used, like Haar, Coiflet, Symlet, or can be built for a special transient analysis [Borghetti et al., 2008]

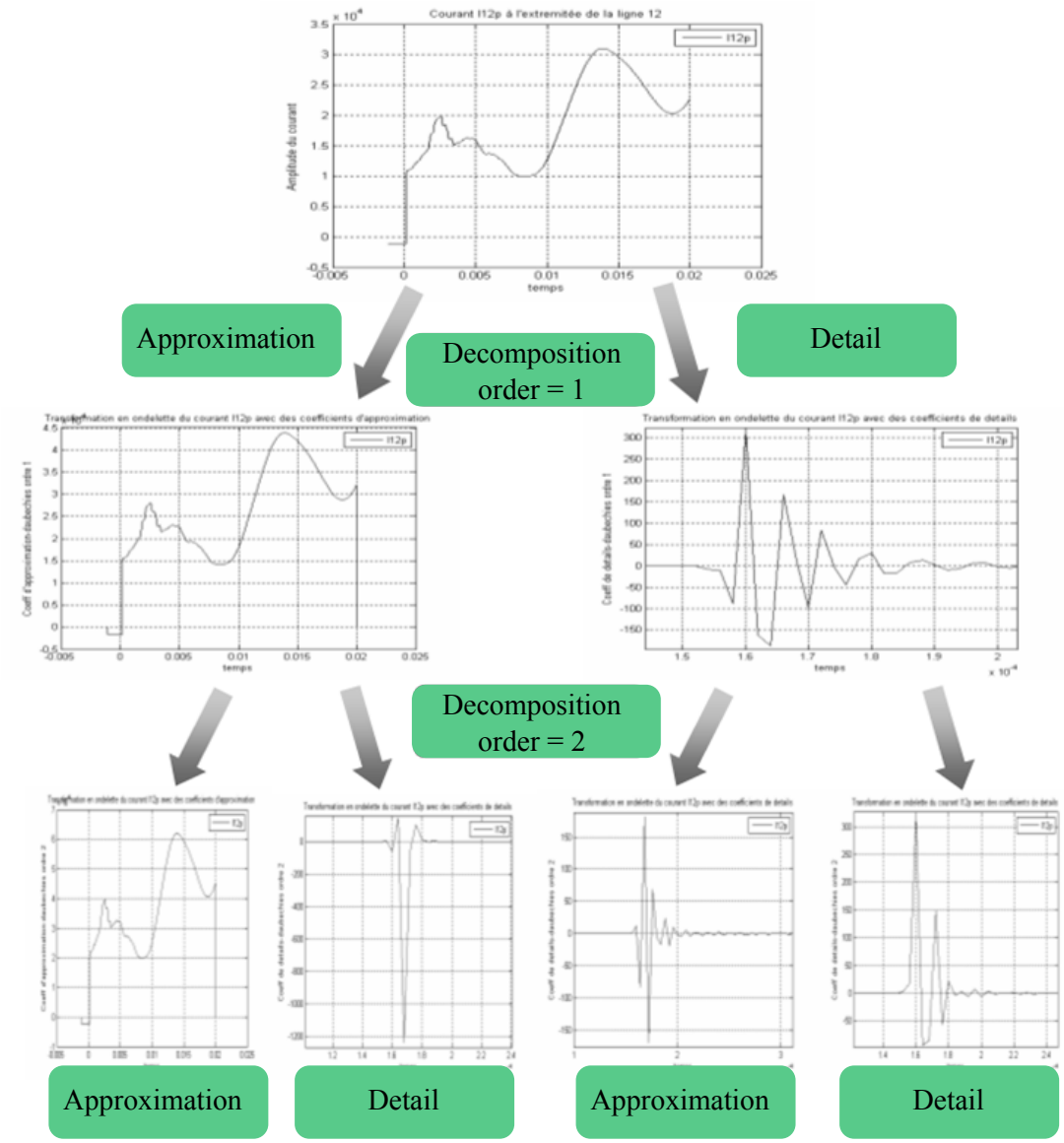

Figure A.10: Current decomposition illustration

Using the DC grid configuration presented on Fig.A.3, the idea was to find a criterion enabling the selective detection of any fault. For a given fault, the currents and voltages decomposition into wavelet detail coefficients (second order, Daubechies) of the signals measured at each cable end was performed (10 currents and 10 voltages). The maximal value of those coefficients, which corresponds to the fault occurrence, was stored in a matrix. This was done for 175 fault cases (the fault can occurred in any of the 5 links, in 7 positions and its resistance can take 5 values: 1Ω, 10Ω, 20Ω, 50Ω, 100Ω).

The goal was to find a threshold for each protection that ensures the selectivity,

meaning that for a given protection, the threshold is exceeded for any fault occurring on the cable it is connected to, and this threshold is not exceeded for any other faults, external to the link. A criterion based on such threshold and assuming a cable-level communication was found, but is similar to the directional criterion developed in Chapter 5 section 3.4.2. In this case, the recourse to complex signal processing methods such as the wavelet transform would be useless, so a criterion assuming no communication was investigated. However, no solution were found considering all those faults. Indeed, the selectivity might be ensured for faults with resistance of 1Ω, but the higher fault resistance cases then are not detected. Even though, a multi-criterion principle was considered, but does not provide any advantages compared to the backup protection proposal of Chapter 5 section 4.

Appendix B

Protection plan validation

1 Worst case faults clearance by the backup protection

As mentioned in Chapter 6 section 2.2 page 165, the worst case faults in terms of current to break are the most likely ones subjected to imply a breaker failure. The operation of the backup protection is shown in this section for those worst case faults.

Those faults are the one used to test the differential current protection in section 2.1.3 b) page 160, where the breaker of the relay located near the fault fails. The current to break and the tripping time of the remote faulty cable end relay (thanks to the differential current protection) is the same than if there is no breaker failure. They were given in Tab.6.10 page 161. The tripping times for the backup protection (the cable end where a breaker failmure occurred) and the current to break are given in Tab.B.1 and Tab.B.2.

Fault location	Relay	Tripping time	Current to break
Near relay PR_{12}	PR_1	2.440ms	33.015kA
	PR_{12}	FAILED	prosp: 52.513kA
	PR_{13}	2.440ms	19.498kA

Table B.1: Relevant operation times related to the clearing process of the fault example, and current to break by the breakers (prosp means prospective current to break if the breaker did not fail

Near relay PR_{13}	PR_1	2.440ms	31.751kA
	PR_{12}	2.440ms	26.654kA
	PR_{13}	FAILED	prosp: 58.416kA
Near relay PR_{21}	PR_2	2.610ms	25.626kA
	PR_{21}	FAILED	prosp: 69.174kA
	PR_{23}	2.610ms	22.444kA
	PR_{24}	2.610ms	21.103kA
Near relay PR_{23}	PR_2	2.610ms	25.774kA
	PR_{21}	2.610ms	23.511kA
	PR_{23}	FAILED	prosp: 70.775kA
	PR_{24}	2.610ms	21.490kA
Near relay PR_{24}	PR_2	2.610ms	27.174kA
	PR_{21}	2.610ms	20.021kA
	PR_{23}	2.610ms	20.466kA
	PR_{24}	FAILED	prosp: 67.762kA
Near relay PR_{31}	PR_3	2.610ms	21.577kA
	PR_{31}	FAILED	prosp: 54.339kA
	PR_{32}	2.610ms	32.762kA
Near relay PR_{32}	PR_3	2.610ms	23.022kA
	PR_{31}	2.610ms	21.186kA
	PR_{32}	FAILED	prosp: 44.075kA
Near relay PR_{42}	PR_4	3.110ms	22.226kA
	PR_{42}	FAILED	prosp: 38.152kA
	PR_{45}	3.110ms	15.926kA
Near relay PR_{45}	PR_4	3.110ms	16.674kA
	PR_{42}	3.110ms	41.334kA
	PR_{45}	FAILED	prosp: 58.009kA
Near relay PR_{54}	PR_5	3.110ms	24.827kA
	PR_{54}	3.110ms	prosp: 24.827kA

Table B.2: Relevant operation times related to the clearing process of the fault example, and current to break by the breakers (prosp means prospective current to break if the breaker did not fail

2 Complete list of conducted tests on the mock-up

The mock-up TWENTIES - DEMO 3 implementation and notations are reminded on Fig.B.1. Several tests were conducted, using other structures, so they will be given at the beginning of the list of their respective tests.

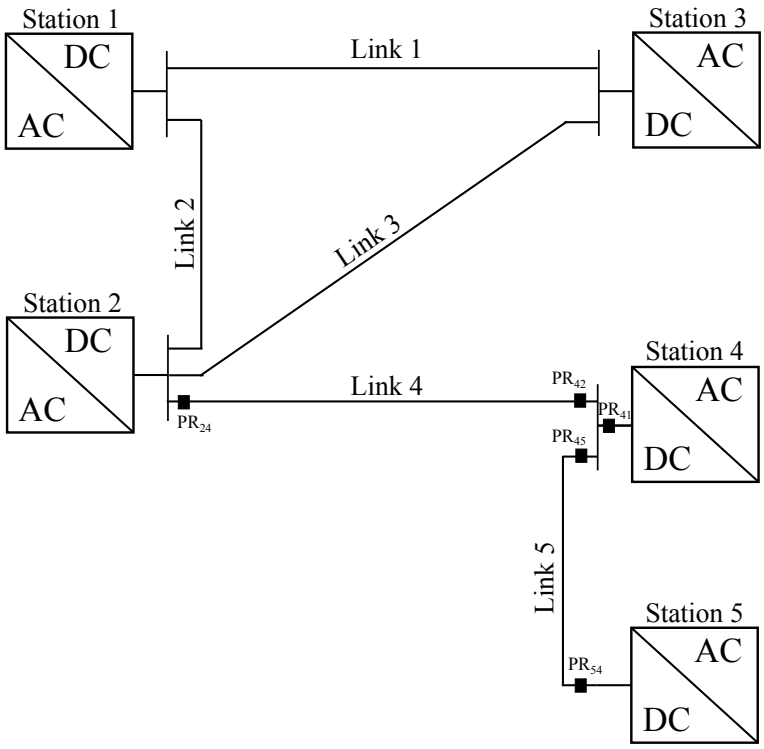

Figure B.1: Mock-up configuration

2.1 Test conducted on March, 25th 2013

2.1.1 First test series - 3 nodes grid

This series of test were performed on the grid configuration given in Fig.B.2. Converters 4 and 5 and power controlled, and converter 2 is voltage controlled.

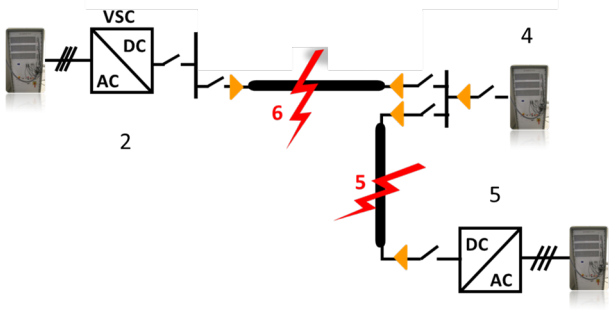

Figure B.2: 3 nodes grid configuration

Only the main cable differential protection was implemented, and the threshold value I_{dTH+} was set to 12A. The fault can be either on link 4 (horizontal) or on link 5 (vertical).

Test	Fault position	R_{fault}	Operation point	Tripping
T1	Link5	10Ω	no power transfer	OK
T2	Link5	10Ω	station 5 injects 300W	OK
T3	Link5	5Ω	no power transfer	OK
T4	Link5	5Ω	station 5 injects 300W	OK
T5	Link4	10Ω	no power transfer	OK

Table B.3: First test series, tripping OK means that the fault is cleared with the main cable differential protection

Between tests T5 and T6, the master and slave controlled converters were exchanged.

Test	Fault position	R_{fault}	Operation point	Tripping
T6	Link4	10Ω	no power transfer	OK
T7	Link4	10Ω	station 5 injects 300W	OK
T8	Link4	5Ω	no power transfer	OK

Table B.4: First test series, tripping OK means that the fault is cleared with the main cable differential protection

2.1.2 Second test series

This test series was conducted on the 5 nodes grid structure given on Fig.B.1. Converters 3, 4 and 5 are power controlled, and converters 1 and 2 are drooped controlled. Only converters 2 and 5 are physical.

Test	Fault position	R_{fault}	Operation point	Tripping
T10	Link4	10Ω	station 5 injects 300W	OK
T11	Link5	10Ω	stations 3, 4 and 5 inject respectively 600W, 390W and 220W	OK
T12	Link5	5Ω	stations 3, 4 and 5 inject respectively 600W, 390W and 220W	OK

Table B.5: First test series, tripping OK means that the fault is cleared with the main cable differential protection

2.2 Test conducted on May, 29th 2013 - Preparation of the backup mode

2.2.1 Test 20

No physical converter is connected, all the stations are the amplifiers. A load is placed near station 5 to create a power transfer.

Cable differential protection threshold is set to 6A.

The fault on link 5, with a resistance of 5Ω is cleared by the differential protection at PR_{54}, but the breaker of PR_{45} is set to trip 10ms after.

2.2.2 Test 21

The node near station 2 is disconnected to the source. Converter of station 5 is physical, and no power transfer is created.

The threshold I_{dTH+} is set to 12A, and the 5Ω fault on link 5 is cleared 3.140ms after its occurrence.

2.2.3 Test 22

The same configuration than test 21 is used and the same fault is done. The differential protection is disconnected at PR_{54}, so the backup can be tested.

The fault is cleared by the cable differential protection at PR_{45}, and by the backup at PR_{54}.

2.2.4 Test 23

The same configuration than the two previous tests is used, and station 5 injects 300W. A fault of 10Ω is done on link 4, and is cleared by the differential protection at both cable ends.

Bibliography

Bibliography

[Aimin et al., 2009] Aimin, L., Zexiang, C., Qizhen, S., Xiaohua, L., Dayong, R., and Zeming, Y. (2009). Study on the dynamic performance characteristics of hvdc control and protections for the hvdc line fault. In *Power and Energy Society General Meeting, PES*.

[Andersen and al., 2005] Andersen, B. and al. (2005). Vsc transmission. Technical report, CIGRE.

[Andrea et al., 2010a] Andrea, J., Schweitzer, P., and Tisserand, E. (2010a). A new dc and ac arc fault electrical model. In *Electrical Contacts (HOLM), 2010 Proceedings of the 56th IEEE Holm Conference on*, pages 1–6.

[Andrea et al., 2010b] Andrea, J., Schweitzer, P., Tisserand, E., Roth, P., and Weber, S. (2010b). Repeatable and calibrated arc fault generator. In *Industrial Electronics (ISIE), 2010 IEEE International Symposium on*, pages 1022–1026.

[Asplund, 2004] Asplund, G. (2004). Sustainable energy systems with hvdc transmission. In *IEEE Power Engineering Society General Meeting*.

[Bahrman et al., 2003] Bahrman, M., Johansson, J., and Nilsson, B. (2003). Voltage source converter transmission technologies: the right fit for the application. In *Power Engineering Society General Meeting, 2003, IEEE*, volume 3, pages –1847 Vol. 3.

[Borghetti et al., 2008] Borghetti, A., Bosetti, M., Di Silvestro, M., Nucci, C. A., and Paolone, M. (2008). Continuous-wavelet transform for fault location in distribution power networks: Definition of mother wavelets inferred from fault originated transients. *Power systems, IEEE Transactions on*, 23(2):380–388.

[Correvon, 2005] Correvon, M. (2005). Mesure de courant, transducers, hes so course on système électroniques.

[Craciun et al., 2011] Craciun, O., Florescu, A., Munteanu, I., Bacha, S., Bratcu, A. I., and Radu, D. (2011). Protection devices testing based on power-hardware-in-the-loop simulation. In *IECON 2011 - 37th Annual Conference on IEEE Industrial Electronics Society*, pages 3736–3741.

[Darwish and Elkalashy, 2005] Darwish, H. and Elkalashy, N. (2005). Universal arc representation using emtp. *Power Delivery, IEEE Transactions on*, 20(2):772–779.

[Darwish et al., 2006] Darwish, H. A., Izzularab, M. A., and Elkalashy, N. I. (2006). Enhanced commutation circuit design of hvdc circuit breaker using emtp. In *IEEE PES Conference and Exhibition*.

[Datta and Chatterjee, 2012] Datta, B. and Chatterjee, S. (2012). A literature review on use of bewley's lattice diagram. In *Power and Energy in NERIST (ICPEN), 2012 1st International Conference on*, pages 1–4.

[Descloux et al., 2013a] Descloux, J., Curis, J., and Raison, B. (2013a). Protection plan for multi-terminal direct current grids. In *PowerTech conference, Grenoble, France*.

[Descloux et al., 2013b] Descloux, J., Gandioli, C., Raison, B., Hadjsaid, N., and Tixador, P. (2013b). Protection system for meshed hvdc network using superconducting fault current limiters. In *PowerTech conference, Grenoble, France*.

[Descloux et al., 2014] Descloux, J., Raison, B., and Curis, J. (2014). Protection algorithm based on differential voltage measurement for mtdc grids, submitted. In *DPSP 2014*.

[Descloux et al., 2012] Descloux, J., Rault, P., Nguefeu, S., Curis, J., Guillaud, X., Colas, F., and Raison, B. (2012). Hvdc meshed grid: Control and protection of a multi-terminal hvdc system. In *CIGRE international conference*.

[Dommel and Meyer, 1974] Dommel, H. and Meyer, W. (1974). Computation of electromagnetic transients. *Proceedings of the IEEE*, 62(7):983 – 993.

[EMTPWorks, 2005] EMTPWorks (2005). *Constant Parameters Transmission Line*. EMTP-rv Library.

[Eric Favre, 2004] Eric Favre, W. T. L. (2004). Capteurs de courant: à chacun son argument. *Mesures électriques*, Solutions(763):49–55.

[Evrenosoglu and Abur, 2005] Evrenosoglu, C. and Abur, A. (2005). Travelling wave based fault location for teed circuits. *Power Delivery, IEEE Transactions on*, 20(2):115–1121.

[Gandioli, 2013] Gandioli, C. (2013). *Du dimensionnement à l'intégration dans le réseau électrique du limiteur supraconducteur de courant*. Thesis, CNRS, Institut Néel, Creta, G2Elab.

[Gang et al., 2005] Gang, W., Min, W., Haifeng, L., and Chao, H. (2005). Transient based protection for hvdc lines using wavelet-multiresolution signal decomposition. In *PES Transmission and Distribution Conference & Exhibition: Asia and Pacific Dalian, China*. IEEE.

[Ghandhari et al., 2011] Ghandhari, M., Van Hertem, D., Curis, J. B., Despouys, O., and Marzin, A. (2011). Protection requirements for a multi-terminal meshed dc grid. In *Cigrè International Symposium THE ELECTRIC POWER SYSTEM OF THE FUTURE Integrating supergrids and microgrids location*. QC 20120113.

[Guo and Zhao, 2009] Guo, C. and Zhao, C. (2009). A new technology for hvdc start-up and operation using vsc-hvdc system. In *IEEE Power & Energy Society General Meeting*.

[Gustavsen, 2001] Gustavsen, B. (2001). Panel session on data for modeling system transients insulated cables. In *Power Engineering Society Winter Meeting, 2001. IEEE*, volume 2, pages 718 –723 vol.2.

[Hafner and Jacobson, 2011] Hafner, J. and Jacobson, B. (2011). Proactive hybrid hvdc breakers - a key innovation for reliable hvdc grids. *CIGRE*.

[http://www.energy.siemens.com,] http://www.energy.siemens.com.

[Idarraga Ospina et al., 2008] Idarraga Ospina, G., Cubillos, D., and Ibanez, L. (2008). Analysis of arcing fault models. In *Transmission and Distribution Conference and Exposition: Latin America, 2008 IEEE/PES*, pages 1–5.

[Ikonen et al., 2005] Ikonen, M., Laakkonen, O., and Kettunen, M. (2005). Two-level and three-level converter comparison in wind power application. In *www.elkraft.ntnu.no/smola2005/Topics/15.pdf*.

[Jadidian, 2009] Jadidian, J. (2009). A compact design for high voltage direct current circuit breaker. *IEEE Transactions on Plasma Science*, 37(6):1084–1091.

[Jovcic et al., 2013] Jovcic, D., Zhang, L., and Hajian, M. (2013). Lcl vsc converter for high-power applications. *Power Delivery, IEEE Transactions on*, 28(1):137–144.

[K. and N., 2005] K., R. and N., Y. (2005). Fault identification using wavelet transform. In *PES Transmission and Distribution Conference & Exhibition: Asia and Pacific, Dalien, China*. IEEE.

[Kocar et al., 2008] Kocar, L., Mahseredjian, J., and Olivier, G. (2008). Weighting method for transient analysis of underground cables. *Power Delivery, IEEE Transactions on*, 23(3):1629–1635.

[Kocar et al., 2010] Kocar, L., Mahseredjian, J., and Olivier, G. (2010). Improvement of numerical stability for the computation of transients in lines and cables. *Power Delivery, IEEE Transactions on*, 25(2):1104–1111.

[Kundur, 1994] Kundur, P. (1994). *Power System Stability And Control*. EPRI power system engineering series. McGraw-Hill Education (India) Pvt Limited.

[LEM, 2012] LEM (2012). *Current Transducer ITL 4000-S*.

[Liu et al., 2007] Liu, X., Osman, A. H., and Malik, O. P. (2007). Stationary wavelet transform based hvdc line protection. In *39th North American Power Symposium*, pages 37–42. IEEE.

[Liu et al., 2009] Liu, X., Osman, A. H., and Malik, O. P. (2009). Hybrid traveling wave/boundary protection for bipolar hvdc line. In *Power and Energy Society General Meeting, PES*. IEEE.

[Maillard, 2013] Maillard, D. (2013). Réseaux: les vrais défis de la transition énergétique. *Les Echos*, 21419.

[Mallat, 2008] Mallat, S. (2008). *A Wavelet Tour of Signal Processing, Third Edition: The Sparse Way*. Academic Press, 3rd edition.

[Marti, 1982] Marti, J. (1982). Accuarte modelling of frequency-dependent transmission lines in electromagnetic transient simulations. *Power Apparatus and Systems, IEEE Transactions on*, PAS-101(1):147 –157.

[Marti, 1988] Marti, L. (1988). Simulation of transients in underground cables with frequency-dependent modal transformation matrices. *Power Delivery, IEEE Transactions on*, 3(3):1099 –1110.

[Marti, 1993] Marti, L. (1993). Simulation of electromagnetic transients in underground cables using the emtp. In *Advances in Power System Control, Operation and Management, 1993. APSCOM-93., 2nd International Conference on*, pages 147 –152 vol.1.

[Meyer et al., 2005] Meyer, C., Kowal, M., and Doncker, R. W. D. (2005). Circuit breaker concepts for future high-power dc-applications. *IEEE IAS*, nan:p. 860–866.

[Mitsubishi, 2009] Mitsubishi (2009). Mitsubishi hvigbt modules cm1500hc-66r. Technical report, Mitsubishi.

[Morched et al., 1999] Morched, A., Gustavsen, B., and Tartibi, M. (1999). A universal model for accurate calculation of electromagnetic transients on overhead lines and underground cables. *Power Delivery, IEEE Transactions on*, 14(3):1032 –1038.

[Naidoo and Ijumba, 2004] Naidoo, D. and Ijumba, N. M. (2004). Hvdc line protection for the proposed future hvdc systems. In *International Conference on Power System Technology, POWERCON, Singapore*, pages 1327–1332. IEEE.

[Naidoo and Ijumba, 2005] Naidoo, D. and Ijumba, N. M. (2005). A protection system for long hvdc transmission lines. In *Inaugural PES Conference and Exposition in Africa, Durban, South Africa*. IEEE.

[Nakao et al., 2001] Nakao, H., Nakagoshi, Y., Hatano, M., Koshizuka, T., Nishiwaki, S., Kobayashi, A., Murao, T., and Yanabu, S. (2001). D.c. current inter-

ruption in hvdc sf6 gas mrtb by means of self-excited oscillation superimposition. *IEEE Transactions on Power Delivery*, 16(4):687–693.

[Nee and Angquist, 2010a] Nee, H.-P. and Angquist, L. (2010a). Perspectives on power electronics and grid solutions for offshore wind farms. Technical Report 10:96, Elforsk.

[Nee and Angquist, 2010b] Nee, H.-P. and Angquist, L. (2010b). Perspectives on power electronics and grid solutions for offshore wind farms. Technical Report 10:96, Elforsk.

[Nexans, 2013] Nexans (2013). Câbles sous-marins, www.nexans.fr. Consulted on February, 2013.

[NEY, 2013] NEY, M. (2013). Bases de l'électromagnétisme. *Techniques de l'ingénieur Électromagnétisme. Propagation*, base documentaire : TIB277DUO.(ref. article : e1020). fre.

[Nguefeu et al., 2011] Nguefeu, S., Rault, P., Grieshaber, W., and Hassan, F. (2011). Twenties delivrable 11.1, demo 3 requirement specifications: detailed specifications for a dc network and detailed specifications for alstom grid's dc breaker. Technical report, RTE, ALSTOM Grid.

[PAYS, 2013a] PAYS, M. (2013a). Câbles de transport d'énergie applications. *Techniques de l'ingénieur Réseaux électriques mixtes - Ingénierie des réseaux*, base documentaire : TIB267DUO.(ref. article : d4521). fre.

[PAYS, 2013b] PAYS, M. (2013b). Câbles de transport d'énergie technologies. caractéristiques. *Techniques de l'ingénieur Réseaux électriques mixtes - Ingénierie des réseaux*, base documentaire : TIB267DUO.(ref. article : d4520). fre.

[Pelenc, 2002] Pelenc, Y. (2002). Interruption des circuits alimentés en courant continu. *Techniques de l'ingénieur*, D4 700:1–16.

[Peralta et al., 2012] Peralta, J., Saad, H., Dennetiere, S., Mahseredjian, J., and Nguefeu, S. (2012). Detailed and averaged models for a 401-level mmc–hvdc system. *Power Delivery, IEEE Transactions on*, 27(3):1501–1508.

[Petersen, 1995] Petersen, A. (1995). Portable optical ac- and proposed dc-current sensor for high voltage applications. *Power Delivery, IEEE Transactions on*, 10(2):595 –599.

[PuissanceAnalyse, 2012] PuissanceAnalyse (2012). *HVDC : système de mesure forts courants http://www.puissance-analyse.com/capteurs-de-courant/hvdc-systeme-de-mesure-forts-courants.html, consulted on March 2013.*

[Rahmatian and Ortega, 2006] Rahmatian, F. and Ortega, A. (2006). Applications of optical current and voltage sensors in high-voltage systems. In *Transmission Distribution Conference and Exposition: Latin America, 2006. TDC '06. IEEE/PES*, pages 1 –4.

[Rault, 2013] Rault, P. (2013). *Control and stability of VSC-based MTDC grids.* Thesis, L2EP, Ecole Centrale Lille.

[RTE, 2006] RTE (2006). *L'interconnexion électrique France – Angleterre (IFA2000), un maillon stratégique au coeur de l'Europe de l'Électricité.*

[Saad et al., 2013] Saad, H., Peralta, J., Dennetiere, S., Mahseredjian, J., Jatskevich, J., Martinez, J., Davoudi, A., Saeedifard, M., Sood, V., Wang, X., Cano, J., and Mehrizi-Sani, A. (2013). Dynamic averaged and simplified models for mmc-based hvdc transmission systems. *Power Delivery, IEEE Transactions on*, 28(3):1723–1730.

[Sabonnadière and Hadjsaïd, 2007] Sabonnadière, J.-C. and Hadjsaïd, N. (2007). *Lignes et réseaux électriques 1.* Hermes Science Publications.

[Schoenemann et al., 2004] Schoenemann, T., Kiefer, J., Leung, S. Y., Oerzen, B., Inkinen, T., and Huguenot, P. (2004). Commutation process in gas circuit breakers: close-operation and commutation failure during an open-operation. In *Electrical Contacts, 2004. Proceedings of the 50th IEEE Holm Conference on Electrical Contacts and the 22nd International Conference on Electrical Contacts*, pages 53–57.

[Shang et al., 2001] Shang, L., Herold, G., Jaeger, J., Krebs, R., and Kumar, A. (2001). High-speed fault identification and protection for hvdc line using wavelet technique. In *Porto Power Tech Conference, Porto, Portugal*, volume 3.

[Siemens, 2008] Siemens (2008). Guide de mise en service et de maintenance, equipement de protection siemens 7sd52, 7sd52-service-v2-7. Technical report, Siemens.

[Takahashi et al., 2010] Takahashi, M., Sasaki, K., Hirata, Y., Murao, T., Takeda, H., Nakamura, Y., Ohtsuka, T., Sakai, T., and Nosaka, N. (2010). Field test of dc optical current transformer for hvdc link. In *Power and Energy Society General Meeting, 2010 IEEE*, pages 1 –6.

[Tang, 2003] Tang, L. (2003). *Control and protection of Multi-Terminal DC transmission systems based on Voltage Source Converters*. Thesis, McGill University, Department of Electrical and Computer Engineering, Montreal, Quebec, Canada.

[TechnoScience, 2012] TechnoScience (2012). Techno-science website. Consulted on February, 2013.

[Thomas et al., 2009] Thomas, D., Sumner, M., Coggins, D., Wang, X., Wang, J., and Geertsma, L. R. (2009). Fault location for dc marine power systems. In *Electric Ship Technologies Symposium, ESTS*, pages 456–460. IEEE.

[Tixador and Brunet, 2007] Tixador, P. and Brunet, Y. (2007). Supraconducteurs, bases théoriques. *Techniques de l'ingénieur*, D2 701.

[Tixador et al., 2011] Tixador, P., Nguyen Nhat, T., Okada Vieira, H., and Ponceau, R. (2011). Impact of conductor inhomogeneity on fcl transient performance. *IEEE transactions on applied superconductivity*, 21.

[Vacquié, 1986] Vacquié, S. (1986). Arc électrique. *Techniques de l'ingénieur*, D 324:1–16.

[Valenza and Cipollini, 1995] Valenza, D. and Cipollini, G. (1995). Hvdc submarine power cables systems state of the art and future developments. In *Energy Management and Power Delivery, 1995. Proceedings of EMPD '95., 1995 International Conference, IEEE.*

[Vissouvanadin Soubaretty, 2011] Vissouvanadin Soubaretty, B. (2011). *Matériaux de câble à isolation synthétique pour des applications au transport d'énergie HVDC*. Thesis, Univerité de Toulouse.

[You et al., 2009] You, M., Zhang, B.-H., Cao, R.-F., Xu, J.-D., Zhang, S., Bo, Z.-Q., and Klimek, A. (2009). Study of non-unit transient-based protection for hvdc transmission lines. In *Power and Energy Engineering Conference, APPEC Asia Pacific*.

[Zhen-Qiang and Lv, 2008] Zhen-Qiang and Lv, Y.-P. (2008). A novel scheme of hvdc transmission line voltage traveling wave protection based on wavelet transform. In *International Conference on High Voltage Engineering and Application, Chongqing, China*. IEEE.

Résumé étendu

Résumé étendu

La recherche et le développement de nouvelles solutions de transmission d'électricité sont soutenus par la nécessité de transition énergétique globale, de par les préoccupations relatives à l'augmentation de la consommation et au développement durable, actuellement sujets de larges débats.

Dans ce contexte, l'Union Européenne a lancé un paquet nommé climat et énergie, adopté par le Parlement Européen en décembre 2008. Ce paquet se concentre notamment sur la réduction des émissions de gaz à effet de serre, la pénétration des énergies renouvelables, l'efficacité énergétique, et soutient le célèbre objectif des 3x20, à savoir :

- 20% de réduction des émissions de gaz à effet de serre d'ici 2020,
- L'augmentation de l'efficacité énergétique de manière à économiser 20% de la consommation énergétique européenne d'ici 2020,
- L'atteinte d'un taux de pénétration de 20% d'énergie renouvelable dans la consommation énergétique totale de l'union européenne d'ici 2020.

Dans le cadre de la transition énergétique, les attentes en termes de réduction de consommation et d'augmentation de productions décentralisées peuvent laisser sous-entendre une baisse des besoins en transport d'électricité. Par ailleurs, le réseau de transport est souvent associé à la production centralisée due à la forte proportion de production nucléaire dans le mix énergétique français. Dans [Maillard, 2013], le président du directoire de RTE revisite cette idée. Entre autres, l'éloignement géographique des ressources solaires ou éoliennes par rapport aux lieux de consommation, l'impossibilité d'absorber localement de fortes puissances produites et les limites en termes de capacité de stockage sont soulignés. L'exemple allemand est rappelé puisque le pays fait actuellement l'expérience d'un gâchis économique dû

aux lacunes du réseau de transport, ce qui entraine parfois l'obligation de restreindre la production d'origine renouvelable. Ses conclusions montrent que l'adaptation du réseau de transport est un réel challenge à relever, sans quoi la transition énergétique n'est pas possible, et ce indépendamment des choix retenus pour le futur.

Dans ce cadre, RTE participe au renforcement d'un réseau pan-européen, et à long terme à la création d'un supergrid. Des projets européens émergent dans ce sens, et plusieurs concepts de supergrid voient le jour. Alors que le projet Desertec considère la liaison de l'Europe à des parcs photovoltaïques de grande ampleur en Afrique, d'autres réseaux maillant la mer du Nord sont investigués.

Figure 6.3: Exemple de réseau maillé: http://www.greenunivers.com

Ces supergrids apparaissent comme des solutions complémentaires et nécessaires à l'intégration des énergies d'origine renouvelable dans les mécanismes de marché qui existent déjà. Grâce au renforcement des interconnexions entre tous les pays européens, et à la mutualisation de l'électricité produite par les infrastructures les plus efficaces, ces supergrids permettraient éventuellement une réduction du coût total de l'énergie pour chaque pays participant, et l'amélioration de l'indépendance énergétique de l'Europe.

Dans ce contexte, la Commission Européenne a démarré en 2010 le projet nommé Twenties, qui vise à soutenir l'intégration de production d'électricité d'origine renouvelable à large échelle dans le réseau de transport. Les 26 partenaires sont majori-

tairement des gestionnaires de réseau de transport, des constructeurs de composants et des universités, pour un budget total de 56.8M€.

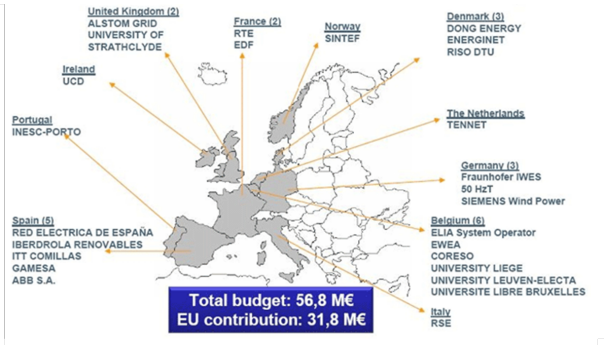

Figure 6.4: TWENTIES, source: http://www.twenties-project.eu

En tant que partenaire du projet Twenties et conducteur de 2 groupes de travail (WP5 et WP11), RTE a pour rôle d'étudier la faisabilité technique et économique de réseaux offshore à courant continu. En effet, cette solution de transmission est considérée pour relier des parcs éoliens éloignés des côtes au réseau de transport alternatif continental. Alors que le WP5 est plutôt relié à des aspects de R&D, le WP11 conduit à la création d'un démonstrateur (DEMO3) afin de prouver les résultats issus des études théoriques sur les réseaux à courant continu.

En effet, il n'existe aucun réseau maillé à courant continu puisque le courant alternatif est utilisé à l'échelle mondiale pour la transmission d'énergie électrique. Les transformateurs électromagnétiques étaient la clé de ce succès, puisque la transformation de courant continu était trop complexe à effectuer, chère, et soumise à un faible rendement. Néanmoins, le développement récent des composants d'électronique de puissance implique de nouveaux potentiels pour l'utilisation de transmission en courant continu. Grâce à ces améliorations technologiques, de nombreuses interconnections en courant continu ont été construites dans plusieurs pays, où le transport en courant alternatif s'avérait moins avantageux. Une liaison à courant continu permet entre autres l'interconnexion de deux réseaux de fréquences différentes, mais surtout, les caractéristiques des systèmes HVDC (High Voltage Direct Current) sont très appréciées pour la transmission de forte puissance lorsque de grandes distances sont considérées (à partir de 40 km, selon la puissance transitée). En effet, l'utilisation de liaisons souterraines ou sous-marines en courant alternatif impose la compensation des pertes dues à l'effet capacitif des câbles. Le transport utilisant les

liaisons HVDC possède donc un avantage puisque cet effet n'existe pas en courant continu. La figure 6.5 justifie le choix du courant continu, en illustrant la capacité à transporter de la puissance pour les différents types de câbles en fonction de la distance et pour différents niveaux de contrainte de tension.

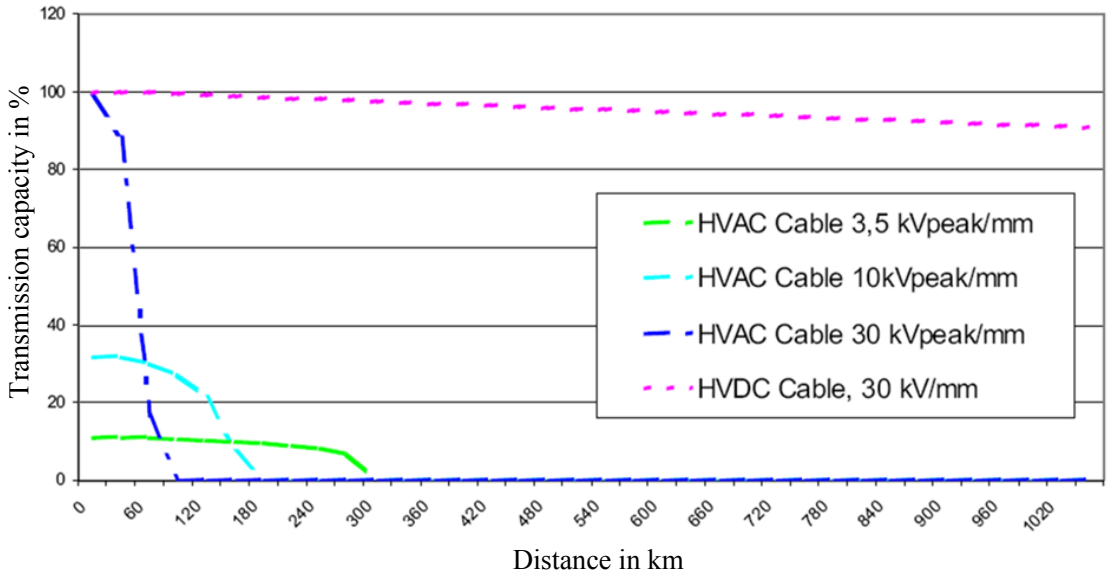

Figure 6.5: Capacité de transmission des liaisons HVAC et HVDC, [Asplund, 2004]

Pour ces raisons, qui sont présentées dans le premier chapitre du manuscrit, les réseaux à courant continu sont l'objet d'investigations dans le cadre du projet Twenties. RTE étudia deux problématiques distinctes, à savoir :

- le contrôle des stations de conversion AC/DC composant le réseau,
- la protection des réseaux DC.

La réalisation du travail de recherche donna lieu à deux thèses supervisées par RTE. La première, sur les aspects de contrôle-commande des stations de conversion AC/DC, a été conduite par Pierre Rault au laboratoire L2EP de Lille, et la seconde sur les protections de ces réseaux a été effectuée au laboratoire G2Elab à Grenoble, et est présentée dans ce manuscrit.

Cette thèse traite de la protection des réseaux à courant continu, élément clé de l'exploitation de ces futures infrastructures et complément indispensable aux futurs disjoncteurs à courant continu. L'étude se concentre sur des réseaux multi-terminaux bouclés et/ou maillés, et propose d'étudier la faisabilité d'un plan de

protection comportant plusieurs principes, composés d'algorithmes principal et de secours en cas de défaillance de celui-ci ou d'un disjoncteur.

Le chapitre 1 détaille la pertinence du recours au courant continu, et discute les différentes technologies utilisées. Les liaisons HVDC consistent à convertir l'énergie produite sous forme de courant alternatif en courant ou tension continue grâce à des stations de conversion, puis de transformer cette énergie en courant alternatif triphasé. Outre l'avantage de faciliter l'exploitation grâce à l'absence de puissance réactive, les liaisons HVDC présentent une souplesse dans les réglages des dispositifs d'électronique de puissance. Le schéma 6.6 présente le principe de fonctionnement.

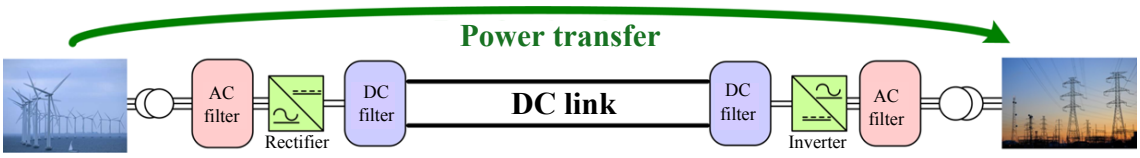

Figure 6.6: Schéma de liaison HVDC

Les filtres assurent le lissage du courant et le maintien d'une tension constante côté continu, ainsi que la compensation des harmoniques du courant côté alternatif. Les transformateurs, quant à eux, sont dimensionnés de manière à supporter les fortes variations de courant susceptibles de se produire dans la partie continue, et doivent posséder une forte impédance de court-circuit afin d'en limiter l'impact sur le réseau. La liaison DC peut être constituée de lignes aériennes ou de câbles souterrains ou sous-marins, et différentes topologies peuvent être appliquées.

Que ce soit au niveau d'une source de production ou pour le raccord de la liaison HVDC à un réseau alternatif, la conversion AC/DC ou DC/AC est nécessaire. Les deux types de convertisseurs les plus connus sont les LCCs (Line-Commutated Converters), qui utilisent des thyristors, et les VSCs (Voltage Source Converters), qui sont constitués de transistors. Les VSC sont les convertisseurs les plus récents et les transistors (IGBT) peuvent être passants ou bloqués sur commande. Un grand nombre d'IGBTs sont connectés en série dans chaque bras. Ils sont commandés pour changer d'état simultanément, avec une précision de l'ordre de la fraction de µs. Le principal avantage du VSC repose sur la possibilité du contrôle simultané des puissances active et réactive échangées entre le convertisseur et le réseau qui y est

connecté. Les VSCs sont d'autant plus utiles dans le cas où la liaison HVDC consiste à relier un parc éolien. En effet, les générateurs asynchrones ont besoin d'une tension de référence et absorbent de la puissance réactive, que le VSC est capable de fournir. Ainsi, l'utilisation d'un VSC permet de se passer des condensateurs généralement employés au niveau des fermes éoliennes. De plus, le changement de direction du transfert de puissance n'implique pas l'inversion du signe de la tension, contrairement aux LCCs, ce qui permet d'utiliser des câbles à isolation synthétique. Les VSCs sont par conséquent appropriés aux liaisons multi-terminal puisque la polarité et le niveau de tension sont maintenus constants. Les topologies les plus classiques sont constituées de deux ou trois niveaux.

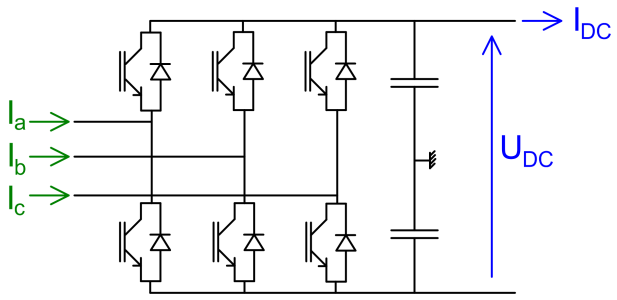

Figure 6.7: Convertisseur à deux niveaux

Cependant, de nouvelles structures, dites multi-niveaux se développent. Le convertisseur est alors composé de sous-modules constitués d'une capacité DC et d'un demi-pont. Chaque bras contient des connexions en séries de ces sousmodules, comme illustré Figure 6.8. Le demi-pont permet d'insérer ou de by-passer la capacité dans la chaîne de sous-modules connectés en série. Le système de contrôle maintient à un niveau constant la moyenne du nombre de sous-modules insérés dans les deux bras, afin d'équilibrer la tension DC. Le potentiel désiré du terminal est construit par la variation de la différence entre le nombre de sous-modules insérés dans les bras supérieur et inférieur.

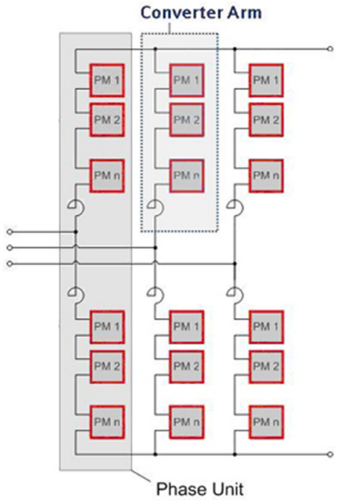

Figure 6.8: Schéma de convertisseur multi-niveaux, [http://www.energy.siemens.com,]

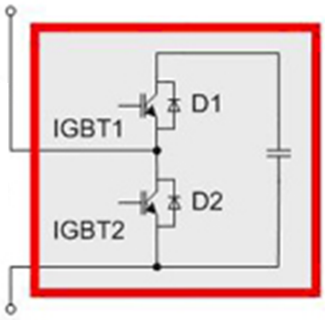

Figure 6.9: Sous-modeule demi pont, [http://www.energy.siemens.com,]

Dans le cas d'une structure multi-niveaux, chaque échelon de l'onde de sortie résulte de l'opération d'un seul sous-module dans chaque bras. La moyenne de la fréquence de commutation par semi-conducteur peut être réduite de manière significative par rapport à une topologie 2 niveaux. Le contenu harmonique de l'onde produite est très faible, réduisant ainsi la taille des filtres nécessaires. Ces technologies sont très récentes et commencent juste à se développer. Des variantes existent chez les principaux fabricants, et sont connues sous le nom de M2C (Modular Multilevel Converter) pour Siemens et CTL (Cascaded Two Level converter) pour ABB. Alstom Grid propose lui aussi une variante du M2C en remplaçant les demi-ponts des sous-modules par des ponts complets. Cette topologie offre la possibilité d'inverser le signe de la tension côté DC, permettant ainsi la connexion d'un VSC à un LCC.

Elle permet aussi de bloquer la circulation de courant provenant du côté DC, ce qui est particulièrement utile lors d'un défaut intervenant dans la partie DC. Cela permettrait notamment l'économie de disjoncteurs DC. Néanmoins, le nombre de composants d'électronique de puissance de cette dernière technologie est prohibitif.

Le chapitre 2 se concentre sur le phénomène de défaut et en révisant les philosophies de protection possibles qui ont été trouvées dans la littérature. La stratégie retenue dans le cadre de cette thèse repose sur celle déjà utilisée dans le cas de la protection des réseaux de transport AC et qui a déjà fait ses preuves en exploitation, c'est-à-dire que la sélectivité est obtenue grâce au recours à des disjoncteurs à courant continu disposés à chaque extrémité de câble et à chaque point de raccordement des stations de conversion. La technologie de coupure d'un courant DC est discutée dans ce même chapitre mais la disponibilité de ces disjoncteurs est une hypothèse forte dans cette étude, puisqu'actuellement ce type de dispositif ultra rapide est en phase de prototypage. Le partenaire industriel en charge de l'évaluation de la faisabilité de ces objets est Alstom Grid dans le cadre de Twenties. Cette thèse se concentre sur la détection sélective des défauts, point clé pour commander les disjoncteurs.

Etant donné l'impossibilité de test on-site vue l'inexistence de ce type de réseau, le recours à la modélisation est nécessaire et la représentation des éléments constituant le système électrique à courant continu est une étape clé de cette étude, qui a été réalisée sous le logiciel de simulation de transitoires électromagnétiques EMTP-rv. Chaque élément est détaillé dans le chapitre trois du manuscrit, dont les deux principaux sont les câbles conducteurs et les convertisseurs AC/DC. Les câbles sont représentés par un modèle tenant compte de la dépendance fréquentielle des caractéristiques. Les convertisseurs sont quant à eux représentés par un modèle détaillé, et le modèle de contrôle commande de ceux-ci a été réalisé au sein du laboratoire L2EP par Pierre Rault.

Le chapitre 4 utilise le modèle de réseau complet sous EMTP-rv pour étudier le comportement d'un réseau DC en conditions de défaut, et montrer l'influence de chaque paramètre sur les grandeurs représentatives d'un défaut d'isolement, grâce à une étude paramétrique.

L'objectif est d'être capable d'éliminer, et ce de manière sélective, un défaut d'isolement intervenant au niveau des câbles ou jeux de barre DC. Les relais de protection doivent donc inclure des algorithmes de détection sélectifs, afin de contrôler les disjoncteurs à courant continu localisés à chaque bout de câble.

Le chapitre 5 est le cœur des travaux puisqu'après des indications sur les éléments régissant les contraintes de rapidité du système de protection, les algorithmes envisageables sont développés, pour finalement fournir une proposition de plan de protection complet.

La problématique majeure repose sur la rapidité d'action du système de protection. Cette contrainte temporelle est nécessaire pour assurer la tenue du matériel et l'opérabilité des convertisseurs AC/DC. Effectivement, un défaut se traduit d'une part par une circulation de courant destructrice pour les diodes qui composent les convertisseurs, et une chute de tension impliquant l'impossibilité de commander les IGBTs.

La faible résistivité des câbles DC ne permet pas de limiter l'apport des capacités phase/terre de ces mêmes câbles au courant de défaut. Les amplitudes limites sont ainsi atteintes en un temps de l'ordre de 5ms.

La contrainte de rapidité s'applique aussi aux organes de coupure, et est bien connue des constructeurs qui l'ont prise en compte dans leurs technologies de disjoncteur à courant continu haute tension. La problématique de la forte amplitude des courants à couper demeure, celle-ci pouvant se résoudre par l'ajout d'éléments capables de limiter le courant ou sa montée (limiteur supraconducteur, inductance, ...). Ces éléments permettent par ailleurs de relaxer la contrainte temporelle qui est intrinsèquement liée aux amplitudes. Néanmoins, la compatibilité de leur dimensionnement en vue d'un développement du réseau DC (nouveau raccordement notamment) reste à prouver.

En conclusion à ces éléments, la méthode qui a été choisie consiste à détecter de manière sélective le défaut dès l'arrivée du premier front aux capteurs les plus

proches, et d'envisager les éléments limitant le courant pour soutenir le fonctionnement des disjoncteurs, voire leur donner une marge supplémentaire (en terme d'amplitude de courant à couper), ce qui augmenterait la fiabilité du système de protection DC global.

Par conséquent, les algorithmes doivent travailler dans le domaine de la centaine de kiloHertz, engageant un besoin de captation des grandeurs haute tension cohérent avec cette valeur. Le système de protection qui a été défini est composé de 4 algorithmes résumés ci-dessous.

Une fréquence de 100kHz a été supposée pour la réalisation des calculs par les relais de protection. Etant donné la simplicité des opérations effectuées (sommes, comparaison à un seuil), le résultat du calcul est supposé connu au pas de temps suivant, soit 10µs plus tard. Un retard a été ajouté afin de tenir compte des temps de transmission entre relais, soit 20µs intra-poste, auxquels on ajoute un retard de 1ms par 200km pour une transmission inter-poste.

Protection différentielle de câble

Le courant différentiel est mesuré à chaque relais localisé en bout de câble, l'ordre d'ouverture est envoyé après dépassement d'un seuil, avec une validation effectuée sur 3 échantillons consécutifs, ce qui ajoute un délai de 30µs. Si un premier front de courant négatif est observé (i.e. présence de défaut mais externe au câble considéré), la protection se bloque pendant la durée du transitoire suivant le défaut et son élimination. Le temps de détection dépend de la longueur du câble (délai de transmission par fibre optique directe inter-poste 200km/ms). Pour une liaison de 100km, ordre envoyé environ 600µs (y compris temps de traitement) après l'apparition du défaut. Il faut ajouter à cela le temps d'action du disjoncteur, inconnu pour le moment.

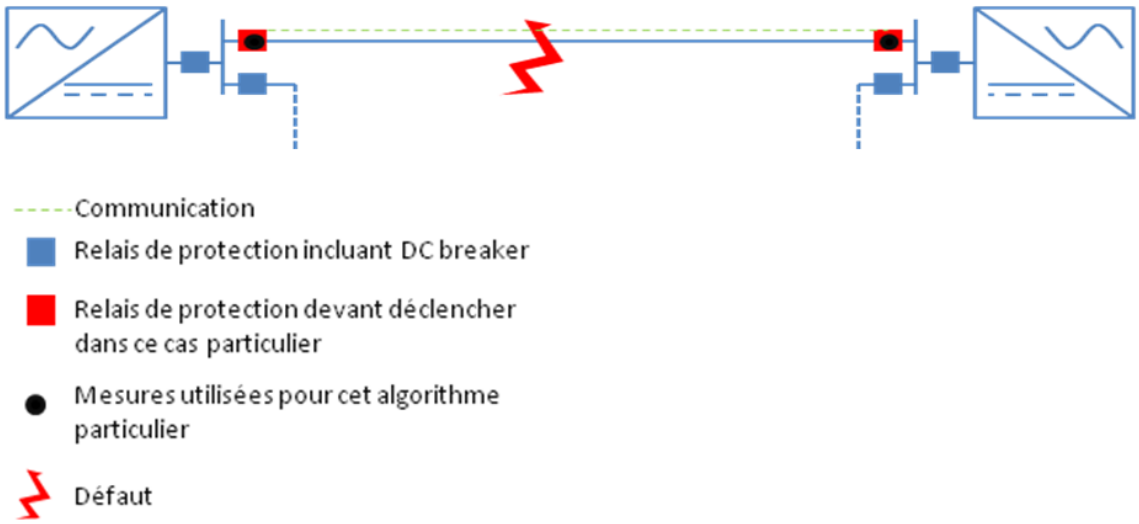

Figure 6.10: Protection différentielle de câble

Protection différentielle de barre

Protection différentielle classique, l'ordre d'ouverture est envoyé instantanément après traitement par l'algorithme (transmission intra-poste et validation sur 3 échantillons) dès l'apparition du défaut puisqu'il n'y a pas de délais de transmission de mesure vue la proximité des relais.

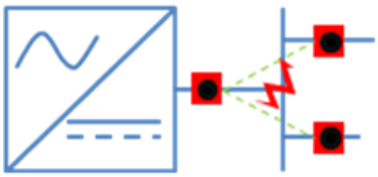

Figure 6.11: Protection différentielle de barre

Différentielle de tension – secours défaillance fibre optique

Ce principe suppose une inductance en série en extrémité de câble DC. L'algorithme repose sur la mesure des tensions aux bornes des inductances, et dépassement d'un seuil avec critère directionnel. L'inductance atténue la montée du courant provenant des câbles sains, et permet d'être sélectif sans communication. Cet algorithme pour-

rait aussi être utilisé en tant que protection principale, mais vue l'absence de communication, le déclenchement à chaque extrémité du câble en défaut n'est pas simultané. Pour cette raison, il est utilisé comme secours à la protection différentielle de câble. L'ordre d'ouverture est envoyé environ 1ms après l'apparition du défaut.

Figure 6.12: Protection différentielle de tension

Secours défaillance disjoncteur

Ce principe s'applique dans le cas d'un défaut câble, éliminé par la protection différentielle d'un côté, dans le cas d'une défaillance d'un disjoncteur de l'autre.

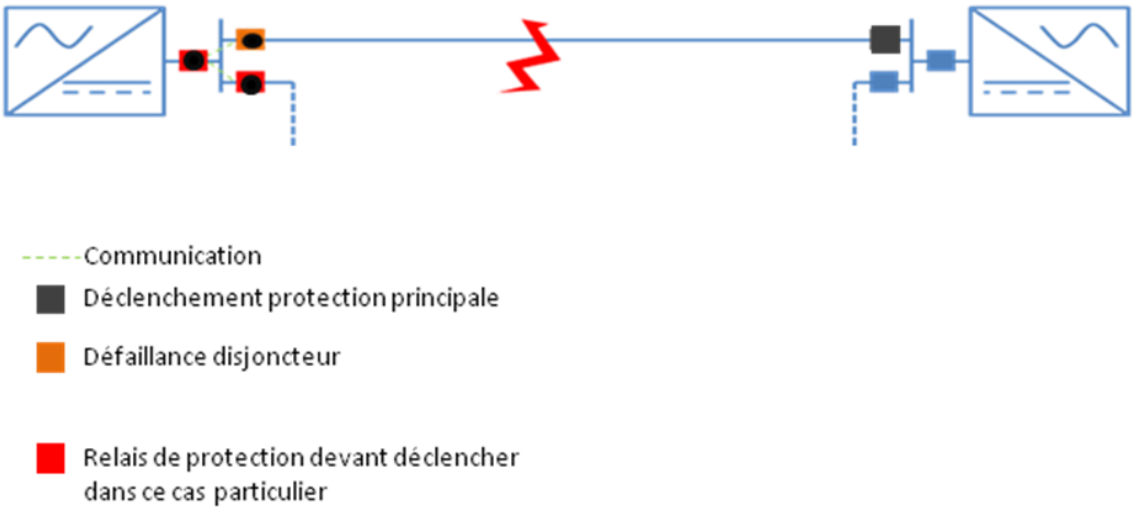

Figure 6.13: Protection de secours défaillance disjoncteur

Le courant mesuré côté convertisseur permet la détection (critère 1) et d'appliquer les règles de sélectivité (critère 2). Si le seuil est dépassé, la mesure des courants dans les départs permet de vérifier qu'un disjoncteur est défaillant (critère 3). Si les 3 critères sont validés, l'ordre d'ouverture est envoyé à tous les disjoncteurs connectés au jeu de barre. Le déclenchement du secours implique la perte d'une station et est donc moins sélectif.

Le temps d'action du disjoncteur influe directement sur le temps de validation du critère 3, puisque pour pouvoir vérifier une défaillance, une temporisation correspondant à l'élimination du défaut est ajoutée.

Par ailleurs, le développement des algorithmes a été réalisé grâce à des simulations EMTP-rv et leur principe de fonctionnement (chaîne d'action) a été validé grâce au démonstrateur Twenties-DEMO3 implanté au L2EP (Lille). Cette validation est présentée dans le sixième et dernier chapitre du manuscrit, à laquelle sont associées les limites d'utilisation des algorithmes.

En conclusion de ces travaux, un plan de protection complet a été proposé, celui-ci étant composé de deux algorithmes principaux (l'un traitant les défauts d'isolement dans les câbles et le second au niveau des jeux de barres), and deux secours (l'un en cas de perte de communication et l'autre pour palier à une défaillance disjoncteur). Par ailleurs, l'insertion d'un autre algorithme dans ce plan de protection permet la vérification de l'état du câble en phase de connexion, renforçant ainsi la sécurité lors de manœuvres sur le réseau en évitant le raccordement de câbles dégradés. Les performances théoriques du système ont été évaluées grâce aux simulations sous le logiciel EMTP-rv, en tenant compte des effets d'atténuation des capteurs dans les entrées du système de protection. La robustesse des principes face au bruit ainsi qu'aux autres perturbations relatives aux composants physiques a été vérifiée grâce à un démonstrateur hybride à échelle réduite (tension nominale de 250 volts) composés de câbles et convertisseurs physiques eux-mêmes connectés à des éléments simulés en temps réel. Les principes de courant différentiel et de secours défaillance disjoncteur ont été vérifiés sur ce démonstrateur. Cette maquette prouve aussi l'efficacité des principes de protection sur d'autres topologies de réseau.

Toutefois, la faisabilité d'un tel système de protection dépend de la performance des futurs disjoncteurs à courant continu, dont la rapidité influence directement les réglages des seuils et temporisations des relais de protection. Par ailleurs, la capacité de coupure limitée de ces mêmes disjoncteurs incite à chercher des solutions de limitation de courant viables, et les questionnements relevant de la validité des modèles de câbles demeurent.

Cette thèse a donné lieu à 4 publications dans des conférences internationales:

[Descloux et al., 2012]: J. Descloux , P. Rault, S. Nguefeu, J-B. Curis, X. Guillaud, F. Colas, B. Raison (RTE, L2EP, G2Elab, France), HVDC meshed grid : Control and protection of a multi-terminal HVDC system, CIGRE 2012, B4, Paris, France

[Descloux et al., 2013a]: J. Descloux, B. Raison, J-B. Curis (G2Elab, RTE, France), Protection Plan for Multi-Terminal Direct Current Grids, PowerTech 2013, Grenoble, France

[Descloux et al., 2013b]: J. Descloux, C. Gandioli, B. Raison, N. Hadjsaid, P. Tixador (G2Elab, RTE, France), Protection system for meshed HVDC network using superconducting fault current limiters, PowerTech 2013, Grenoble, France

[Descloux et al., 2014]: J. Descloux, J-B. Curis, Bertrand Raison, (G2Elab, RTE, France), Protection algorithm based on differential voltage measurement for MTDC grids, submitted, DPSP 2014, Copenhagen, Denmark

et deux valorisations orales :

IEEE Power and Energy Society French Chapter, Soirée Doctorants, February 10th, 2012, Paris, France

2013 IEEE Power and Energy Society General Meeting, HVDC Panel Session, July, 2013, Vancouver, Canada

Protection contre les courts-circuits des réseaux électriques à courant continu de forte puissance

Résumé Dans le domaine du transport de l'électricité, les qualités intrinsèques des réseaux alternatifs s'estompent devant la difficulté imposée par le transport de la puissance réactive lorsque les lignes aériennes ou, plus particulièrement, les câbles souterrains ou sous-marins atteignent des longueurs critiques. Dans le cadre des réflexions visant à exploiter au mieux les énergies renouvelables d'origine éolienne off-shore ou hydrolienne, l'hypothèse de la création d'un réseau électrique à haute tension continue pour acheminer ces énergies jusqu'aux centres de consommation est considérée. Ce travail de thèse, encadrée par RTE et le laboratoire de Génie Electrique de Grenoble (G2Elab), est en lien avec le projet TWENTIES, financé dans le cadre du programme FP7 de la Commission Européenne, qui a pour vocation d'analyser les obstacles à l'intégration de volumes croissants d'énergie renouvelable dans le système électrique européen, et de proposer des solutions pour lever ces verrous technologiques. Les travaux traitent de la protection des réseaux à courant continu, élément clé de l'exploitation de ces futures infrastructures et complément indispensable aux futurs disjoncteurs à courant continu. L'étude se concentre sur des réseaux multi-terminaux bouclés et/ou maillés, et propose d'étudier la faisabilité d'un plan de protection comportant plusieurs principes, composés d'algorithmes principal et de secours en cas de défaillance de celui-ci ou d'un disjoncteur.

Mots clés *Réseau de transport d'électricité, courant continu, câble, plan de protection, système de protection, court-circuit.*

Protection plan for a Multi-Terminal and High Voltage Direct Current grid

Abstract In electricity transmission, the inherent qualities of alternative grids fade in front of the difficulty imposed by the reactive power transportation, when overhead lines or, particularly underground or submarine cables reach critical lengths. In the frame of the thought aiming to operate at best renewable energy resources, coming from wind or hydro power stations, the creation of a high voltage direct current grid is assumed to dispatch those energies to the consumption centers. Indeed, from a certain amount of power to transmit, there is a critical length beyond which AC transmission is not viable anymore, and where DC links becomes both more efficient and less costly. The new conversion technologies, namely the voltage source converters, now enables the connection of several terminals and therefore, the creation of a true grid, which can either have a looped, meshed, or radial structure. The advantages of such grid structure in relation to point-to-point links are obvious in terms of reliability of the transmission grid. Nevertheless, some technological locks remain, and the protection against faults of those grids is currently largely debates. This Ph.D work, advised by RTE and Grenoble Electrical Engineering laboratory (G2Elab) is linked with the TWENTIES project, which aims to analyse the potential obstacles to the integration of renewable resources in the European electrical system, and to propose solutions to lift those technological barriers.This Ph.D thesis aims to propose a complete protection plan against insulation faults in cable or busbar, including a main protection and two backups in case of failure of a component, for a submarine DC grid. The target application would be a grid linking offshore wind farms and countries through the North Sea.

Keywords *Transmission power grid, direct current, cable, protection plan, protection system, short-circuit.*